THE UNIVERSITY OF READING
DEPARTMENT OF MATHEMATICS

Development of Linear Models for Data Assimilation in Numerical Weather Prediction

by

Amos S. Lawless

Thesis submitted for the degree of
Doctor of Philosophy

May 2001

Abstract

Four-dimensional variational data assimilation requires the development of a discrete linear model with which to predict the evolution of a perturbation to the initial state of a nonlinear system. There are two ways in which this linear model may be derived. Beginning with the continuous nonlinear equations we may first discretize them and then linearize the numerical scheme thus formed, or we may first linearize the continuous equations and then apply some suitable discretization. In this thesis we compare these two methods.

Using simple models of an ODE and a PDE problem we show how the two methods may lead to models with different stability and accuracy characteristics. An important factor in determining the accuracy of the second method is found to be the representation of the background trajectory around which the model is linearized. We find that natural approximations to this trajectory may not only reduce the accuracy of the overall scheme but, within the context of semi-Lagrangian advection, may lead to a scheme which is no longer consistent.

As part of our analysis we identify a difficulty in testing the linear model formed by first linearizing and then discretizing. In order to overcome this we propose a new method for testing such models, which we demonstrate both theoretically and numerically.

Finally we consider the implementation of these ideas for operational weather forecasting, by developing the linearization of a three-dimensional weather forecasting model. For this case only the linear model formed by first linearizing and then discretizing is found. Numerical tests are performed using this model and the results interpreted in the light of the analysis of the simple problems.

Acknowledgements

My first acknowledgement is to my academic supervisor, Prof Nancy Nichols. I am extremely grateful for the careful attention she has given to this work and for her patience in explaining the finer mathematical points which I often overlooked. My gratitude goes also to my supervisor at the Met Office, Sue Ballard, for her constant support throughout this work, particularly for her help with the work on the three-dimensional model of Chapter 6 and for ensuring that I had sufficient time for this project.

I wish to thank Andrew Staniforth of the Met Office for his guidance in setting up the shallow water model of Chapter 5. My thanks go also to past and present members of the dynamics and data assimilation research and development groups at the Met Office, who have worked with me to build the model used in Chapter 6. I particularly acknowledge Mike Cullen who produced the initial design for this model.

I would like to thank my family, for their love and encouragement over many years. I also thank my friends who have been a continual source of support and strength during the last few years.

Finally I would like to acknowledge the financial support of the Met Office, who supported this PhD project as part of my full time work.

Contents

Chapter 1

Introduction

L.F. Richardson proposed a method of forecasting the weather numerically using the already well-known equations of a fluid in 1922 [70]. His idea was not realized until much later when, in the 1950s, simple models of the atmosphere were run on the very first digital computers [89]. However, it was soon realized that to be able to forecast a physically realistic state of the atmosphere it was necessary to specify the initial conditions with care, so as to avoid the growth of non-physical gravity waves within the numerical model. It was the absence of techniques to do this that lead to large errors in Richardson's own first forecast [52].

The difficulty with the specification of initial conditions for a weather forecasting model is that the underlying initial value problem being solved is very much underdetermined. For the operational resolution of most global models today it is necessary to specify of the order $10^6 - 10^7$ data values to begin a model forecast, but at any one time the number of observations of the atmosphere is only of the order 10^5. Besides the obvious lack in the number of data, the data that are available are not evenly spread and so for example we have many useful data over the continents, but little over the oceans. Thus to obtain a reasonable estimate of the initial fields for the forecast model it is necessary to combine the data we do have with some first estimate of the initial state. This estimate is known as a *background field* and

is usually obtained from a previous short period forecast. The process of using the data to improve on this estimate is called *data assimilation.*

Until recently most methods of data assimilation have relied on a statistical combination of the data and background field. A review of such methods is given in [31] and [51]. A limitation of these methods is that they do not explicitly use the known model equations to constrain the problem in any way. This was changed by the proposal of the method of four-dimensional variational data assimilation (4D-Var) (e.g. [48], [80]). This method treats the data assimilation problem as a problem of minimizing the distance between the observations and the trajectory of the numerical model in a given time window, while still staying close to the background solution. Thus the numerical model itself is used as a constraint in the problem. The proposal of this method led to much experimentation in 4D-Var systems (e.g. [85], [14], [49], [86], [95], [50], [94]). However the full 4D-Var system as originally proposed was thought to be too expensive for any operational implementation.

The development of a 4D-Var system for use in real-time weather forecasting became a realistic possibility when in 1994 Courtier et al. [17] proposed an incremental formulation. In this formulation the linearization of the nonlinear model is used to predict the evolution of a perturbation around a given trajectory of the nonlinear model. The distance from the perturbed trajectory to the observations is then minimized, with the adjoint of the linear model being used to provide the required gradient information for the minimization. In this way the full 4D-Var problem is approximated by a quadratic problem. This guarantees a unique solution to the minimization and also allows faster convergence to this solution. This formulation also allows an approximation to the true linearization of the model to be used, thus allowing further savings in the computational cost.

In order to develop an incremental 4D-Var system we must first develop a linearization of our nonlinear model and the adjoint of this linear model. This require-

ment is not particular to 4D-Var, however, since the linearization of a nonlinear model is often used as a means of obtaining the adjoint model in other applications. Adjoint models are an efficient method of providing gradient information for many large scale optimization problems. They are used within meteorology not only for data assimilation, but also for the study of forecast error, the determination of initial perturbations for ensemble forecasts, sensitivity analyses and the targetting of atmospheric observations [27], [13], [12], [56], [63], [68], [69]. They also arise in many applications in other fields, such as aerodynamic design [1], [60] and oil reservoir problems [15]. Thus the question as to which is the best method to obtain the linear model and the adjoint model is one which is of interest in many fields.

There are three different ways in which one may develop a discrete adjoint model beginning from a continuous nonlinear model and these are illustrated in Figure 1.1. Method 1, which is called the *continuous method*, is to find the adjoint of the continuous nonlinear equations and then apply a suitable discretization. This method has been used for example in aerodynamic design [40]. However, it is not suitable for the problem of incremental 4D-Var since it does not provide a discrete linear model with which to predict the evolution of a perturbation.

Method 2 is first to discretize the nonlinear equations and then linearize the discrete numerical scheme in order to form a discrete linear model. This method is known as the *discrete method* and the discrete linear model formed in this way is called the *tangent linear model* (TLM). The adjoint model can be found directly from the tangent linear model by a transposition of the matrix representation of the discrete tangent linear model. This method has the advantage that the tangent linear model can be found by directly linearizing the nonlinear model source code, a process known as *automatic differentiation*. The adjoint model can then be found by transposing the tangent linear model source code ([5], [9], [10], [14], [32], [34], [75]).

The third method is one which we propose in this thesis. We begin from the

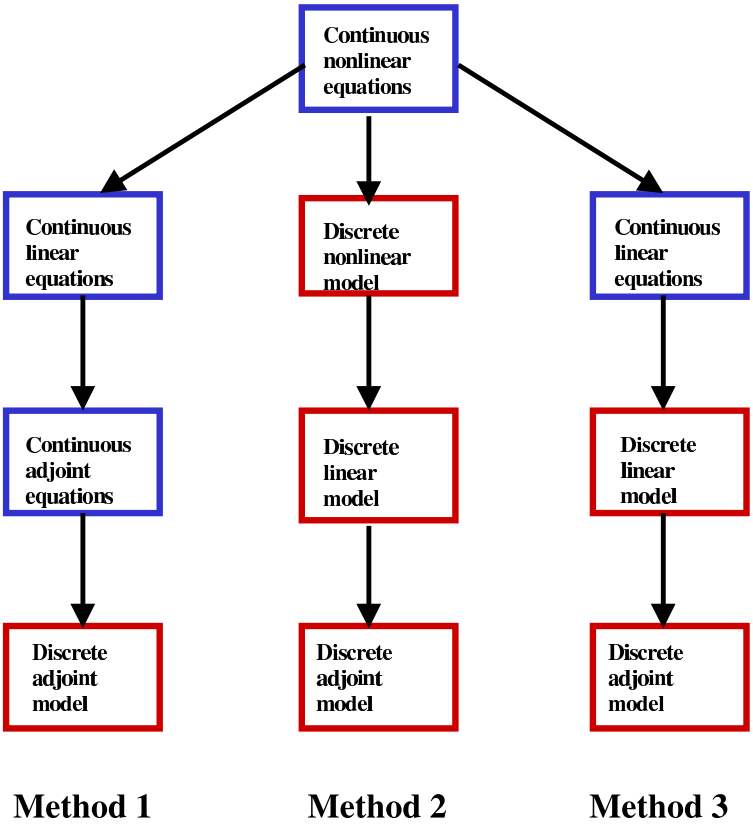

Figure 1.1: A schematic explanation of the various ways to derive a discrete adjoint model.

continuous nonlinear equations and linearize them, to form a set of continuous linear equations. These linear equations are then discretized using a suitable numerical scheme to form the discrete linear model, which we call a *perturbation forecast model* (PFM). The adjoint model can then be obtained from the perturbation forecast model in the same way as in Method 2 and so within the incremental 4D-Var scheme we still have the exact adjoint of our discrete linear model. We call this approach the *semi-continuous* method.

There are two main advantages to the semi-continuous method. The first is based on the premise that although the tangent linear model is valid for infinitesimal perturbations, what we actually want to model are finite perturbations of the size of uncertainties in the initial conditions [26]. The perturbation forecast model can be designed with this aim in mind. Thus it can be based on physical principles and can make some small approximations to the true tangent linear model. If the magnitude of such approximations is no greater than the error made by linearizing, then this should not affect the accuracy of the calculations, but will allow significant savings to be made to the running costs of the models. In fact, within the field of aerodynamics some attempt has been made to simplify the adjoint model to reduce its cost [60]. Our approach allows such simplifications to be made both in the equations of the linear model before any discretization by appealing to scale analysis and in the actual implementation of the numerical scheme.

A second advantage to this approach is that it is possible to avoid some of the problems which occur with numerical schemes which are difficult to linearize. Such difficulties will be reviewed in more detail in Section 3.2. For the present we note that one such problem can occur when deciding how to linearize an iterative scheme [64]. The semi-continuous method avoids this question by applying a suitable numerical scheme to the linearized equations.

In this thesis we do not treat the adjoint model, but concentrate our attention only on the discrete linear models formed by the discrete method (Method 2) and

the semi-continuous method (Method 3). We wish to compare the properties of the linear models formed in this way and to examine some of the issues which arise when discretizing the linear equations in the semi-continuous method. We begin in Chapter 2 by reviewing some of the principles of numerical analysis and some particular numerical schemes, which we make use of in the remainder of the thesis. In Chapter 3 we review some of the studies that have already been carried out on linear models, first looking at how linear models have generally been assessed and then presenting some known results on the different ways to find a linear and adjoint model. At the end of the chapter we propose a new method for the testing of a perturbation forecast model. We then move on to our own studies of particular examples of linear models. In Chapter 4 we look at a simple example of an ordinary differential equation problem and develop the linear model by both methods, comparing the tangent linear model (TLM) and the perturbation forecast model (PFM) analytically and numerically. Chapter 5 then considers a simple system of partial differential equations. We again develop and compare the TLM and PFM, in a study of the one-dimensional shallow water equations, this time using numerical schemes more similar to those used in the three-dimensional weather forecasting model being developed for operational use at the Met Office. In Chapter 6 we turn our attention to this three-dimensional weather forecasting model. For this model it is not practical to develop the linearization by both methods, so we develop only the PFM. We explain some of the choices made for the numerical scheme and show results from numerical experiments. Finally in Chapter 7 we draw together the conclusions from the various models we have looked at and propose some questions to be answered in future work.

Chapter 2

Numerical methods for differential equations

In this chapter we review some of the concepts of numerical analysis and the numerical methods which we make use of in the remainder of the thesis. We begin in Section 2.1 by reviewing the analysis of initial value problems of ordinary differential equations (ODEs) and then move on to partial differential equations (PDEs) in Section 2.2. For each of these we review three essential properties of any numerical scheme, accuracy, convergence and stability. The accuracy of a numerical scheme is a measure of how well the numerical method approximates the original continuous equation. To measure this we introduce the definitions of the truncation error, order and consistency of a numerical scheme. However these only measure the error in the approximation of the equation and do not give information about how close the numerical solution is to the analytical solution. To obtain this we introduce the concept of convergence. Finally we have stability, which is a property of the discrete equations and makes no direct reference to the continuous problem. Stability together with consistency ensures that the numerical solution does not grow faster than the analytical solution. For most stability analyses we need to make some simplifying assumptions about the problem being solved. For example, the analysis is

usually applied to a linear problem and sometimes we are required to ensure that we have constant coefficients. Thus such analyses often provide only necessary, but not sufficient, conditions for stability. Within this thesis we restrict our analysis to the stability of a linear system. For both the ODE and PDE problems we discuss the concepts of accuracy, convergence and stability with respect to a general problem and then introduce examples of particular numerical schemes in Sections 2.3 and 2.4.

2.1 Ordinary differential equations

For our study of ordinary differential equations we limit discussion to the system of first order equations

$$\frac{d\mathbf{y}}{dt} - \mathbf{F}(\mathbf{y}, t) = 0, \tag{2.1}$$

where $\mathbf{y} = \mathbf{y}(t)$ is a real-valued vector, $t \in [0, T]$ and $\mathbf{y}(0) = \mathbf{y_0}$ is given. We interpret the independent variable t as a temporal variable. In order to represent general numerical schemes applied to these equations we first introduce some notation. We define the step size Δt for the independent variable t. Then we have at time t_n the analytical value of $\mathbf{y}$, which we write $\mathbf{y}(t_n) = \mathbf{y}(n\Delta t)$. The numerical approximation to this is written $\mathbf{y}_n$. Then we can write a general one-step numerical scheme to solve the system (2.1) as

$$\mathbf{y}_{n+1} - \boldsymbol{\mathcal{F}}_n(\mathbf{y}_n, \Delta t) = 0 \tag{2.2}$$

with initial condition $\mathbf{y}_0$, where for an implicit scheme the solvability of the implicit equations is assumed.

2.1.1 Accuracy

The accuracy of the numerical scheme (2.2) is defined by its *global truncation error* as follows:

Definition 2.1 *For the ODE problem (2.1), the global truncation error* $\boldsymbol{\tau}_n$ *of the scheme (2.2) at time* t_n *is defined by*

$$\boldsymbol{\tau}_n = \frac{\mathbf{y}(t_{n+1}) - \boldsymbol{\mathcal{F}}_n(\mathbf{y}(t_n), \Delta t)}{\Delta t}, \tag{2.3}$$

where $\mathbf{y}(t_n)$ *is the theoretical solution of the initial value problem (2.1).*

The global truncation error is often simply referred to as the truncation error and we will follow this henceforth. A Taylor series expansion of the truncation error in terms of the step size Δt allows us define the *order of accuracy* of the scheme ([44], p.225):

Definition 2.2 *The method (2.2) is said to have order* p *if* p *is the lowest integer for which*

$$\mathbf{y}(t_{n+1}) - \boldsymbol{\mathcal{F}}_n(\mathbf{y}(t_n), \Delta t) = O(\Delta t^{p+1}) \tag{2.4}$$

holds, where $\mathbf{y}(t_n)$ *is assumed to be a sufficiently differentiable solution of the initial value problem (2.1).*

The requirement that the accuracy of the scheme increase as a smaller step size is used is then given by the property of *consistency*:

Definition 2.3 *The numerical method (2.2) is consistent if* $\boldsymbol{\tau}_n \to 0$ *as* $\Delta t \to 0$ *with* $n\Delta t$ *constant.*

This is equivalent to requiring that the order of the scheme be at least one.

2.1.2 Convergence

The convergence of a numerical scheme relates the analytical and numerical solutions. We first need to choose an appropriate norm to measure the distance between the solutions, which we write $\| \, . \, \|$. Commonly chosen norms for a vector $\mathbf{x} = \{x_j\}$ of length N are the maximum norm

$$\| \, \mathbf{x} \, \|_\infty = \max_{1 \le j \le N} |x_j| \tag{2.5}$$

and the Euclidean, or l_2 norm

$$\| \mathbf{x} \|_2 = \left(\sum_{j=1}^{N} |x_j|^2 \right)^{\frac{1}{2}}. \tag{2.6}$$

We define the *global error* $\mathbf{e}_n$ of the numerical solution at time t_n by

$$\mathbf{e}_n = \mathbf{y}(n\Delta t) - \mathbf{y}_n. \tag{2.7}$$

Then we have:

Definition 2.4 *The numerical scheme (2.2) is a convergent approximation to the initial-value problem (2.1) if* $\| \mathbf{e}_n \| \to 0$ *as* $n \to \infty$ *with* $n\Delta t$ *constant.*

Convergence is related to consistency by means of the following theorem:

Theorem 2.1 *Let* $\boldsymbol{\mathcal{F}}_n$ *be a continuous function of its arguments and let there exist a constant* L *such that for all points* $(\mathbf{y}_n, \Delta t), (\mathbf{y}_n^*, \Delta t)$,

$$\| \boldsymbol{\mathcal{F}}_n(\mathbf{y}_n, \Delta t) - \boldsymbol{\mathcal{F}}_n(\mathbf{y}_n^*, \Delta t) \| \leq (1 + L\Delta t) \| \mathbf{y}_n - \mathbf{y}_n^* \| . \tag{2.8}$$

Then the one-step method (2.2) is consistent if and only if it is convergent ([44], p.116).

The condition (2.8) is called the *Lipschitz condition.*

2.1.3 Stability

The general definition of stability ensures that a numerical method is not over-sensitive to small perturbations in the initial conditions of the problem. We use the definition from [45], p.32. We define perturbations $\{\boldsymbol{\delta}_n, n = 0, 1, \ldots, M\}$ and perturbed solutions $\{\mathbf{z}_n, n = 0, 1, \ldots, M\}$ to the discrete system (2.2) by

$$\begin{aligned} \mathbf{z}_{n+1} &= \boldsymbol{\mathcal{F}}_n(\mathbf{z}_n, \Delta t) - \boldsymbol{\delta}_n = 0, \\ \mathbf{z}_0 &= \mathbf{y}_0 + \boldsymbol{\delta}_0. \end{aligned} \tag{2.9}$$

Then we have

Definition 2.5 *Let $\boldsymbol{\delta}_n, \boldsymbol{\delta}_n^*$ be any two perturbations of (2.2) and let $\mathbf{z}_n, \mathbf{z}_n^*$ be the resulting perturbed solutions for $n = 0, 1, \ldots, M$. Then if there exists constants S and h_0 such that, for all $\Delta t \in (0, h_0]$,*

$$\| \mathbf{z}_n - \mathbf{z}_n^* \| \leq S\epsilon \tag{2.10}$$

whenever

$$\| \boldsymbol{\delta}_0 - \boldsymbol{\delta}_0^* \| \leq \epsilon \tag{2.11}$$

for $0 \leq n\Delta t \leq T$, we say that the methods (2.2) is zero-stable.

A sufficient condition for the zero-stability of the numerical scheme (2.2) is that the scheme satisfy a Lipschitz condition of the form (2.8).

The definition of zero-stability is concerned with what happens as $\Delta t \to 0$ with $n\Delta t$ fixed. For $\Delta t \neq 0$ we can define a weaker form of stability which considers how a perturbation propagates for a fixed Δt as $n \to \infty$. We determine this weaker stability by applying the numerical scheme to the linear scalar equation

$$\frac{dy}{dt} = \mu y, \qquad \mu < 0. \tag{2.12}$$

If we apply the numerical method (2.2) to this equation, we obtain a one-step difference equation of the form

$$y_{n+1} = \lambda(\mu\Delta t) y_n, \tag{2.13}$$

where $\lambda(\mu\Delta t)$ is called the *amplification factor*. We then have

Definition 2.6 *The numerical scheme (2.2) is absolutely stable on an interval (α, β) if $y_n \to 0$ as $n \to \infty$ for $\mu\Delta t \in (\alpha, \beta)$.*

We see from (2.13) that the numerical scheme is absolutely stable for those values of $\mu\Delta t$ for which $|\lambda(\mu\Delta t)| < 1$ holds ([45], p.199).

2.2 Partial differential equations

The partial differential equation problem we consider is the first order quasi-linear system in two independent variables

$$\frac{\partial \mathbf{u}}{\partial t} + \boldsymbol{F_1}(\mathbf{u}, x, t)\frac{\partial \mathbf{u}}{\partial x} + \boldsymbol{F_0}(\mathbf{u}, x, t) = 0, \tag{2.14}$$

where $\mathbf{u} = \mathbf{u}(x,t)$ is a real-valued vector, $t \in [0,T]$ and $x \in [0,L]$. The boundary conditions on x are periodic, so that $\mathbf{u}(0,t) = \mathbf{u}(L,t)$, and the initial condition $\mathbf{u}(x,0) = \mathbf{u_0}(x)$ is given. The partial derivatives of the vector $\mathbf{u}$ are defined to be the Jacobian of the vector with respect to the variable x or t. We interpret x as a spatial variable and t as a temporal variable. Many of the following results can easily be extended to more spatial dimensions by considering a vector $\mathbf{x} = [x_1, x_2, \ldots, x_k]$, but for the purposes of this chapter we restrict the discussion to one spatial dimension so as to simplify the notation.

In order to represent the numerical schemes we introduce step sizes $\Delta x, \Delta t$ for the independent variables x and t. Then at any spatial point x_i and time t_n the solution to the analytical system (2.14) is written $\mathbf{u}(x_i, t_n) = \mathbf{u}(i\Delta x, n\Delta t)$. The numerical approximation to this we write $\mathbf{u}_i^n$. We also need to define notation for the vector of values over all spatial points at a given time. We assume that we have N gridpoints, with $N\Delta x = L$, and define the vector of numerical solutions on the grid by

$$\mathbf{U}^n = [(\mathbf{u}_1^n)^T, (\mathbf{u}_2^n)^T, \ldots, (\mathbf{u}_N^n)^T]^T. \tag{2.15}$$

This is a numerical approximation to the analytical solution vector

$$\mathbf{U}(t_n) = [\mathbf{u}^T(x_1, t_n), \mathbf{u}^T(x_2, t_n), \ldots, \mathbf{u}^T(x_N, t_n)]^T. \tag{2.16}$$

We can then write a general one-step numerical method for solving the system (2.14) in the form

$$\mathbf{U}^{n+1} - \boldsymbol{\mathcal{G}}^n(\mathbf{U}^n, \Delta x, \Delta t) = 0, \tag{2.17}$$

where $\boldsymbol{\mathcal{G}}^n$ is a continuously differentiable difference operator and $\mathbf{U}^0$ is given.

2.2.1 Accuracy

We define the accuracy of the numerical scheme (2.17) by means of its global truncation error as follows:

Definition 2.7 *For the PDE problem (2.14), the global truncation error* $\boldsymbol{\tau}^n$ *of the scheme (2.17) at time* t_n *is defined by*

$$\boldsymbol{\tau}^n = \frac{\mathbf{U}(t_{n+1}) - \boldsymbol{\mathcal{G}}^n(\mathbf{U}(t_n), \Delta x, \Delta t)}{\Delta t}. \tag{2.18}$$

As for the ODE problem, this then leads to the definitions of order and consistency for the numerical scheme. For this case we may have different orders of accuracy in different variables and so we have,

Definition 2.8 *The method (2.17) is said to have order* p *in* Δx *and order* q *in* Δt *if* p *and* q *are the lowest integers for which*

$$\mathbf{U}(t_{n+1}) - \boldsymbol{\mathcal{G}}^n(\mathbf{U}(t_n), \Delta x, \Delta t) = O(\Delta x^{p+1}) + O(\Delta t^{q+1}) \tag{2.19}$$

holds, where $\mathbf{U}(t_n)$ *is assumed to be a sufficiently differentiable solution of the initial value problem (2.14).*

Definition 2.9 *The numerical method (2.17) is consistent in a given norm if* $\| \boldsymbol{\tau}^n \| \to 0$ *as* $\Delta t \to 0$ *and* $\Delta x \to 0$ *with* $n\Delta t$ *and* $N\Delta x$ *constant.*

It is necessary that there be some additional fixed relationship between Δt and Δx, with $\Delta t = O(\Delta x)$ typical for hyperbolic problems ([57], p.136). We note that the scheme will be consistent if and only if it has order of at least one in all independent variables.

2.2.2 Convergence

To define convergence for the PDE scheme we first define the global error $\mathbf{e}_i^n$ at point x_i and time t_n,

$$\mathbf{e}_i^n = \mathbf{u}(i\Delta x, n\Delta t) - \mathbf{u}_i^n. \tag{2.20}$$

Then we have:

Definition 2.10 *The numerical scheme (2.17) is a convergent approximation to the initial-value problem (2.14) in a given norm if* $\| \mathbf{e}_i^n \| \to 0$ *as* $n \to \infty, i \to \infty$ *with* $n\Delta t, i\Delta x$ *constant.*

2.2.3 Stability

In this section we restrict discussion to the stability of linear schemes for partial differential equations, that is schemes of the form (2.17) where $\boldsymbol{\mathcal{G}}^n$ is a linear function of $\mathbf{U}^n$. Then the stability of the numerical scheme (2.17) can be expressed by the following definition, taken from [42], p.30:

Definition 2.11 *The difference approximation (2.17) is stable in a given norm for a sequence* $\Delta t \to 0, \Delta x \to 0$ *if there are constants* α, K *such that for all* t_0, t_n *with* $t_n \geq t_0$ *and all* $\mathbf{U}^0$

$$\| \mathbf{U}^n \| \leq K e^{\alpha(t_n - t_0)} \| \mathbf{U}^0 \| . \tag{2.21}$$

For a PDE problem, establishing the stability of a numerical system is an important part of demonstrating its convergence. The inherent link between these two properties is expressed by the *Lax equivalence theorem*:

Theorem 2.2 (Lax equivalence) *Given a properly posed initial-value problem and a finite-difference approximation to it that satisfies the consistency condition, stability is the necessary and sufficient condition for convergence, assuming that all conditions hold in the same norm. ([71], p.45).*

However, in general it is difficult to determine a condition such as (2.21) for a variable coefficient problem and so we usually consider only the stability of a constant-coefficient linear system. In this case the numerical scheme (2.17) can be written

$$\mathbf{U}^{n+1} = \mathbf{C_0}(\Delta t, \Delta x)\mathbf{U}^n, \tag{2.22}$$

where $\mathbf{C_0}$ is a time invariant matrix. Assuming a relationship between Δx and Δt we can write such a system in the form

$$\mathbf{U}^{n+1} = \mathbf{C_1}(\Delta t)\mathbf{U}^n, \tag{2.23}$$

with $\mathbf{C_1}$ a time invariant matrix and $0 \leq n\Delta t \leq T$. Since $\mathbf{C_1}$ is time invariant we have $\mathbf{U}^n = [\mathbf{C_1}(\Delta t)]^n\mathbf{U}^0$. The matrix $\mathbf{C_1}$ is the *amplification matrix*. Then to determine the stability of the linear system (2.23) we use the result of Richtmyer and Morton, which limits how much a feature of the initial data can be amplified in the numerical procedure. This leads to the following:

Theorem 2.3 *The finite difference approximation (2.23) is stable in a given norm if for some $\gamma > 0$, the infinite set of operators*

$$\begin{aligned} &[\mathbf{C_1}(\Delta t)]^n, \qquad 0 < \Delta t < \gamma, \\ &\qquad\qquad\quad 0 \leq n\Delta t \leq T, \end{aligned} \tag{2.24}$$

is uniformly bounded in that norm ([71], p.45).

We can determine a necessary condition for stability as follows. We let $\lambda_1, \lambda_2, \ldots, \lambda_n$ be the eigenvalues of $\mathbf{C_1}(\Delta t)$ and recall that these are the solutions of the equation

$$\det |\lambda\mathbf{I} - \mathbf{C_1}| = 0. \tag{2.25}$$

The *spectral radius* $\rho(\mathbf{C_1})$ of $\mathbf{C_1}(\Delta t)$ is defined as

$$\rho(\mathbf{C_1}) = \max_j |\lambda_j| . \tag{2.26}$$

Then, following [71], p. 70, we have

$$\rho(\mathbf{C_1})^n \leq \| [\mathbf{C_1}(\Delta t)]^n \| \tag{2.27}$$

Therefore, using Theorem 2.3, a necessary condition for stability in a given norm is that $\rho(\mathbf{C_1})$ be bounded in that norm. This leads to the following condition ([57], p.144):

Theorem 2.4 (von Neumann condition) *A necessary condition for the linear system (2.23) to be stable is that there exists a constant K such that for each of the eigenvalues λ_i of the amplification matrix $\mathbf{C_1}$*

$$|\lambda_i| \leq 1 + K\Delta t. \tag{2.28}$$

Furthermore we find that if $\mathbf{C_1}$ is a normal matrix, then this condition is both necessary and sufficient for stability ([71], p.70).

In practice we must determine how the numerical solution is amplified from one time step to the next before this theory can be applied. To do this we make use of Fourier analysis. We explain this method next in Section 2.2.4.

2.2.4 Fourier analysis

In order to analyse the amplification of the numerical solution in successive time steps we must separate the effects of the space and time discretizations. To do this we apply a Fourier transformation to the system (2.22). This procedure of Fourier analysis, which is also known as the von Neumann method, is a fairly straightforward procedure. However it can only be applied under a restricted set of conditions: that the system being analysed is linear, the matrix $\mathbf{C_0}$ is constant in time and the boundary conditions for the problem are periodic. Under these conditions the method then proceeds as follows. We assume that the numerical solution to the system (2.22) is given by a single Fourier mode of the form

$$\mathbf{U}_j^n = \mathbf{a}_n e^{ikj\Delta x}, \tag{2.29}$$

where k is the wave number and $\mathbf{a}_n$ is constant in space. Then substituting this into the linear system (2.22) we obtain a relationship of the form

$$\mathbf{a}_{n+1} = \hat{\mathbf{C}}_\mathbf{0}(\Delta t, k)\mathbf{a}_n, \tag{2.30}$$

where $\hat{\mathbf{C}}_\mathbf{0}$ is the discrete Fourier transform of the matrix $\mathbf{C_0}$. This is an equation of the form (2.23), with the transformed matrix $\hat{\mathbf{C}}_\mathbf{0}(\Delta t, k)$ being the amplification matrix for each value of the wavenumber k. We see from (2.29) that $\| \mathbf{U}^n \| = \| \mathbf{a}_n \|$. Hence a stability condition for the transformed system (2.30) is equivalent to a stability condition for the original linear system (2.22). Thus we find that under the assumptions required by this technique, a necessary condition for the linear system (2.22) to be stable is that the amplification matrix $\hat{\mathbf{C}}_\mathbf{0}(\Delta t, k)$ satisfy the von Neumann condition for all possible values of the wavenumber k.

Further useful information about the stability of the scheme and its phase error can be found by modifying the above analysis such that we replace the mode (2.29) by the expression

$$\mathbf{U}_j^n = \mathbf{U_0} e^{i(kj\Delta x + \omega n \Delta t)}, \tag{2.31}$$

where $\mathbf{U_0}$ is constant in time and space and ω is complex. Then substituting into (2.22) leads to the matrix equation

$$(e^{i\omega\Delta t}\mathbf{I} - \hat{\mathbf{C}}_\mathbf{0}(\Delta t, k))\mathbf{U_0} = \mathbf{0}, \tag{2.32}$$

where $\mathbf{0}$ is the zero vector. Taking the determinant we obtain the characteristic equation for the matrix $\hat{\mathbf{C}}_\mathbf{0}(\Delta t, k)$, with $e^{i\omega\Delta t}$ being the eigenvalues of $\hat{\mathbf{C}}_\mathbf{0}(\Delta t, k)$. Then, from Theorem 2.4, a necessary condition for stability is that

$$\left| e^{i\omega\Delta t} \right| \leq 1 + O(\Delta t). \tag{2.33}$$

The advantage of this form of analysis is that by splitting ω into its real and imaginary parts we can obtain information on the amplitude and phase of the scheme separately. Following Durran [21], p.91, we write $\omega = \omega_r + i\omega_i$. Then the Fourier mode (2.31) can be written

$$\begin{aligned} \mathbf{U}_j^n &= \mathbf{U_0} e^{-\omega_i n \Delta t} e^{i(kj\Delta x + \omega_r n \Delta t)} && (2.34) \\ &= \left| \mathbf{U}_j^n \right| e^{i(kj\Delta x + \omega_r n \Delta t)}. && (2.35) \end{aligned}$$

Thus the imaginary part of ω determines the amplitude of the solution and so corresponds to the stability analysis of above, with the solution growing for $\omega_i < 0$. On the other hand the real part ω_r gives information about the phase-speed. The expression for ω_r in terms of the other variables is called the *discrete dispersion relation*. Then ω_r is the frequency of the numerical solution and the phase speed is given by $-\omega_r/k$.

The derivation of such a relation allows comparison with an equivalent expression for the analytical system. We consider the linear analytical equations with constant coefficients. Then substituting Fourier modes of the form

$$\mathbf{u}(x,t) = \mathbf{u_0} e^{i(kx+\omega t)}, \tag{2.36}$$

with $\mathbf{u_0}$ constant in space and time, we can derive an expression for the frequency ω in terms of the wave number k. This analytical expression can be compared with the discrete dispersion relation to determine the change in frequency of a given Fourier mode caused by the numerical scheme. Thus this second form of Fourier mode (2.31) provides both a stability analysis and a phase speed analysis.

As noted above, the Fourier method is limited by the fact that it can be applied only to linear constant-coefficient systems. For systems with variable coefficients and nonlinear systems some information can be gained from an analysis of a frozen-coefficient linearized system if the variable coefficients are smooth and well-resolved and the scheme includes some dissipative smoothing ([21], p.147).

Having reviewed the methods available to examine numerical schemes, we now turn our attention to examples of some schemes which we will make use of later in the thesis. We first treat methods for ODE problems in Section 2.3 and then look at methods for PDE problems in Section 2.4.

2.3 Methods for ODE problems

In this section we restrict our attention to the scalar ODE problem

$$\frac{dy}{dt} - f(y,t) = 0, \tag{2.37}$$

with $t \in [0,T]$ and $y(0) = y_0$. We define two types of numerical scheme for use in later chapters, linear multistep methods and Runge-Kutta methods.

Linear multistep methods for the solution of ODE problems do not follow the general form of the scheme (2.2). We treat these methods only briefly in Chapter 4 and so the definition is included here only for completeness. The general *linear k-step method* for solving (2.37) is written (following [44], p.11),

$$\sum_{j=0}^{k} \alpha_j y_{n+j} = \Delta t \sum_{j=0}^{k} \beta_j f_{n+j}, \tag{2.38}$$

where α_j and β_j are constants and $f_n \equiv f(y_n, t_n)$. It is assumed that $\alpha_k \neq 0$ and that α_0 and β_0 are not both zero. Since the coefficients are arbitrary to the extent of a constant multiplier we assume that $\alpha_k = 1$.

These methods achieve high order accuracy by using function values at several steps in a linear scheme. In order to achieve higher order while retaining a one-step scheme it is necessary to allow nonlinearities to be introduced. This is the idea behind Runge-Kutta schemes. Following [44], p.114, we write a general *R-stage Runge-Kutta method* as

$$y_{n+1} - y_n = \Delta t \phi(y_n, t_n, \Delta t), \tag{2.39}$$

where

$$\phi(y_n, t_n, \Delta t) = \sum_{r=1}^{R} c_r k_r, \tag{2.40}$$

with

$$\sum_{r=1}^{R} c_r = 1 \tag{2.41}$$

and the functions k_r defined such that (2.39) satisfies the original differential equation (2.37) to the required order of accuracy. We note that the scheme (2.39) is of the general form of a one-step method (2.2) and so the theory developed in Section 2.1 is applicable to such schemes. The so-called 'classical' Runge-Kutta methods are derived by setting

$$\begin{aligned} k_1 &= f(y_n, t_n), \\ k_r &= f(y_n + \Delta t \sum_{s=1}^{r-1} b_{rs} k_s, t_n + a_r \Delta t), \\ a_r &= \sum_{s=1}^{r-1} b_{rs}, \\ & \quad r = 2, 3, \ldots, R. \end{aligned} \tag{2.42}$$

A scheme with a given order of accuracy can then be designed by the appropriate choice of the coefficients a_r, b_{rs}, c_r. In Chapter 4 we will make use only of the two-stage Runge-Kutta method defined by choosing $b_{21} = 1$ and $c_1 = c_2 = \frac{1}{2}$, giving the scheme

$$\begin{aligned} k_1 &= f(y_n, t_n), \\ k_2 &= f(y_n + \Delta t f(y_n, t_n), t_n + \Delta t), \\ y_{n+1} &= y_n + \frac{\Delta t}{2}(k_1 + k_2). \end{aligned} \tag{2.43}$$

2.4 Methods for PDE problems

When we turn to PDE problems we find a wide selection of schemes available. Many of these are reviewed in [57] for general PDE problems and in [21] specifically for wave equations of geophysical fluid dynamics. Here we only treat the particular numerical schemes which we use in the one-dimensional shallow water model of Chapter 5 and the three-dimensional weather forecasting model of Chapter 6. We introduce the semi-implicit semi-Lagrangian treatment of a forced advection equation. A review

of the use of semi-Lagrangian schemes in atmospheric models is given in [79]. We begin with semi-Lagrangian advection in the context of a passive advection equation and then show how this is extended to treat the forced advection problem.

Following [79] we first illustrate the principle of semi-Lagrangian advection by considering the passive advection equation in one dimension. Thus we have

$$\frac{D\theta}{Dt} \equiv \frac{\partial \theta}{\partial t} + U(x,t)\frac{\partial \theta}{\partial x} = 0, \tag{2.44}$$

where θ is a scalar function being advected and $U(x,t)$ is a given wind field. This system is of the same form as our general PDE problem (2.14). Along the curve

$$\frac{dx}{dt} = U(x,t) \tag{2.45}$$

the scalar θ remains constant. We can consider the set of curves given by (2.45) as the set of trajectories of individual fluid particles. In a fully Lagrangian framework we would follow each of these particles in consecutive time steps. The problem with such a scheme is that an initially regular distribution of particles would soon be distributed irregularly [79]. The semi-Lagrangian method follows trajectories of fluid particles, but on each time step a different set of particles is chosen such that at the end of the time step the particles lie on a regular grid.

A semi-Lagrangian method is usually discretized over two or three time levels. Here we consider only a two-time-level scheme. These have the advantage over three-time-level schemes that they can use twice the time step of a three-time-level scheme to obtain the same order of time accuracy [83]. We illustrate the method with reference to Figure 2.1, which is adapted from Figure 2 of [79]. The general principle is that for each grid point at time level $t_n + \Delta t$ we can trace back the trajectory of a particle arriving at that point by integrating (2.45) backwards from time $t_n + \Delta t$ to time t_n. This is illustrated in Figure 2.1 by the line CA. The value of the scalar θ at point C and time level $t_n + \Delta t$ is then equal to the value of θ at point A at time level t_n. Since point A will not usually lie on a grid point, its value

must be determined by interpolation from surrounding grid points at time t_n. In practice we approximate the exact trajectory of the particle AC by the approximate straight line trajectory $A'C$. This is calculated by assuming a constant velocity U_0 along the trajectory. Then if the point C has x coordinate x_j, the point A' has x coordinate $x_j - U_0\Delta t$. We refer to point C as the *arrival point*, denoted by the subscript a and point A' as the departure point, denoted by the subscript d. Then we approximate (2.44) by

$$\frac{\theta_a^{n+1} - \theta_d^n}{\Delta t} = 0. \tag{2.46}$$

We note that this scheme is of the general one-step form given by (2.17) and so the theory for PDE problems developed in Section 2.2 is applicable to two-time-level semi-Lagrangian schemes.

Two important components of such a scheme are the determination of the advecting velocity U_0 and the interpolation of values at time level t_n to the departure point. The advecting velocity should be an estimate of the velocity at the mid-point of the trajectory at time level $t_n + \Delta t/2$, which corresponds to point B in Figure 2.1. The problem which occurs in real atmospheric models is that the velocity U is itself being advected and so is not known *a priori* at time level t_{n+1}. The solution to this, proposed independently by Temperton and Staniforth [83] and McDonald and Bates [55], is to extrapolate the winds to time level $t_n + \Delta t/2$ using the winds at times t_n and t_{n-1}. The displacement α in Figure 2.1 is computed by solving iteratively

$$\alpha^{(k+1)} = \Delta t U^*(x_j - \frac{\alpha^{(k)}}{2}, t_n + \frac{\Delta t}{2}), \tag{2.47}$$

with

$$U^*(x_i, t_n + \frac{\Delta t}{2}) = \frac{3}{2}U(x_i, t_n) - \frac{1}{2}U(x_i, t_n - \Delta t) \tag{2.48}$$

and

$$\alpha^{(0)} = 0. \tag{2.49}$$

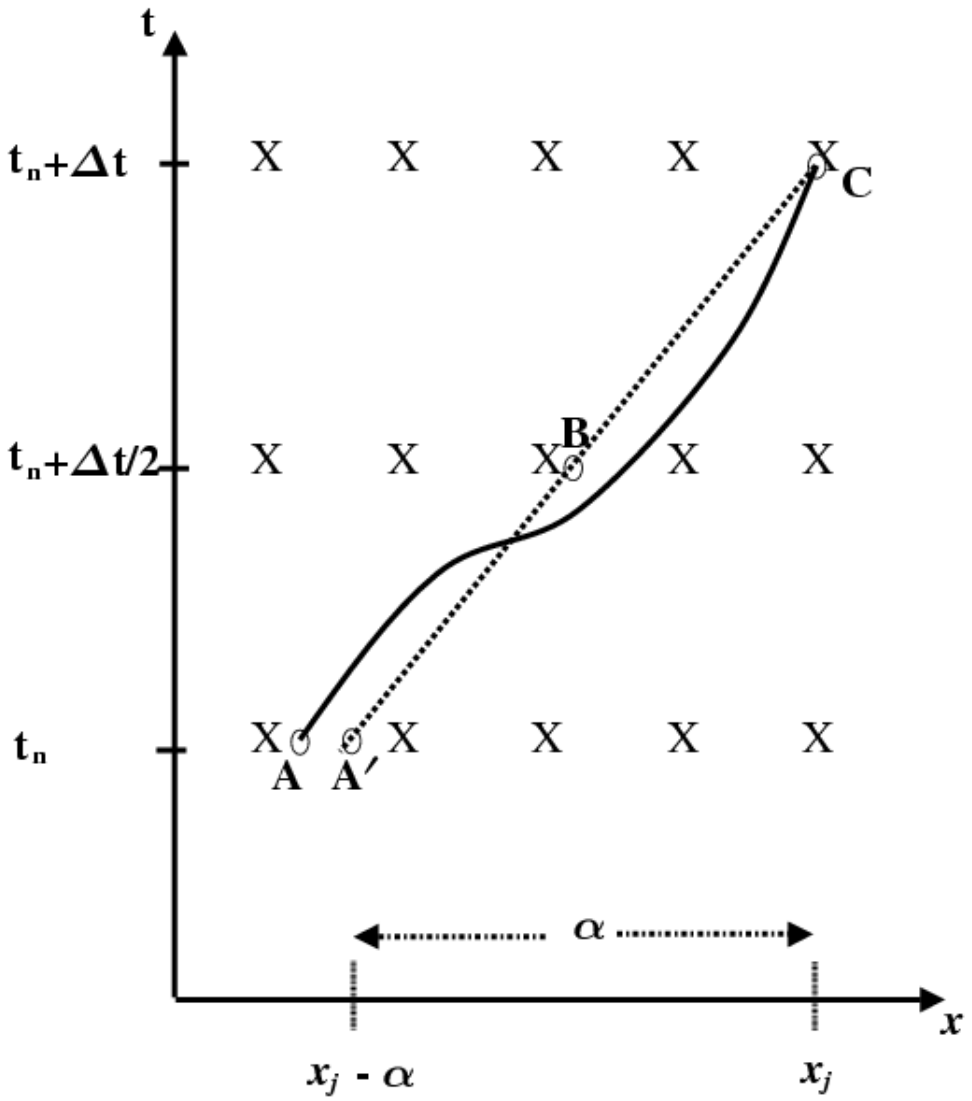

Figure 2.1: A schematic representation of two-time-level semi-Lagrangian advection.

Pudykiewicz et al. [66] proved that this iteration will converge provided that

$$\Delta t \max \left| \frac{\partial U}{\partial x} \right| < 1 \tag{2.50}$$

for this one-dimensional case. We note that the use of this iteration introduces values of the wind at time level $n-1$ into the scheme and so the scheme is not exactly a one-step scheme. However for most purposes of analysis we can consider the determination of the displacement separately and still consider the rest of the scheme as if it were just one-step.

The calculation of U^* requires values to be calculated at points which do not necessarily lie on the grid. Thus an interpolation must be made using values at surrounding grid points. It is sufficient to use a linear interpolation for this step [79]. However, the choice of interpolation scheme to interpolate values of θ to the departure point is more important. A comparison of the properties of various polynomial interpolations is contained in [53]. It is found that linear interpolation for this step has too large a damping. Cubic interpolation is often used as the best compromise between accuracy and computational cost [79].

The main advantage of semi-Lagrangian schemes is that the stability of such schemes is not restricted by the CFL condition and so the maximum time step depends only on the convergence criterion (2.50). For a three-dimensional atmospheric model Pudykiewicz et al. [66] conclude that the maximum permitted time step is of the order of approximately 3 hours. This is much larger than can be used in an Eulerian scheme. Whereas the time step of an Eulerian model must be chosen according to stability considerations, the semi-Lagrangian method thus allows the time step to be chosen on the basis of accuracy considerations. However, in order to obtain the benefit from using larger time steps, it is important that the iteration (2.47) be solved to at least $O(\Delta t^2)$ accuracy in order to avoid degrading the accuracy of the scheme as a whole [54]. Two iterations of this displacement calculation are found to be sufficient to achieve this [79].

The potential benefits of semi-Lagrangian schemes have led many operational weather forecasting centres to move towards the implementation of such schemes in recent years. The operational models at the European Centre for Medium-range Weather Forecasting and the Canadian Meteorological Centre both use such schemes in their models [37], [16] and the Met Office is moving towards implementing such a scheme [18]. However, in order to use a larger time step it is necessary to combine a semi-Lagrangian treatment of advection with a semi-implicit treatment of terms responsible for gravity waves, so that the speed of the gravity waves does not itself determine the stability criterion of the scheme.

To illustrate how this is done we consider the forced advection of a scalar θ in one dimension

$$\frac{\partial \theta}{\partial t} + U(x,t)\frac{\partial \theta}{\partial x} + G(\theta, x, t) = 0. \tag{2.51}$$

Then following the scheme of [83] we can discretize (2.51) as

$$\frac{\theta_a^{n+1} - \theta_d^n}{\Delta t} + \frac{1}{2}G_d^n + \frac{1}{2}G_a^{n+1} = 0. \tag{2.52}$$

Again the particular problem (2.51) is an example of the general problem (2.14) and the scheme (2.52) can be rearranged to be a one-step scheme of the general form (2.17) and so the definitions of Section 2.2 apply. The scheme is second order accurate in time and is unconditionally stable for the linearized equations [83]. However, Rivest et al. [74] showed that the scheme allows a spurious orographic resonance. To avoid this they propose a first order and a second order off-centering of the implicit part of the scheme. The first order version is typically used, which discretizes (2.51) with the scheme

$$\frac{\theta_a^{n+1} - \theta_d^n}{\Delta t} + (1-\alpha)G_d^n + \alpha G_a^{n+1} = 0, \tag{2.53}$$

with $\alpha \in [0.5, 1]$. When $\alpha = 0.5$ we have the original scheme (2.52) and $\alpha = 1$ gives a fully implicit time updating. For values of α not equal to 0.5 the scheme is first order accurate in time, but it is close to second order for α close to 0.5.

In later chapters we look at the linearizations of models using the schemes introduced in this section. First we review some of the work which has already been published on linear models.

Chapter 3

Development and testing of linear models

In the previous chapter we introduced some concepts of numerical analysis and also some of the numerical schemes that we wish to use in this thesis. The theory of numerical analysis can be used not only to study the nonlinear model, but also to compare the linear models formed by the discrete method (the tangent linear model) and the semi-continuous method (the perturbation forecast model). The definitions of the previous chapter allow us to assess the properties of these discrete models and also compare them with the linear continuous system. In the present chapter we consider work directly concerned with the development and testing of linear models. We begin in Section 3.1 by looking at an alternative way in which tangent linear models have been assessed, by comparison with the discrete nonlinear model. Then, in Section 3.2, we review some previous studies which have looked at the properties of linear models. Finally, in Section 3.3, we propose a new method for evaluating a perturbation forecast model.

3.1 Comparison with discrete nonlinear model

3.1.1 Theory

In the meteorological literature the usual method of testing a tangent linear model follows that of Rabier and Courtier [67], which compares the evolution of a perturbation in the discrete linear model with the evolution of the same perturbation in the discrete nonlinear model. The method is based on a Taylor series expansion of the solution operator of the discrete nonlinear model. We illustrate the method with respect to a PDE initial value problem, but the following can easily be adapted for the ODE case.

We consider a general numerical scheme of the same form as equation (2.17)

$$\mathbf{U}^{n+1} - \boldsymbol{\mathcal{G}}^n(\mathbf{U}^n, \Delta x, \Delta t) = 0 \tag{3.1}$$

with $n\Delta t \in [0, T]$ and $\mathbf{U^0}$ given. Let the Jacobian of $\boldsymbol{\mathcal{G}}^n$ with respect to the model state vector evaluated at $\mathbf{U}^n$ be written

$$\left.\frac{\partial \boldsymbol{\mathcal{G}}^n}{\partial \mathbf{U}}\right|_{\mathbf{U}^n}. \tag{3.2}$$

We define $\boldsymbol{S}(t_n, t_0, \mathbf{U^0})$ to be the solution operator which maps an initial state $\mathbf{U^0}$ to a state $\mathbf{U}^n$ at time level n, so that

$$\mathbf{U}^n = \boldsymbol{S}(t_n, t_0, \mathbf{U^0}) \tag{3.3}$$

with

$$\boldsymbol{S}(t_n, t_0, \mathbf{U^0}) = \boldsymbol{\mathcal{G}}^{n-1}(\boldsymbol{\mathcal{G}}^{n-2}(\ldots(\boldsymbol{\mathcal{G}}^0(\mathbf{U^0}, \Delta x, \Delta t))\ldots)). \tag{3.4}$$

Now suppose that to the initial state $\mathbf{U^0}$ of the model we apply a small perturbation $\alpha\boldsymbol{\delta}\mathbf{U^0}$, where $\boldsymbol{\delta}\mathbf{U^0}$ controls the shape of the perturbation and α is a scalar parameter which controls its magnitude. We can run the discrete nonlinear model starting from the unperturbed state $\mathbf{U^0}$ and then again from the perturbed state

$\mathbf{U^0} + \alpha\boldsymbol{\delta}\mathbf{U^0}$. Then at any time t_n the difference between the two model runs is the perturbation $\boldsymbol{N}^n[\alpha\boldsymbol{\delta}\mathbf{U^0}]$ evolved in the nonlinear model, given by

$$\boldsymbol{N}^n[\alpha\boldsymbol{\delta}\mathbf{U^0}] = \boldsymbol{S}(t_n, t_0, \mathbf{U^0} + \alpha\delta\mathbf{U^0}) - \boldsymbol{S}(t_n, t_0, \mathbf{U^0}). \tag{3.5}$$

By a Taylor series expansion of $\boldsymbol{S}$ in (3.5) we have

$$\boldsymbol{N}^n[\alpha\boldsymbol{\delta}\mathbf{U^0}] = \frac{\partial \boldsymbol{S}(t_n, t_0, \mathbf{U^0})}{\partial \mathbf{U^0}}\alpha\boldsymbol{\delta}\mathbf{U^0} + O(\alpha^2) \tag{3.6}$$

where the Jacobian $\partial\boldsymbol{S}(t_n, t_0, \mathbf{U^0})/\partial\mathbf{U}$ is calculated along the time-evolving trajectory defined by $\boldsymbol{S}(t_n, t_0, \mathbf{U^0})$. We apply the chain rule to (3.4) to obtain

$$\frac{\partial \boldsymbol{S}(t_n, t_0, \mathbf{U^0})}{\partial \mathbf{U^0}} = \frac{\partial \boldsymbol{\mathcal{G}}^{n-1}}{\partial \boldsymbol{\mathcal{G}}^{n-2}}\frac{\partial \boldsymbol{\mathcal{G}}^{n-2}}{\partial \boldsymbol{\mathcal{G}}^{n-3}}\cdots\frac{\partial \boldsymbol{\mathcal{G}}^{1}}{\partial \boldsymbol{\mathcal{G}}^{0}}\frac{\partial \boldsymbol{\mathcal{G}}^{0}}{\partial \mathbf{U^0}} \tag{3.7}$$

$$= \prod_{k=0}^{n-1}\left.\frac{\partial \boldsymbol{\mathcal{G}}^{k}}{\partial \mathbf{U}}\right|_{\mathbf{U^k}}. \tag{3.8}$$

using (3.2). Then substituting into (3.6) and defining the operator

$$\mathbf{G}(t_n, t_0) = \prod_{k=0}^{n-1}\left.\frac{\partial \boldsymbol{\mathcal{G}}^{k}}{\partial \mathbf{U}}\right|_{\mathbf{U^k}} \tag{3.9}$$

we have

$$\boldsymbol{N}^n[\alpha\boldsymbol{\delta}\mathbf{U^0}] = \mathbf{G}(t_n, t_0)\alpha\boldsymbol{\delta}\mathbf{U^0} + O(\alpha^2). \tag{3.10}$$

We note that the operator $\mathbf{G}(t_n, t_0)$ has been derived by a differentiation of each step of the discrete nonlinear model. Hence this is the solution operator of the linear model derived by linearizing the discrete nonlinear model. In other words, (3.9) defines the tangent linear model. Thus (3.10) tells us that to first order in α the solution of the tangent linear model applied to $\alpha\delta\mathbf{U^0}$ is equal to the perturbation $\boldsymbol{N}^n[\alpha\boldsymbol{\delta}\mathbf{U^0}]$ calculated from the two runs of the nonlinear model.

This relationship is used as a standard test of a tangent linear model. An initial model state $\mathbf{U^0}$ and perturbation $\boldsymbol{\delta}\mathbf{U^0}$ are generated and the nonlinear model run from the states $\mathbf{U^0}$ and $\mathbf{U^0} + \alpha\boldsymbol{\delta}\mathbf{U^0}$. The difference between these two runs at any time can be compared with the output of the tangent linear model, linearized around

the state defined by the trajectory $\boldsymbol{S}(t_n, t_0, \mathbf{U^0})$ and acting on the perturbation $\alpha\boldsymbol{\delta}\mathbf{U^0}$. Such a comparison enables us to understand how well the tangent linear model represents the true evolution of a perturbation in the discrete nonlinear model. The trajectory around which the tangent linear model is linearized is referred to as the *linearization state*. An important component of these experiments is the choice of the initial $\mathbf{U^0}$ used to generate this linearization state and of the initial perturbation $\alpha\boldsymbol{\delta}\mathbf{U^0}$. However, since these will depend on which particular model we are using, we leave discussion of this to the sections on numerical experiments in later chapters.

Within this thesis we wish to apply this test not only to the tangent linear model, but also to the linear model formed by discretizing the continuous linear equations, the perturbation forecast model. Thus we introduce the notation $\mathbf{L}(t_n, t_0)$ to mean the solution operator of a linear model formed by either discretizing first and then linearizing, or linearizing first and then discretizing. In the case where we linearize the discrete nonlinear model we have the tangent linear model and so usually $\mathbf{L}(t_n, t_0) = \mathbf{G}(t_n, t_0)$. For the perturbation forecast model we have a different linear operator $\mathbf{L}(t_n, t_0) = \mathbf{P}(t_n, t_0)$ and in general

$$\mathbf{P}(t_n, t_0) = \mathbf{G}(t_n, t_0) + \mathbf{R}(t_n, t_0) \tag{3.11}$$

where $\mathbf{R}(t_n, t_0)$ is a non-zero linear operator. We use the notation $(\boldsymbol{\delta}\mathbf{U^n})^L$ to represent the perturbation evolved in the linear model, and so

$$(\boldsymbol{\delta}\mathbf{U^n})^L = \mathbf{L}(t_n, t_0)\boldsymbol{\delta}\mathbf{U^0}. \tag{3.12}$$

The linear models are assumed to be linearized around a state which satisfies the discrete nonlinear system.

Before comparing a perturbation evolution in the nonlinear and linear models in the way we have described it is important to have clear the purpose of the test. For this we make use of the concepts of correctness and validity introduced by Polavarapu et al. [65]. We first define the *linearization error*:

Definition 3.1 *The linearization error* $\mathbf{E}^n$ *at time* t_n *is the difference between the nonlinear and linear variations. Thus*

$$\mathbf{E}^n = \boldsymbol{\mathcal{N}}^n[\alpha\boldsymbol{\delta}\mathbf{U}^{\mathbf{0}}] - \mathbf{L}(t_n, t_0)\alpha\boldsymbol{\delta}\mathbf{U}^{\mathbf{0}}. \tag{3.13}$$

Then the concept of correctness refers to whether the linear model represents the linear part of the nonlinear evolution. This is an objective property of a given discrete model and does not depend on the particular linearization state or initial perturbation. Thus following [65] we have

Definition 3.2 *The linear model* $\mathbf{L}(t_n, t_0)$ *is correct for any time* t_n *if*

$$\mathbf{L}(t_n, t_0) = \prod_{k=0}^{n-1} \left. \frac{\partial \boldsymbol{\mathcal{G}}^k}{\partial \mathbf{U}} \right|_{\mathbf{U}^k}. \tag{3.14}$$

Thus a correct linear model differs from the nonlinear model only in terms which are second order or higher. This allows us to formulate a necessary and sufficient condition for correctness as follows:

Lemma 3.1 *The linear model* $\mathbf{L}(t_n, t_0)$ *is correct if and only if for all initial perturbation directions* $\boldsymbol{\delta}\mathbf{U}^{\mathbf{0}}$

$$\lim_{\alpha \to 0} \frac{\| \mathbf{E}^n \|}{|\alpha|} = 0. \tag{3.15}$$

However we note that although Lemma 3.1 allows us to test for correctness by considering the limit of small perturbations, the concept of correctness is not itself dependent on the perturbation size.

Validity on the other hand is a more subjective property, since it is a judgement as to how well the linear variation approximates the nonlinear variation. This depends on the particular value of the linearization state and perturbation being used. The judgement as to whether a linear model is valid in a given situation will also depend somewhat on the application for which the model is required. We use the concepts of [65] to define validity as follows:

Definition 3.3 *The linear model* $\mathbf{L}(t_n, t_0)$ *is valid at time* t_n *for a given background trajectory* $\boldsymbol{S}(t_n, t_0, \mathbf{U^0})$ *and initial perturbation* $\alpha\boldsymbol{\delta}\mathbf{U^0}$ *if*

$$\| \mathbf{E}^n \| \ll \| (\alpha\boldsymbol{\delta}\mathbf{U^n})^L \| . \tag{3.16}$$

More discussion of the choice of norm is made in Section 3.1.2. This definition is equivalent to the requirement that the true nonlinear evolution of a given finite perturbation be dominated by the part of the evolution predicted by the linear model.

For the purpose of comparing the two different methods for deriving the linear model, we note that in general only the tangent linear model will be correct according to Definition 3.2 of correctness. However, since for most applications we are concerned with predicting the evolution of a finite perturbation in a given situation, it is the validity of the linear model which is most of interest. In the following chapters therefore we concern ourselves more with comparing the validity of the tangent linear and perturbation forecast models, though some discussion of correctness will be made. We now consider some of the ways in which correctness and validity can be determined in practice.

3.1.2 Quantifying the error

Using the above notation we have from the linear model at time level n the vector of perturbations $(\boldsymbol{\delta}\mathbf{U^n})^L$ and from the nonlinear difference the vector of perturbations $\boldsymbol{N}^n[\alpha\boldsymbol{\delta}\mathbf{U^0}]$. In order to compare these we must define some way of measuring the difference between them. We describe various methods for measuring this difference proposed in the literature. Rabier and Courtier [67] measure the difference between the nonlinear and linear perturbations relative to the size of the linear perturbation. They define the *relative error* E_R which compares the error in the linear evolution with the size of the linear perturbation. Thus they define

$$E_R = 100 \frac{\| \boldsymbol{N}^n[\alpha\boldsymbol{\delta}\mathbf{U^0}] - \mathbf{L}(t_n, t_0)[\alpha\boldsymbol{\delta}\mathbf{U^0}] \|}{\| \mathbf{L}(t_n, t_0)[\alpha\boldsymbol{\delta}\mathbf{U^0}] \|}, \tag{3.17}$$

where $\| \, . \, \|$ is a given norm. We look more closely at the choice of norm later. For the moment we note that the relative error can be used to test both the correctness and validity of the linear model. The correctness of a tangent linear model can be proved by showing that this error measure reduces to zero as the perturbation size α decreases. This method was used by Li et al. [50], who tested their linear model by changing α logarithmically, that is by putting $\alpha = 10^{-p}$, where p is an integer. For a tangent linear model, which we usually expect to be correct according to Definition 3.2, this test is a useful way of proving that the tangent linear model has been correctly coded. However, for a perturbation forecast model we find that the relative error does not tend exactly to zero, but to a non-zero constant dependent on the linearization state. In order to understand the reason for this we note with reference to (3.10) and (3.11) that for the perturbation forecast model

$$\boldsymbol{N}^n[\alpha\boldsymbol{\delta}\mathbf{U^0}] - \mathbf{L}(t_n, t_0)[\alpha\boldsymbol{\delta}\mathbf{U^0}] = -\mathbf{R}(t_n, t_0)[\alpha\boldsymbol{\delta}\mathbf{U^0}] + O(\alpha^2). \tag{3.18}$$

Hence from (3.17) we have

$$E_R = \frac{\| \, \mathbf{R}(t_n, t_0)[\alpha\boldsymbol{\delta}\mathbf{U^0}] + O(\alpha^2) \, \|}{\| \, \mathbf{P}(t_n, t_0)[\alpha\boldsymbol{\delta}\mathbf{U^0}] \, \|}. \tag{3.19}$$

Thus we see that as $\alpha \to 0$, E_R will not itself tend to zero, but will tend to a value given by

$$\frac{\| \, \mathbf{R}(t_n, t_0) \, \|}{\| \, \mathbf{P}(t_n, t_0) \, \|}, \tag{3.20}$$

which will be constant for a given value of t_n. This presents a problem for testing a perturbation forecast model, since we do not have the same objective test as we have for a tangent linear model. In Section 3.3 we propose a different method for assessing the error of a perturbation forecast model.

Despite this problem, the relative error is still useful for assessing both linear models when we consider a finite perturbation. For a tangent linear model known to be correct the relative error is a measure of the validity in a given situation. When the relative error is low it indicates that the evolution in the nonlinear model

is reasonably linear and so the tangent linear approximation is valid. A high relative error on the other hand indicates that nonlinear effects are having a big influence on the evolution. For the perturbation forecast model the relative error is dependent on a combination of the nonlinearity of the evolution and the closeness of the discrete scheme to the tangent linear model. For a given situation it gives information as to how well the linear model approximates the nonlinear evolution, taking into account both of these effects.

As we have already mentioned, an important component of this measure is the definition of the norm. In [67] Rabier and Courtier choose an energy based norm. Such a norm has the advantage of being physically and mathematically meaningful, since it is weighted by the grid box area and so the discrete norm converges to the corresponding continuous norm as the grid size is reduced. In this way we do not give too much weight to polar points on a regular latitude-longitude grid. However, when we are testing a model for correctness (or near correctness for a perturbation forecast model) it may be more desirable to give equal weight to all grid points, to ensure that any problems near the poles show up immediately. In this case the root mean square (rms) value may be a more useful norm. This norm is defined for a vector $\mathbf{x} = \{x_j\}$ of length N by the formula

$$rms(\mathbf{x}) = \left(\frac{1}{N} \sum_{i=1}^{N} x_i^2 \right)^{\frac{1}{2}}. \tag{3.21}$$

The root mean square norm is simply the l_2 norm (2.6) scaled by the square root of the length of the vector. We note that in spherical geometry this norm does not converge to a continuous norm as the grid size is reduced. Vukićević and Bao [88] use this norm for their experiments. They measure the total error with respect to the size of the nonlinear perturbation rather than the linear perturbation, defining the *solution error* E_S by

$$E_S = 100 \frac{rms(\boldsymbol{N}^n[\alpha \boldsymbol{\delta} \mathbf{U_0}] - \mathbf{L}(t_n, t_0)[\alpha \boldsymbol{\delta} \mathbf{U_0}])}{rms(\boldsymbol{N}^n[\alpha \boldsymbol{\delta} \mathbf{U_0}])}. \tag{3.22}$$

A final measure of the difference between the linear and nonlinear perturbations is the correlation coefficient, used for example by Errico et al. [28]. If we have two vectors of length N, $\mathbf{x} = \{x_j\}$ and $\mathbf{y} = \{y_j\}$, then we define the correlation coefficient $C[\mathbf{x}, \mathbf{y}]$ between $\mathbf{x}$ and $\mathbf{y}$ by

$$C[\mathbf{x}, \mathbf{y}] = \frac{\sum_{i=1}^{N}(x_i - \bar{x})(y_i - \bar{y})}{\left(\sum_{i=1}^{N}(x_i - \bar{x})^2 \sum_{i=1}^{N}(y_i - \bar{y})^2\right)^{\frac{1}{2}}}, \tag{3.23}$$

where

$$\begin{aligned} \bar{x} &= \frac{1}{N}\sum_{i=1}^{N} x_i, \\ \bar{y} &= \frac{1}{N}\sum_{i=1}^{N} y_i. \end{aligned} \tag{3.24}$$

A value of $C[\mathbf{x}, \mathbf{y}]$ close to unity indicates a good agreement between $\mathbf{x}$ and $\mathbf{y}$. However, the authors of [28] note that

> "The correlation measure of the accuracy tends to suggest closer agreement between figures than some other measures do."

This effect can be seen in a study by Li et al. [50], who calculate correlations of greater than 0.9 even when the relative error exceeds 40%.

A closer examination of the correlation measure shows that it is dominated by errors in phase between the linear and nonlinear perturbations and, unlike the other error measures discussed, is not sensitive to a pure amplitude error. We illustrate this using an idealised nonlinear perturbation in a one-dimensional advection problem with 10 data points, as shown in Figure 3.1. We consider two scenarios, Case I in which the linear perturbation has only an amplitude error (Figure 3.2) and Case II in which the linear perturbation has only a phase error (Figure 3.3). The linearization errors for these experiments as defined by Definition 3.1 are shown in Figures 3.4 and 3.5 respectively. Table 3.1 shows the correlation, the relative error and the solution error for these two cases.

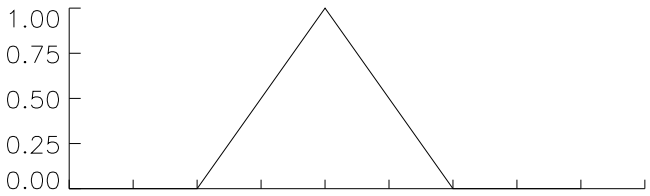

Figure 3.1: Nonlinear perturbation.

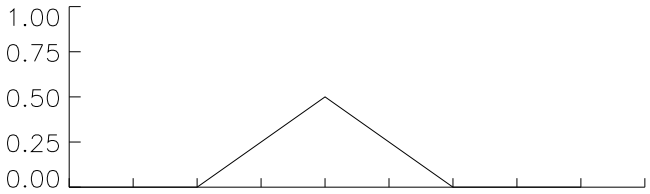

Figure 3.2: Linear perturbation with amplitude error.

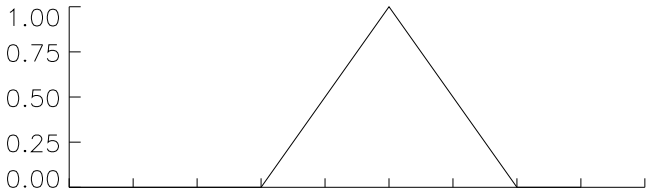

Figure 3.3: Linear perturbation with phase error.

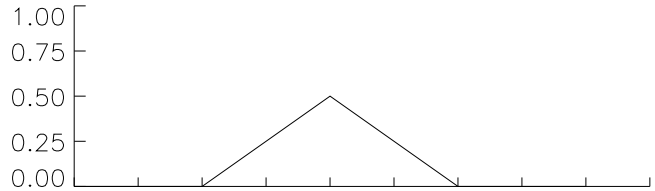

Figure 3.4: Linearization error for perturbation of Figure 3.2

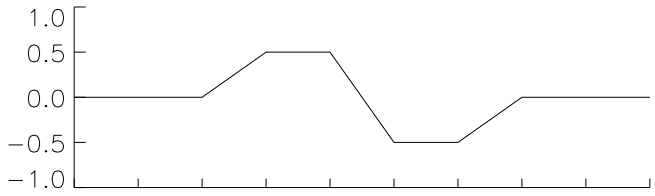

Figure 3.5: Linearization error for perturbation of Figure 3.3

	Case I	Case II
Correlation	1.0	0.54
E_R	100%	82%
E_S	50%	82%

Table 3.1: Comparison of different error measures for amplitude and phase errors.

From this simple example we see that if the linear and nonlinear perturbations are exactly in phase (Case I) then the correlation measure shows a perfect correlation, even if there is a large amplitude difference between the perturbations. For this reason it is important to quote some measure of the perturbation amplitudes whenever the correlation measure is used alone. The relative error and solution error on the other hand are sensitive to both amplitude and phase errors. When only a phase error is present so that the nonlinear and linear perturbations have the same amplitude, we have $\| \boldsymbol{N}[\alpha\boldsymbol{\delta}\mathbf{U^0}] \| = \| \mathbf{L}(t_n,t_0)[\alpha\boldsymbol{\delta}\mathbf{U^0}] \|$ and we find that the relative error and solution error have the same value. We note that the relative size of the relative error and solution error is given by the ratio

$$\frac{E_R}{E_S} = \frac{\| \boldsymbol{N}[\alpha\boldsymbol{\delta}\mathbf{U^0}] \|}{\| \mathbf{L}(t_n,t_0)[\alpha\boldsymbol{\delta}\mathbf{U^0}] \|}, \tag{3.25}$$

which is independent of the magnitude of the linearization error $\| \mathbf{E}^n \|$. Thus the actual values of the different error measures depend not only on the linearization error, but also on the magnitudes of the linear or nonlinear perturbations.

It is clear from this analysis that no single measure can be relied on to tell the whole story. In order to assess the validity of linear models for different perturbations in different situations it will be necessary to consider different measures, with an understanding of the limitations of each. It must also be recognized that all the measures discussed in this section are calculated as norms over a whole field or a given area of a field and do not differentiate between large and small scales. For the application of incremental 4D-Var we wish to ensure that the linear model is

valid primarily for perturbations of meteorological significance and so a subjective assessment of the perturbation fields is also useful.

So far we have seen essentially two different methods of examining the properties of linear models, the techniques of numerical analysis discussed in Chapter 2 and the method of comparison with the discrete nonlinear model discussed in this section. In Section 3.3 we propose a new method which we have designed specifically for perturbation forecast models. First however we review some studies of linear models already published.

3.2 A review of studies of linear models

There is very little published work which looks at the specific question of the comparative properties of the linear model generated by first discretizing and then linearizing (the tangent linear model, or TLM) and that generated by first linearizing and then discretizing (the perturbation forecast model, or PFM). The question was looked at in the context of an ordinary differential equation problem by Ortega and Rheinboldt [61]. Using the theory of functional analysis they showed that for a class of discretization operators satisfying a compatability condition, the TLM and PFM were equivalent. This work was extended by Krishna [43] who, noting that the compatability condition of [61] was difficult to verify in practice, developed a theory to show the equivalence of the TLM and PFM without verification of this condition. However, it is observed that the theory does not apply to some commonly used difference schemes, such as Runge-Kutta methods. We shall look in more detail at an example of a Runge-Kutta scheme in Chapter 4.

Other work in this area has concentrated either on the properties of tangent linear models, or on a comparison of the adjoint models formed by the continuous method and the discrete method (Methods 1 and 2 of Figure 1.1). This work on adjoint models is also useful to review here, since the accuracy of the adjoint model

is inherently linked to that of the linear model [28]. In fact the tangent linear model could be found by taking the adjoint of the adjoint model formed by the continuous method. We first look at the work which has concentrated solely on the tangent linear model.

Studies of the properties of the direct linearization of a discrete nonlinear model have been made within meteorology and within the more general field of automatic differentiation (AD), but surprisingly the interaction between the two has been very limited. Certainly meteorologists have made use of the techniques of AD in deriving linear and adjoint models (e.g. [14], [93]), but little reference is made to the theoretical results of AD in the meteorological literature. A particular example of this is the study of the linearization of iterative processes. These are important in meteorological models, particularly when semi-implicit semi-Lagrangian schemes are used. These schemes contain iterative processes within the departure point calculation of the semi-Lagrangian scheme and in the solution of the elliptic pressure equation which arises from the implicitly treated terms. Within the meteorological literature the problem of linearizing such processes has been studied by Polavarapu and Tanguay [64]. They examine the direct linearization of each step of a fixed-point iterative procedure and also an approximation to this which does not vary the linearization state from iteration to iteration. They establish that the direct linearization converges more slowly than the nonlinear reference iteration. This problem has also been looked at in detail within the field of AD and studies therein have looked at the theoretical properties of some simplifications [35], [4].

Another area of difficulty which has been studied in the context of meteorological tangent linear models is the treatment of interpolation, which is an important part of semi-Lagrangian schemes. As we saw in our review of such schemes in Section 2.4, the values of a field at the departure point must be found by interpolation from the values at surrounding grid points. In order to calculate which are the nearest grid points it is necessary to calculate the nearest integer value to the departure

point displacement from the coordinate origin. In Fortran this is provided by the intrinsic function INT. However, this process is non-differentiable and so may lead to problems if the departure point of the perturbed trajectory lies in a different grid interval from the background trajectory. Polavarapu et al. [65] examined the linearization of various piecewise-continuous interpolation schemes in this context for correctness, as defined by Definition 3.2. They found that assuming infinitesimal perturbations it is necessary that the first derivative of the interpolating functions be continuous in order to ensure the correctness of the tangent linear model. This implies that if the perturbed departure point lies in a grid interval adjacent to that of the linearization state departure point, then the first derivatives of the interpolation function used in each interval must be equal at the grid point in between. If the perturbations are assumed to be finite then this continuity of the first derivative is no longer sufficient to ensure correctness. In a later study of the effect of such errors in the tangent linear model it was shown that the errors can amplify in time. However, for a realistic wind field it was found not to be a problem [81].

The problem of treating non-differentiable processes when developing a tangent linear model has also been looked at in the context of the parametrization of sub-grid scale processes within numerical weather prediction models. The modelling of processes such as convection (intended in the meteorological sense as a thermally-induced circulation) includes many discontinuous operators, for example on-off switches, which cause difficulties for the linearization. There have been two approaches to coping with this problem. One is to assume that the switches are not sensitive to changes in the initial conditions (e.g. [3], [92]) and so the tangent linear and adjoint models follow the same path through the code as the nonlinear integration. In the context of 4D-Var in its full, non-incremental form, this gives errors in the gradient required for the minimization. Vukićević and Bao [88] showed that linearization errors caused by treating convective processes in this way could lead to slower convergence and consequently locally bad 4D-Var data assimilation results in

the areas where the linearization error was highest. However they conclude that in practice this problem was unlikely to cause errors larger than those associated with other approximations within the data assimilation system.

A second method of treating the problem of discontinuous processes within physical parametrizations is to redesign the nonlinear schemes such that these discontinuities do not occur ([2], [94], [90]). At ECMWF and Meteo-France this path has been pursued and a simplified set of nonlinear physical parametrizations has been developed for use in the incremental 4D-Var scheme [41]. They have been designed in such a way that their linearizations and adjoints are straightforward to obtain. However, the original physical parametrizations are used in the calculation of the nonlinear trajectory.

At this point we highlight one of the benefits of the semi-continuous approach to forming the linear model. Since we work from the continuous linear equations, we have no need to linearize discrete schemes and so the problems highlighted in this section do not arise. We see this more clearly in an example of a one-dimensional shallow water system in Chapter 5, where we develop a model including some of the difficulties discussed here.

It is also important to consider the stability of the linear models. We have previously shown that the tangent linear model may become unstable for time steps at which the perturbation forecast model is still stable [46]. Further details of this study are given in Chapter 4. More recently it has been demonstrated that in the context of a diffusion problem the linearization of a discrete nonlinear model which is unconditionally stable may lead to a tangent linear model which is only conditionally stable [91]. Hence for large enough time steps the tangent linear model may become unstable, even if the nonlinear model is stable. This is possible even when the underlying continuous problem is stable. Thus it is important to understand well the stability properties of the linear model. We intend to demonstrate in the forthcoming chapters that this is most easily done by following the semi-continuous method to

derive a perturbation forecast model, rather than linearizing the discrete numerical schemes.

In the published studies on adjoint models, there have been various comparisons made of the adjoint model formed by the continuous and the discrete methods, but no work on the adjoint model formed by the semi-continuous method. Although the continuous method is not of great interest for the application of incremental 4D-Var, since it does not provide a discrete linear model directly, some of the results of these studies are relevant to the present argument and so we review these here.

One important area which has been studied is the adjoints of advection schemes. Sirkes and Tziperman [76] demonstrated that the adjoint of a leapfrog scheme formed using the discrete method shows a sensitivity to a computational mode which does not appear when the adjoint is formed by the continuous method. This occurs because the adjoint formed by the discrete method gives a sensitivity with respect to the discrete numerical model, of which the leapfrog computational mode is an important component. On the other hand, the adjoint formed by the continuous method approximates a sensitivity with respect to the continuous system. Although the authors conclude that both adjoints are valid if only a gradient at the initial time is needed, as is true for incremental 4D-Var, they do state that this is symptomatic of a wider problem of ensuring the stability of an adjoint model.

More recently Thuburn and Haine [87] investigated the adjoints of nonoscillatory advection schemes. Such schemes, in order to be monotone and better than first-order accurate, are necessarily nonlinear. The authors show that for a large class of such schemes the sensitivities calculated using the discrete adjoint do not agree with those calculated from a direct perturbation of the forward model. Moreover they prove that the discontinuities in the advection schemes cannot be smoothed out in some way to prevent this without sacrificing some desirable properties of the schemes.

A comparison of the continuous and discrete approaches to adjoints in the context

of aeronautical design is made by Giles and Pierce [33]. They comment that while the continuous approach has the advantage that the physical significance of the adjoint variables and the role of the boundary conditions is clearer, the discrete approach is more conceptually straightforward and allows the exact gradient of the discrete cost function to be obtained. However they conclude that for the moment there is no clear evidence as to which is the best method to follow and both methods seem to perform well in practice. Similar results are reported by Nadarajah and Jameson [59], who study this problem for the Euler equations in aerodynamic design. For their particular optimization problem they show that the difference between the gradients calculated from the continuous and discrete methods becomes smaller as the mesh is made finer, but the adjoint formed by the discrete method is computationally more expensive. To some extent the choice of method used will depend on the problem being solved. For example, Anderson and Ventkatakrishnan [1] look at a problem of aerodynamic design on unstructured grids. For their case the continuous approach is found not to be suitable, since for example it does not provide sensitivities due to the grid, which in their problem are essential to obtain accurate derivatives.

It is clear from the work reviewed here that whether we need only an adjoint model or whether we need the discrete linear model as well, both the continuous method and the discrete method have their difficulties. The question we now wish to answer is: *Can the semi-continuous method provide us with a linear model which is as accurate as the tangent linear model formed by the discrete method while avoiding some of the problems associated with linearizing discrete numerical models?* It is this question which we examine in the remainder of the thesis. The adjoint model formed from the semi-continuous method will not be discussed. One important part of this question is to decide what we mean by an accurate linear model. The concepts of numerical analysis from Chapter 2 and the comparison with the discrete nonlinear model as described in Section 3.1 both provide methods of assessing the accuracy of a linear model. However, we saw in Section 3.1 that the test described there favours

the linear model formed by linearizing the discrete scheme, the tangent linear model. We now propose a new method designed to evaluate the accuracy of a perturbation forecast model.

3.3 Comparison with estimated tangent linear model error

One of the difficulties in testing a perturbation forecast model which we referred to in Section 3.1.2 is the fact that the linearization error does not tend to zero as a perturbation becomes infinitesimally small. For experiments with finite size perturbations it would be useful to know how much of the linearization error we do see is due to nonlinear effects and how much is due to the fact of using a perturbation forecast model instead of a tangent linear model. In this section we develop a new method of assessing this, which uses the nonlinear model to estimate the linearization error that we would obtain if we had a tangent linear model. This can then be compared with the actual linearization error from the perturbation forecast model.

We consider our discrete nonlinear model to be of the form (3.3). In order to derive our formula for the estimate of the linearization error we first need to expand the nonlinear model using a Taylor series. To do this we follow [67]. We assume that the vector $\mathbf{U}$ is represented by p components U_l and that the model $\boldsymbol{S}$ is represented by p scalar components S_l with $l = 1, \ldots, p$, so that

$$U_l^n = S_l(t_n, t_0, \mathbf{U^0}). \tag{3.26}$$

Then from [67] we have the expansion

$$\begin{aligned} S_l(t_n, t_0, \mathbf{U^0} + \boldsymbol{\delta}\mathbf{U^0}) &= S_l(t_n, t_0, \mathbf{U^0}) \\ &+ \sum_{i=1}^{p} \frac{\partial S_l}{\partial U_i}(t_n, t_0, \mathbf{U^0})\delta U_i^0 \\ &+ \frac{1}{2!}\sum_{i=1}^{p}\sum_{j=1}^{p} \frac{\partial^2 S_l}{\partial U_i \partial U_j}(t_n, t_0, \mathbf{U^0})\delta U_i^0 \delta U_j^0 \\ &+ \frac{1}{3!}\sum_{i=1}^{p}\sum_{j=1}^{p}\sum_{k=1}^{p} \frac{\partial^3 S_l}{\partial U_i \partial U_j \partial U_k}(t_n, t_0, \mathbf{U^0})\delta U_i^0 \delta U_j^0 \delta U_k^0 \\ &+ h.o.t. \end{aligned} \tag{3.27}$$

We wish to use this Taylor series expansion to derive an estimate of the linearization error we would obtain if we used the tangent linear model to evolve an initial perturbation $\boldsymbol{\delta}\mathbf{U^0}$ around an evolving linearization state $\boldsymbol{S}(t_n, t_0, \mathbf{U^0})$.

The method proceeds as follows. We first run the nonlinear model from three different initial conditions, $\mathbf{U^0}, \mathbf{U^0} + \boldsymbol{\delta}\mathbf{U^0}$ and $\mathbf{U^0} + \gamma\boldsymbol{\delta}\mathbf{U^0}$, where γ is a small scalar parameter. From these runs we can use (3.5) to calculate the two nonlinear perturbations

$$\boldsymbol{N}^n[\boldsymbol{\delta}\mathbf{U^0}] = \boldsymbol{S}(t_n, t_0, \mathbf{U^0} + \boldsymbol{\delta}\mathbf{U^0}) - \boldsymbol{S}(t_n, t_0, \mathbf{U^0}), \tag{3.28}$$

$$\boldsymbol{N}^n[\gamma\boldsymbol{\delta}\mathbf{U^0}] = \boldsymbol{S}(t_n, t_0, \mathbf{U^0} + \gamma\boldsymbol{\delta}\mathbf{U^0}) - \boldsymbol{S}(t_n, t_0, \mathbf{U^0}), \tag{3.29}$$

consisting of the components $N_l^n[\boldsymbol{\delta}\mathbf{U^0}], N_l^n[\gamma\boldsymbol{\delta}\mathbf{U^0}]$ respectively, with $l = 1, \ldots, p$. We now note that the linearization error $\mathbf{E}^n$ we would obtain by applying the tangent linear model to the perturbation $\boldsymbol{\delta}\mathbf{U^0}$ is given by

$$\mathbf{E}^n = \boldsymbol{N}^n[\boldsymbol{\delta}\mathbf{U^0}] - \mathbf{G}(t_n, t_0)\boldsymbol{\delta}\mathbf{U^0} \tag{3.30}$$

using Definition 3.1, where $\mathbf{G}(t_n, t_0)$ is the tangent linear model operator defined by

(3.9). Then from (3.27) we see that $\mathbf{E}^n$ consists of the p components E_l^n given by

$$\begin{aligned} E_l^n &= \frac{1}{2!}\sum_{i=1}^{p}\sum_{j=1}^{p}\frac{\partial^2 S_l}{\partial U_i \partial U_j}(t_n, t_0, \mathbf{U^0})\delta U_i^0 \delta U_j^0 \\ &+ \frac{1}{3!}\sum_{i=1}^{p}\sum_{j=1}^{p}\sum_{k=1}^{p}\frac{\partial^3 S_l}{\partial U_i \partial U_j \partial U_k}(t_n, t_0, \mathbf{U^0})\delta U_i^0 \delta U_j^0 \delta U_k^0 \\ &+ h.o.t. \end{aligned} \tag{3.31}$$

It is this quantity which we seek to estimate.

We now define a function $\boldsymbol{\mathcal{E}}^n$ by

$$\boldsymbol{\mathcal{E}}^n = \frac{\boldsymbol{N}^n[\gamma\boldsymbol{\delta}\mathbf{U^0}] - \gamma\boldsymbol{N}^n[\boldsymbol{\delta}\mathbf{U^0}]}{\gamma^2 - \gamma} \tag{3.32}$$

with components $\mathcal{E}_l^n$. Then using (3.27) we find that

$$\begin{aligned} \mathcal{E}_l^n &= \frac{1}{2!}\sum_{i=1}^{p}\sum_{j=1}^{p}\frac{\partial^2 S_l}{\partial U_i \partial U_j}(t_n, t_0, \mathbf{U^0})\delta U_i^0 \delta U_j^0 \\ &+ (1+\gamma)\frac{1}{3!}\sum_{i=1}^{p}\sum_{j=1}^{p}\sum_{k=1}^{p}\frac{\partial^3 S_l}{\partial U_i \partial U_j \partial U_k}(t_n, t_0, \mathbf{U^0})\delta U_i^0 \delta U_j^0 \delta U_k^0 \\ &+ h.o.t. \end{aligned} \tag{3.33}$$

A comparison of this expression with (3.31) shows that for small values of γ and small perturbations we have for each of the p components $\mathcal{E}_l^n \approx E_l^n$ and so $\boldsymbol{\mathcal{E}}^n \approx \mathbf{E}^n$. Since the expression (3.32) is calculated by using only the nonlinear model, it provides an estimate of the expected linearization error $\mathbf{E}^n$ of a tangent linear model without the need for such a model. Thus this formula allows us to estimate how much of the linearization error we see in tests of the perturbation forecast model is due to nonlinear effects.

As a corollary of this analysis we can also estimate the solution error we would obtain if we were to use an exact tangent linear model. From (3.22) we find that the solution error E_S can be written

$$E_S = 100\frac{rms(\mathbf{E}^n)}{rms(\boldsymbol{N}^n[\boldsymbol{\delta}\mathbf{U^0}])}. \tag{3.34}$$

Since the size of the nonlinear perturbation is known and we have an estimate for the linearization error, we can also calculate the estimated solution error $\hat{E}_s$ using

$$\hat{E}_S = 100 \frac{rms(\boldsymbol{\mathcal{E}}^n)}{rms(\boldsymbol{N}^n[\boldsymbol{\delta}\mathbf{U}^0])}. \tag{3.35}$$

This can then be compared with the actual solution error for a perturbation forecast model, calculated using the linearization error $\mathbf{E}^n$ from (3.13). This gives a more quantitive estimate of the difference from a tangent linear model.

Although these formulae are analytically robust, it is necessary to test them numerically to see how well they hold in practice. In Chapter 5 we develop the tangent linear and perturbation forecast models of a semi-implicit semi-Lagrangian shallow water model. In experiments with these simple models in Section 5.6 we are able to validate the formulae developed in this section and we consider there how to choose practically the value of the parameter γ in (3.32). Once these formulae are demonstrated to be useful we can apply them in our study of a three-dimensional weather forecasting model in Chapter 6. First however we study a very simple ordinary differential equation initial value problem in Chapter 4. This problem is used to prove the concept of the semi-continuous method and to examine the accuracy and stability properties of the linear model formed in this way.

Chapter 4

An ODE initial value problem

In this chapter we wish to investigate the principle of the semi-continuous method for developing a linear model by looking at a very simple problem. The results of this chapter we have also published separately in a technical report of the Met Office [46]. The problem we study is an initial value problem of a scalar ordinary differential equation. The aim of looking at this problem is to see in a simple context what kind of results we may expect in more complicated models.

We consider a general ODE initial value problem for a scalar function $y(t)$ of the form

$$\frac{dy}{dt} = f(y), \quad t \in [0, T], \; y(0) = y_0, \tag{4.1}$$

where f is explicitly a function in y only. This is a scalar equation of the same form as the general equation (2.1) introduced in Section 2.1. The linearization of (4.1) is

$$\frac{d(\delta y)}{dt} = f'(y)\delta y, \tag{4.2}$$

where

$$f'(y) \equiv \left.\frac{df}{dy}\right|_{y(t)}. \tag{4.3}$$

We note that since $y = y(t)$, the coefficient of δy in (4.2) will in general vary with time. This must be taken into account when applying schemes that require

coefficients from different time levels. In order to develop the linear model by the discrete method we apply a numerical scheme to equation (4.1) and then linearize this scheme. This gives the tangent linear model (TLM). We wish to compare this linear model with that derived by the semi-continuous method, that is by applying the original numerical scheme directly to equation (4.2). This second linear model is the perturbation forecast model (PFM). Within this chapter we compare the TLM and PFM for a particular numerical scheme, looking particularly at the properties of accuracy and stability.

Before we continue it is desirable to say something about the existence of solutions to these equations. We assume that f is continuous on some interval $[y_0, y_T]$ and satisfies a Lipschitz condition

$$\| f(y_1) - f(y_2) \| \leq L \ \| y_1 - y_2 \| \tag{4.4}$$

for all $y_1, y_2 \in [y_0, y_T]$. L is the Lipschitz constant. This ensures that (4.1) has a unique solution while y remains in the region $[y_0, y_T]$ ([30], section 1.1).

In order to show that the tangent linear problem (4.2) has a Lipschitz condition and therefore a unique solution, we first note that for given perturbations $\delta y_1, \delta y_2$ to a state $y(t)$, we have

$$\| f'(y)\delta y_1 - f'(y)\delta y_2 \| \leq \| f'(y) \| \| \delta y_1 - \delta y_2 \| . \tag{4.5}$$

Hence, if $f'(y)$ is bounded in $[y_0, y_T]$, we can choose

$$L = \max\{\| f'(y) \| : y \in [y_0, y_T]\} \tag{4.6}$$

to give the required condition. A bound on $f'(y)$ is then provides a sufficient condition for a solution to exist and so this is assumed in our analysis.

4.1 Linear multistep methods

We consider the general linear k-step method as defined by (2.38) of Chapter 2. Applying such a scheme to (4.1), we have

$$\sum_{j=0}^{k} \alpha_j y_{n+j} = \Delta t \sum_{j=0}^{k} \beta_j f_{n+j}, \tag{4.7}$$

where $f_n \equiv f(y_n)$. A linearization of this scheme produces the tangent linear model

$$\sum_{j=0}^{k} \alpha_j \delta y_{n+j} = \Delta t \sum_{j=0}^{k} \beta_j f'_{n+j} \delta y_{n+j}. \tag{4.8}$$

It is clear that exactly the same result would be obtained by applying the original scheme (2.38) to the linear equation (4.2). Hence, for the case of a general linear multistep method, the discrete method and the semi-continuous method are equivalent.

4.2 Nonlinear methods

The conclusion of the previous section does not necessarily hold when we apply a nonlinear numerical method to the problem. To illustrate this, we use the example of a two-stage Runge-Kutta scheme defined by equation (2.43) of Chapter 2, which we restate here:

$$\begin{aligned} k_1 &= f(y_n, t_n), \\ k_2 &= f(y_n + \Delta t f(y_n, t_n), t_n + \Delta t), \\ y_{n+1} &= y_n + \frac{\Delta t}{2}(k_1 + k_2). \end{aligned} \tag{4.9}$$

For the nonlinear problem we are considering we note that the function f does not depend explicitly on t and therefore we have the scheme

$$\begin{aligned} k_1 &= f(y_n), \\ k_2 &= f(y_n + \Delta t\, f(y_n)), \\ y_{n+1} &= y_n + \frac{\Delta t}{2}(k_1 + k_2). \end{aligned} \tag{4.10}$$

Applying this scheme to the nonlinear equation (4.1) gives the discrete nonlinear model

$$y_{n+1} = y_n + \frac{\Delta t}{2}\left\{f(y_n) + f(y_n + \Delta t\, f(y_n))\right\}. \tag{4.11}$$

In order to form the TLM we linearize this scheme to obtain

$$\begin{aligned} \delta y_{n+1} &= \delta y_n + \frac{\Delta t}{2}\{f'(y_n)\delta y_n \\ &+ f'(y_n + \Delta t\, f(y_n))[1 + \Delta t\, f'(y_n)]\delta y_n\}. \end{aligned} \tag{4.12}$$

However, if we apply the nonlinear scheme (4.9) to the tangent linear equation (4.2), noting the time dependence of the coefficient of δy, we obtain the PFM

$$\begin{aligned} \delta y_{n+1} &= \delta y_n + \frac{\Delta t}{2}\{f'(y_n)\delta y_n \\ &+ f'(y_{n+1})[1 + \Delta t\, f'(y_n)]\delta y_n\}. \end{aligned} \tag{4.13}$$

A comparison of (4.12) and (4.13) shows that they are very similar, but with y_{n+1} in the second equation being replaced by an estimate of this in the first. In the second scheme, however, y_{n+1} is given by the more accurate estimate obtained from (4.11), which implies that

$$\begin{aligned} \delta y_{n+1} &= \delta y_n + \frac{\Delta t}{2}\{f'(y_n)\delta y_n \\ &+ f'(y_n + \frac{\Delta t}{2}\left\{f(y_n) + f(y_n + \Delta t\, f(y_n))\right\})[1 + \Delta t\, f'(y_n)]\delta y_n\}. \end{aligned} \tag{4.14}$$

It is clear from equations (4.12) and (4.14) that the TLM and PFM are not the same for a general function f. Hence for this scheme the processes of discretization

and linearization are not commutative. We note however that if we were to apply the Runge-Kutta scheme to the coupled system given by the continuous nonlinear equation (4.1) and the continuous linear equation (4.2), then the resulting linear model would be the same as the tangent linear model. This is the commutativity of discretization and linearization which is usually referred to in the literature (for example [61]). However, by applying the scheme first to the nonlinear equation and then to the linear equation afterwards, a different linear model results. Since this is the method followed in practice to obtain the linearization of a weather forecasting model at the Met Office (details of which are given in Chapter 6), it is useful to study the effect of forming the PFM in this way. We now examine in more detail the TLM (4.12) and the PFM (4.14) to see if we can say something about their comparative properties. We begin with an analysis of their truncation errors.

4.2.1 Truncation error analysis

We wish to calculate the truncation errors in both the linear models, to check the accuracy to which they solve the continuous linear equation (4.2). It is informative to compare with the truncation error of the scheme applied to the nonlinear equation, and so this is calculated first.

Let us denote the truncation error of the nonlinear model as τ_{NL}. Then by the definition of truncation error given by Definition 2.1 and using (4.11), we have

$$\tau_{NL} = \frac{y(t_{n+1}) - y(t_n)}{\Delta t} - \frac{1}{2}\left\{f(y(t_n)) + f(y(t_n) + \Delta t\, f(y(t_n))\right\}. \tag{4.15}$$

Noting that $y(t_{n+1}) = y(t_n + \Delta t)$, we can perform a Taylor series expansion around time t_n and also expand the second function about $f(y(t_n))$. Then using relation-

ships

$$\begin{aligned}
\frac{dy}{dt} &= f(y(t)), \\
\frac{d^2y}{dt^2} &= f(y(t))f'(y(t)), \\
\frac{d^3y}{dt^3} &= [f'(y(t))]^2 f(y(t)) + f''(y(t))[f(y(t))]^2,
\end{aligned}$$

we find that the truncation error is given by

$$\begin{aligned}
\tau_{NL} &= \left(\frac{1}{6}f(y(t_n))[f'(y(t_n))]^2 - \frac{1}{12}f''(y(t_n))[f(y(t_n))]^2\right)\Delta t^2 \\
&+ O(\Delta t^3). \qquad (4.16)
\end{aligned}$$

By this we see that the scheme is second order in time.

Now we wish to examine the truncation errors for the two linear models (4.12) and (4.14), which we denote τ_1 and τ_2 respectively. First we must be clear about what these quantities mean. The PFM (4.14) is a scheme written to approximate the linear equation (4.2) and so the truncation error is defined in the usual way with respect to the analytical solution of the linear equation. However, when we look at the TLM (4.12), we do not have a clear definition of truncation error, since this scheme is not designed as an approximation to any particular equation. For comparison therefore, we take the truncation error with respect to the solution of the same linear equation (4.2).

For the TLM (4.12) the truncation error is found to be

$$\begin{aligned}
\tau_1 &= \frac{\delta y(t_{n+1}) - \delta y(t_n)}{\Delta t} - \frac{1}{2}\{f'(y(t_n))\delta y(t_n) \\
&+ f'(\, y(t_n) + \Delta t f(y(t_n))\,)[1 + \Delta t f'(y(t_n))]\delta y(t_n)\}. \qquad (4.17)
\end{aligned}$$

Now we expand $\delta y(t_{n+1}) = \delta y(t_n + \Delta t)$ in a Taylor series around t_n and expand the

last term of the equation around $f'(y(t_n))$. Then using the relationships

$$\begin{aligned}
\frac{d(\delta y)}{dt} &= f'(y(t))\delta y + O(\delta y^2), \\
\frac{d^2(\delta y)}{dt^2} &= f''(y(t))f(y(t))\delta y + [f'(y(t))]^2\delta y + O(\delta y^2), \\
\frac{d^3(\delta y)}{dt^3} &= f'''(y(t))[f(y(t))]^2\delta y + 4f''(y(t))f'(y(t))f(y(t))\delta y \\
&+ [f'(y(t))]^3\delta y + O(\delta y^2),
\end{aligned}$$

we find that to order δy

$$\begin{aligned}
\tau_1 &= \left(\frac{1}{6}[f'(y(t_n))]^3 + \frac{1}{6}f''(y(t_n))f'(y(t_n))f(y(t_n))\right. \\
&- \left.\frac{1}{12}f'''(y(t_n))[f(y(t_n))]^2\right)\delta y(t_n)\Delta t^2 + O(\delta y(t_n)\Delta t^3). \qquad (4.18)
\end{aligned}$$

We note first of all that this is second order. A simple manipulation shows that it is equal to the linearization of the nonlinear model truncation error (4.16).

Turning now to what happens when we discretize the continuous linear equation, we find that the truncation error for the PFM (4.14) is

$$\begin{aligned}
\tau_2 &= \frac{\delta y(t_{n+1}) - \delta y(t_n)}{\Delta t} - \frac{1}{2}\{f'(y(t_n))\delta y(t_n) + f'(y(t_n) \\
&+ \frac{\Delta t}{2}\{f(y(t_n)) + f(y(t_n) + \Delta t\, f(y(t_n)))\})[1 + \Delta t f'(y(t_n))]\delta y(t_n)\}, \qquad (4.19)
\end{aligned}$$

and with the same cancellations as in the previous case, this reduces to

$$\begin{aligned}
\tau_2 &= \left(\frac{1}{6}[f'(y(t_n))]^3 - \frac{1}{12}f''(y(t_n))f'(y(t_n))f(y(t_n))\right. \\
&- \left.\frac{1}{12}f'''(y(t_n))[f(y(t_n))]^2\right)\delta y(t_n)\Delta t^2 + O(\delta y(t_n)\Delta t^3). \qquad (4.20)
\end{aligned}$$

Again we see that this is second order, but this time it is not the linearization of the truncation error of the nonlinear scheme.

4.3 Example

To illustrate the above theory we consider the simple example of the initial value problem (4.1) with $f(y) = y^2$, which gives

$$\frac{dy}{dt} = y^2, \tag{4.21}$$

and we assume $t \in [0, 10]$ and $y(0) = y_0$. The analytical solution to this equation is given by

$$y = \frac{y_0}{1 - y_0 t}. \tag{4.22}$$

By considering a perturbation δy to the problem (4.21), we obtain the analytical solution for the nonlinear evolution of a perturbation,

$$\delta y(t) = \frac{\delta y_0}{(1 - (y_0 + \delta y_0)t)(1 - y_0 t)}. \tag{4.23}$$

The analytical linear system obtained from the linearization of (4.21) is

$$\frac{d(\delta y)}{dt} = 2y\delta y, \tag{4.24}$$

which has the solution

$$\delta y(t) = \frac{\delta y_0}{(1 - y_0 t)^2}. \tag{4.25}$$

To obtain the numerical models we first apply the Runge-Kutta scheme (4.10) to (4.21), to obtain the discrete nonlinear model

$$y_{n+1} = y_n + y_n^2 \Delta t + y_n^3 \Delta t^2 + \frac{y_n^4 \Delta t^3}{2}, \tag{4.26}$$

which is second order in time, with truncation error

$$\tau_{NL} = \frac{y(t_n)^4 \Delta t^2}{2} + \sum_{k=4}^{\infty} y(t_n)^{k+1} \Delta t^{k-1}. \tag{4.27}$$

To find the linear model by the discrete method, we linearize the discrete scheme (4.26) to obtain the TLM

$$\delta y_{n+1} = (1 + 2y_n \Delta t + 3y_n^2 \Delta t^2 + 2y_n^3 \Delta t^3)\delta y_n. \tag{4.28}$$

The linear model by the semi-continuous method is determined by applying the numerical scheme (4.9) to the analytical linear equation (4.24). This gives the PFM

$$\delta y_{n+1} = \delta y_n + y_n \Delta t \delta y_n + y_{n+1} \Delta t [1 + 2 y_n \Delta t] \delta y_n. \tag{4.29}$$

Then, using the estimate of y_{n+1} from (4.26), we have

$$\begin{aligned} \delta y_{n+1} &= \delta y_n + y_n \Delta t \delta y_n \\ &+ \left(y_n + y_n^2 \Delta t + y_n^3 \Delta t^2 + \frac{y_n^4 \Delta t^3}{2} \right) \Delta t [1 + 2 y_n \Delta t] \delta y_n \\ &= (1 + 2 y_n \Delta t + 3 y_n^2 \Delta t^2 + 3 y_n^3 \Delta t^3 + \frac{5}{2} y_n^4 \Delta t^4 + y_n^5 \Delta t^5) \delta y_n. \end{aligned} \tag{4.30}$$

Then using equations (4.21) and (4.24) and their derivatives, the truncation errors as defined by Definition 2.1 are as follows:

• for the discrete method (TLM)

$$\begin{aligned} \tau_1 &= 2 y(t_n)^3 \Delta t^2 \delta y(t_n) + 5 y(t_n)^4 \Delta t^3 \delta y(t_n) + 6 y(t_n)^5 \Delta t^4 \delta y(t_n) \\ &+ \sum_{k=6}^{\infty} (k+1) y(t_n)^k \Delta t^{k-1} \delta y(t_n); \end{aligned} \tag{4.31}$$

• for the semi-continuous method (PFM)

$$\begin{aligned} \tau_2 &= y(t_n)^3 \Delta t^2 \delta y(t_n) + \frac{5}{2} y(t_n)^4 \Delta t^3 \delta y(t_n) + 5 y(t_n)^5 \Delta t^4 \delta y(t_n) \\ &+ \sum_{k=6}^{\infty} (k+1) y(t_n)^k \Delta t^{k-1} \delta y(t_n). \end{aligned} \tag{4.32}$$

We note that both linear models are second order in time. For the PFM this would be expected, since we know from the analysis of the discrete nonlinear model that the scheme we are applying is a second order scheme. For the TLM we see that the scheme is also second order, with truncation error (4.31) equal to the linearization of the nonlinear model truncation error (4.27). However the form of the truncation error is different for the two linear models, with that of the PFM having a smaller principal term than that of the TLM. In order to understand any differences in behaviour between the TLM and PFM we now consider some numerical experiments.

4.4 Numerical experiments

We use the method described in Section 3.1 to compare the linear and nonlinear evolution of the perturbations in the numerical models. The schemes were coded and the nonlinear model was run from two slightly different initial conditions y_0 and $y_0 + \delta y_0$ at time $t = 0$. The difference between these two runs was then compared with each of the linear models initialized with the perturbation δy_0 at $t = 0$. The first experiment used values of $y_0 = -2.5$ and $\delta y_0 = -0.1$ and a time step $\Delta t = 0.25$. The output is shown in Figure 4.1. The solid line shows the difference between the two nonlinear runs, the dashed line shows the TLM scheme formed by linearizing the discrete scheme (4.28) and the dotted line shows the PFM scheme formed by discretizing the linear equation (4.30). Also plotted with diamonds is the true nonlinear variation of a perturbation calculated from the analytical expression (4.23). For this experiment the solid line and the dashed line are almost identical. We see that both linear models approximate well the true nonlinear variation.

The experiment was then repeated with larger time steps, first for $\Delta t = 0.35$ and then for $\Delta t = 0.5$. The output from the first of these is shown in Figure 4.2. The solution trajectory from the PFM moves away from the other curves. This model thus seems to be less accurate in representing both the true nonlinear variation and the evolution in the discrete nonlinear model, despite having a smaller truncation error.

However, when the time step is increased even further, to a value of 0.5, a different behaviour is seen. The output from this experiment is shown in Figure 4.3. In this case the difference between the two runs of the discrete nonlinear model is quite different from the true nonlinear evolution of the perturbation. The TLM follows closely the difference between the two discrete nonlinear runs, whereas the PFM is closer to the true nonlinear variation.

To explain the peak in these results which makes the two linear schemes so dif-

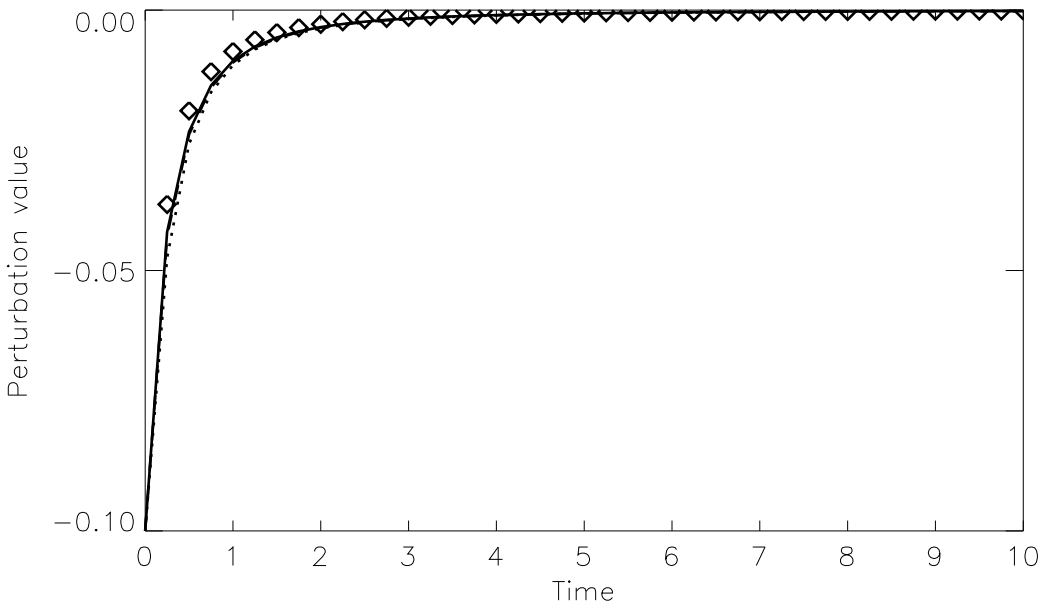

Figure 4.1: Plot of perturbation against time for $\Delta t = 0.25$. The solid line indicates the evolution in the nonlinear model, the dashed line shows the tangent linear model evolution, the dotted line shows the perturbation forecast model evolution and the diamonds indicate the true nonlinear variation.

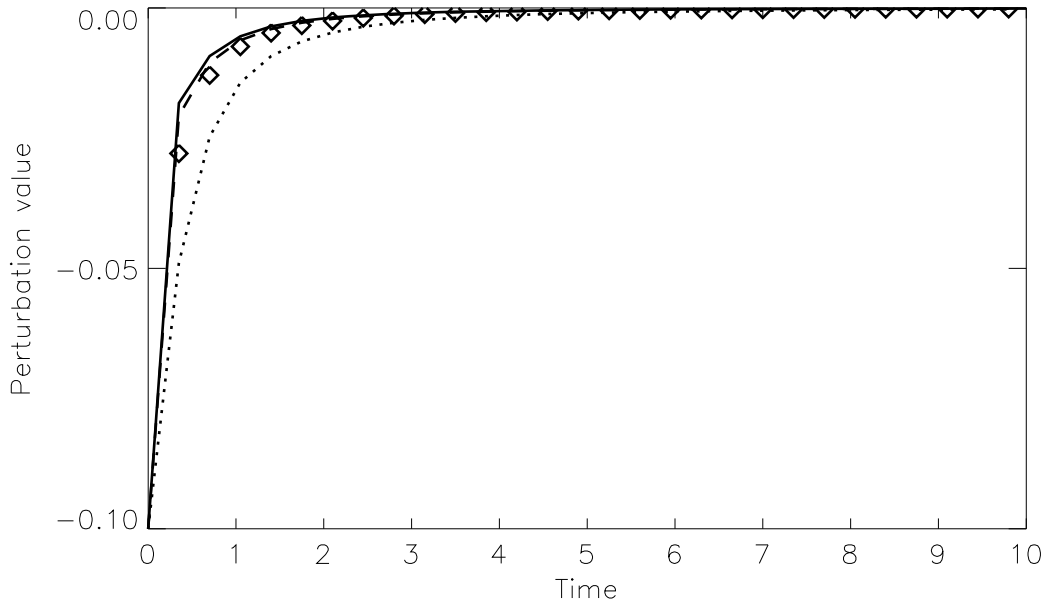

Figure 4.2: As Figure 4.1, with $\Delta t = 0.35$.

ferent, it is useful to look at the behaviour of the numerical solution of the nonlinear equation. The solution from the runs of the nonlinear model is shown in Figure 4.4. The dotted line indicates the model run with $\Delta t = 0.25$, the dashed line with $\Delta t = 0.5$ and the solid line is the analytical solution. We show in Figure 4.5 the absolute value of the global error e_n for each of these runs, as defined by (2.7). It can be seen that doubling the time step gives a large increase in the error of the model solution, showing that the scheme itself is inaccurate with the larger time step. The effect of this inaccuracy on the difference between the perturbed and unperturbed runs is that the perturbation can change sign. This can be seen in Figure 4.3; the solid line shows the initial negative perturbation becoming positive during the nonlinear model run, whereas the true nonlinear variation, shown by the diamonds, remains always negative.

If we consider the true nonlinear variation (4.23), then for given initial values y_0 and δy_0 both less than zero, we see that $\delta y(t)$ cannot change sign. If we examine the

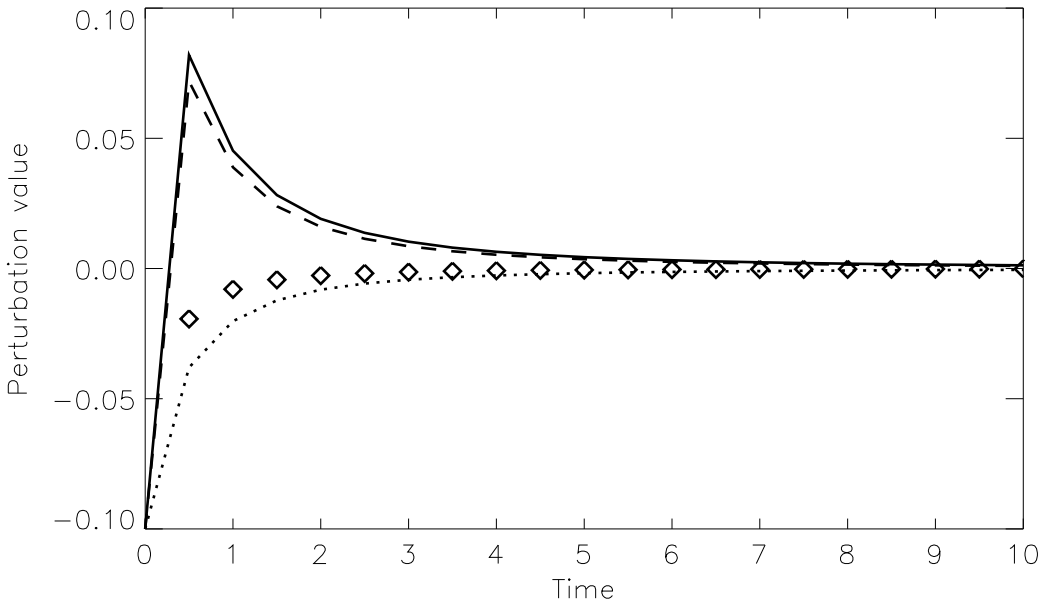

Figure 4.3: Plot of perturbation against time for $\Delta t = 0.5$. The solid line indicates the evolution in the nonlinear model, the dashed line shows the tangent linear model evolution, the dotted line shows the perturbation forecast model evolution and the diamonds indicate the true nonlinear variation.

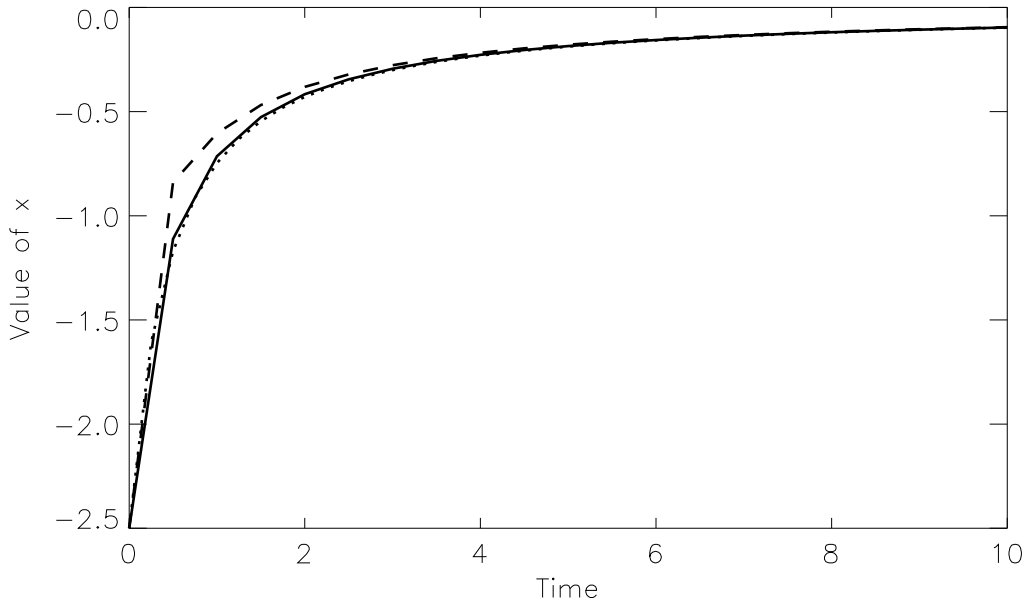

Figure 4.4: Solution of nonlinear model runs. The dotted line is for $\Delta t = 0.25$ and the dashed line is for $\Delta t = 0.5$. The solid line indicates the analytical solution of the nonlinear problem.

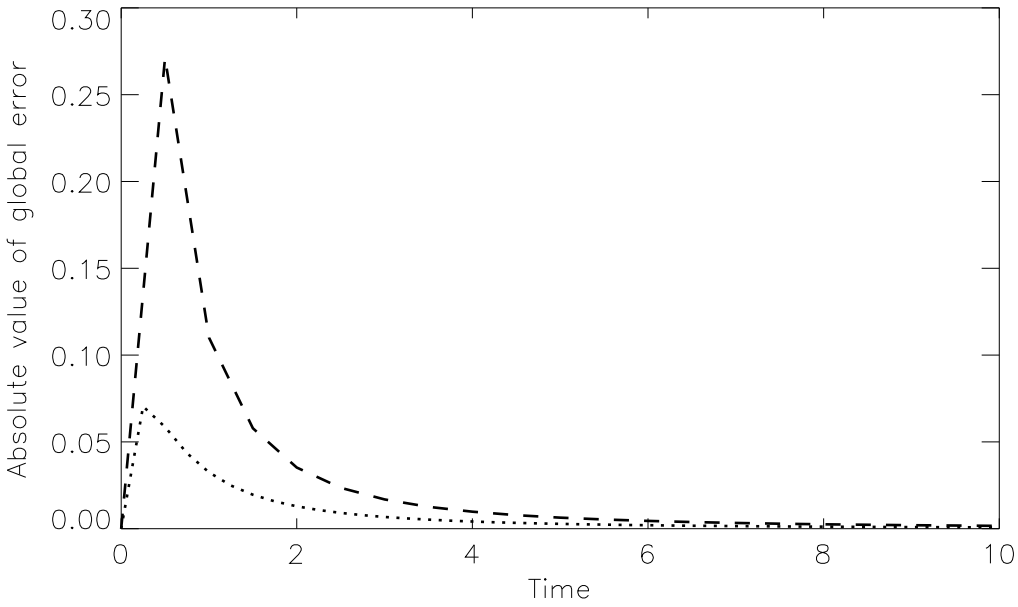

Figure 4.5: Absolute value of the global error for the nonlinear model runs. The dotted line is for $\Delta t = 0.25$ and the dashed line is for $\Delta t = 0.5$.

analytical solution to the linear equation (4.25), we see also that δy at any time t is always a positive factor times the initial δy and thus cannot change sign. Hence the analytical solutions to both the nonlinear and linear problems tell us that an initial negative perturbation must remain negative throughout the model run. Thus the behaviour of the perturbation in the discrete nonlinear model is one which is not allowed by the analytical solution.

Turning now to the linear models, we wish to understand why the solution of the model formed by the discrete method (the dashed line in Figure 4.3) follows the erroneous nonlinear model solution. In particular, we wish to determine whether this is an effect of an incorrect linearization state or a feature of the scheme itself. The experiments were therefore repeated, using a time step of $\Delta t = 0.25$ in the nonlinear model run, and then using the linearization state from this to force the linear models with a time step of $\Delta t = 0.5$. The result of this is shown in Figure 4.6. From this experiment we see that a more correct linearization state is not enough to prevent the perturbation from changing sign in the linear model formed by the discrete method (the TLM). The linear model is unstable even though the nonlinear model is well-behaved. The problem must therefore be inherent in the scheme of the TLM. We therefore analyse further the linear schemes, to understand how their behaviour changes with time step.

4.4.1 Analysis of numerical results

We first consider the numerical stability of the schemes. To investigate the linear stability limit of the Runge-Kutta scheme (4.10) we follow the method of Section 2.1.3 and apply the scheme to the scalar system

$$\frac{dy}{dt} = \mu y, \qquad \mu < 0. \tag{4.33}$$

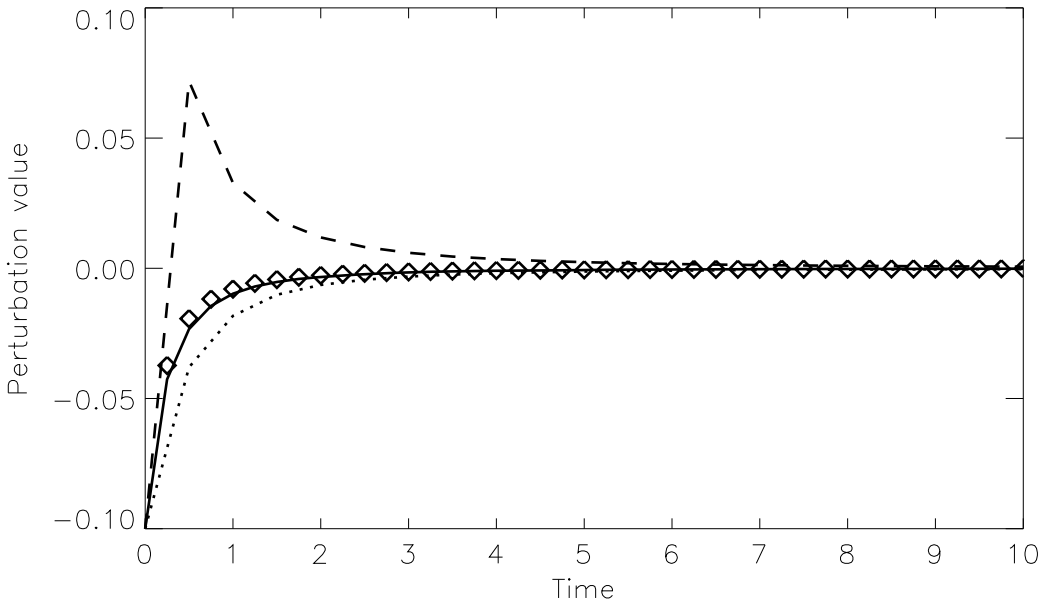

Figure 4.6: As Figure 4.3, but with the nonlinear model run with $\Delta t = 0.25$ and the linear models run with $\Delta t = 0.5$.

Then requiring that the modulus of the amplification factor be less than one, we find a limit on the time step Δt for this scheme of

$$\Delta t < -\frac{2}{\mu}. \tag{4.34}$$

Hence with μ set to $2y$, as in our linear equation (4.24), we find that for stability we require

$$\Delta t < -\frac{1}{y}. \tag{4.35}$$

For $y = -2.5$ this gives a time step limit of $\Delta t < 0.4$.

This limit also holds for the linear model formed by the discrete method (the TLM). The amplification factor λ_n of the linear scheme is given by

$$\lambda_n = \frac{\delta y_{n+1}}{\delta y_n}. \tag{4.36}$$

For an initial negative perturbation to remain negative we require that λ_n is always positive. A simple analysis of the TLM (4.28) shows that (4.35) is a necessary and sufficient condition for this.

To illustrate this we plot λ_n for the scheme, for a range of values of y and Δt. This is shown in Figure 4.7. We see that for $y = -2.5$ the amplification factor becomes negative for time steps Δt greater than 0.4, as predicted by the analysis.

In contrast, the scheme formed by the semi-continuous method allows a larger time step for any particular value of y than that given by the above analysis. In this case, the scheme allows for the variation of μ in time, thus making it more stable for larger time steps than the model formed by linearizing the discrete nonlinear scheme. This can be seen in the plot of its amplification factor in Figure 4.8. A comparison with Figure 4.7 shows a greater range of values for which λ_n remains positive. In particular, for $y = -2.5$ and time step $\Delta t = 0.5$, λ_n is positive with value 0.38.

In order to compare the accuracy of the linear schemes, we define the *local* error

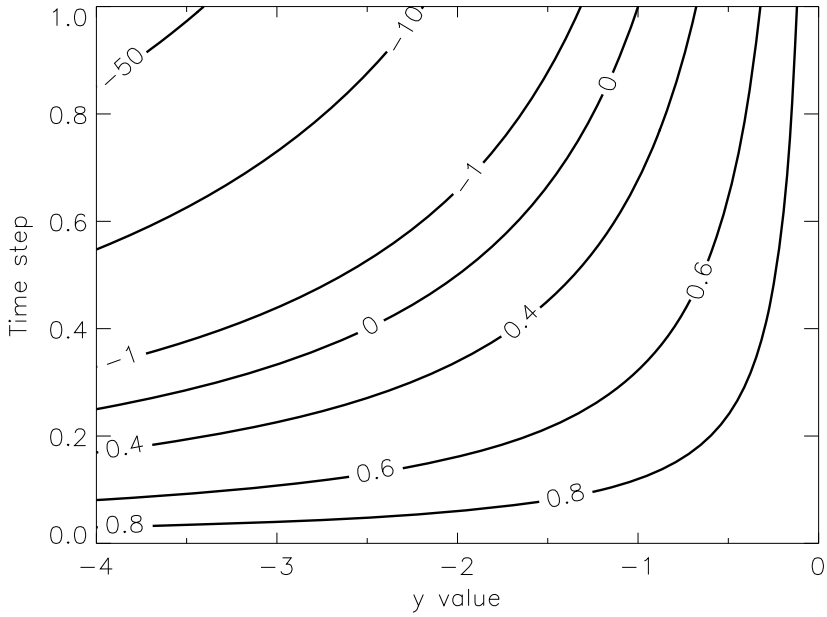

Figure 4.7: Amplification factor for various time steps and values of y: Tangent linear model.

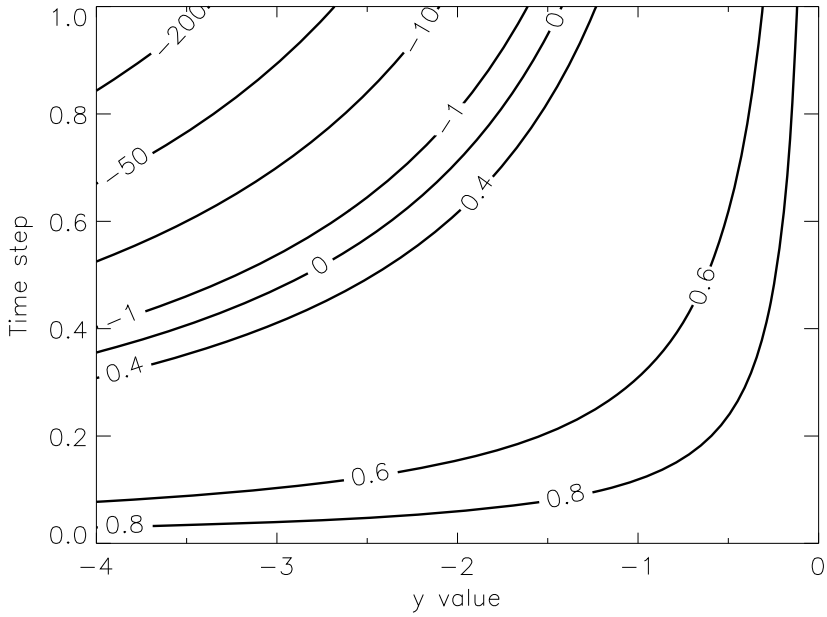

Figure 4.8: Amplification factor for various time steps and values of y: Perturbation forecast model.

of each scheme at time t_{n+1} by

$$E = \delta y(t_{n+1}) - \delta y_{n+1}, \tag{4.37}$$

where we assume $\delta y_n = \delta y(t_n)$ and $y_n = y(t_n)$. Then, expanding about time t_n we find the following local errors after one time step:

• for the discrete method (TLM)

$$E_1 = [2y(t_n)^3\Delta t^3 + 5y(t_n)^4\Delta t^4 + 6y(t_n)^5\Delta t^5 + O(y(t_n)^6\Delta t^6)]\delta y(t_n); \tag{4.38}$$

• for the semi-continuous method (PFM)

$$E_2 = [y(t_n)^3\Delta t^3 + \frac{5}{2}y(t_n)^4\Delta t^4 + 5y(t_n)^5\Delta t^5 + O(y(t_n)^6\Delta t^6)]\delta y(t_n). \tag{4.39}$$

The higher order terms of these errors are identical, and so we can write an exact expression for their difference,

$$E_1 - E_2 = [y(t_n)^3\Delta t^3 + \frac{5}{2}y(t_n)^4\Delta t^4 + y(t_n)^5\Delta t^5]\delta y(t_n). \tag{4.40}$$

A simple analysis shows that within the limits of stability, the magnitude of the error E_2 is greater than that of E_1 wherever

$$-1 < y\Delta t < -\frac{1}{2}. \tag{4.41}$$

For a value of $y = -2.5$ this corresponds to a time step range of $0.2 < \Delta t < 0.4$, and so explains the relative accuracy of the two linear solutions when $\Delta t = 0.35$. When the time step is less than 0.2, we find that the scheme formed by the semi-continuous method is more accurate.

4.5 Linearization state

Within each of the linear models we find a dependence on the linearization state $y(t)$ about which the model has been linearized. From equation (4.13) we note that

the discretization of the linear equation depends on $f'(y(t))$ at two different time levels t_n and t_{n+1}. In real applications we may want to replace both of these with some average value of the linearization state, since storing the values at every time step may be too costly. There are different ways that this can be done. One way is just to use the value of the linearization state at time t_n everywhere. However, calculation of the truncation error for this scheme shows it to be first order in time, that is the accuracy of the original scheme is reduced.

Since a reduction in accuracy is undesirable, the next natural thing to try is to find an average state in the middle of the time step, which we will write y_m. This gives the scheme

$$\begin{aligned} \delta y_{n+1} &= \delta y_n + \frac{\Delta t}{2}\{f'(y_m)\delta y_n \\ &+ f'(y_m)[1 + \Delta t f'(y_m)]\delta y_n\}. \end{aligned} \tag{4.42}$$

We note that this is not just the same scheme (2.43) with values at the intermediate time level, since this formula would imply that $k_1 = f'(y_m)\delta y_n$, which contains variables at two different time levels. Applying the scheme (4.42) to the general linear equation, we find that the truncation error τ_3 is given by

$$\begin{aligned} \tau_3 &= \frac{\delta y(t_{n+1}) - \delta y(t_n)}{\Delta t} - \frac{1}{2}\Big[2f'(y(t_m))\delta y(t_n) \\ &+ \Delta t[f'(y(t_m))]^2\delta y(t_n)\Big]. \end{aligned} \tag{4.43}$$

We consider two different ways of calculating the intermediate value. We could either take the average of the values of y at the ends of the time step, *i.e.*

$$y_m = \frac{1}{2}\Big(y_n + y_{n+1}\Big), \tag{4.44}$$

or we could take the value of the model state at the middle of the time step

$$y_m = y_{n+\frac{1}{2}}. \tag{4.45}$$

This second option requires the nonlinear model, which generates the linearization state, to be run at a higher time resolution than the linear model in order to produce

the intermediate values. An expansion of the truncation error finds that both of these options are second order accurate.

Although it may be argued that this is not a fair comparison, since by changing the time of the linearization state we are changing the numerical scheme, this is in fact what we do in practice. In the three-dimensional perturbation forecast model being developed at the Met Office, of which we speak in detail in Chapter 6, we apply the scheme of the nonlinear model to the linear equations, and afterwards decide where to take our linearization state. Hence it is important to know to what extent the choice of linearization state can affect the accuracy of the model.

To illustrate the effects of this choice we repeat the numerical experiment of the previous section using the scheme given by (4.42) and a time step of 0.5. We run two different experiments. For the first y_m is taken to be equal to y_n, and for the second the value of y_m defined by (4.44) is used. The results are shown by the asterisks in Figures 4.9 and 4.10 respectively. It is seen that using the value at the start of the time step, giving only a first order approximation, does indeed degrade the results. The evolution is no longer monotonic, but has an undershoot in the early stages of the run. Averaging the linearization state to the midpoint of the time step instead results in a much closer solution to the true discretization of the linear equation.

4.6 Summary

Although we have only considered a very simple numerical model in this chapter, the analysis and numerical experiments have provided an insight into the two different methods for developing a linear model. It is clear that at least for some schemes applying the numerical scheme to the continuous linearized equations is not the same as linearizing the discrete nonlinear scheme. The linear models thus formed may have different stability characteristics and so may exhibit different behaviours in some circumstances. In the example considered the tangent linear model has

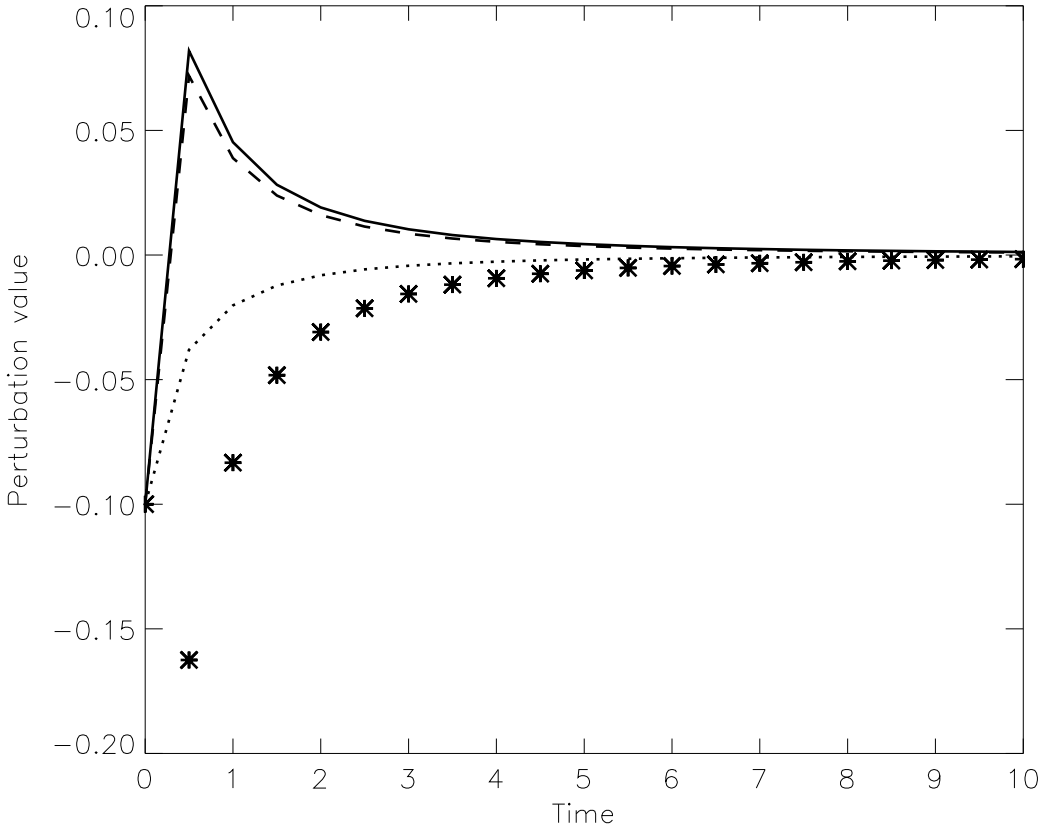

Figure 4.9: As Figure 4.3, with the asterisks showing the evolution of the perturbation forecast model when the linearization state is taken at the start of the time step.

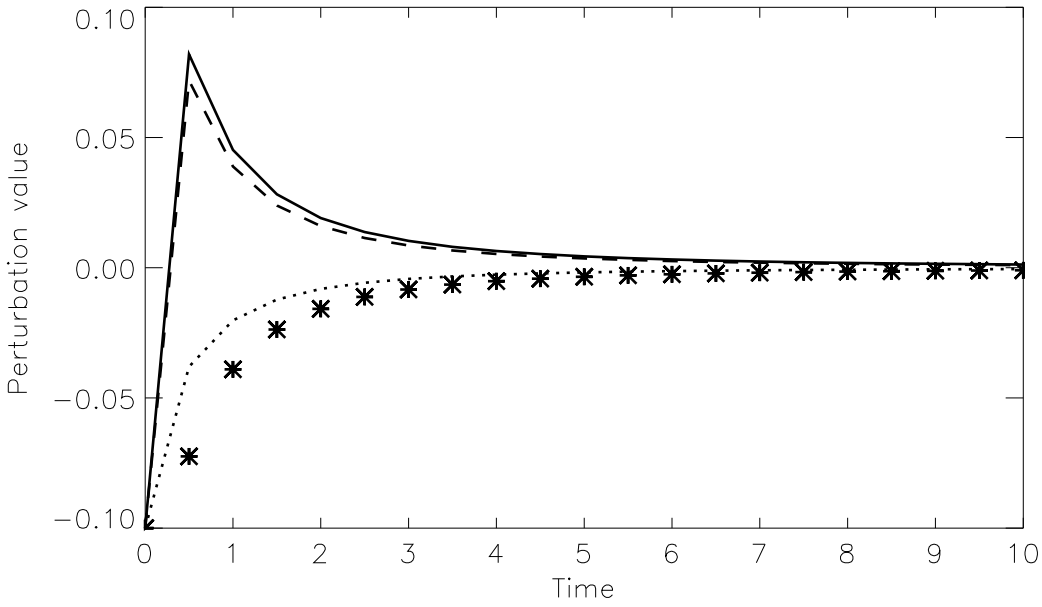

Figure 4.10: As Figure 4.3, with the asterisks showing the evolution of the perturbation forecast model when the linearization state is taken at the midpoint of the time step.

the linear stability limit of the discrete nonlinear model, whereas the perturbation forecast model allows larger time steps. Hence it is possible that the TLM may become unstable for time steps at which the PFM is still stable. Such a difference may be important if we wish to run the linear model at a lower temporal resolution than the nonlinear model. In practice this may be the case for incremental 4D-Var, since many iterations of the linear model will be required and means to reduce the cost of the linear model must therefore be sought. There may of course be situations in which the TLM is more stable than the PFM. However an advantage we see of the semi-continuous method is that the stability of the linear model may be better controlled *a priori* by careful choice of the numerical scheme used to discretize the linear equations.

For the numerical experiments in which both linear models remained stable, we find that the relative accuracy of the TLM and PFM compared with the analytical solution is dependent upon the value of the time step and the value of the linearization state. Thus it is not clear that either method holds an advantage over the other from an accuracy point of view.

A corollary of the results in this chapter is that testing the validity of the linear model must be performed with a good understanding of the nature of the numerical scheme. The usual method of testing such a model by comparing its output to the evolution of a perturbation in a nonlinear model will indicate how well the linear model represents the behaviour of the discrete nonlinear model. This is expected from the theoretical analysis and has been illustrated with numerical experiments. However, if the limitations of the numerical scheme are not understood, the linear model will not necessarily indicate the true evolution of a perturbation in reality, for example a perturbation to the atmosphere, and so may not be valid for applications which require this. It is therefore necessary to keep in mind the particular application for which the model is required whenever we are interpreting the results of such tests.

Finally in this chapter we have seen that if we apply a slightly modified version of

the scheme to the continuous linear equation, for example by using the linearization state at a different time level, then the order of accuracy may be reduced. In practice we may want to make such approximations, since for example it may be too expensive to store the linearization state at every time step. It is clear from the simple example considered that any approximations made must take into account the effect on the truncation error. We next consider such questions in the context of a one-dimensional shallow-water model.

Chapter 5

A 1-D shallow water model

In the previous chapter we have shown that for a simple ordinary differential equation problem linearizing a discrete nonlinear model is not necessarily the same as discretizing the linearized continuous equations. We now examine this problem for a partial differential equation system, using some of the numerical schemes that are used in operational weather forecasting models. We begin in Section 5.1 by setting up the analytical model. We state the systems of nonlinear and linearized equations and examine some of their properties. In Section 5.2 we then present the various numerical schemes. We set out in detail the scheme for our nonlinear model and then discretize it to form the tangent linear model (TLM). We then present the result of applying a numerical scheme to the linearized equations, that is the perturbation forecast model (PFM). In dealing with partial differential equations we find that there is more freedom in how to apply the numerical scheme to the linearized equations and so two alternatives for the PFM are presented. Some analysis of the schemes is made in Section 5.3 before presenting the results from numerical experiments in Section 5.4. We then consider the effect of altering the time level of the linearization state in Section 5.5. In Section 5.6 we discuss further the testing of linear models and verify the method for testing a perturbation forecast model which we proposed in Section 3.3. Finally Section 5.7 summarizes the results of the

chapter, particularly concentrating on those results which help our understanding of the three-dimensional models.

5.1 The analytical model

5.1.1 The nonlinear equations

The model we wish to consider is the one-dimensional shallow water system describing the flow of a single-layer fluid over an obstacle in the absence of rotation. The governing equations can be written

$$\frac{Du}{Dt} + \frac{\partial \phi}{\partial x} = -g\frac{\partial H}{\partial x}, \tag{5.1}$$

$$\frac{D\phi}{Dt} + \phi\frac{\partial u}{\partial x} = 0, \tag{5.2}$$

where

$$\frac{D}{Dt} = \frac{\partial}{\partial t} + u\frac{\partial}{\partial x} \tag{5.3}$$

is the material derivative. In these equations $H = H(x)$ is the height of the bottom orography, u is the velocity of the fluid and $\phi = gh$ is the geopotential, where g is the gravitational constant and $h > 0$ the depth of the fluid above the orography. The problem is defined on the domain $x \in [0, L]$ with periodic boundary conditions such that $x(0) = x(L)$ and we let $t \in [0, T]$. The values of u and ϕ are specified everywhere at the initial time, such that

$$\begin{aligned} u(x,0) &= u_0(x), \\ \phi(x,0) &= \phi_0(x). \end{aligned}$$

We note that the mass continuity equation (5.2) can also be written in its logarithmic form

$$\frac{D(\ln \phi)}{Dt} + \frac{\partial u}{\partial x} = 0. \tag{5.4}$$

When we implement the numerical model we find this form of the equation easier to work with, since the last term on the left hand side is linear. However, for work on the properties of the analytical equations, the two forms are equivalent and so we use (5.2).

5.1.2 Properties of the analytical system

In order to understand some properties of the nonlinear system, it is useful first to examine the constant coefficient linear system. This is derived by linearizing the homogeneous system around an equilibrium state U_0, Φ_0 which is constant in time and space. We put $H(x) = 0$ for all x and set

$$\begin{aligned} u(x,t) &= U_0 + \delta u(x,t), \\ \phi(x,t) &= \Phi_0 + \delta\phi(x,t). \end{aligned}$$

Then substituting into (5.1) and (5.2) we find

$$\frac{\partial \delta u}{\partial t} + U_0 \frac{\partial \delta u}{\partial x} + \frac{\partial \delta \phi}{\partial x} = 0, \tag{5.5}$$

$$\frac{\partial \delta \phi}{\partial t} + U_0 \frac{\partial \delta \phi}{\partial x} + \Phi_0 \frac{\partial \delta u}{\partial x} = 0, \tag{5.6}$$

to first order in the perturbations. Following the methods of Section 2.2.4, we obtain the dispersion relation for this linear system by searching for wave solutions of the form

$$\begin{aligned} \delta u(x,t) &= \delta u_0 e^{i(kx+\omega t)}, \\ \delta \phi(x,t) &= \delta \phi_0 e^{i(kx+\omega t)}, \end{aligned}$$

where k is the wave number and ω is the frequency. Substituting these solutions into the linearized system we obtain

$$i\omega \delta u_0 + ikU_0 \delta u_0 + ik\delta\phi_0 = 0, \tag{5.7}$$

$$i\omega \delta \phi_0 + ikU_0 \delta \phi_0 + ik\Phi_0 \delta u_0 = 0, \tag{5.8}$$

from which we can derive the analytical dispersion relation

$$\omega = -kU_0 \pm k\sqrt{\Phi_0}. \tag{5.9}$$

The phase speed of a wave is then given by

$$-\frac{\omega}{k} = U_0 \pm \sqrt{\Phi_0}. \tag{5.10}$$

Thus for the linearized homogeneous analytical system the phase speed is independent of the wave number k.

For the complete nonlinear inhomogeneous system (5.1), (5.2), it is more difficult to obtain analytical properties. We can however find steady state solutions to the equations. To find such solutions we set $\partial u/\partial t = 0$ in (5.1) and $\partial \phi/\partial t = 0$ in (5.2). Then following [38] we integrate with respect to x to obtain the steady state solutions

$$\frac{u^2}{2} + \phi + gH = K_1 = \text{constant} \tag{5.11}$$

and

$$u\phi = K_2 = \text{constant}, \tag{5.12}$$

where $u = u(x)$, $\phi = \phi(x)$ and K_1, K_2 are constants of integration which are independent of x. We note that the invariance of these quantities in the steady state is simply Bernoulli's theorem for this system ([6], Section 3.5). We use these solutions in Section 5.4 to help validate our numerical models and to understand the behaviour of the linearizations.

5.1.3 The analytical linear system

In order to form the set of linear equations we consider the fields u, ϕ as perturbations $\delta u, \delta\phi$ about a spatially and temporally varying basic state $\bar{u}, \bar{\phi}$ which satisfies the nonlinear equations. This basic state is also called the linearization state. Thus we

have

$$u(x,t) = \bar{u}(x,t) + \delta u(x,t), \tag{5.13}$$

$$\phi(x,t) = \bar{\phi}(x,t) + \delta\phi(x,t). \tag{5.14}$$

These expressions are substituted into the nonlinear equations (5.1), (5.2) and products of perturbations neglected, to give the linear equations. We obtain, for the linearization of the momentum equation (5.1)

$$\frac{D\delta u}{Dt} + \delta u \frac{\partial \bar{u}}{\partial x} + \frac{\partial \delta\phi}{\partial x} = 0; \tag{5.15}$$

for the linearization of the continuity equation in its original form (5.2)

$$\frac{D\delta\phi}{Dt} + \delta u \frac{\partial \bar{\phi}}{\partial x} + \delta\phi \frac{\partial \bar{u}}{\partial x} + \bar{\phi}\frac{\partial(\delta u)}{\partial x} = 0; \tag{5.16}$$

and for the linearization of the continuity equation in its logarithmic form (5.4)

$$\frac{D}{Dt}\Big(\frac{\delta\phi}{\bar{\phi}}\Big) + \delta u \frac{\partial(\ln\bar{\phi})}{\partial x} + \frac{\partial(\delta u)}{\partial x} = 0. \tag{5.17}$$

The material derivative D/Dt is defined as in (5.3), but using the linearization state wind $\bar{u}$. As for the nonlinear model, we treat the logarithmic form of the continuity equation (5.17) in the discrete numerical model developed here, but the alternative form (5.16) is easier to use when deriving analytical properties of the system.

By setting the partial time derivative to zero in (5.15) and (5.16) we can find two steady state solutions, which are equal to the linearizations of the steady state solutions of the nonlinear equations. Thus we have

$$\bar{u}\delta u + \delta\phi = \delta K_1 \tag{5.18}$$

and

$$\bar{u}\delta\phi + \delta u\bar{\phi} = \delta K_2, \tag{5.19}$$

with δK_1 and δK_2 constant.

5.2 The numerical schemes

5.2.1 The nonlinear model

The governing equations we discretize are the momentum equation (5.1) and the logarithmic form of the continuity equation (5.4). Using this form of the continuity equation has the advantage that we avoid having to treat the nonlinear term of the product of the geopotential and divergence seen in (5.2), which can lead to instabilities if extrapolated quantities are used [79]. The scheme we will use is a two-time-level semi-implicit semi-Lagrangian scheme as described in Section 2.4. It is based on the scheme of [83], but with an off-centred time averaging of the forcing terms along the trajectory, as in [74]. The time discretization is thus written

$$\frac{u_a^{n+1} - u_d^n}{\Delta t} + (1-\alpha_1)\left(\frac{\partial \phi}{\partial x} + g\frac{\partial H}{\partial x}\right)_d^n + \alpha_1\left(\frac{\partial \phi}{\partial x} + g\frac{\partial H}{\partial x}\right)_a^{n+1} = 0, \tag{5.20}$$

$$\frac{(\ln\phi)_a^{n+1} - (\ln\phi)_d^n}{\Delta t} + (1-\alpha_2)\left.\frac{\partial u}{\partial x}\right|_d^n + \alpha_2\left.\frac{\partial u}{\partial x}\right|_a^{n+1} = 0, \tag{5.21}$$

where d indicates a value at the departure point and a indicates a value at the arrival point. The coefficients α_1, α_2 are time-weighting parameters chosen to lie in the interval $[\frac{1}{2}, 1]$. This scheme is chosen to match as closely as possible the new integration scheme being developed for the Unified Model at the Met Office [18], [19], which we outline in Chapter 6. It is also similar to the scheme being used operationally in the GEM model of the Canadian Meteorological Centre [16].

The spatial discretization chosen is a staggering of the points on which the variables u and ϕ are held, which is essentially a one-dimensional representation of the Arakawa C-grid being used at the Met Office. The points are regularly spaced such that the distance between neighbouring points holding u and ϕ values is $\frac{\Delta x}{2}$. We identify a general point at which ϕ is evaluated (a ϕ-point) as x_i, where i is an integer. The points either side of it on which u is evaluated (u-points) are written $x_{i-\frac{1}{2}}$ and $x_{i+\frac{1}{2}}$. The grid is defined with N ϕ-points and N u-points and with cyclic

boundary conditions, such that the point ϕ_{N+1} is identical to the point ϕ_1 and $u_{N+\frac{1}{2}}$ is identical to $u_{\frac{1}{2}}$. Interpolation of quantities between u-points and ϕ-points is performed using a linear interpolation. The introduction of such a staggering means that for a general ϕ-point x_i and a general u-point $x_{i+\frac{1}{2}}$ the departure points will differ. Henceforth we indicate the departure point for the ϕ-point using the subscript $d\phi$ and the departure point for a u-point using the subscript du.

We first give an outline of the solution method for the scheme, before writing out all the details needed in order to perform a linearization. We follow a predictor-corrector method, with one prediction step followed by one correction step. The first step is to calculate the departure points x_{du} and $x_{d\phi}$ for each of the u and ϕ gridpoints at time level $n+1$. This allows us to calculate the time level n terms in (5.20) and (5.21). Thus we obtain

$$\begin{aligned} u_{i+\frac{1}{2}}^{n+1} \quad + \quad & \alpha_1 \Delta t \left(\left. \frac{\partial \phi}{\partial x} \right|_{i+\frac{1}{2}}^{n+1} + g \left. \frac{\partial H}{\partial x} \right|_{i+\frac{1}{2}} \right) \\ & = u_{du}^n - (1-\alpha_1)\Delta t \left(\left. \frac{\partial \phi}{\partial x} \right|_{du}^{n} + g \left. \frac{\partial H}{\partial x} \right|_{du} \right), \qquad (5.22) \\ (\ln \phi)_i^{n+1} \quad + \quad & \alpha_2 \Delta t \left. \frac{\partial u}{\partial x} \right|_{i}^{n+1} = \left(\ln \phi - (1-\alpha_2)\Delta t \frac{\partial u}{\partial x} \right)_{d\phi}^{n}, \qquad (5.23) \end{aligned}$$

with all the terms on the right hand sides of (5.22) and (5.23) known. Then after discretizing the derivative terms we are left with a system of coupled linear equations for u and ϕ at time level $n+1$ at all spatial points. These equations can be solved by eliminating u at time level $n+1$ and solving the remaining set of equations for ϕ_i^{n+1} at each ϕ-point x_i. The result can then be substituted back into (5.22) to find the values of $u_{i+\frac{1}{2}}^{n+1}$ for each u-point $x_{i+\frac{1}{2}}$.

The scheme in detail proceeds as follows:

1. First we must find the departure points x_{du}, $x_{d\phi}$ for each of the u-points and ϕ-points at time level $n+1$. We consider the calculation for a general point x_j, where x_j can be either a u-point or a ϕ-point. Then the departure point

x_d can be calculated from

$$x_d = x_j - \alpha_j \tag{5.24}$$

where the displacement α_j is calculated using the iterative procedure introduced in Section 2.4,

$$\alpha_j^{(k+1)} = \Delta t u^*(x_j - \frac{\alpha_j^{(k)}}{2}, t_n + \frac{\Delta t}{2}) \tag{5.25}$$

with $\alpha_j^{(0)} = 0$. The velocity u^* is an estimate of the velocity at the mid-point of the trajectory. In order to estimate the velocity at time $t_n + \Delta t/2$ we use the extrapolation formulae

$$u^*(x_{i+\frac{1}{2}}, t_n + \frac{\Delta t}{2}) = \frac{3}{2}u(x_{i+\frac{1}{2}}, t_n) - \frac{1}{2}u(x_{i+\frac{1}{2}}, t_n - \Delta t) \tag{5.26}$$

at u points and

$$u^*(x_i, t_n + \frac{\Delta t}{2}) = \frac{3}{2}\overline{u}^x(x_i, t_n) - \frac{1}{2}\overline{u}^x(x_i, t_n - \Delta t) \tag{5.27}$$

at ϕ points, with

$$\overline{u}^x(x_i, t_n) = \frac{1}{2}(u(x_{i-\frac{1}{2}}, t_n) + u(x_{i+\frac{1}{2}}, t_n)). \tag{5.28}$$

The evaluation of (5.25) requires u to be calculated at the point $x_j - \alpha_j^{(k)}/2$. This may not lie on a grid point and so the value must be found by interpolation from surrounding grid points. For this step a linear interpolation is used. We set out the details with reference to Figure 5.1. In order to calculate u at $x_m = x_j - \alpha_j^{(k)}/2$, point B in the figure, we need to interpolate between the grid points either side of x_m, which we write x_{j-s-1} and x_{j-s}. The value of s, which will depend on the arrival point index j and the iteration count k, is given by

$$s_j^{(k)} = \mathrm{INT}\left(\frac{\alpha_j^{(k)}}{2\Delta x}\right) \tag{5.29}$$

where INT(x) means the integer value of x. Now define $\gamma_j^{(k)}$ to be the fraction of the grid interval $x_{j-s} - x_{j-s-1}$ which is covered by the length $x_{j-s} - x_m$, so that

$$\gamma_j^{(k)} = -s_j^{(k)} + \frac{\alpha_j^{(k)}}{2\Delta x}. \tag{5.30}$$

Then u at point x_m can be calculated from the linear interpolation formula

$$\begin{aligned} u(m\Delta x, (n+\frac{1}{2})\Delta t) &= \gamma_j^{(k)} u((j - s_j^{(k)} - 1)\Delta x, (n+\frac{1}{2})\Delta t) \\ &+ (1 - \gamma_j^{(k)}) u((j - s_j^{(k)})\Delta x, (n+\frac{1}{2})\Delta t). \end{aligned} \tag{5.31}$$

Having performed K iterations of (5.25) the departure point is situated at $j\Delta x - \alpha_j^{(K)}$. It is normally found that there is no advantage to performing more than two iterations of this part of the solution procedure [79]. We now let

$$p = INT\left(\frac{\alpha_j^{(K)}}{\Delta x}\right) \tag{5.32}$$

and define

$$\beta_j = -p + \left(\frac{\alpha_j^{(K)}}{\Delta x}\right). \tag{5.33}$$

Then the departure point x_d lies between the points x_{j-p-1} and x_{j-p} and is a distance $\beta_j \Delta x$ from the point x_{j-p}, as shown in Figure 5.1. We note here that the INT function used in (5.29) and (5.32) is non-differentiable. Thus it will require special attention when we look at the tangent linear model.

2. Having found the departure points, we can calculate the right hand sides of (5.22) and (5.23). We first define the variables X, Y,

$$X = u - (1-\alpha_1)\Delta t\left(\frac{\partial \phi}{\partial x} + g\frac{\partial H}{\partial x}\right), \tag{5.34}$$

$$Y = \ln\phi - (1-\alpha_2)\Delta t\frac{\partial u}{\partial x}, \tag{5.35}$$

where the derivative terms are approximated using the standard centred differences

$$\left.\frac{\partial \phi}{\partial x}\right|_{i+\frac{1}{2}} \approx \frac{\phi_{i+1} - \phi_i}{\Delta x}, \tag{5.36}$$

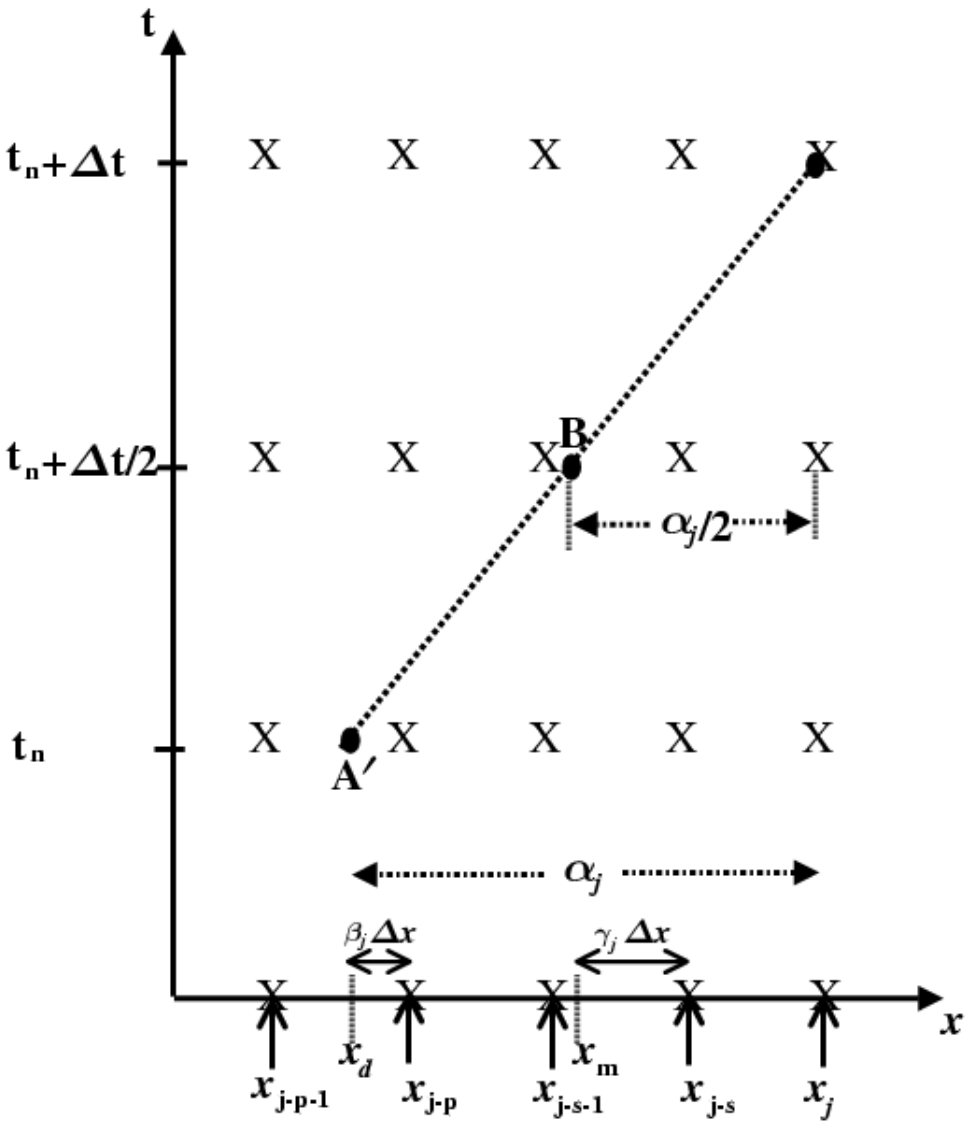

Figure 5.1: A schematic representation of two-time-level semi-Lagrangian advection.

$$\left.\frac{\partial u}{\partial x}\right|_i \approx \frac{u_{i+\frac{1}{2}} - u_{i-\frac{1}{2}}}{\Delta x}. \tag{5.37}$$

Equations (5.22) and (5.23) thus become

$$u_{i+\frac{1}{2}}^{n+1} + \alpha_1 \Delta t \left(\left.\frac{\partial \phi}{\partial x}\right|_{i+\frac{1}{2}}^{n+1} + g \left.\frac{\partial H}{\partial x}\right|_{i+\frac{1}{2}} \right) = X_{du}^n, \tag{5.38}$$

$$(\ln \phi)_i^{n+1} + \alpha_2 \Delta t \left.\frac{\partial u}{\partial x}\right|_i^{n+1} = Y_{d\phi}^n. \tag{5.39}$$

The variables X and Y are calculated at gridpoints at time level n, defining X on u-points and Y on ϕ-points. The values at the departure points can then be calculated from these values by interpolation. As discussed in Section 2.4 a cubic interpolation is often used and here we use the cubic Lagrange formula. Hence we obtain

$$\begin{aligned}
X_{du}^n &= (-\frac{1}{6}\beta_{i+\frac{1}{2}} + \frac{1}{6}\beta_{i+\frac{1}{2}}^3) X_{i+\frac{1}{2}-p-2}^n + (\beta + \frac{1}{2}\beta_{i+\frac{1}{2}}^2 - \frac{1}{2}\beta_{i+\frac{1}{2}}^3) X_{i+\frac{1}{2}-p-1}^n \\
&+ (1 - \frac{1}{2}\beta_{i+\frac{1}{2}} - \beta_{i+\frac{1}{2}}^2 + \frac{1}{2}\beta_{i+\frac{1}{2}}^3) X_{i+\frac{1}{2}-p}^n \\
&+ (-\frac{1}{3}\beta_{i+\frac{1}{2}} + \frac{1}{2}\beta_{i+\frac{1}{2}}^2 - \frac{1}{6}\beta_{i+\frac{1}{2}}^3) X_{i+\frac{1}{2}-p+1}^n, \qquad (5.40) \\
Y_{d\phi}^n &= (-\frac{1}{6}\beta_i + \frac{1}{6}\beta_i^3) Y_{i-p-2}^n + (\beta_i + \frac{1}{2}\beta_i^2 - \frac{1}{2}\beta_i^3) Y_{i-p-1}^n \\
&+ (1 - \frac{1}{2}\beta_i - \beta_i^2 + \frac{1}{2}\beta_i^3) Y_{i-p}^n \\
&+ (-\frac{1}{3}\beta_i + \frac{1}{2}\beta_i^2 - \frac{1}{6}\beta_i^3) Y_{i-p+1}^n, \qquad (5.41)
\end{aligned}$$

where the values of β for each point are defined by (5.33). We note that the variable p will also depend on the coordinates of the arrival point by means of (5.32), but this dependence is omitted for clarity in (5.40) and (5.41).

3. The next step is to solve the implicit part of the procedure. From (5.38) and (5.39) we have two sets of N equations

$$u_{i+\frac{1}{2}}^{n+1} + \alpha_1 \Delta t \left(\left. \frac{\partial \phi}{\partial x} \right|_{i+\frac{1}{2}}^{n+1} + g \left. \frac{\partial H}{\partial x} \right|_{i+\frac{1}{2}} \right) = X_{du}^n, \tag{5.42}$$

$$(\ln \phi)_i^{n+1} + \alpha_2 \Delta t \left. \frac{\partial u}{\partial x} \right|_i^{n+1} = Y_{d\phi}^n, \tag{5.43}$$

valid for all values $i = 1, \ldots, N$, with periodic boundary conditions closing the system. Then eliminating $u_{i+\frac{1}{2}}$ for all values of i we obtain the set of equations

$$-\frac{\alpha_1 \alpha_2 \Delta t^2}{\Delta x^2} \phi_{i+1}^{n+1} + 2\frac{\alpha_1 \alpha_2 \Delta t^2}{\Delta x^2} \phi_i^{n+1} - \frac{\alpha_1 \alpha_2 \Delta t^2}{\Delta x^2} \phi_{i-1}^{n+1} + (\ln \phi)_i^{n+1} = R_i, \tag{5.44}$$

with

$$R_i = Y_{d\phi}^n - \frac{\alpha_2 \Delta t}{\Delta x} [\tilde{X}_{i+\frac{1}{2}}^n - \tilde{X}_{i-\frac{1}{2}}^n] \tag{5.45}$$

and

$$\tilde{X}_{i+\frac{1}{2}}^n = X_{du}^n - \alpha_1 \Delta t g \left. \frac{\partial H}{\partial x} \right|_{i+\frac{1}{2}}. \tag{5.46}$$

The equation (5.44) is a discretization of an elliptic equation on the domain and is weakly nonlinear through the presence of the $\ln \phi$ term on the left hand side.

4. A suitable procedure must now be obtained to solve the system (5.44) for all values of ϕ_i at time level $n+1$. The method we choose is to apply a fixed point iteration, solving a linear problem on each iteration. A natural way of choosing such an iteration would be to consider a scheme such as

$$-\frac{\alpha_1 \alpha_2 \Delta t^2}{\Delta x^2} \phi_{i+1}^{(m)} + 2\frac{\alpha_1 \alpha_2 \Delta t^2}{\Delta x^2} \phi_i^{(m)} - \frac{\alpha_1 \alpha_2 \Delta t^2}{\Delta x^2} \phi_{i-1}^{(m)} = R_i - (\ln \phi)_i^{(m-1)}, \tag{5.47}$$

where the superscript m is the iteration counter. However the tridiagonal matrix given by left hand side of this equation is singular and so this iteration is not well-defined.

To obtain a suitable linear equation to iterate we shift the solution about a reference state Φ_{ref} which is constant in time and space. We write

$$\phi_i^{n+1} = \Phi_{ref} + \phi_i' \tag{5.48}$$

and put

$$C = \frac{\alpha_1 \alpha_2 \Delta t^2}{\Delta x^2}. \tag{5.49}$$

Then substituting into (5.44) and moving the nonlinear term to the right hand side we have

$$-C\phi'_{i+1} + 2C\phi'_i - C\phi'_{i-1} = R_i - \ln(\Phi_{ref} + \phi'_i). \tag{5.50}$$

We now add a term ϕ'_i/Φ_{ref} to both sides of (5.50) to obtain

$$-C\phi'_{i+1} + \Big(2C + \frac{1}{\Phi_{ref}}\Big)\phi'_i - C\phi'_{i-1} = R_i - \ln(\Phi_{ref} + \phi'_i) + \frac{\phi'_i}{\Phi_{ref}}. \tag{5.51}$$

We note that this equation is mathematically equivalent to the original equation (5.44). However the left hand side now consists of a strictly diagonally dominant tridiagonal matrix and is therefore invertible. Hence we can successively solve the series of equations

$$\begin{aligned} -C{\phi'_{i+1}}^{(m+1)} \quad &+ \quad \Big(2C + \frac{1}{\Phi_{ref}}\Big){\phi'_i}^{(m+1)} - C{\phi'_{i-1}}^{(m+1)} \\ &= \quad R_i - \ln(\Phi_{ref} + {\phi'_i}^{(m)}) + \frac{{\phi'_i}^{(m)}}{\Phi_{ref}}, \end{aligned} \tag{5.52}$$

where m is the iteration count and ${\phi_i}'^{(0)} = 0$ for all i. On each iteration we apply a direct solution method to solve the linear equation using the solver of Appendix A.2 of [21]. The iteration (5.52) is a fixed point iteration which we have designed for this particular model. We show in Appendix A that it converges to the solution of (5.44) provided that

$$|\phi'| < \frac{\Phi_{ref}}{2}. \tag{5.53}$$

The iteration is repeated until (5.44) is satisfied to some specified tolerance. Assuming that this occurs after M iterations we obtain an updated value of ϕ from

$$\phi_i^{n+1} = \Phi_{ref} + {\phi'_i}^{(M)}. \tag{5.54}$$

5. As a final step we use these new values of ϕ_i to calculate values of u at each grid point at the new time level from (5.38), thus completing one time step of the scheme.

5.2.2 The tangent linear model

The normal procedure to obtain a tangent linear model is to linearize directly the source code of the nonlinear model, and this is the practice which we also follow. However, to enable analysis of the scheme produced in this way, it is instructive to write out the equivalent scheme that this produces. We do this by linearizing the discrete nonlinear scheme described in Section 5.2.1. We first set

$$\begin{aligned} u^n_{i+\frac{1}{2}} &= \bar{u}^n_{i+\frac{1}{2}} + \delta u^n_{i+\frac{1}{2}}, \\ \phi^n_i &= \bar{\phi}^n_i + \delta \phi^n_i, \end{aligned} \tag{5.55}$$

where $\bar{u}^n_{i+\frac{1}{2}}, \bar{\phi}^n_i$ are solutions of the discrete nonlinear model at time level n. The linearization is then obtained by substituting these expressions into the nonlinear scheme and neglecting products of perturbations. We now derive the discrete equations this produces for each stage of the model solution procedure.

1. The first stage is the linearization of the departure point calculation. We show only the calculation for u-points, since that for ϕ-points follows the same pattern with some extra horizontal averaging. The scheme for the nonlinear model can be summarized by the three steps

$$s^{(k)}_j = \mathrm{INT}\left(\frac{\alpha^{(k)}_j}{2\Delta x}\right), \tag{5.56}$$

$$\gamma^{(k)}_j = -s^{(k)}_j + \frac{\alpha^{(k)}_j}{2\Delta x}, \tag{5.57}$$

$$
\begin{aligned}
\alpha_j^{(k+1)} &= \Delta t\left[\frac{3}{2}\left(\gamma_j^{(k)}u((j-s_j^{(k)}-1)\Delta x, n\Delta t)\right.\right.\\
&\quad \left.+(1-\gamma_j^{(k)})u((j-s_j^{(k)})\Delta x, n\Delta t)\right)\\
&- \frac{1}{2}\left(\gamma_j^{(k)}u((j-s_j^{(k)}-1)\Delta x, (n-1)\Delta t)\right.\\
&\quad \left.\left.+(1-\gamma_j^{(k)})u((j-s_j^{(k)})\Delta x, (n-1)\Delta t)\right)\right]. \qquad (5.58)
\end{aligned}
$$

The equations resulting from a direct linearization of this discrete scheme are therefore as follows.

$$
\delta s_j^{(k)} = 0, \qquad (5.59)
$$

since the linearization necessarily assumes that the grid interval for interpolation processes does not change. Then we have

$$
\delta\gamma_j^{(k)} = \frac{\delta\alpha_j^{(k)}}{2\Delta x} \qquad (5.60)
$$

and

$$
\begin{aligned}
\delta\alpha_j^{(k+1)} &= \Delta t\left[\frac{3}{2}\left(\bar{\gamma}_j^{(k)}\delta u((j-\bar{s}_j^{(k)}-1)\Delta x, n\Delta t)\right.\right.\\
&\quad \left.+\ (1-\bar{\gamma}_j^{(k)})\delta u((j-\bar{s}_j^{(k)})\Delta x, n\Delta t)\right)\\
&- \frac{1}{2}\left(\bar{\gamma}_j^{(k)}\delta u((j-\bar{s}_j^{(k)}-1)\Delta x, (n-1)\Delta t)\right.\\
&\quad \left.\left.+\ (1-\bar{\gamma}_j^{(k)})\delta u((j-\bar{s}_j^{(k)})\Delta x, (n-1)\Delta t)\right)\right]\\
&+ \Delta t\left[\frac{3}{2}\left(\delta\gamma_j^{(k)}\bar{u}((j-\bar{s}_j^{(k)}-1)\Delta x, n\Delta t)\right.\right.\\
&\quad \left.-\delta\gamma_j^{(k)}\bar{u}((j-\bar{s}_j^{(k)})\Delta x, n\Delta t)\right)\\
&- \frac{1}{2}\left(\delta\gamma_j^{(k)}\bar{u}((j-\bar{s}_j^{(k)}-1)\Delta x, (n-1)\Delta t)\right.\\
&\quad \left.\left.-\delta\gamma_j^{(k)}\bar{u}((j-\bar{s}_j^{(k)})\Delta x, (n-1)\Delta t)\right)\right], \qquad (5.61)
\end{aligned}
$$

with $\delta\alpha_j^{(0)} = 0$. We note here that because we are taking a small predetermined number of iterations, usually two or three, we can consider this as just a two- or three-step calculation and so linearize each iteration separately as if they were just different parts of the numerical scheme. This allows the linearization to be performed at the level of the model source code and is the procedure often followed in deriving the linearization of this part of a semi-Lagrangian scheme in meteorological models [64], [82]. However, when we come to the iterative solution of the elliptic equation later, we iterate to some desired convergence criteria and the number of iterations may differ between time steps. In that case we use a different method to find the tangent linear model.

Now we assume that the perturbed departure point lies in the same grid interval as the original departure point, and so $\delta p = 0$. As discussed in Section 3.2 this assumption will ensure a correct tangent linear model for infinitesimal perturbations if and only if for a piecewise-continuous interpolation function the first derivative of the interpolating function is continuous, as shown in [65]. For the cubic Lagrange scheme which we are using this condition does not hold. However the authors of [65] state that for this scheme the error in the linearization is not large. Then after K iterations of this calculation we calculate the linearization of (5.33)

$$\delta\beta_j = \frac{\delta\alpha_j^{(K)}}{\Delta x}. \tag{5.62}$$

2. The next stage is to calculate perturbations to the expressions of known terms X, Y. We linearize (5.34) and (5.35) to obtain

$$\delta X_{i+\frac{1}{2}} = \delta u_{i+\frac{1}{2}} - (1-\alpha_1)\,\Delta t \frac{\partial \delta\phi}{\partial x}\bigg|_{i+\frac{1}{2}}, \tag{5.63}$$

$$\delta Y_i = \frac{\delta\phi}{\bar{\phi}} - (1-\alpha_2)\Delta t \frac{\partial \delta u}{\partial x}. \tag{5.64}$$

Then using these expressions we can evaluate the linearization of the cubic

Lagrange interpolation to the departure points. Thus from (5.40) we have

$$\begin{aligned}
\delta X^n_{du} &= (-\frac{1}{6}\beta_{i+\frac{1}{2}} + \frac{1}{6}\beta^3_{i+\frac{1}{2}})\delta X^n_{i+\frac{1}{2}-p-2} + (\beta_{i+\frac{1}{2}} + \frac{1}{2}\beta^2_{i+\frac{1}{2}} - \frac{1}{2}\beta^3_{i+\frac{1}{2}})\delta X^n_{i+\frac{1}{2}-p-1} \\
&+ (1 - \frac{1}{2}\beta_{i+\frac{1}{2}} - \beta^2_{i+\frac{1}{2}} + \frac{1}{2}\beta^3_{i+\frac{1}{2}})\delta X^n_{i+\frac{1}{2}-p} \\
&+ (-\frac{1}{3}\beta_{i+\frac{1}{2}} + \frac{1}{2}\beta^2_{i+\frac{1}{2}} - \frac{1}{6}\beta^3_{i+\frac{1}{2}})\delta X^n_{i+\frac{1}{2}-p+1} \\
&+ (-\frac{1}{6} + \frac{1}{2}\beta^2_{i+\frac{1}{2}})\delta\beta_{i+\frac{1}{2}}\bar{X}^n_{i+\frac{1}{2}-p-2} + (1 + \beta_{i+\frac{1}{2}} - \frac{3}{2}\beta^2_{i+\frac{1}{2}})\delta\beta_{i+\frac{1}{2}}\bar{X}^n_{i+\frac{1}{2}-p-1} \\
&+ (-\frac{1}{2} - 2\beta_{i+\frac{1}{2}} + \frac{3}{2}\beta^2_{i+\frac{1}{2}})\delta\beta_{i+\frac{1}{2}}\bar{X}^n_{i+\frac{1}{2}-p} \\
&+ (-\frac{1}{3} + \beta_{i+\frac{1}{2}} - \frac{1}{2}\beta^2_{i+\frac{1}{2}})\delta\beta_{i+\frac{1}{2}}\bar{X}^n_{i+\frac{1}{2}-p+1} \qquad (5.65)
\end{aligned}$$

and from (5.41) we have

$$\begin{aligned}
\delta Y^n_{d\phi} &= (-\frac{1}{6}\beta_i + \frac{1}{6}\beta^3_i)\delta Y^n_{i-p-2} + (\beta_i + \frac{1}{2}\beta^2_i - \frac{1}{2}\beta^3_i)\delta Y^n_{i-p-1} \\
&+ (1 - \frac{1}{2}\beta_i - \beta^2_i + \frac{1}{2}\beta^3_i)\delta Y^n_{i-p} + (-\frac{1}{3}\beta_i + \frac{1}{2}\beta^2_i - \frac{1}{6}\beta^3_i)\delta Y^n_{i-p+1} \\
&+ (-\frac{1}{6} + \frac{1}{2}\beta^2_i)\delta\beta_i\bar{Y}^n_{i-p-2} + (1 + \beta_i - \frac{3}{2}\beta^2_i)\delta\beta_i\bar{Y}^n_{i-p-1} \\
&+ (-\frac{1}{2} - 2\beta_i + \frac{3}{2}\beta^2_i)\delta\beta_i\bar{Y}^n_{i-p} + (-\frac{1}{3} + \beta_i - \frac{1}{2}\beta^2_i)\delta\beta_i\bar{Y}^n_{i-p+1}. \qquad (5.66)
\end{aligned}$$

The values of p and β in (5.65) and (5.66) are in fact linearization state values defined by (5.32) and (5.33), but the overbars have been omitted for clarity. The value of $\delta\beta$ is that calculated from (5.62). Finally for this part of the scheme we linearize (5.46) to obtain

$$\delta\tilde{X}^n_{i+\frac{1}{2}} = \delta X^n_{du}. \qquad (5.67)$$

We note that the perturbation to X^n_{du}, written δX^n_{du}, is not equal to the per-

turbation of X evaluated at the point X_{du} and similarly for $\delta Y^n_{d\phi}$. We define

$$\begin{aligned}
(\delta X)^n_{du} &= (-\frac{1}{6}\beta_{i+\frac{1}{2}} + \frac{1}{6}\beta^3_{i+\frac{1}{2}})\delta X^n_{i+\frac{1}{2}-p-2} \\
&+ (\beta_{i+\frac{1}{2}} + \frac{1}{2}\beta^2_{i+\frac{1}{2}} - \frac{1}{2}\beta^3_{i+\frac{1}{2}})\delta X^n_{i+\frac{1}{2}-p-1} \\
&+ (1 - \frac{1}{2}\beta_{i+\frac{1}{2}} - \beta^2_{i+\frac{1}{2}} + \frac{1}{2}\beta^3_{i+\frac{1}{2}})\delta X^n_{i+\frac{1}{2}-p} \\
&+ (-\frac{1}{3}\beta_{i+\frac{1}{2}} + \frac{1}{2}\beta^2_{i+\frac{1}{2}} - \frac{1}{6}\beta^3_{i+\frac{1}{2}})\delta X^n_{i+\frac{1}{2}-p+1}, \qquad (5.68) \\
(\delta Y)^n_{d\phi} &= (-\frac{1}{6}\beta_i + \frac{1}{6}\beta^3_i)\delta Y^n_{i-p-2} + (\beta_i + \frac{1}{2}\beta^2_i - \frac{1}{2}\beta^3_i)\delta Y^n_{i-p-1} \\
&+ (1 - \frac{1}{2}\beta_i - \beta^2_i + \frac{1}{2}\beta^3_i)\delta Y^n_{i-p} \\
&+ (-\frac{1}{3}\beta_i + \frac{1}{2}\beta^2_i - \frac{1}{6}\beta^3_i)\delta Y^n_{i-p+1} \qquad (5.69)
\end{aligned}$$

and put

$$\delta u^* = \frac{\delta \alpha^{(K)}_j}{\Delta t}. \qquad (5.70)$$

Here δu^* is the perturbation to the estimate of the velocity at the mid-point of the trajectory. Then the equations for δX^n_{du} and $\delta Y^n_{d\phi}$ can be written

$$\begin{aligned}
\delta X^n_{du} &= (\delta X)^n_{du} + \frac{\Delta t}{\Delta x}\delta u^* \left(\bar{u} - (1-\alpha_1)\Delta t \left(\frac{\partial \bar{\phi}}{\partial x} + g\frac{\partial H}{\partial x}\right)\right)^n_{d'}, \qquad (5.71) \\
\delta Y^n_{d\phi} &= (\delta Y)^n_{d\phi} + \frac{\Delta t}{\Delta x}\delta u^* \left(\ln \bar{\phi} - (1-\alpha_2)\Delta t \frac{\partial \bar{u}}{\partial x}\right)^n_{d'}, \qquad (5.72)
\end{aligned}$$

where d' indicates not the perturbed departure point, but the linearization of the interpolation scheme. A Taylor series expansion shows that this linearization divided by Δx is an $O(\Delta x)$ approximation to the first derivative $\partial/\partial x$. Then also noting that $\delta u^* = \delta u^n_{du} + O(\Delta t)$ we can consider (5.71) and (5.72) as the equations

$$\begin{aligned}
\delta X^n_{du} &= (\delta X)^n_{du} + \Delta t \delta u^n_{du} \left(\frac{\partial \bar{u}}{\partial x} - (1-\alpha_1)\Delta t \left(\frac{\partial^2 \bar{\phi}}{\partial x^2} + g\frac{\partial^2 H}{\partial x^2}\right)\right)^n_{du} \\
&+ O(\Delta t \Delta x), \qquad (5.73) \\
\delta Y^n_{d\phi} &= (\delta Y)^n_{d\phi} + \Delta t \delta u^n_{du} \left(\frac{\partial \ln \bar{\phi}}{\partial x} - (1-\alpha_2)\Delta t \frac{\partial^2 \bar{u}}{\partial x^2}\right)^n_{d\phi} \\
&+ O(\Delta t \Delta x). \qquad (5.74)
\end{aligned}$$

We note that the first term of each bracket on the right hand sides of (5.73) and (5.74) also appear in the analytical linear equations (5.15) and (5.17). However the second term of each bracket consisting of second derivatives of the linearization state do not appear in the analytical equations and thus do not appear in the perturbation forecast models. These terms arise from the perturbation to the departure point calculation. We see later in Section 5.3.3 that these terms contribute to the first order part of the truncation error for this scheme.

3. The next part of the nonlinear scheme is the iterative solution of the discrete elliptic equation. In order to find the tangent linear model we do not linearize this iterative procedure, but instead linearize the discrete equation of the non-linear model and then solve this linear equation, thus following the normal procedure of automatic differentiation [5]. The equation which we solve in the nonlinear model is (5.51), but since this is mathematically equivalent to the original form (5.44), a linearization of the latter is sufficient. Linearizing (5.44) we obtain

$$-C\delta\phi_{i+1}^{n+1} + \left(2C + \frac{1}{\bar{\phi}_i^{n+1}}\right)\delta\phi_i^{n+1} - C\delta\phi_{i-1}^{n+1} = \delta R_i, \tag{5.75}$$

with C defined by (5.49) and

$$\delta R_i = \delta Y_{d\phi}^n - \frac{\alpha_2 \Delta t}{\Delta x}[\delta\tilde{X}_{i+\frac{1}{2}}^n - \delta\tilde{X}_{i-\frac{1}{2}}^n]. \tag{5.76}$$

This is a linear equation which can be solved directly for $\delta\phi_i^{n+1}$ at all points x_i. Hence we see that for this system an iterative procedure is not needed in the tangent linear model.

4. From the updated values of $\delta\phi_i$, the time level $n+1$ values of $\delta u_{i+\frac{1}{2}}$ at each point $x_{i+\frac{1}{2}}$ are then found from the linearization of (5.38)

$$\delta u_{i+\frac{1}{2}}^{n+1} = \delta\tilde{X}_{i+\frac{1}{2}}^n - \alpha_1 \Delta t \frac{(\delta\phi_{i+1}^{n+1} - \delta\phi_i^{n+1})}{\Delta x}. \tag{5.77}$$

This completes one time step of the tangent linear model.

5.2.3 The perturbation forecast model

To develop the perturbation forecast model we begin by taking the continuous linearized equations (5.15), (5.17) and seek some suitable discretization, following as closely as possible the numerical scheme of the nonlinear model. The most natural method of treating these equations in a semi-implicit semi-Lagrangian context is to treat all the nonadvective terms as off-centred averages along the trajectory. Thus we propose the scheme

$$\begin{aligned}\frac{1}{\Delta t}\left(\delta u_{i+\frac{1}{2}}^{n+1}-\delta u_{du}^{n}\right) &+ (1-\alpha_1)\frac{\partial\delta\phi}{\partial x}\bigg|_{du}^{n}+\alpha_1\frac{\partial\delta\phi}{\partial x}\bigg|_{i+\frac{1}{2}}^{n+1}\\ &+ (1-\alpha_3)\left(\delta u\frac{\partial\bar{u}}{\partial x}\right)_{du}^{n}+\alpha_3\left(\delta u\frac{\partial\bar{u}}{\partial x}\right)_{i+\frac{1}{2}}^{n+1}=0, \quad (5.78)\end{aligned}$$

$$\begin{aligned}&\frac{1}{\Delta t}\left(\left(\frac{\delta\phi}{\bar{\phi}}\right)_i^{n+1}-\left(\frac{\delta\phi}{\bar{\phi}}\right)_{d\phi}^{n}\right)+(1-\alpha_2)\frac{\partial\delta u}{\partial x}\bigg|_{d\phi}^{n}+\alpha_2\frac{\partial\delta u}{\partial x}\bigg|_{i}^{n+1}\\ +\;&(1-\alpha_4)\left(\overline{(\delta u)}^{x}\frac{\partial(\ln\bar{\phi})}{\partial x}\right)_{d\phi}^{n}+\alpha_4\left(\overline{(\delta u)}^{x}\frac{\partial(\ln\bar{\phi})}{\partial x}\right)_{i}^{n+1}=0, \quad (5.79)\end{aligned}$$

where

$$(\overline{\delta u}^{x})_i^n=\frac{1}{2}(\delta u_{i-\frac{1}{2}}^n+\delta u_{i+\frac{1}{2}}^n) \quad (5.80)$$

and α_i are time-weighting coefficients for $i=1,\ldots,4$. The finite difference form of the derivatives $\partial\delta\phi/\partial x$ in (5.78) and $\partial\delta u/\partial x$ in (5.79) are defined by (5.36) and (5.37), as for the nonlinear model. For the perturbation forecast model we also require the approximations

$$\frac{\partial\bar{u}}{\partial x}\bigg|_{i+\frac{1}{2}} \approx \frac{\bar{u}_{i+\frac{3}{2}}-\bar{u}_{i-\frac{1}{2}}}{2\Delta x}, \quad (5.81)$$

$$\frac{\partial(\ln\bar{\phi})}{\partial x}\bigg|_{i} \approx \frac{(\ln\bar{\phi})_{i+1}-(\ln\bar{\phi})_{i-1}}{2\Delta x}. \quad (5.82)$$

The outline of the scheme is very similar to that of the nonlinear model.

1. We first calculate the departure points. Since the semi-Lagrangian part of our scheme is only considering advection by the linearization state wind, these departure points and hence their derivation is exactly the same as in the nonlinear model.

2. The next step is to calculate all the time level n terms in (5.78) and (5.79). We first define

$$\begin{aligned} \delta X &= \delta u - (1-\alpha_1)\Delta t \frac{\partial \delta\phi}{\partial x} - (1-\alpha_3)\Delta t \delta u \frac{\partial \bar{u}}{\partial x}, && (5.83) \\ \delta Y &= \frac{\delta\phi}{\bar{\phi}} - (1-\alpha_2)\Delta t \frac{\partial \delta u}{\partial x} \\ &\quad -(1-\alpha_4)\Delta t (\overline{\delta u}^x) \frac{\partial (\ln \bar{\phi})}{\partial x} && (5.84) \end{aligned}$$

   in a similar way to X and Y in equations (5.34) and (5.35) of the nonlinear model. Then the values δX^n_{du}, $\delta Y^n_{d\phi}$ at the departure points x_{du}, $x_{d\phi}$ are calculated by interpolation from nearby gridpoints using the cubic Lagrange interpolation formulae (5.40), (5.41) respectively.

3. Having calculated the time level n terms we substitute into (5.78), (5.79) to obtain the implicit system

$$\begin{aligned} \delta u^{n+1}_{i+\frac{1}{2}} &+ \alpha_1 \Delta t \left.\frac{\partial \delta\phi}{\partial x}\right|^{n+1}_{i+\frac{1}{2}} + \alpha_3 \Delta t \delta u^{n+1}_{i+\frac{1}{2}} \left.\frac{\partial u}{\partial x}\right|^{n+1}_{i+\frac{1}{2}} \\ &= \delta X^n_{du}, && (5.85) \\ \left(\frac{\delta\phi}{\bar{\phi}}\right)^{n+1}_i &+ \alpha_2 \Delta t \left.\frac{\partial \delta u}{\partial x}\right|^{n+1}_{i} + \alpha_4 \Delta t (\overline{\delta u}^x)^{n+1}_i \left.\frac{\partial (\ln \bar{\phi})}{\partial x}\right|^{n+1}_{i} \\ &= \delta Y^n_{d\phi}. && (5.86) \end{aligned}$$

   In order to solve this system we wish to eliminate $\delta u^{n+1}_{i+\frac{1}{2}}$ for all values of i to form a system of equations for $\delta\phi^{n+1}_i$. We first rewrite (5.85)

$$\delta u^{n+1}_{i+\frac{1}{2}} \left(1 + \alpha_3 \Delta t \left.\frac{\partial \bar{u}}{\partial x}\right|^{n+1}_{i+\frac{1}{2}}\right) = \delta X^n_{du} - \alpha_1 \Delta t \left.\frac{\partial \delta\phi}{\partial x}\right|^{n+1}_{i+\frac{1}{2}}. \qquad (5.87)$$

We can eliminate δu provided that

$$1 + \alpha_3 \Delta t \frac{\partial \bar{u}}{\partial x}\bigg|_{i+\frac{1}{2}}^{n+1} \neq 0. \tag{5.88}$$

This leads to a restriction on the time step

$$\Delta t < \frac{1}{\alpha_3 |\partial \bar{u}/\partial x|}, \tag{5.89}$$

This may seem to be an extra restriction which is not present in the tangent linear model. However, we recall from Section 2.4 that the iterative procedure by which we calculate the departure point itself imposes the restriction $\Delta t \max |\partial \bar{u}/\partial x| < 1$. Hence for values of α_3 in the range $[0, 1]$, (5.89) must hold in any case. We define

$$\bar{Z}_{i+\frac{1}{2}} = \left(1 + \alpha_3 \Delta t \frac{(\bar{u}_{j+\frac{3}{2}} - \bar{u}_{j-\frac{1}{2}})}{2\Delta x}\right)^{-1}, \tag{5.90}$$

so that (5.87) gives

$$\delta u_{i+\frac{1}{2}}^{n+1} = \bar{Z}_{i+\frac{1}{2}}^{n+1} \left(\delta X_{du}^n - \alpha_1 \Delta t \left.\frac{\partial \delta\phi}{\partial x}\right|_{i+\frac{1}{2}}^{n+1}\right). \tag{5.91}$$

Then substituting this expression into (5.86) and rearranging, we obtain the system of linear equations

$$\begin{aligned} - \quad & C_{2i+\frac{1}{2}}(C_{1i} + C_3)\delta\phi_{i+1}^{n+1} \\ + \quad & \left[\frac{1}{\phi_i^{n+1}} + C_{2i-\frac{1}{2}}(-C_{1i} + C_3) + C_{2i+\frac{1}{2}}(C_{1i} + C_3)\right]\delta\phi_i^{n+1} \\ + \quad & C_{2i-\frac{1}{2}}(C_{1i} - C_3)\delta\phi_{i-1}^{n+1} \\ & = \delta R_i, \end{aligned} \tag{5.92}$$

with

$$\begin{aligned}
C_{1i} &= \frac{\alpha_4 \Delta t}{2} \frac{\partial (\ln \bar{\phi})_i^{n+1}}{\partial x}, \\
C_{2_{i+\frac{1}{2}}} &= \frac{\alpha_1 \Delta t}{\Delta x} \bar{Z}_{i+\frac{1}{2}}^{n+1}, \\
C_3 &= \frac{\alpha_2 \Delta t}{\Delta x}, \\
\delta R_i &= \delta Y_j - C_{1j}(\bar{Z}_{j-\frac{1}{2}}^{n+1} \delta X_{j-\frac{1}{2}}^n + \bar{Z}_{j+\frac{1}{2}}^{n+1} \delta X_{j+\frac{1}{2}}^n) \\
&\quad -C_3(\bar{Z}_{j+\frac{1}{2}}^{n+1} \delta X_{j+\frac{1}{2}}^n - \bar{Z}_{j-\frac{1}{2}}^{n+1} \delta X_{j-\frac{1}{2}}^n).
\end{aligned}$$

The system (5.92) is represented by a strictly diagonally dominant tridiagonal matrix and so can be directly solved for all values of $\delta \phi_i^{n+1}$ using the same solver as in the nonlinear model.

4. The result of the previous step is then substituted into (5.91) to calculate the updated values $\delta u_{i+\frac{1}{2}}^{n+1}$ and so complete one time step of the perturbation forecast model.

5.2.4 A second version of the perturbation forecast model

One possible difficulty with the perturbation forecast model scheme discussed in Section 5.2.3 is in the treatment of the term arising from the linearization of advection, in which the perturbation wind multiplies the gradient of the linearization state field. In the analytical linear equations (5.15), (5.17) we have the terms

$$\delta u \frac{\partial \bar{u}}{\partial x}, \qquad \delta u \frac{\partial (\ln \bar{\phi})}{\partial x}. \tag{5.93}$$

The averaging of these terms along the trajectory as in the scheme of the first perturbation forecast model (5.78), (5.79) couples the equations in a way that may cause difficulties in a three-dimensional model. In order to avoid this coupling, we consider an alternative scheme for the perturbation forecast model, which matches more closely the scheme implemented at the Met Office. On the assumption that

the perturbation wind is likely to be small, we treat this term explicitly and in an Eulerian fashion. Hence for both equations the term is evaluated at the arrival point, but at time level n. Thus we have the scheme

$$\begin{aligned}\frac{1}{\Delta t}\left(\delta u^{n+1}_{i+\frac{1}{2}} - \delta u^{n}_{du}\right) &+ \left(\delta u \frac{\partial \bar{u}}{\partial x}\right)^{n}_{i+\frac{1}{2}} \\ &+ (1-\alpha_1)\frac{\partial \delta\phi}{\partial x}\bigg|^{n}_{du} + \alpha_1 \frac{\partial \delta\phi}{\partial x}\bigg|^{n+1}_{i+\frac{1}{2}} = 0, \end{aligned} \tag{5.94}$$

$$\begin{aligned}\frac{1}{\Delta t}\left(\left(\frac{\delta\phi}{\bar{\phi}}\right)^{n+1}_{i} - \left(\frac{\delta\phi}{\bar{\phi}}\right)^{n}_{d\phi}\right) &+ \left(\overline{\delta u}^{x}\frac{\partial(\ln\bar{\phi})}{\partial x}\right)^{n}_{i} \\ &+ (1-\alpha_2)\frac{\partial \delta u}{\partial x}\bigg|^{n}_{d\phi} + \alpha_2 \frac{\partial \delta u}{\partial x}\bigg|^{n+1}_{i} = 0, \end{aligned} \tag{5.95}$$

with $\overline{\delta u}^{x}$ defined by (5.80). The method for solving this scheme is very similar to the previous section, with just a few terms changed. The departure point calculation is the same, from which we calculate the known terms

$$\delta X^{n}_{du} = \left(\delta u - (1-\alpha_1)\Delta t \frac{\partial \delta\phi}{\partial x}\right)^{n}_{du} - \Delta t \delta u \frac{\partial \bar{u}}{\partial x}\bigg|^{n}_{i+\frac{1}{2}}, \tag{5.96}$$

$$\delta Y^{n}_{d\phi} = \left(\frac{\delta\phi}{\bar{\phi}} - (1-\alpha_2)\Delta t \frac{\partial \delta u}{\partial x}\right)^{n}_{d\phi} - \Delta t \overline{\delta u}^{x}\frac{\partial(\ln\bar{\phi})}{\partial x}\bigg|^{n}_{i}. \tag{5.97}$$

We then have the system

$$\delta u^{n+1}_{i+\frac{1}{2}} + \alpha_1 \Delta t \left.\frac{\partial \delta\phi}{\partial x}\right|^{n+1}_{i+\frac{1}{2}} = \delta X^{n}_{du}, \tag{5.98}$$

$$\left(\frac{\delta\phi}{\bar{\phi}}\right)^{n+1}_{i} + \alpha_2 \Delta t \left.\frac{\partial \delta u}{\partial x}\right|^{n+1}_{i} = \delta Y^{n}_{d\phi}. \tag{5.99}$$

From these equations we can eliminate all values of $\delta u^{n}_{i+\frac{1}{2}}$ to obtain the linear system

$$\begin{aligned} - \; & C_{2i+\frac{1}{2}} C_3 \delta\phi^{n+1}_{i+1} + \left[\frac{1}{\phi^{n+1}_{i}} + 2C_{2i-\frac{1}{2}}C_3\right]\delta\phi^{n+1}_{i} \\ + \; & C_{2i-\frac{1}{2}} C_3 \delta\phi^{n+1}_{i-1} = \delta R_i, \end{aligned} \tag{5.100}$$

where $C_{2i-\frac{1}{2}}$, $C_{2i+\frac{1}{2}}$ and C_3 are defined as in the previous section and

$$\delta R_i = \delta Y_j - C_3(\bar{Z}^{n+1}_{j+\frac{1}{2}}\delta X^{n}_{j+\frac{1}{2}} - \bar{Z}^{n+1}_{j-\frac{1}{2}}\delta X^{n}_{j-\frac{1}{2}}). \tag{5.101}$$

Again we have a strictly diagonally dominant system, which can be solved for $\delta\phi_i$ at each point x_i for time level $n+1$. The result is then used to update $\delta u_{i+\frac{1}{2}}$ for all values of i by means of (5.98).

5.3 Analysis of numerical schemes

In order to proceed with an assessment of the different linear models, we wish to look at the properties of the numerical schemes developed in Section 5.2. However, we also need to understand the properties of the nonlinear discrete model and so these are also discussed.

5.3.1 Stability of nonlinear model

In Section 2.4 we referred to studies which have shown that the scheme developed from the nonlinear model in Section 5.2.1 will be unconditionally linearly stable for values of $\alpha_1, \alpha_2 \in [0.5, 1]$. Here we develop the discrete dispersion relation for the constant-coefficient linear system of our model, to illustrate this stability and give information on the phase speed of the numerical solution. We follow the method of Fourier analysis described in Section 2.2.4 and substitute Fourier modes of the form (2.31) in order to provide the dispersion relation.

First we must define the linearized constant-coefficient problem for the numerical system (5.20), (5.21). We let

$$\begin{aligned} u^n_{i+\frac{1}{2}} &= U_0 + \delta u^n_{i+\frac{1}{2}}, \\ \phi^n_i &= \Phi_0 + \delta\phi^n_i, \end{aligned}$$

with U_0, Φ_0 constant and $\Phi_0 > 0$ and assume a constant advective wind U_0. Then substituting into (5.20), (5.21) we obtain the linear system

$$\frac{\delta u^{n+1}_{i+\frac{1}{2}} - \delta u^n_{du}}{\Delta t} + (1-\alpha_1)\left.\frac{\partial \delta\phi}{\partial x}\right|^n_{du} + \alpha_1 \left.\frac{\partial \delta\phi}{\partial x}\right|^{n+1}_{i+\frac{1}{2}} = 0, \tag{5.102}$$

$$\frac{\delta\phi_i^{n+1} - \delta\phi_{d\phi}^n}{\Phi_0 \Delta t} + (1-\alpha_2)\left.\frac{\partial \delta u}{\partial x}\right|_{d\phi}^{n} + \alpha_2 \left.\frac{\partial \delta u}{\partial x}\right|_{i}^{n+1} = 0, \tag{5.103}$$

where $x_{du} = x_{i+\frac{1}{2}} - U_0\Delta t$, $x_{d\phi} = x_i - U_0\Delta t$ and the spatial derivatives are approximated according to the centred difference formulae (5.36), (5.37).

We seek solutions of the form

$$\delta u = \delta u_0 e^{i(kx+\omega t)}, \quad \delta\phi = \delta\phi_0 e^{i(kx+\omega t)}, \tag{5.104}$$

where $\delta u_0, \delta\phi_0$ are constant in space and time and ω is complex. For the purposes of the analysis we will assume that all interpolation is exact, that is we assume no errors arising from the interpolation to the departure point nor from the interpolation between u- and ϕ- points. In general there will be an error from the interpolation, which will depend upon the distance of the departure point from the grid point and hence on the assumed constant velocity U_0. A more complete study of the error due to interpolation is given by McDonald [53], who showed that a cubic interpolation scheme has the smallest phase error of the low order Lagrangian interpolations. He also found that the amplitude error when the interpolation point is close to a grid point is small, with an amplifying factor of less than one as the interpolation point moves away from the grid point. Hence we do not expect the errors due to interpolation to cause an amplification and so this approximation is reasonable for our present analysis.

We first calculate the Fourier representation of the spatial derivatives at the departure points by substituting the finite difference formulae of the derivatives (5.36), (5.37) into the cubic Lagrange interpolation formula and then substituting in the Fourier modes (5.104). We find that

$$\left.\frac{\partial \delta u}{\partial x}\right|_{d\phi} = \frac{2i \sin\frac{k\Delta x}{2}}{\Delta x}\delta u_{d\phi}, \tag{5.105}$$

$$\left.\frac{\partial \delta \phi}{\partial x}\right|_{du} = \frac{2i \sin\frac{k\Delta x}{2}}{\Delta x}\delta \phi_{du}. \tag{5.106}$$

Then substituting these expressions and (5.104) into (5.102) and (5.103) we obtain

an equation of the form

$$\mathbf{M}\begin{pmatrix} \delta u_0 \\ \delta \phi_0 \end{pmatrix} = \begin{pmatrix} 0 \\ 0 \end{pmatrix}, \tag{5.107}$$

where

$$\mathbf{M} = \begin{pmatrix} E'-1 & 2i\sin\frac{k\Delta x}{2}\frac{\Delta t}{\Delta x}[(1-\alpha_1)+\alpha_1 E'] \\ 2i\sin\frac{k\Delta x}{2}\frac{\Delta t}{\Delta x}\Phi_0[(1-\alpha_2)+\alpha_2 E'] & E'-1 \end{pmatrix} \tag{5.108}$$

with $E = e^{i\omega\Delta t}$, $E' = e^{ikU_0\Delta t}E$ and $|E'| = |E|$. A comparison with the theory developed in Section 2.2.4 shows that (5.107) can be used to obtain the characteristic equation for the amplification matrix of the numerical scheme, by setting $\det\mathbf{M} = 0$. Then the eigenvalues of the amplification matrix are the values of E which satisfy this equation. It follows from Theorem 2.4, the von Neumann condition, that a necessary condition for stability is that

$$|E| \leq 1 + O(\Delta t). \tag{5.109}$$

In fact from the analytical dispersion relation (5.9) we find that ω is real and so there is no growth in the analytical solution. Hence for the numerical scheme we seek the stability condition $|E| \leq 1$, without allowing any growth in the solution. We set $\det\mathbf{M} = 0$ from which we obtain the relation

$$\begin{aligned} (1+\alpha_1\alpha_2 C^2)E'^2 &+ (C^2(\alpha_2(1-\alpha_1)+\alpha_1(1-\alpha_2))-2)E' \\ &+ (1-\alpha_1)(1-\alpha_2)C^2+1 = 0, \end{aligned} \tag{5.110}$$

with

$$C^2 = 4\Phi_0\frac{\Delta t^2}{\Delta x^2}\sin^2\frac{k\Delta x}{2}. \tag{5.111}$$

If we assume that α_1 and α_2 are equal to a common value α, then the solution of (5.110) is given by

$$E' = \frac{1+(\alpha^2-\alpha)C^2 \pm Ci}{1+\alpha^2 C^2}. \tag{5.112}$$

Since $|E| = |E'|$, the condition $|E| \leq 1$ is satisfied only for values of $\alpha \geq 0.5$ and thus this is a necessary condition for stability. For a value of $\alpha = 0.5$ we find that $|E| = 1$ and so there is no amplitude error in the numerical solution. However Rivest et al. [74] showed that it is necessary to use a value of α slightly greater than 0.5 to avoid spurious resonance in the solution.

Again following Section 2.2.4 we can separate ω into its real and imaginary parts, putting $\omega = \omega_r + i\omega_i$. Then substituting into (5.112) we obtain the numerical phase speed

$$-\frac{\omega_r}{k} = U_0 \pm \frac{1}{k\Delta t} \tan^{-1}\left(\frac{C}{1 + (\alpha^2 - \alpha)C^2}\right). \tag{5.113}$$

A comparison with the analytical phase speed (5.10) shows that there is an error in phase in the numerical solution dependent upon the wave number k.

5.3.2 Time accuracy of nonlinear model

We now examine the truncation error for the scheme used in the nonlinear model, as stated by Definition 2.7 of Section 2.2. In deriving the truncation error we consider only the time discretization, that is we assume that there is no error due to spatial discretization or interpolation. The reason for this is twofold. Firstly, a good spatial accuracy can easily be obtained by the choice of an appropriate interpolation scheme and so in order to preserve the accuracy of the overall scheme it is important to consider the time accuracy of the scheme. In fact, the truncation errors for various polynomial interpolations within semi-Lagrangian schemes have been derived in [54]. The second reason for looking at the time truncation error is so that we can also understand the effect of approximating the linearization state of the perturbation forecast models at different time levels, which we discuss in Section 5.5.

For ease of notation we make use of subscripts x and t to indicate partial derivatives with respect to those variables. We expand the truncation errors around the mid-point (x_m, t_m) of the semi-Lagrangian trajectory. Then for the nonlinear model

described in Section 5.2.1 we find that the semi-discrete scheme (5.20) satisfies the analytical momentum equation (5.1) with truncation error

$$\tau_u^{NL} = (2\alpha_1 - 1)\frac{\Delta t}{2}(\phi_{xt} + u\phi_{xx} + ugH_{xx})_{x_m}^{t_m} + O(\Delta t^2) \tag{5.114}$$

and that the scheme (5.21) satisfies the analytical continuity equation (5.4) with truncation error

$$\tau_\phi^{NL} = (2\alpha_2 - 1)\frac{\Delta t}{2}(u_{xt} + uu_{xx})_{x_m}^{t_m} + O(\Delta t^2). \tag{5.115}$$

We see that if we have $\alpha_1 = 0.5, \alpha_2 = 0.5$ then the scheme is second order accurate, whereas for the off-centred scheme, with α_1, α_2 greater than 0.5, there is a first order time truncation error. However, if the values are chosen to be close to 0.5, then we can write $\alpha_i = (1 + \epsilon_i)/2$, with $i = 1, 2$, for some small parameters ϵ_i. In this case we have for both equations

$$\tau_v^{NL} = O(\epsilon_i \Delta t) + O(\Delta t^2), \tag{5.116}$$

where $v = u$ or ϕ. Then for small enough values of ϵ_i, that is for values of α_i close enough to 0.5, the scheme will be close to second order.

5.3.3 Time accuracy of linear models

An important question to answer with respect to the linear models is to what truncation error their time discretizations approximate the analytical linear system. We apply Definition 2.7 to calculate the truncation error in the usual way and then expand in a Taylor series around the mid-point of the trajectory defined by the linearization state wind.

For the tangent linear model described in Section 5.2.2 we do not have an obvious form of the time discretizations to which we can apply a truncation error analysis. We can calculate a general form of the tangent linear model by perturbing the nonlinear model time discretizations (5.20) and (5.21), including a perturbation to

the departure point, and then dropping products of perturbations in the expansion of the truncation error. We find that the tangent linear model satisfies the linearized momentum equation (5.15) with truncation error

$$\tau_u^{TL} = (2\alpha_1 - 1)\frac{\Delta t}{2}\left[\delta\phi_{xt} + \bar{u}\delta\phi_{xx} + \delta u\bar{\phi}_{xx} + \delta u g H_{xx}\right]_{x_m}^{t_m} + O(\Delta t^2) \qquad (5.117)$$

and the linearized continuity equation (5.17) with truncation error

$$\tau_\phi^{TL}(2\alpha_2 - 1)\frac{\Delta t}{2}\left[\delta u_{xt} + \bar{u}\delta u_{xx} + \delta u\bar{u}_{xx}\right]_{x_m}^{t_m} + O(\Delta t^2). \qquad (5.118)$$

In order to verify the method used here we note that a general time discretization for the equation for δu can also be found by combining equations (5.67), (5.73) and (5.77) from Section 5.2.2 and ignoring the discretization of the spatial derivatives. An expansion of the truncation error for the expression thus formed gives exactly the same as (5.117).

We see from (5.117) and (5.118) that the tangent linear model is a second order in time approximation to the continuous linear system for time-weightings $\alpha_1 = \alpha_2 = 0.5$ and $O(\Delta t)$ otherwise. A comparison of the truncation error with that of the nonlinear model, given by (5.114) and (5.115), shows that the leading order terms in the error for the tangent linear model are equal to the linearization of the leading order terms in the nonlinear model truncation error. This was also true for the example of the ODE problem in Chapter 4.

In order to calculate the time accuracy of the perturbation forecast model scheme of Section 5.2.3 we consider the time discretizations (5.78) and (5.79). We find that (5.78) approximates the continuous linearized momentum equation (5.15) with truncation error

$$\begin{aligned}\tau_u^{P1} &= (2\alpha_1 - 1)\frac{\Delta t}{2}\left(\delta\phi_{xt} + \bar{u}\delta\phi_{xx}\right)_{x_m}^{t_m} \\ &+ (2\alpha_3 - 1)\frac{\Delta t}{2}\left((\delta u\bar{u}_x)_t + \bar{u}(\delta u\bar{u}_x)_x\right)_{x_m}^{t_m} + O(\Delta t^2). \qquad (5.119)\end{aligned}$$

and the discretization of the linearized continuity equation (5.79) approximates the

analytical linear equation (5.17) with truncation error

$$\begin{aligned}\tau_{\phi}^{P1} &= (2\alpha_2 - 1)\frac{\Delta t}{2}\left(\delta u_{xt} + \bar{u}\delta u_{xx}\right)_{x_m}^{t_m} \\ &+ (2\alpha_4 - 1)\frac{\Delta t}{2}((\delta u(\ln\bar{\phi})_x)_t + \bar{u}(\delta u(\ln\bar{\phi})_x)_x)_{x_m}^{t_m} + O(\Delta t^2). \quad (5.120)\end{aligned}$$

It is informative to compare the truncation errors of the tangent linear model and the first perturbation forecast model for our shallow water system. We consider first the approximation to the linearized momentum equation. A comparison of (5.117) and (5.119) shows that if $\delta u = 0$ so that there is no perturbation to the back trajectory of the semi-Lagrangian scheme, then the truncation errors are identical. Where $\delta u \neq 0$ an extra $O(\Delta t)$ error is added depending on how the perturbation to the trajectory has been treated. For the tangent linear model the truncation error (5.117) contains a term of the form $\delta u(\bar{\phi}_{xx} + gH_{xx})$. A comparison of these terms with equation (5.73) reveals that they arise from the linearization of the interpolation within the semi-Lagrangian scheme. In the perturbation forecast model however we do not have such a linearization, since we treat the perturbation wind term $\delta u\bar{u}_x$ as a forcing averaged along the trajectory. As a result of this we find in the truncation error (5.119) a dependence on the rate of change of this term along the trajectory.

The truncation errors for the mass continuity equation show a similar picture. We compare the tangent linear model error (5.118) with the perturbation forecast model error (5.120). The tangent linear model contains a term involving the perturbation wind multiplied by $\bar{u}_{xx}$. A comparison with (5.74) shows again that this comes from the linearization of the interpolation scheme. The perturbation forecast model error on the other hand depends on the rate of change of the term $\delta u(\ln\bar{\phi})_x$ along the trajectory.

We now consider the second perturbation forecast model scheme described by equations (5.94) and (5.95) of Section 5.2.4. For this scheme we find the truncation

error

$$\begin{aligned} \tau_u^{P2} &= (2\alpha_1 - 1)\frac{\Delta t}{2}\left(\delta\phi_{xt} + \bar{u}\delta\phi_{xx}\right)_{x_m}^{t_m} \\ &+ \frac{\Delta t}{2}\left(-(\delta u\bar{u}_x)_t + \bar{u}(\delta u\bar{u}_x)_x\right) + O(\Delta t^2) \end{aligned} \tag{5.121}$$

in the approximation of the linearized momentum equation (5.15) and the truncation error

$$\begin{aligned} \tau_\phi^{P2} &= (2\alpha_2 - 1)\frac{\Delta t}{2}(\delta u_{xt} + \bar{u}\delta u_{xx})_{x_m}^{t_m} \\ &+ \frac{\Delta t}{2}(-(\delta u(\ln\bar{\phi})_x)_t + \bar{u}(\delta u(\ln\bar{\phi})_x)_x) + O(\Delta t^2) \end{aligned} \tag{5.122}$$

in the approximation of (5.17). Thus we see that for this second version of the perturbation forecast model the accuracy is only first order in time even with the time weightings α_i set equal to 0.5. This appears to be a serious deficiency with this version of the model.

5.4 Numerical experiments

5.4.1 Verification of nonlinear model

The numerical experiment we use to test the different models is one of a motion forced by some orography, based on an experiment described by Houghton and Kasahara [38]. For time $t < 0$ the fluid is at rest and the geopotential ϕ is equal to $\phi_0 - H(x)$, with ϕ_0 constant. At $t = 0$ the fluid is impulsively set in motion with a constant velocity u_0 for all x. From this impulse a wave motion develops and moves away from the obstacle in both directions, while the solution in the vicinity of the obstacle becomes a steady state solution and thus satisfies (5.11) and (5.12). For a continuous flow the analytical values of the steady state constants K_1 and K_2 are

given by

$$K_1 = \frac{u_0^2}{2} + \phi_0, \tag{5.123}$$

$$K_2 = u_0\phi_0. \tag{5.124}$$

This problem is defined over an infinite domain $-\infty < x < \infty$, but the authors of [38] use a periodic domain with boundaries far enough away from the obstacle that the asymptotic conditions are established around the obstacle before any of the wave motions can feed back into this area. We also follow this approach.

In [38] Houghton and Kasahara describe different motions depending on the initial conditions u_0, ϕ_0 and the size of the obstacle. For some combinations of these parameters jumps will form in the fields. However, since in our study we wish to consider the behaviour of linear approximations, we want only motions which are not too highly nonlinear and so we restrict the experiments to ones in which a jump does not form.

In order to test our nonlinear model, we first run an experiment based on Case A of [38]. The height of the obstacle H is given by

$$H(x) = H_c\left(1 - \frac{x^2}{a^2}\right) \qquad \text{for} \qquad 0 \leq |x| \leq a, \tag{5.125}$$

and $H(x) = 0$ otherwise. H_c is the maximum height of the obstacle and a is half the length over which the base of the obstacle extends. The values of the various parameters needed are taken from [38]. The domain is defined to be periodic over 1000 gridpoints, with a distance $\Delta x = 0.01m$ between them, so that $x \in [0m, 10m]$. The value of a is taken to be $40\Delta x = 0.4m$ and the height of the obstacle $H_c = 0.05m$. At time $t = 0$ we have $\phi(x) = g(h_0 - H(x))$, where we take $h_0 = 0.2m$ and $g = 10ms^{-2}$. The initial velocity u_0 is taken to be $0.1ms^{-1}$. We run for a total of 500 time steps using a time step Δt of $4.6 \times 10^{-3}s$.

It is also necessary to choose the variable parameters in the numerical scheme that we are using, which was outlined in Section 5.2.1. We set the time-weighting

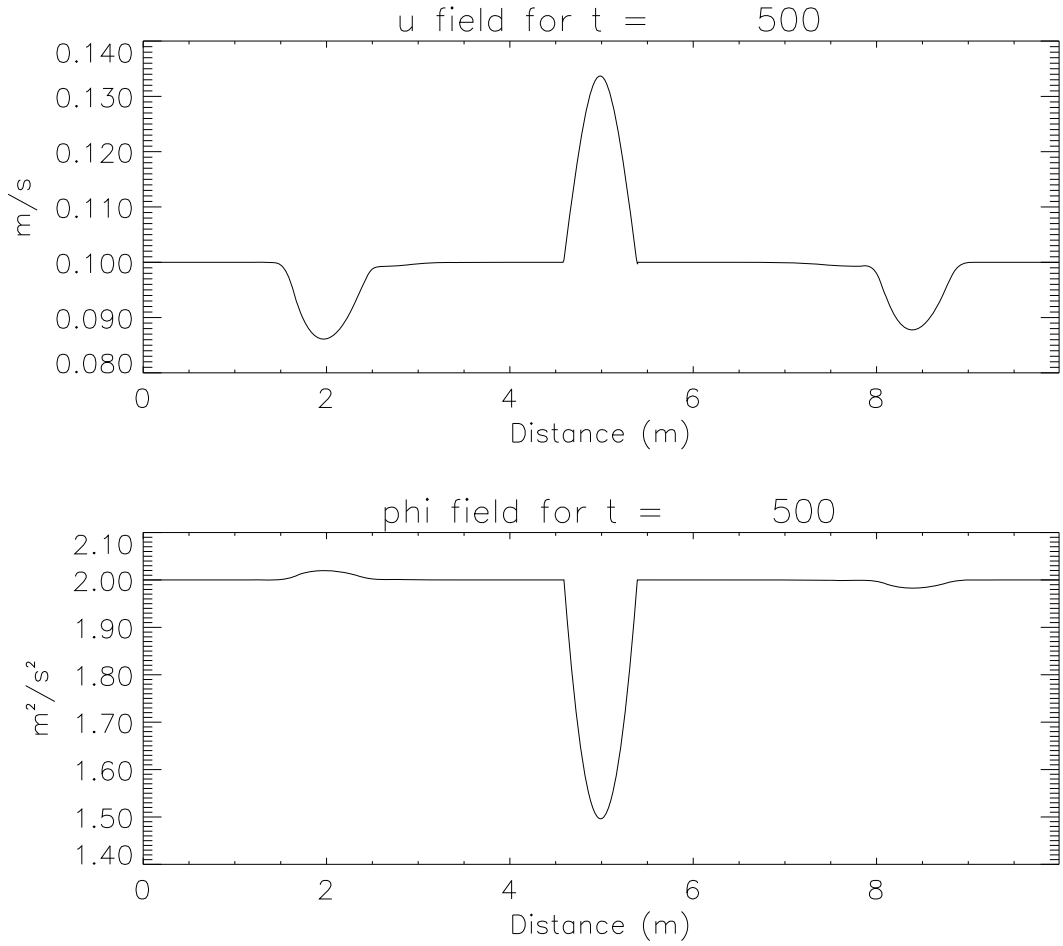

Figure 5.2: Fields of u and ϕ from the nonlinear model after 500 time steps = 2.3s.

parameters α_1, α_2 to 0.6, thus satisfying the stability criteria of Section 5.3.1, while still keeping close to the more accurate centred time differencing. These α values are typical of those used in practice, for example in the regional model of the Canadian Meteorological Centre [16]. The reference geopotential Φ_{ref} in the iterative procedure (5.52) is taken to be $1.5 m^2 s^{-2}$.

Figure 5.2 shows the fields after 500 time steps, which is equivalent to $2.3s$ of real time. The fields in the centre of the domain match well the corresponding figures in [38]. The average velocity of the outgoing waves in the first 500 time

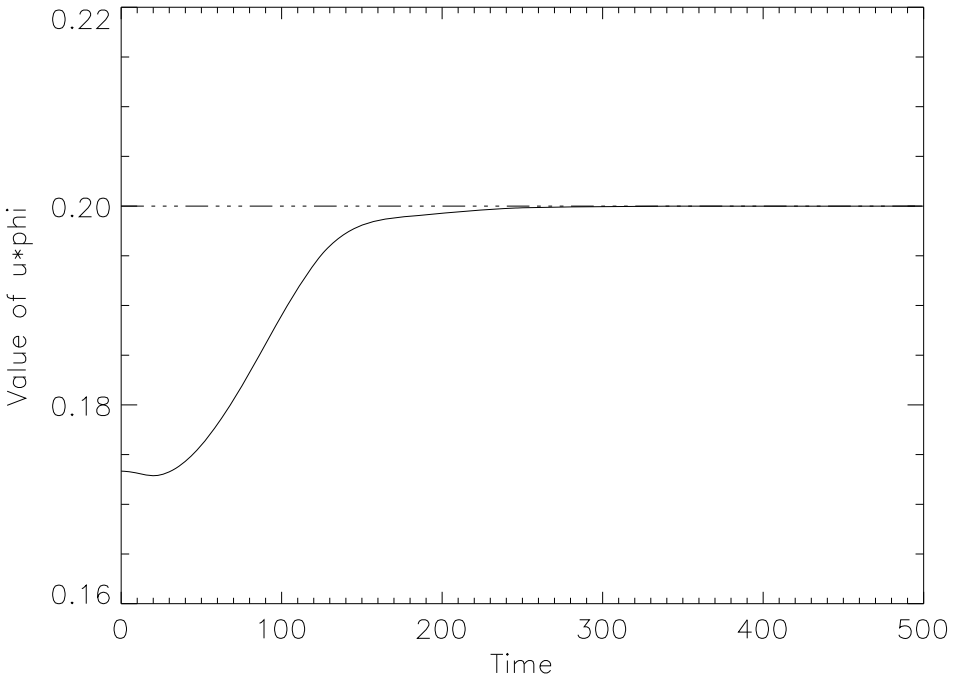

Figure 5.3: Variation of $u\phi$ in the centre of the domain with time. The dot-dashed line shows the asymptotic value $u_0\phi_0$.

steps (calculated from the distance from the centre divided by $2.3s$) is found to be $-1.31ms^{-1}$ and $1.47ms^{-1}$. These compare with the analytical values calculated for the homogeneous linearized problem using (5.10) of $-1.31ms^{-1}$ and $1.51ms^{-1}$. They do not match exactly since the analytical results are based on the constant-coefficient linearized homogeneous system. In Figure 5.3 we plot the value of the quantity $u\phi$ summed over the interval from 4.5m to 5.5m, which is where the stationary part of the solution forms. From Section 5.1.2 we expect this quantity to asymptote to the value of K_2, which for this problem is equal to $u_0\phi_0 = 0.2$, and we see that this is indeed the case. Thus it seems that our nonlinear scheme with the given parameter settings models well the true solution of the problem. With confidence in the nonlinear model, we can now look at how the various linearizations behave.

5.4.2 Verification of linear models

Before comparing the behaviour of the various linear models, we need to ensure that they are coded correctly. To do this we make use of the method described in Section 3.1 and compare the evolution of a perturbation in runs of each linear model with the difference between two runs of the nonlinear model. We take the experiment of Section 5.4.1 as our unperturbed run and add perturbations $(\gamma\delta u_0, \gamma\delta\phi_0)$ to the initial conditions in order to generate the perturbed runs. The initial perturbations are taken at $t = 0$ to be

$$\begin{aligned} \delta u_0 &= 0.01 m s^{-1}, \\ \delta\phi_0 &= -0.2 m^2 s^{-2}, \end{aligned}$$

representing a change of 10% in each field, and we set $\gamma = 10^p$ for $p = 0, -1, \ldots, -5$. For the first version of the perturbation forecast model we must also choose values of the extra time-weightings α_3 and α_4. We set these to be 0.6, as for the other values of α_i. In order to measure the error between nonlinear perturbations and the solution from the various linear models, we calculate the relative error E_R and the solution error E_S as defined by equations (3.17) and (3.22) of Section 3.1.2. The norm used in both cases is the root mean square norm defined by (3.21). These error measures are calculated for the u and ϕ fields separately.

In Figure 5.4 we plot the relative error against perturbation size for the u and ϕ fields for each linear model. The solid line shows the error for the tangent linear model described in Section 5.2.2, the dashed line shows the first version of the perturbation forecast model derived in Section 5.2.3, hereafter written PFM1, and the dotted line shows the second version of the perturbation forecast model from Section 5.2.4, hereafter PFM2. We see that for the tangent linear model the relative error tends linearly towards zero, showing that the model is correctly coded. For the two versions of the perturbation forecast model the relative error tends towards a non-zero constant, as predicted by the theory of Section 3.1.2. However, it is

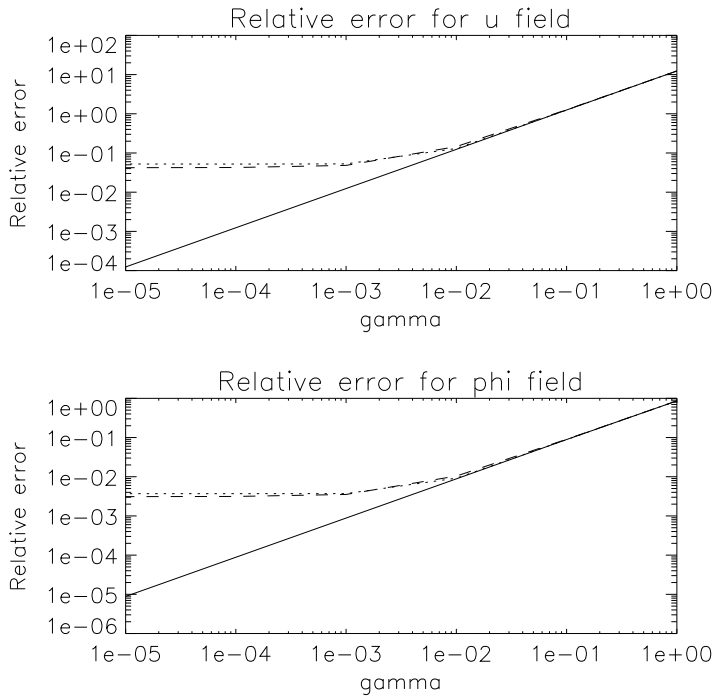

Figure 5.4: Plot of relative error E_R against perturbation size after 500 timesteps. The solid line is for the tangent linear model, the dashed line for PFM1 and the dotted line for PFM2.

encouraging that for the larger perturbations both perturbation forecast models give the same relative error as the tangent linear model. This indicates that all the linear models are an equally valid approximation for reasonably sized perturbations. A plot of the solution error E_S against perturbation size, seen in Figure 5.5, also shows this error tending linearly towards zero for the tangent linear model. For this measure the error for the perturbation forecast models does not asymptote to a constant value, but does show a greater error than the tangent linear model for small perturbations. However, as for the relative error, the solution error indicates that all models are comparable for reasonably sized perturbations. A more detailed comparison between the models is made in Section 5.4.3.

The result of this test is of interest, since it demonstrates that the correct coding

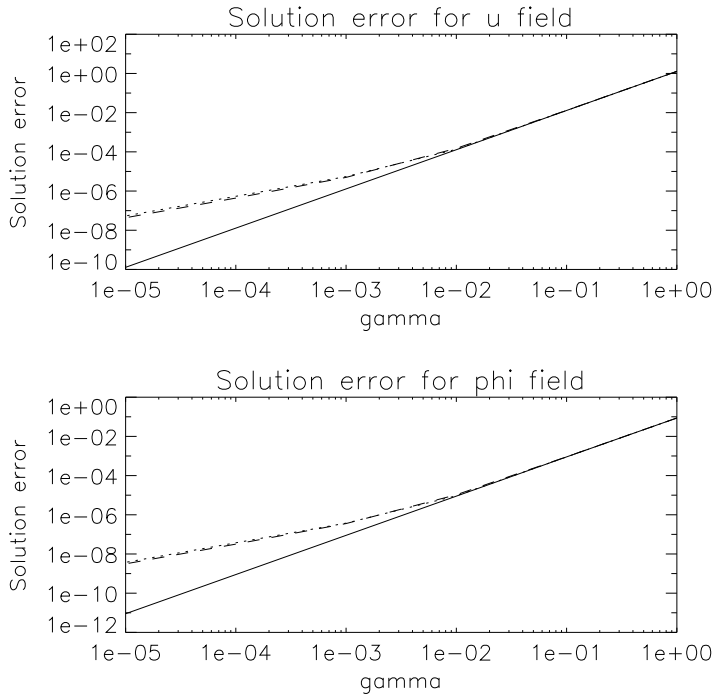

Figure 5.5: Plot of solution error E_S against perturbation size after 500 timesteps. The solid line is for the tangent linear model, the dashed line for PFM1 and the dotted line for PFM2.

of a perturbation forecast model cannot be proved as easily as that of a tangent linear model. The analysis of Section 3.1.2 and the experimental evidence from these experiments show that the relative error will tend to a non-zero constant. However, it is not possible to tell from the value of that constant the significance of the difference between the perturbation forecast model and a tangent linear model. In Section 5.6 we test how well the method for testing a perturbation forecast model which we proposed in Section 3.3 can be used to assess this difference. First however we examine further the performance of the linear models with various numerical experiments.

5.4.3 Experiments with linear models

To begin we take the experiment of Section 5.4.1 as our nonlinear model run to produce the basic state, but we now use a time step of $\Delta t = 9.2 \times 10^{-3} s$. This is double the step we used previously, but we have found that the scheme remains stable with no noticeable loss in accuracy compared to runs with the smaller time step. The initial perturbation is taken to be

$$\begin{aligned} \delta u_0 &= 0.01 m s^{-1}, \\ \delta \phi_0 &= -0.2 m^2 s^{-2}. \end{aligned}$$

For each of the linear models we compare the perturbation produced by the linear model with the difference between the perturbed and unperturbed runs of the nonlinear model. Figures 5.6, 5.7 and 5.8 show the nonlinear and linear perturbations after 250 time steps (2.3s) for the tangent linear model, PFM1 and PFM2 respectively. In each case the top picture shows the perturbation of u and the bottom picture the perturbation of ϕ, with the solid line indicating the nonlinear model perturbation and the dashed line indicating the perturbation as evolved in the linear model.

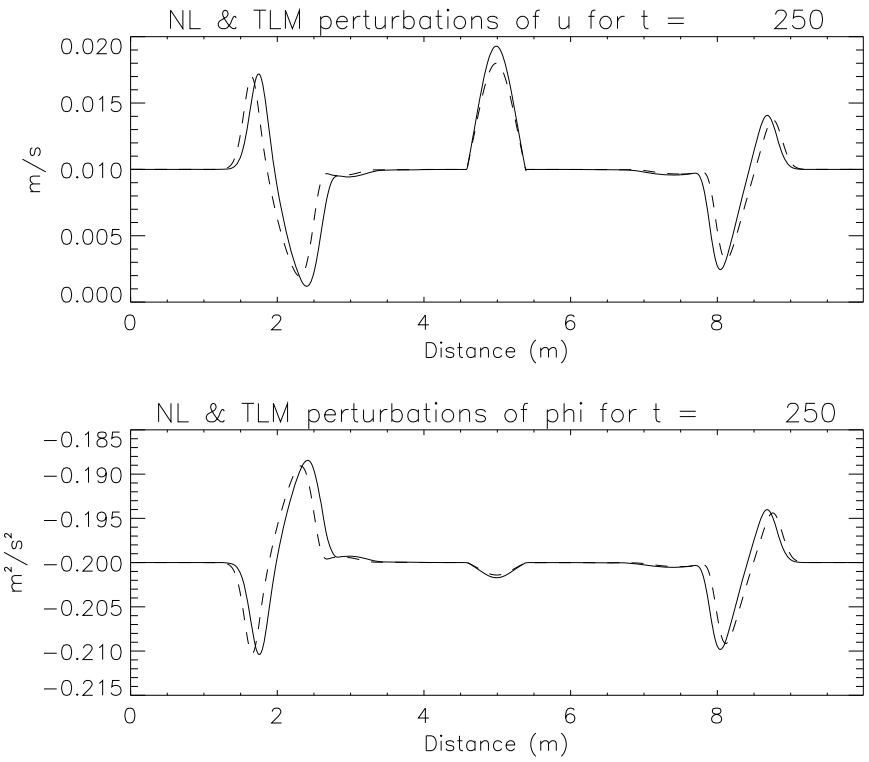

Figure 5.6: Comparison of nonlinear and linear perturbations for tangent linear model after 250 time steps. The solid line shows the nonlinear perturbation and the dashed line the output from the tangent linear model.

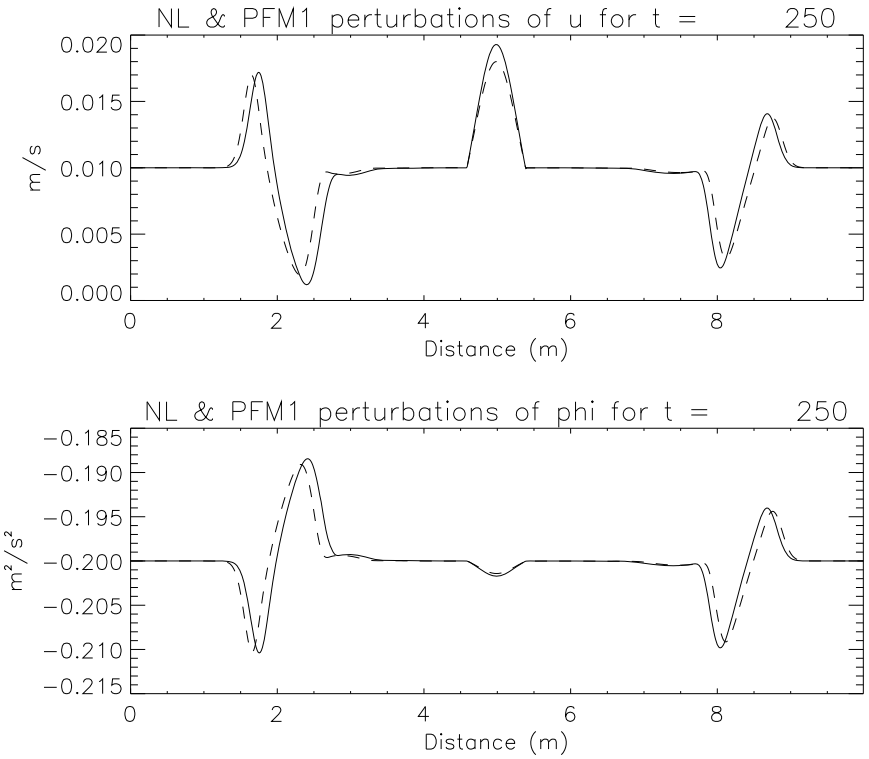

Figure 5.7: Comparison of nonlinear and linear perturbations for the first perturbation forecast model after 250 time steps. The solid line shows the nonlinear perturbation and the dashed line the output from the first perturbation forecast model.

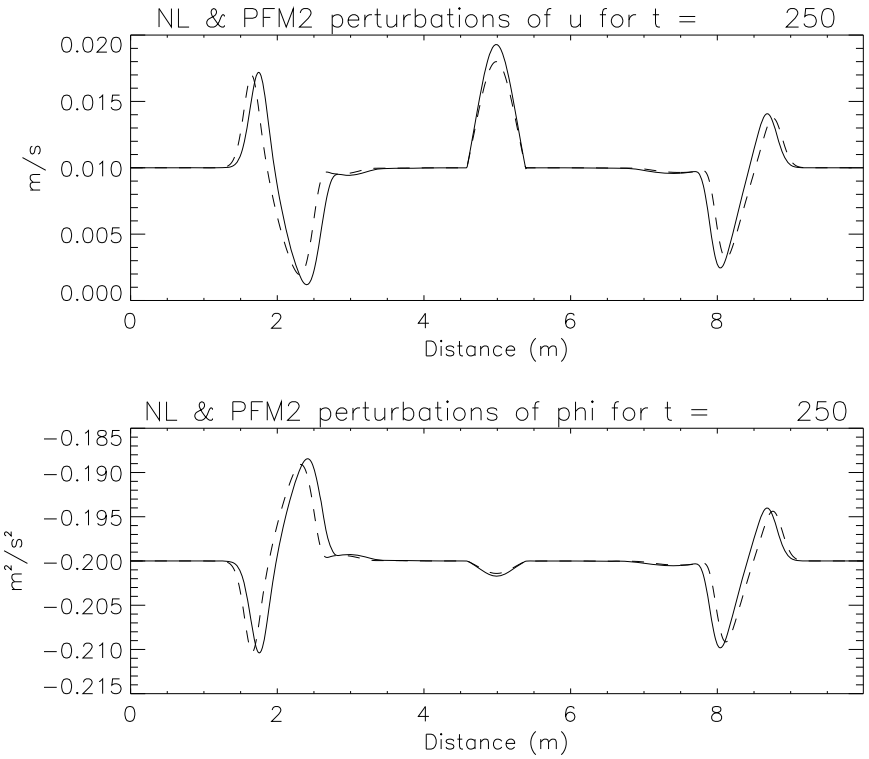

Figure 5.8: Comparison of nonlinear and linear perturbations for the second perturbation forecast model after 250 time steps. The solid line shows the nonlinear perturbation and the dashed line the output from the second perturbation forecast model.

The first thing we notice from these pictures is that all the linear models seem to behave in the same way. For each of the models we see two main errors in the representation of the nonlinear perturbation. The first is that there is an amplitude error in the stationary solution in the centre of the domain. The second error is a phase error in the outwardly moving gravity waves. We examine the source of each of these in turn.

In order to understand the amplitude errors in the stationary solution, we refer back to the solutions derived in Section 5.1.2. There we found that that the stationary solution of the nonlinear model satisfies

$$u(x)\phi(x) = K_2 \tag{5.126}$$

and for this problem we have $K_2 = u_0\phi_0$. From this we can define a relationship between the perturbed quantities

$$\begin{aligned} E_N(x) &\equiv (\bar{u}(x) + \delta u(x))(\bar{\phi}(x) + \delta\phi(x)) - \bar{u}(x)\bar{\phi}(x) \\ &= \bar{u}(x)\delta\phi(x) + \delta u(x)\bar{\phi}(x) + \delta u(x)\delta\phi(x). \end{aligned} \tag{5.127}$$

Then using the asymptotic solutions we find that for the nonlinear problem the analytical value of $E_N(x)$ asymptotes to a constant value E_N^A, given by

$$E_N^A = u_0\delta\phi_0 + \delta u_0\phi_0 + \delta u_0\delta\phi_0. \tag{5.128}$$

We can define a similar quantity for the perturbations from the linear models. In Section 5.1.3 we found that the perturbation to the stationary solution satisfies two analytical expressions, given by (5.18) and (5.19). For the problem being described in this section we find that the constants $\delta K_1, \delta K_2$ are given by

$$\delta K_1 = u_0\delta u_0 + \delta\phi_0, \tag{5.129}$$

$$\delta K_2 = u_0\delta\phi_0 + \delta u_0\phi_0. \tag{5.130}$$

Then defining

$$E_L(x) \equiv \bar{u}(x)\delta\phi(x) + \delta u(x)\bar{\phi}(x), \tag{5.131}$$

we find that for perturbations calculated from the linear problem $E_L(x)$ asymptotes to a constant value E_L^A given by

$$E_L^A = u_0 \delta\phi_0 + \delta u_0 \phi_0. \tag{5.132}$$

For the initial values used in the experiment of this section we find that $E_N^A = -0.02$ and $E_L^A = 0$.

For the numerical solutions we calculate E_N and E_L at the centre of the domain. We first interpolate u and δu to ϕ-points and then calculate the average value of $\bar{E_N}$ and $\bar{E_L}$ over an interval $[x_a, x_b]$ using the trapezoidal quadrature rule, which gives

$$\begin{aligned} \bar{E_N} &= \frac{1}{(x_b - x_a)} \left(\frac{1}{2} E_N(x_a) + \sum_{i=a+1}^{b-1} E_N(x_i) + \frac{1}{2} E_N(x_b) \right), \\ \bar{E_L} &= \frac{1}{(x_b - x_a)} \left(\frac{1}{2} E_L(x_a) + \sum_{i=a+1}^{b-1} E_L(x_i) + \frac{1}{2} E_L(x_b) \right). \end{aligned} \tag{5.133}$$

In Figure 5.9 we plot the variation over time of $\bar{E_N}$ calculated from the nonlinear perturbation and $\bar{E_L}$ calculated from the tangent linear model over the interval $x \in [4.5m, 5.5m]$, together with their analytical asymptotic values. For each quantity we plot the absolute value. We see that after approximately 200 time steps both $\bar{E_N}$ and $\bar{E_L}$ asymptote to a constant value and that this value matches the analytical asymptotic value of E_N^A and E_L^A respectively. Also shown on this figure by the dotted line is the quantity $\bar{E_N}$ calculated using the perturbations from the tangent linear model. The asymptotic value of this quantity does not equal that of the the nonlinear model, but has a larger value. Thus it appears that above the orography the linear model asymptotes to a solution consistent with the linear equations and this explains the difference between the linear and nonlinear solutions in the centre of the domain. Graphs of $\bar{E_L}$ and $\bar{E_N}$ from both perturbation forecast models (not shown) are very similar to those of the tangent linear model.

In order to understand the phase differences seen in perturbations to the outgoing gravity waves, we first wish to understand whether this difference is mainly caused

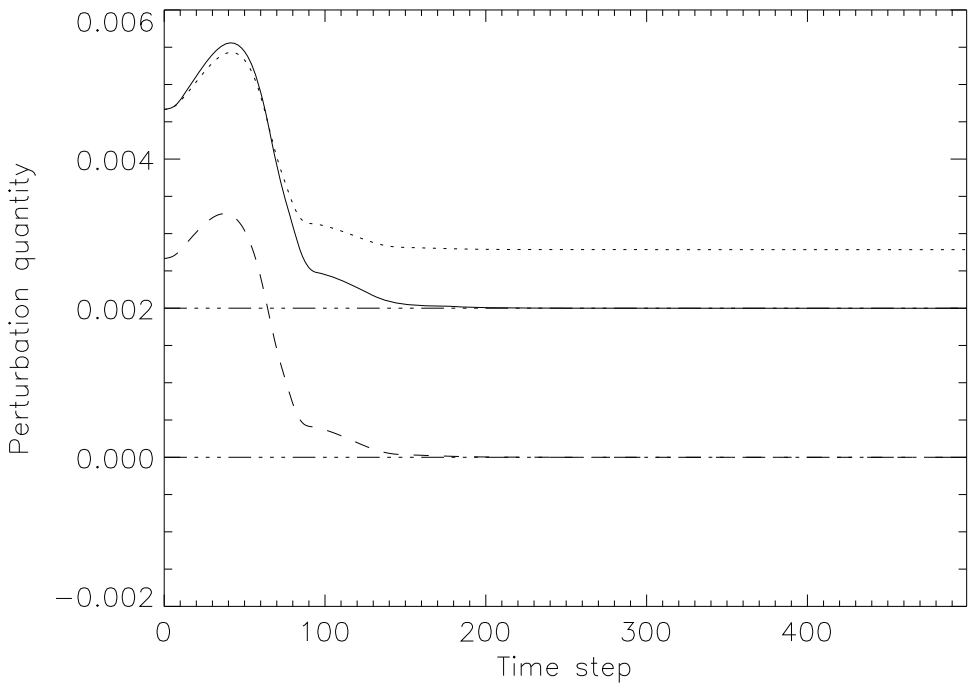

Figure 5.9: Variation of linear and nonlinear perturbations to $u\phi$ in the centre of the domain with time. The solid line is the variation of $\bar{E_N}$ from the nonlinear perturbations, the dashed line is the variation of $\bar{E_L}$ from the tangent linear model and the dotted line is the value of $\bar{E_N}$ from the tangent linear model. The dot-dashed lines show the asymptotic values E_N^A and E_L^A. In each case the absolute value is shown.

by the perturbation to u or the perturbation to ϕ. We therefore run again the previous experiment setting each of the initial perturbations to zero in turn. Thus for the first experiment we use

$$\delta u_0 = 0.01 m s^{-1}, \quad \delta\phi_0 = 0 m^2 s^{-2}, \tag{5.134}$$

and for the second

$$\delta u_0 = 0 m s^{-1}, \quad \delta\phi_0 = -0.2 m^2 s^{-2}. \tag{5.135}$$

Figure 5.10 shows the nonlinear and tangent linear perturbations from the first of these after 250 time steps, and Figure 5.11 shows the same thing for the second of these experiments. We see that when the $\delta\phi$ perturbation is zero, there is no phase error in the waves in the u field. However, if only the initial δu perturbation is zero, then the phase error does appear in the subsequent waves.

We can understand this result by looking again at the analytical phase speed (5.10) for the constant coefficient linear system. Although this was calculated assuming the absence of orography, most of the gravity wave movement is away from the orography in this problem and so we do not expect orographic effects to have a large effect on the wave speed. A perturbation to (5.10) tells us that the difference in phase speed between the two nonlinear model runs is given by

$$-\frac{\delta\omega}{k} = \delta U_0 \pm \left(\sqrt{\Phi_0 + \delta\Phi_0}) - \sqrt{\Phi_0}\right). \tag{5.136}$$

We see then that the difference in phase speed is linear in δU_0 and nonlinear in $\delta\Phi_0$. Thus when the perturbation to ϕ is zero, we would expect the linear model to represent well the phase difference between the two nonlinear model runs and this is reflected in Figure 5.10. However, when $\delta\phi$ is non-zero, then we would expect a difference between the linear and nonlinear models. The same result is also seen by consideration of the numerical dispersion relation for the constant-coefficient linear system (5.113). It is clear that a perturbation in U_0 will lead to a linear perturbation to the phase, while a perturbation to Φ_0 leads to a nonlinear perturbation of the phase.

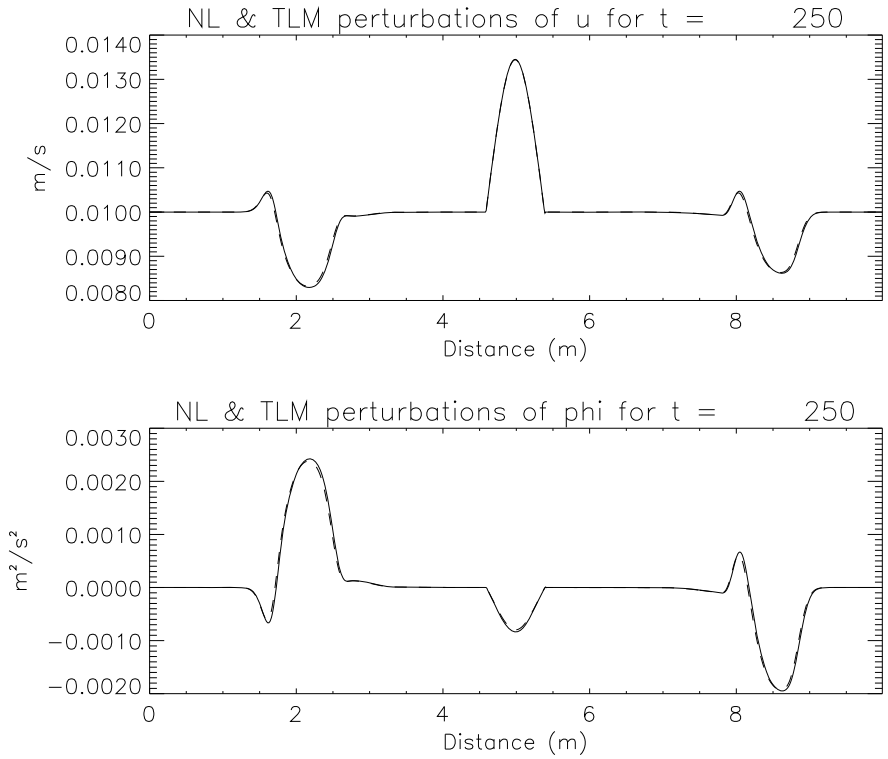

Figure 5.10: Comparison of nonlinear and linear perturbations for tangent linear model after 250 time steps, for the experiment with $\delta\phi_0 = 0$. The solid line shows the nonlinear perturbation and the dashed line the output from the tangent linear model.

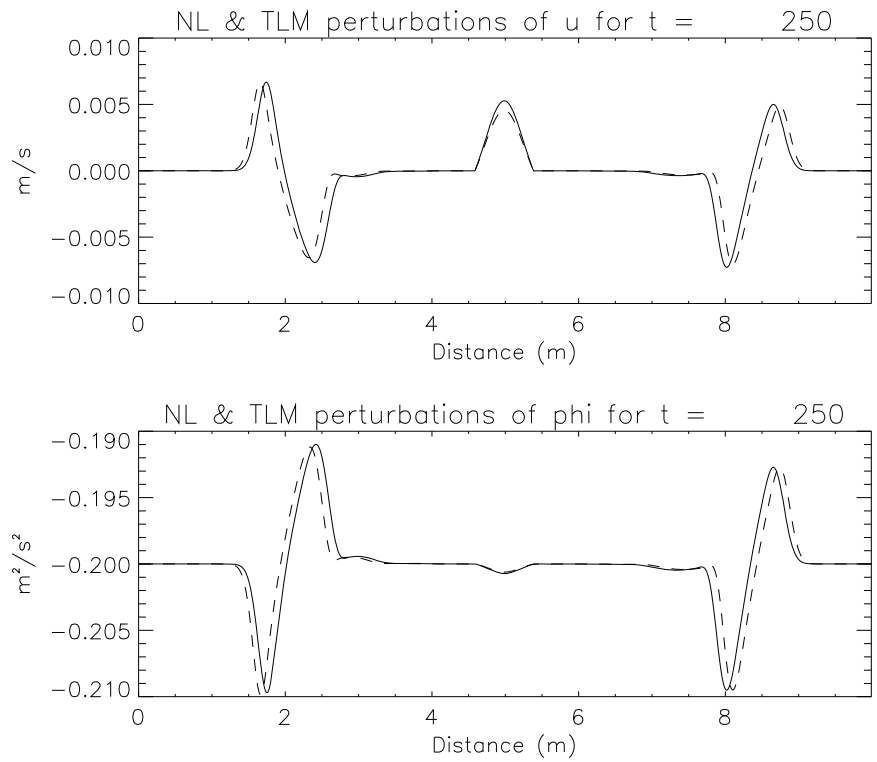

Figure 5.11: Comparison of nonlinear and linear perturbations for tangent linear model after 250 time steps, for the experiment with $\delta u_0 = 0$. The solid line shows the nonlinear perturbation and the dashed line the output from the tangent linear model.

For each of these last two cases we still find an amplitude error in the centre of the domain. The reason for this is that when one of the perturbations is zero, then the asymptotic values E_N^A and E_L^A are equal. In the nonlinear model the nonlinear perturbation to $u\phi$ asymptotes to this expected value. In the linear model it is the linear perturbation to $u\phi$ which asymptotes to this quantity, and so an error is present according to the asymptotic value of the nonlinear term $\delta u(x)\delta\phi(x)$ calculated from the linear model. For the above experiment this quantity remains small for the case in which $\delta\phi_0$ is zero, which is why the amplitude error is less noticeable in Figure 5.10.

5.4.4 Behaviour for large Courant number

The experiments in the previous section were restricted to a small Courant number in order to avoid conditions in which a jump forms in the solution. We would like to check that the linear models are also suitable for values of the linearization state Courant number $\bar{u}\Delta t/\Delta x$ greater than unity and for values of the perturbed Courant number $\delta u\Delta t/\Delta x$ greater than unity. In particular we wish to ensure that the second version of the perturbation forecast model PFM2, described in Section 5.2.4, is stable for such values. In order to run with higher Courant numbers we introduce another experiment taken from [24]. For this experiment there is no orography, that is $H(x) = 0$ everywhere. We have a total of 1000 grid points, separated by a grid length $\Delta x = 1000m$, and we run for a total time of $10,000s$. The reference geopotential for the iterative procedure (5.52) is chosen to be $\Phi_{ref} = 980m^2s^{-2}$. We set the time-weightings $\alpha_1 = \alpha_2 = 0.7$ for all the models and $\alpha_3 = \alpha_4 = 0.7$ for the first perturbation forecast model. These values for α_i were chosen by experiment; values lower than this produced too many trailing waves in the nonlinear model

solution. The initial conditions are

$$\begin{aligned} u(x,0) &= 10ms^{-1}, \\ \phi(x,0) &= 1000m^2s^{-2} + 100\exp\left[-\left(\frac{x-x_0}{5000}\right)^2\right] m^2s^{-2}. \end{aligned}$$

Then the solution of the ϕ field is two gravity waves which move in opposite directions. This is illustrated by Figure 5.12 which shows the initial and final fields of ϕ from a nonlinear model run using a time step $\Delta t = 1$. The average velocity of the waves in the numerical solution, calculated from the distance moved by each wave in the integration period, is $-22.7ms^{-1}$ for the left-moving wave and $42.7ms^{-1}$ for the right-moving wave. These values verify well with the analytical values of $-21.6ms^{-1}$ and $41.6ms^{-1}$ calculated from the phase speed (5.10) of the constant-coefficient homogeneous system given by (5.5) and (5.6). However, the amplitude of the waves is damped, with an amplitude of $1042m^2s^{-2}$ compared with the analytical solution of $1050m^2s^{-2}$. This damping can be reduced by using a smaller time-weighting coefficient, but at the expense of introducing some trailing waves. For the purpose of comparing the linear models we prefer the solution to be as clean as possible, and so we choose to remain with the damped solution.

We now look at two experiments with the linear models. The above experiment is taken as the linearization state and we obtain the perturbed state by adding perturbations

$$\begin{aligned} \delta u(x,0) &= 3ms^{-1}, \\ \delta\phi(x,0) &= -10\exp\left[-\left(\frac{x-x_0}{5000}\right)^2\right] m^2s^{-2}. \end{aligned}$$

For the two experiments we run for a total of $10,000s$. The first experiment uses a time step of $250s$ and the second a time step of $500s$. For the first of these the linearization state Courant number $\bar{u}\Delta t/\Delta x$ is equal to 2.5, whereas the perturbed Courant number $\delta u\Delta t/\Delta x$ is still less than one. For the second experiment the linearization state Courant number is equal to 5, while the perturbed Courant number

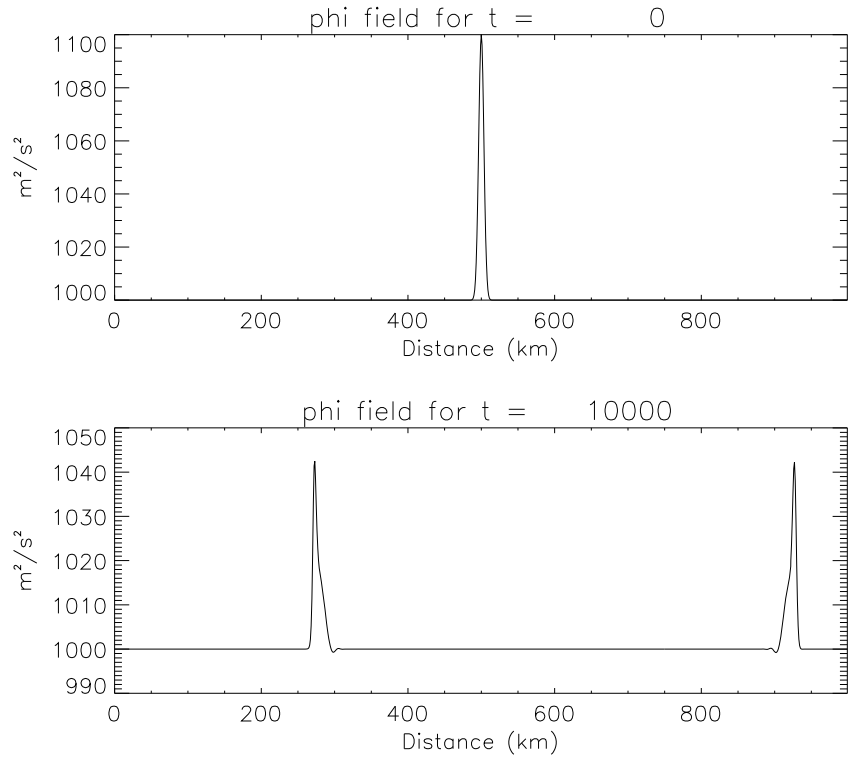

Figure 5.12: ϕ field for initial time and after $10,000s$ from a nonlinear model run with $\Delta t = 1$.

has a value of 1.5. The effect of increasing the time step for the linearization state run is to further dampen and disperse the outward moving gravity waves. This can be seen from Figure 5.13, which shows the final field of ϕ from the nonlinear model for each of these two experiments. The comparison of the nonlinear and linear perturbations of ϕ is shown in Figure 5.14 for the run with $\Delta t = 250s$ and in Figure 5.15 for the run with $\Delta t = 500s$, with the two experiments plotted on a different scale. For each figure we have a comparison with the tangent linear model and both versions of the perturbation forecast model. We find that as for the experiments in Section 5.4.3 the linear model introduces a phase error and an amplitude error with respect to the nonlinear model solution. As the time step increases the perturbations are damped in both the linear and nonlinear models. For a time step of $250s$ we notice no significant difference between the three linear models. However when the time step is increased to $500s$ so that the perturbed Courant number is greater than one, we do notice a slight degradation for the second perturbation forecast model in the representation of the right-moving wave. Thus it seems that the discretization of the $\delta u \partial \bar{u}/\partial x$ and $\delta u \partial(\ln \bar{\phi})/\partial x$ terms in (5.94) and (5.95), which we have shown to be only first order, may lead to errors when the perturbation Courant number is greater than one. However a run of this experiment over a longer time period showed no evidence of the error becoming unstable with time.

5.5 Linearization state of PFM

Within both versions of the perturbation forecast model we find a dependence on the linearization state at both the departure point at time level n and the arrival point at time level $n+1$. In this section we consider whether it is possible to approximate these by using the linearization state at one time level only. We consider first an approximation of the linearization state which uses the value at the correct spatial point, but uses values at time level $n + \frac{1}{2}$. In Section 4.5 we found that for the ODE

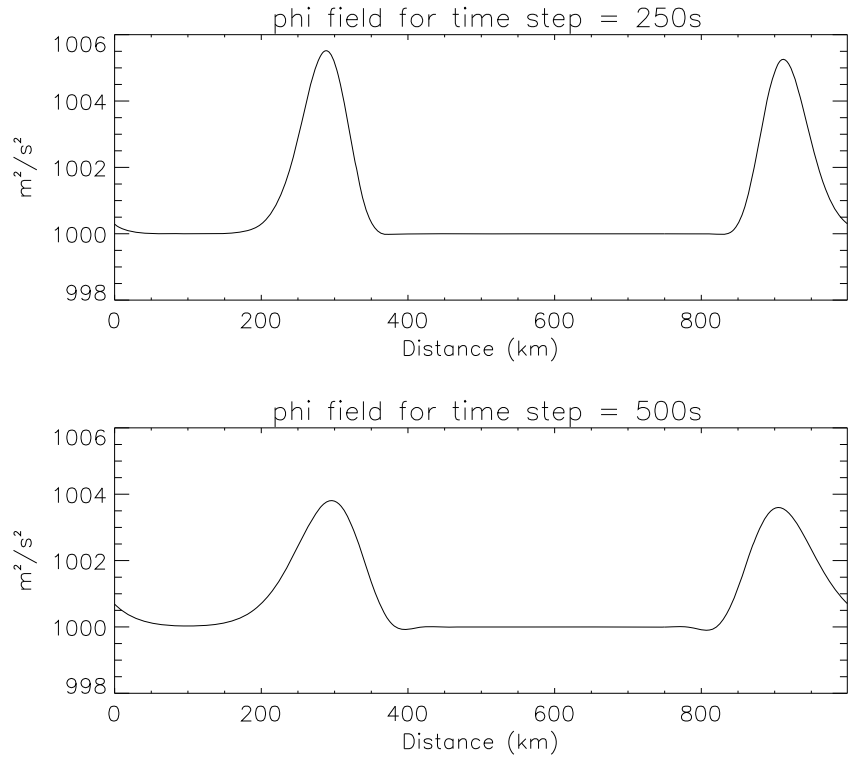

Figure 5.13: ϕ field at final time from nonlinear model runs with $\Delta t = 250s$ and $\Delta t = 500s$.

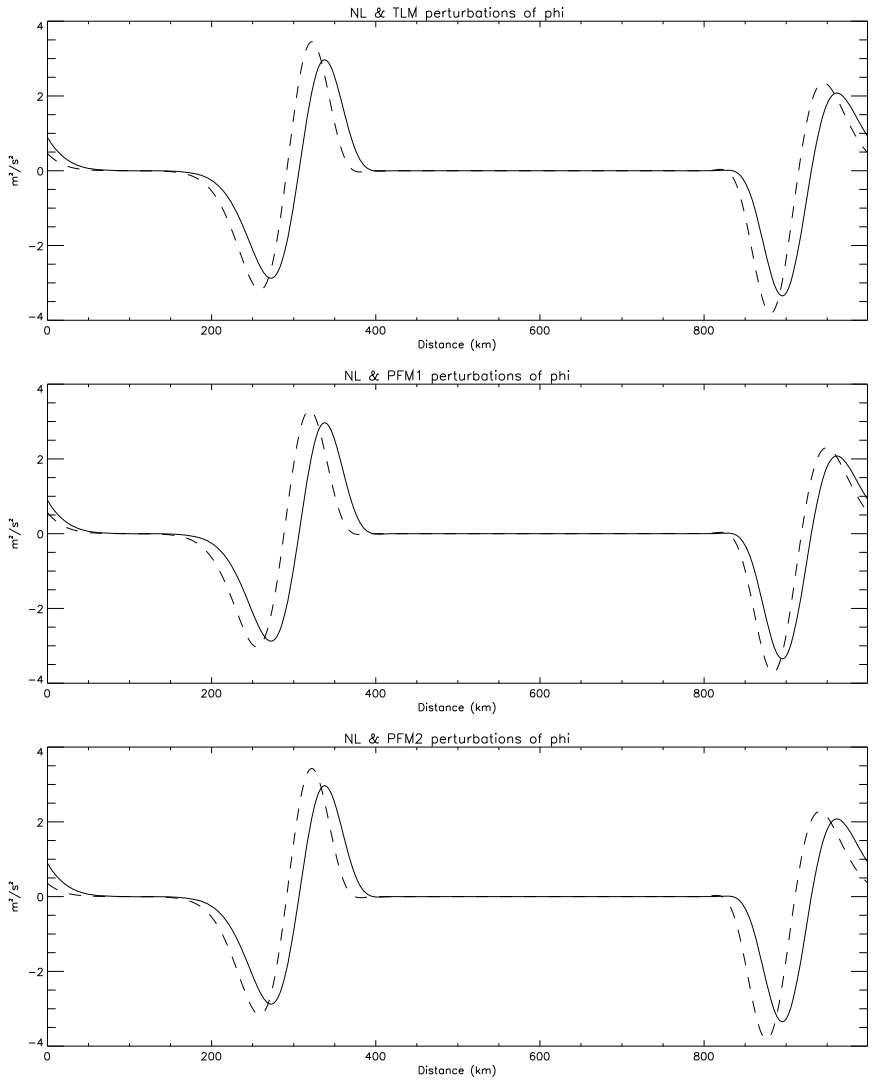

Figure 5.14: Comparison of final nonlinear ϕ perturbation with the corresponding perturbation from each of the linear models after $10,000s$, for $\Delta t = 250s$. The top figure is for the tangent linear model, the centre figure for the first perturbation forecast model and the bottom figure for the second perturbation forecast model.

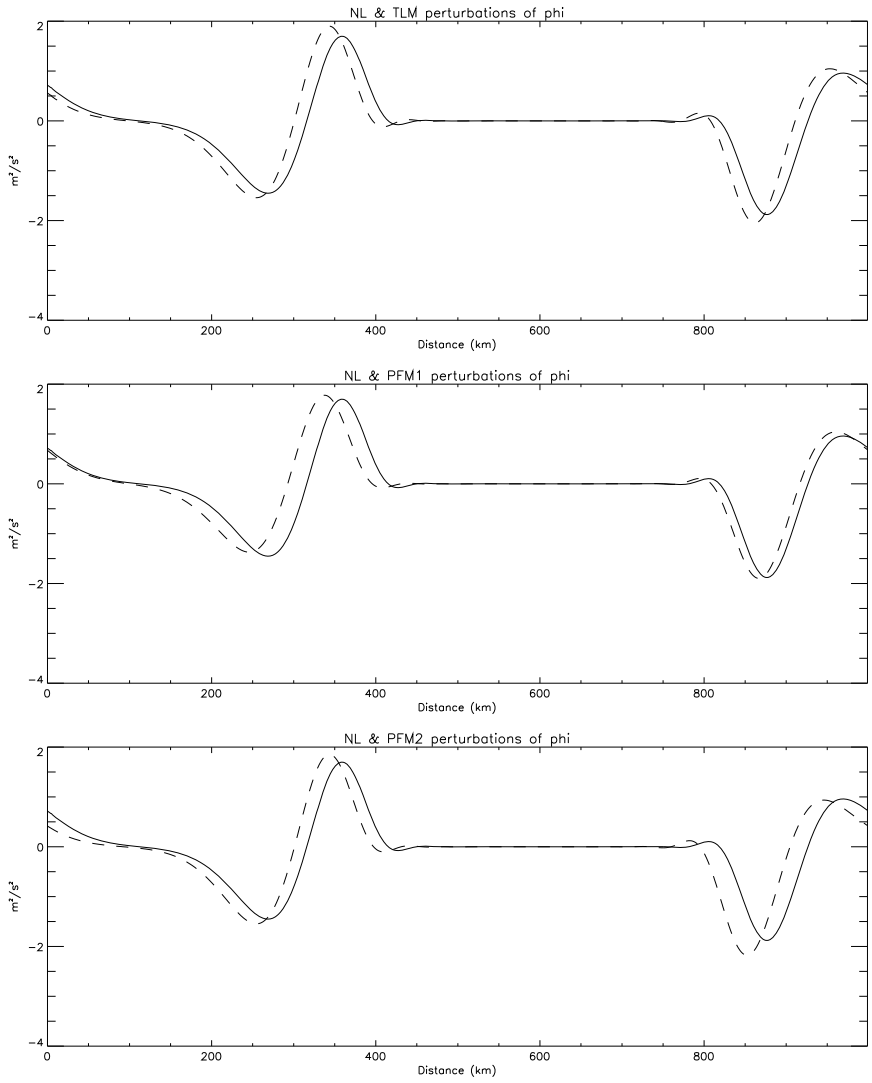

Figure 5.15: Comparison of final nonlinear ϕ perturbation with the corresponding perturbation from each of the linear models after $10,000s$, for $\Delta t = 500s$. The top figure is for the tangent linear model, the centre figure for the first perturbation forecast model and the bottom figure for the second perturbation forecast model.

problem of Chapter 4 this approximation still had the same second order accuracy as the original scheme. Thus for the first perturbation forecast model we replace (5.78) and (5.79) by

$$\begin{aligned}
&\frac{1}{\Delta t}\left(\delta u_{i+\frac{1}{2}}^{n+1}-\delta u_{du}^{n}\right)+(1-\alpha_1)\frac{\partial\delta\phi}{\partial x}\bigg|_{du}^{n}+\alpha_1\frac{\partial\delta\phi}{\partial x}\bigg|_{i+\frac{1}{2}}^{n+1}\\
+\;&(1-\alpha_3)(\delta u)_{du}^{n}\left(\frac{\partial\bar{u}}{\partial x}\right)_{du}^{n+\frac{1}{2}}+\alpha_3(\delta u)_{i+\frac{1}{2}}^{n+1}\left(\frac{\partial\bar{u}}{\partial x}\right)_{i+\frac{1}{2}}^{n+\frac{1}{2}}=0, \qquad (5.137)
\end{aligned}$$

$$\begin{aligned}
&\frac{1}{\Delta t}\left(\frac{\delta\phi_i^{n+1}}{\bar{\phi}_i^{n+\frac{1}{2}}}-\frac{\delta\phi_{d\phi}^{n}}{\bar{\phi}_{d\phi}^{n+\frac{1}{2}}}\right)+(1-\alpha_2)\frac{\partial\delta u}{\partial x}\bigg|_{d\phi}^{n}+\alpha_2\frac{\partial\delta u}{\partial x}\bigg|_{i}^{n+1}\\
+\;&(1-\alpha_4)\,\overline{(\delta u)}^{x}\bigg|_{d\phi}^{n}\left(\frac{\partial(\ln\bar{\phi})}{\partial x}\right)_{d\phi}^{n+\frac{1}{2}}\\
+\;&\alpha_4\,\overline{(\delta u)}^{x}\bigg|_{i}^{n+1}\left(\frac{\partial(\ln\bar{\phi})}{\partial x}\right)_{i}^{n+\frac{1}{2}}=0. \qquad (5.138)
\end{aligned}$$

A calculation of the truncation error around the mid-point of the trajectory shows that for the momentum equation the truncation error is exactly as for the unapproximated version of the model and is given by (5.119). However for the mass continuity equation we now get a truncation error

$$\begin{aligned}
\tau_{\phi}^{P1} &= -\left(\frac{1}{\bar{\phi}}\right)_t\delta\phi\\
&+ (2\alpha_2-1)\frac{\Delta t}{2}\left(\delta u_{xt}+\bar{u}\delta u_{xx}\right)_{x_m}^{t_m}\\
&+ (2\alpha_4-1)\frac{\Delta t}{2}((\delta u(\ln\bar{\phi})_x)_t+\bar{u}(\delta u(\ln\bar{\phi})_x)_x)_{x_m}^{t_n}+O(\Delta t^2). \qquad (5.139)
\end{aligned}$$

We see that for $(\bar{\phi}^{-1})_t\neq 0$ the first term of the truncation error is of order zero and so the scheme (5.138) is not a consistent approximation to the continuous linear equation (5.17). Further analysis shows that this zero order term arises from the approximation of the linearization state within the discretization of the advective term

$$\frac{D}{Dt}\left(\frac{\delta\phi}{\bar{\phi}}\right). \qquad (5.140)$$

An alternative method of approximating the linearization state at one time level only would be to average the time level n and time level $n+1$ values. However, since this averaging is an $O(\Delta t^2)$ approximation to the value at the middle of the time step, the zero order truncation error term appears in the same way.

We illustrate this error by repeating the first experiment of Section 5.4.3 for the first perturbation forecast model, which previously gave the result shown in Figure 5.7. We first rerun the experiment using a linearization state defined by the average of the time level n and time level $n+1$ values at the correct spatial point. The output at the end of the run is shown in Figure 5.16. It is clear that for both the u and ϕ fields the linear model solution is completely incorrect. If however we replace the linearization state in the $\delta\phi/\bar{\phi}$ terms of (5.138) with the correct values, but use the averaged values of the linearization state elsewhere in (5.137) and (5.138), then such a large error does not occur. The output from this experiment is shown in Figure 5.17, which is hard to distinguish from Figure 5.7.

It is possible to extend this analysis to show that a zero order term will occur with such an approximation to the linearization state wherever a time-varying linearization state is included within an advective term of the perturbation forecast model. In general this will be the case if the nonlinear model contains the semi-Lagrangian advection of a quantity which is a nonlinear function of the model variables. For example, in the nonlinear model of this chapter we advect $\ln\phi$ and so this leads to a $1/\bar{\phi}$ term in the perturbation forecast model advection. If we had chosen to discretize the alternative form of the mass continuity equation (5.2), which advects ϕ itself, then we would not have had a problem with consistency even with the time-averaged linearization state.

For the three-dimensional model being developed at the Met Office, which we discuss in Chapter 6, the problem of the zero-order term does not arise since all the quantities being advected are linear in the model variables. However, treating the logarithmic form of the continuity equation with a semi-Lagrangian scheme is

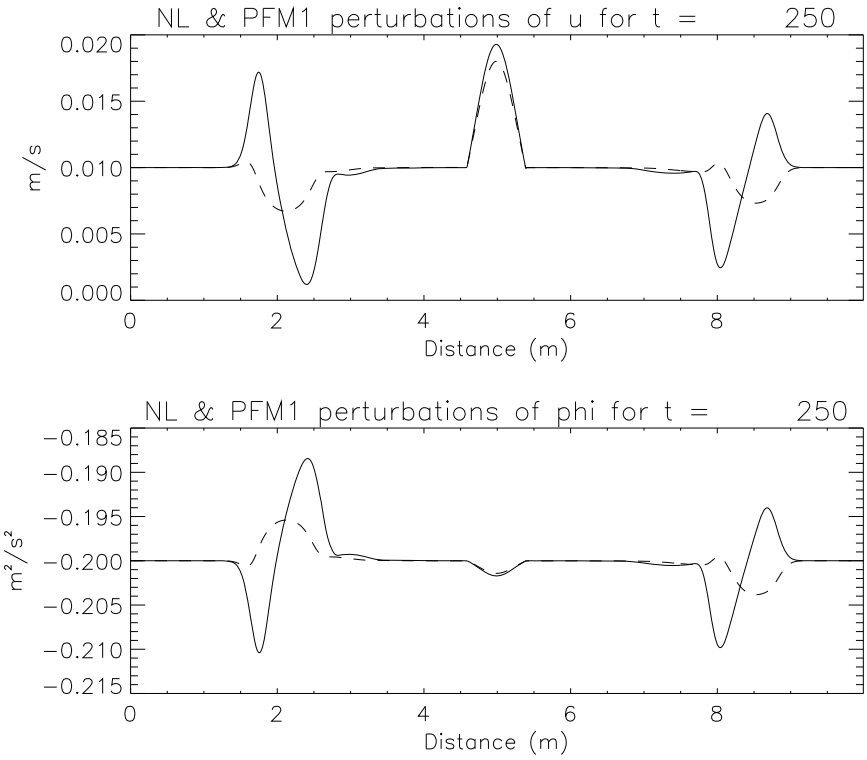

Figure 5.16: Comparison of nonlinear and linear perturbations for the first perturbation forecast model after 250 time steps, with the linearization state averaged to the middle of the time step. The solid line shows the nonlinear perturbation and the dashed line the output from the perturbation forecast model.

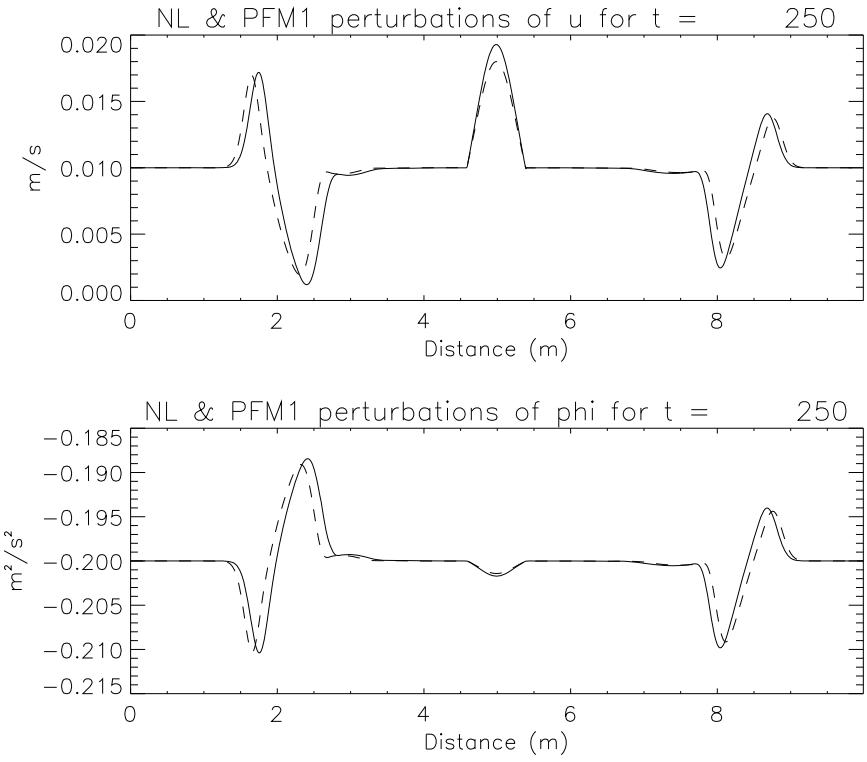

Figure 5.17: Comparison of nonlinear and linear perturbations for the first perturbation forecast model after 250 time steps, with the linearization state averaged to the middle of the time step in all parts of the scheme except the advection of $\delta\phi/\bar{\phi}$. The solid line shows the nonlinear perturbation and the dashed line the output from the perturbation forecast model.

not uncommon. For example the operational models of the European Centre for Medium-range Weather Forecasting [84], [37], and of the Canadian Meteorological Centre [16], both use the semi-Lagrangian advection of a logarithmic quantity within the discretization of the continuity equation. The development of a perturbation forecast version for these models would therefore require great care to ensure consistency of the underlying scheme.

Finally, if we choose to approximate the linearization state outside of the advection terms by using the time level n values in place of the time level $n+1$ values in (5.78) and (5.79), then we obtain the truncation errors

$$\begin{aligned} \tau_u^{P1} &= (2\alpha_1 - 1)\frac{\Delta t}{2}\left(\delta\phi_{xt} + \bar{u}\delta\phi_{xx}\right)_{x_m}^{t_m} \\ &+ (2\alpha_3 - 1)\frac{\Delta t}{2}\left(\delta u_t \bar{u}_x + \bar{u}(\delta u \bar{u}_x)_x\right)_{x_m}^{t_m} \\ &- \frac{\Delta t}{2}(\delta u \bar{u}_{xt})_{x_m}^{t_m} + O(\Delta t^2) \end{aligned} \tag{5.141}$$

for the momentum equation and

$$\begin{aligned} \tau_\phi^{P1} &= (2\alpha_2 - 1)\frac{\Delta t}{2}\left(\delta u_{xt} + \bar{u}\delta u_{xx}\right)_{x_m}^{t_m} \\ &+ (2\alpha_4 - 1)\frac{\Delta t}{2}(\delta u_t(\ln\bar{\phi})_x + \bar{u}(\delta u(\ln\bar{\phi})_x)_x)_{x_m}^{t_m} \\ &- \frac{\Delta t}{2}(\delta u(\ln\bar{\phi})_{xt})_{x_m}^{t_m} + O(\Delta t^2) \end{aligned} \tag{5.142}$$

for the mass continuity equation. We see that the resulting scheme is only first order accurate in time for all choices of the time-weighting parameters α_i. This agrees with the results for the ordinary differential problem in Section 4.5. For that problem we also found that approximating the time level $n+1$ linearization state with time level n values reduced the scheme from second to first order in time.

5.6 Estimating the tangent linear model error

In Section 5.4.2 we illustrated the difficulty of verifying a perturbation forecast model, since although it may be comparable with a tangent linear model for finite

perturbations, the errors do not tend to zero as a perturbation becomes infinitesimally small. In the experiments so far in this chapter we have been able to verify the output of the perturbation forecast models by comparison with the tangent linear model. For the three-dimensional models being used at the Met Office we do not have this opportunity, since we only have the perturbation forecast model and do not have the tangent linear of the discrete nonlinear model. As a proposal for overcoming this problem we developed in Section 3.3 formulae for estimating the linearization error and solution error we would obtain if we were to use a tangent linear model. Since for the shallow water model of this chapter we have the true tangent linear available, we are able to verify the usefulness of these formulae.

In order to validate the formulae developed in Section 3.3 we run again the first experiment from Section 5.4.3. The nonlinear model is then run perturbed by a perturbation $(\gamma\delta u_0, \gamma\delta\phi_0)$, where we use values of $\gamma = 0.5, 0.1, 0.02, 0.01$. For each value of γ we can calculate the estimated linearization error using (3.32) and the estimated solution error using (3.35). These can then be compared with the actual linearization error and solution error of the tangent linear model initialized with the perturbation $(\delta u_0, \delta\phi_0)$.

We first consider the evolution of the solution error with time for each value of γ. We can consider the contributions to the solution error from the u and ϕ fields separately. We choose to plot the values for u rather than ϕ since we find that the values of the solution error are higher and so this will provide a better test of the accuracy of our theory. In Figure 5.18 we plot the true and estimated solution error of the perturbation to the u field. For each of the individual figures the true solution error of the tangent linear model is shown by the solid line and the solution error $\hat{E}_S$ estimated using (3.35) is shown by the dashed line. We see that for a value of $\gamma = 0.5$ the estimate is only good for approximately the first 70 time steps. However as the value of γ is reduced the estimate $\hat{E}_S$ provides a better approximation to the true solution error throughout the period of the run. Hence we see that for a

suitably chosen value of the parameter γ the estimated solution error $\hat{E}_S$ provides a good estimate to the actual solution error obtained using a tangent linear model.

One problem we have is how to choose a suitable value of γ in practice when we do not have the true error to compare with. The value needs to be small enough to provide a good estimate, but still large enough to avoid too much rounding error in the calculation of $\boldsymbol{\mathcal{E}}^n$. We see from Figure 5.18 that as the value of γ is reduced, the estimates of the solution error converge to the true value. Thus by calculating the estimated solution error for different values of γ it is possible to see at what value the estimates begin to converge. The largest value of γ which appears to match the converged solution can then be taken as the most suitable value of the parameter with which to calculate the error in the fields. For example in this experiment we would take $\gamma = 0.02$. This is the method which we will use in Chapter 6 to obtain a suitable value of γ for our three-dimensional model.

Thus we have illustrated that the estimated solution error $\hat{E}_S$ is a good approximation to the true solution error and also provides a method of choosing the value of γ. We now look at the estimate of the linearization error itself. In Figure 5.19 we plot the true linearization error for the u field after 250s and the estimated linearization error $\boldsymbol{\mathcal{E}}^n$ for values of $\gamma = 0.1, 0.02, 0.01$. We see that qualitatively $\boldsymbol{\mathcal{E}}^n$ is a good estimate of the true linearization error. In Figure 5.20 we plot the differences of the estimated error from the true linearization error for each of these values of γ. We see that using a value of $\gamma = 0.02$ compared with $\gamma = 0.1$ introduces approximately a five-fold decrease in the maximum difference. The values of the maxima for these values of γ are 3.43×10^{-4} and 6.78×10^{-5} respectively. Such a difference would be expected, since we see from (3.31) and (3.33) that

$$E_l^n - \mathcal{E}_l^n = -\gamma \frac{1}{3!} \sum_{i=1}^{p} \sum_{j=1}^{p} \sum_{k=1}^{p} \frac{\partial^3 S_l}{\partial U_i \partial U_j \partial U_k}(t_n, t_0, \mathbf{U^0}) \delta U_i^a \delta U_j^a \delta U_k^a + h.o.t., \quad (5.143)$$

which is proportional to γ. The size of this difference should be compared to the maximum value of the linearization error itself, which is 4.5×10^{-3}. We find that

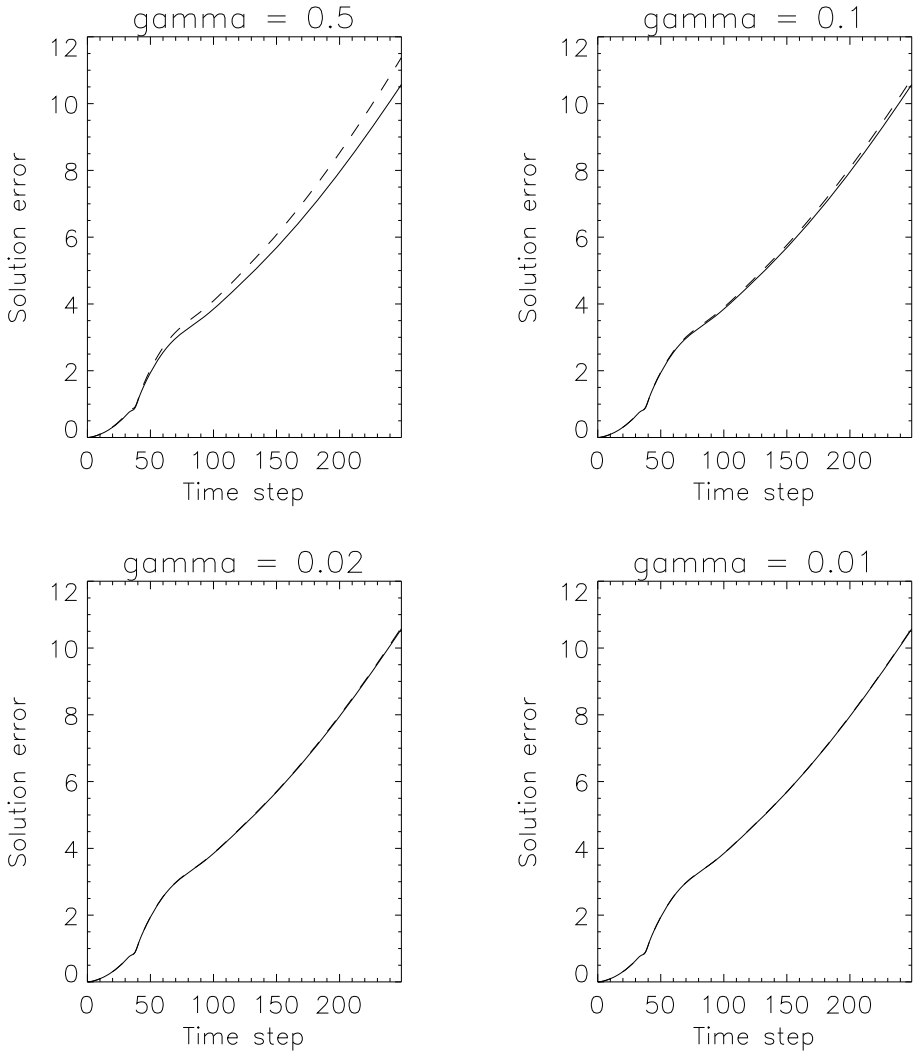

Figure 5.18: Comparison of the evolution of the estimated solution error $\hat{E}_S$ with that of the true solution error of the tangent linear model E_S for values of $\gamma = 0.5, 0.1, 0.02, 0.01$. The dashed line shows the estimated value and the solid line shows the true value. The errors are calculated for the perturbations to the u field.

using the estimate with $\gamma = 0.02$ introduces an error of approximately 1.5% in the calculation of the linearization error. Thus the estimate with this value of the parameter is also quantitatively very good. For the stationary solution in the centre of the domain the true linearization error is 1.3×10^{-3} and the estimate differs from this by approximately 0.25%. A further reduction in γ by a factor of 2 to 0.01 reduces the maximum difference by another factor of 2 to 3.4×10^{-5}. However, this is at the expense of introducing some noise due to rounding error, as can be seen from the third difference plot of Figure 5.20. Thus it seems that the values of $\gamma = 0.02$, which from the plots of solution error was conjectured to be the most suitable value of the parameter, does indeed provide a good compromise between accuracy of the formulae and rounding error.

The experiments of this section have shown that the formulae we derived in Section 3.3 can provide an accurate estimate of the linearization error and solution error of a tangent linear model using only the nonlinear model. This estimate is useful both qualitatively and quantitatively. Having demonstrated this numerically we can have some confidence in the use of these estimates in the three-dimensional model of Chapter 6, for which we do not have an exact tangent linear model. The numerical experiments have also provided a method of choosing the parameter γ such that we obtain a good balance between accuracy and the introduction of spurious noise.

5.7 Summary

In this chapter we have investigated the semi-continuous approach for producing a linear model in the context of a partial differential equation problem, using numerical schemes similar to those used in weather forecasting models. Beginning with a one-dimensional shallow water system we developed two versions of a perturbation forecast model and compared them to the tangent linear model derived by the

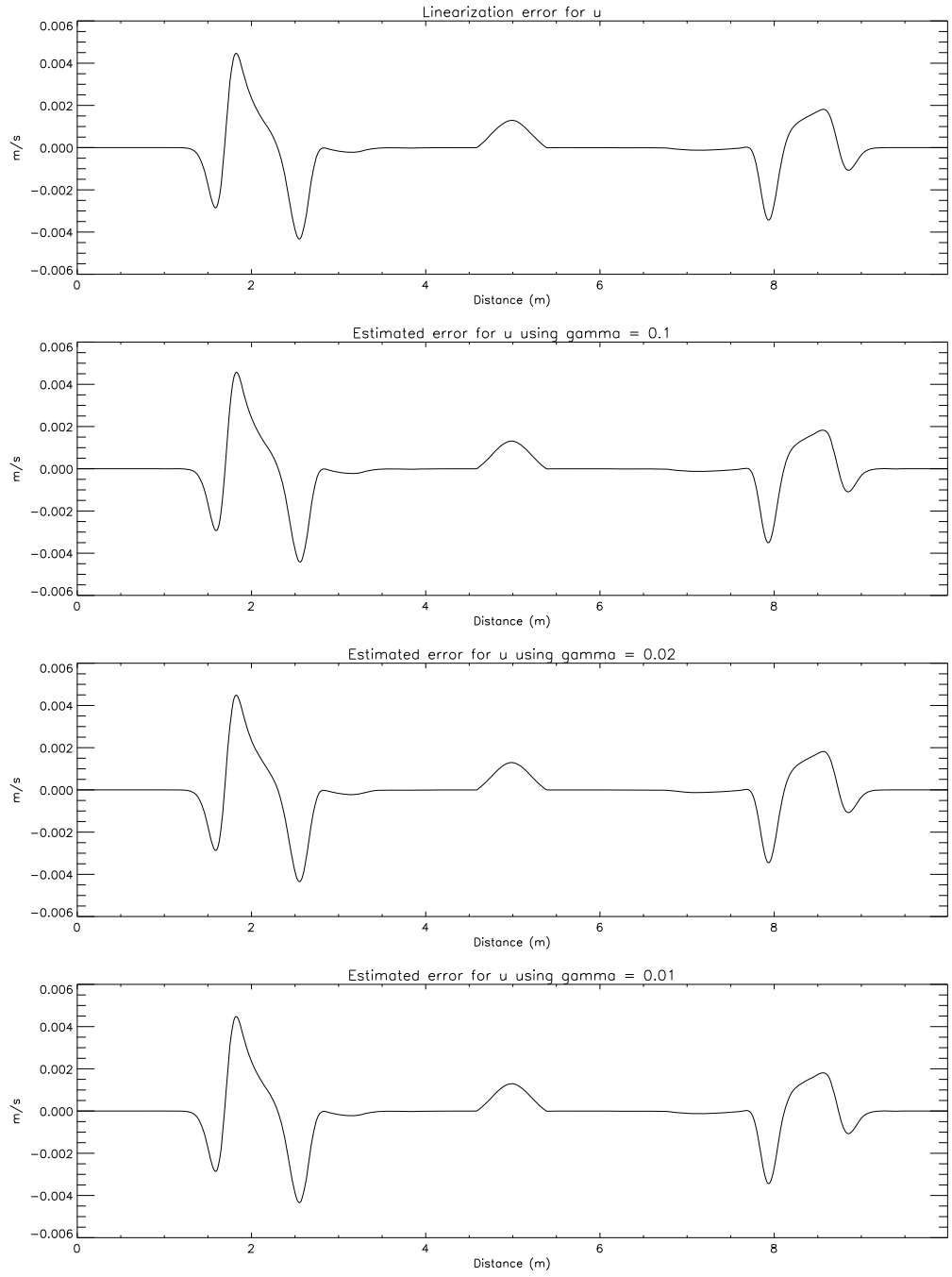

Figure 5.19: Linearization error for u field at the end off the run. The top figure shows the true linearization error and the other figures show the estimated linearization error using values of $\gamma = 0.1, 0.02, 0.01$.

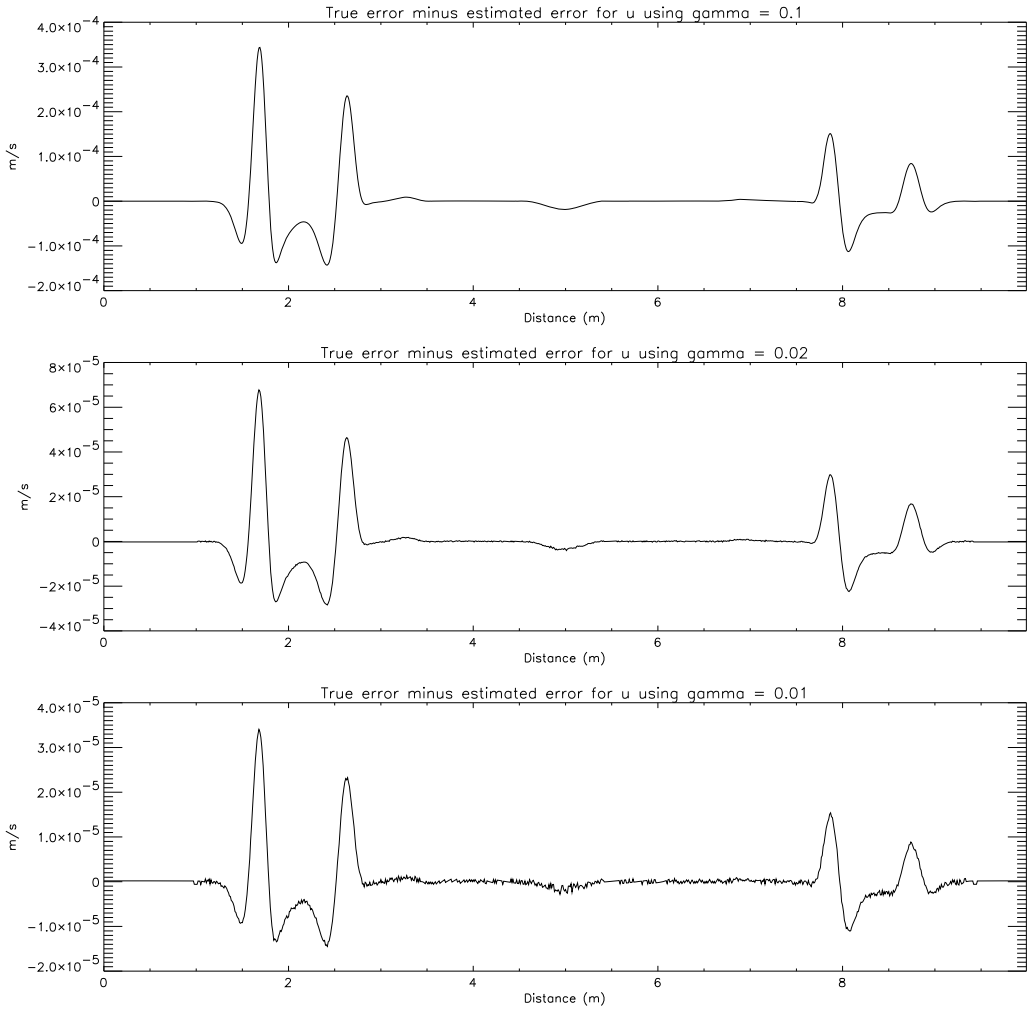

Figure 5.20: True linearization error minus estimated linearization error for values of $\gamma = 0.1, 0.02, 0.01$.

discrete approach. We have shown that the semi-continuous method can be used to design a linear model which is as equally valid as the tangent linear model for finite perturbations. However, this chapter has also illustrated several problems which can occur when using this approach and which must be taken into account when it is applied to a full weather forecasting model.

Firstly, it is clear that when we are treating a system of partial differential equations, there is some extra degree of freedom in deriving a perturbation forecast model which is not present in the ordinary differential equation problem. The linearization of the analytical equations can produce terms in the linear equations which have no obvious counterpart in the nonlinear model and so no obvious discretization. This was seen in the shallow water model of this chapter. The linearization of the analytical equations produced terms containing the perturbation wind multiplied by the gradient of the linearization state field. In the two versions of the perturbation forecast model described in Sections 5.2.3 and 5.2.4 we proposed two different ways of discretizing this term. Our analysis showed that one of these models was second order accurate in time for a centred time averaging, while the other remained first order for all choices of the time weightings. The tangent linear model was also second order for a centred time averaging. Thus we find that the development of a perturbation forecast model for a partial differential equation problem introduces the possibility of choosing a numerical scheme which is detrimental to the accuracy of the model. This illustrates the necessity of applying the semi-continuous method with great care and with a good understanding of the underlying numerical schemes.

We have also shown that the perturbation forecast model requires the time level of the linearization state to be chosen carefully. In the ordinary differential equation problem of Chapter 4 taking the linearization state at the centre of the time step was sufficient to retain second order accuracy, while using the linearization state at the start of the time step reduced the accuracy to first order. This was also true for the shallow water model of this chapter, provided that the correct linearization state

was used within the semi-Lagrangian advection scheme. However, if approximations were made to the linearization state within the advection scheme, then the resulting perturbation forecast model was no longer consistent. This reinforces the conclusion of Chapter 4 that any approximations in the linearization state must be considered in the context of the whole scheme.

Finally we have illustrated that a perturbation forecast model is more difficult to test than a tangent linear model since it is not correct in the sense of Definition 3.2 and so the relative error or solution error do not reduce to zero as the perturbation size is reduced. This provides a problem for testing our three-dimensional weather forecasting model, since we do not have the tangent linear model solution to compare with. To overcome this we developed in Chapter 3 a method of estimating the linearization error and solution error that a tangent linear model would have, by using only the nonlinear model. In this chapter we have been able to demonstrate that this method gives useful estimates and we have also introduced a practical method of specifying a value for the variable parameter γ which the method requires. Thus we can be more confident in the use of this estimate to assess the accuracy of our three-dimensional perturbation forecast model in Chapter 6.

Chapter 6

Application to a Three-Dimensional Model

In Chapters 4 and 5 we have illustrated the viability of developing a linear model by the semi-continuous method. We now apply these ideas to a three-dimensional weather forecasting model. The model we use is the adiabatic version of the new integration scheme being developed at the Met Office for future operational use. The linearization of this model and the adjoint of the linear model are needed as part of the development of an incremental four-dimensional variational data assimilation scheme. However, as we discuss in Section 6.1.2, certain properties of the numerical scheme in the nonlinear model would cause difficulties if we tried to linearize the discrete scheme directly. We have therefore chosen to develop the linear model by applying the semi-continuous method and discretizing the linearized analytical equations. In following this method some of the choices for discretization in the linear model are then constrained by the need to be able to derive the adjoint model easily. In this chapter the scheme for the linear model is set out in detail and then numerical experiments are used to determine the validity of the model for forecasting the evolution of a perturbation. Since it is not straightforward to derive a linearization of the discrete scheme to compare with, we must use other measures

to assess the validity of the model. These will be outlined as we discuss specific numerical results in Section 6.3.

6.1 The nonlinear model

6.1.1 The continuous equations

The nonlinear model is based on the fully compressible Navier-Stokes equations on a sphere. The equations are written in spherical coordinates (r, λ, ϕ), with a height based vertical coordinate, where r defines the distance from the centre of the Earth. The horizontal coordinates λ, ϕ are the longitudinal and latitudinal directions on a regular latitude-longitude grid. The vertical levels in the numerical model are defined by a coordinate η, with the levels following the terrain near the surface of the model and gradually becoming flat higher in the atmosphere. We assume that the coordinate η is a smooth, differentiable function of r, with $\partial\eta/\partial r > 0$. The coordinate is defined such that $\eta = 0$ on the model level following the Earth's surface and $\eta = 1$ on the top model level. Then derivatives along constant r surfaces can be written in terms of derivatives along constant η surfaces using the transformation

$$\left.\frac{\partial}{\partial s}\right|_r = \left.\frac{\partial}{\partial s}\right|_\eta - \left.\frac{\partial r}{\partial s}\right|_\eta \left.\frac{\partial}{\partial r}\right|_{\lambda,\phi,t}, \tag{6.1}$$

where $s = \lambda, \phi$ or t. This relationship also allows us to define a generalized vertical velocity $\dot{\eta}$ with respect to the coordinate system. Noting that the material derivative in height coordinates is given by

$$\frac{D}{Dt} \equiv \left.\frac{\partial}{\partial t}\right|_r + \frac{u}{r\cos\phi}\left.\frac{\partial}{\partial \lambda}\right|_r + \frac{v}{r}\left.\frac{\partial}{\partial \phi}\right|_r + w\frac{\partial}{\partial r} \tag{6.2}$$

we define a vertical velocity $\dot{\eta} = D\eta/Dt$. Then we find that $\dot{\eta}$ is related to w by means of the formula

$$\dot{\eta} = \frac{1}{\partial r/\partial \eta}\left[w - \frac{u}{r\cos\phi}\left.\frac{\partial r}{\partial \lambda}\right|_\eta - \frac{v}{r}\left.\frac{\partial r}{\partial \phi}\right|_\eta\right]. \tag{6.3}$$

The material derivative in the η coordinate system becomes

$$\frac{D}{Dt} \equiv \left.\frac{\partial}{\partial t}\right|_\eta + \frac{u}{r\cos\phi}\left.\frac{\partial}{\partial\lambda}\right|_\eta + \frac{v}{r}\left.\frac{\partial}{\partial\phi}\right|_\eta + \dot{\eta}\frac{\partial}{\partial\eta}. \tag{6.4}$$

The adiabatic form of the continuous model consists of the momentum equations in three dimensions, the mass continuity equation, the thermodynamic equation and the equation of state. These equations then take the following form in the model coordinates, where the notation is set out in Table 6.1, adapted from Table 1 of [18]:

$$\frac{Du}{Dt} - 2\Omega\sin\phi v + 2\Omega\cos\phi w - \frac{uvtan\phi}{r} + \frac{uw}{r} + \frac{c_p\theta}{rcos\phi}\left(\frac{\partial\Pi}{\partial\lambda} - \frac{\partial\Pi}{\partial r}\frac{\partial r}{\partial\lambda}\right) = 0, \tag{6.5}$$

$$\frac{Dv}{Dt} + 2\Omega\sin\phi u + \frac{u^2 tan\phi}{r} + \frac{vw}{r} + \frac{c_p\theta}{r}\left(\frac{\partial\Pi}{\partial\phi} - \frac{\partial\Pi}{\partial r}\frac{\partial r}{\partial\phi}\right) = 0, \tag{6.6}$$

$$\frac{Dw}{Dt} - 2\Omega\cos\phi u - \frac{(u^2+v^2)}{r} + g + c_p\theta\frac{\partial\Pi}{\partial r} = 0, \tag{6.7}$$

$$\frac{D\rho}{Dt} + \rho\nabla.\underline{u}_\eta = 0, \tag{6.8}$$

$$\frac{D\theta}{Dt} = 0, \tag{6.9}$$

$$\Pi^{\frac{\kappa-1}{\kappa}}\rho\theta = \frac{p_0 r^2}{\kappa c_p}. \tag{6.10}$$

The symbol $\underline{u}_\eta$ in (6.8) denotes the velocity vector $(u, v, \dot{\eta})$.

The terms in (6.5), (6.6) and (6.7) involving the Earth's rotation rate Ω arise because the coordinate system we are using is rotating with the Earth and so is a noninertial reference frame. These terms are known as the *Coriolis terms*. The other terms arising in these equations from the choice of coordinate system are the terms proportional to a quadratic function of the velocity components divided by r. We refer to these terms as the *metric terms*. They come from the fact that we use the spherical coordinates λ, ϕ in the horizontal direction, with unit vectors $\mathbf{i}, \mathbf{j}$ directed in an eastward and northward direction respectively. Thus, with respect to a cartesian coordinate system, these vectors are a function of position on the Earth and this is accounted for by these metric terms in the equations.

(r, λ, ϕ)	Spherical polar coordinates relative to centre of Earth
η	Terrain-following vertical coordinate
u, v, w	Velocity components
$\dot{\eta}$	Generalized vertical velocity
p, p_0	Pressure and reference value of pressure
Π	Exner pressure $\left(\frac{p}{p_0}\right)^{\kappa}$
c_p	Specific heat of dry air at constant pressure
κ	Gas constant divided by c_p
ρ	Density scaled by r^2
θ	Potential temperature
Ω	Earth's rotation rate
f	$2\Omega \sin \phi$ (Coriolis parameter)
g	Gravitational constant

Table 6.1: Symbols used in equations. Table adapted from Table 1 of [18].

6.1.2 The discrete nonlinear model

We present here a brief outline of the numerical scheme used in the nonlinear model. Fuller details of the implementation and justification for some of the choices made can be found in [18] and [19]. The model is implemented on a staggered grid, using an Arakawa C staggering in the horizontal and a Charney-Phillips staggering in the vertical. The scheme itself combines a semi-Lagrangian treatment of advection with a semi-implicit treatment of terms responsible for sound and gravity waves. The procedure used is a predictor-corrector method and consists of the following steps:

1. Predict initial estimates of updates to the wind components, density and potential temperature.

2. Use these predicted values and the equation of state to form an equation for the update to the pressure variable. The resulting equation is a three-dimensional elliptic equation with variable coefficients.

3. Solve this elliptic equation and update the pressure variable.

4. Use the updated value of pressure to correct the other variables.

The initial estimates are obtained by means of the two-time-level semi-Lagrangian scheme of Bates et al. [8], using information from the current time level. The departure points are determined from the algorithm of Ritchie and Beaudoin [73] with linear interpolation. This is the first point where we would encounter difficulties if we were to attempt a linearization of the discrete nonlinear scheme. We have seen from the studies reviewed in Section 3.2 and from the shallow water model in Chapter 5 that this part of the scheme includes an iterative process and non-differentiable functions, both of which which must be taken account of in the linearization. Although it is possible to treat such functions, as was illustrated in the tangent linear model of Section 5.2.2, the approach of discretizing the continuous linear equations avoids such complications.

Within the three-dimensional nonlinear model there are various predictor-corrector steps before the formation of the elliptic equation. This is to enable the nonlinear terms to be calculated as accurately as possible. However, if we were to linearize this discrete scheme we would require values of the linearization state from each predictor-corrector step either to be stored from the nonlinear model base state run or to be recalculated during each run of the linear model. We see in the scheme developed for the perturbation forecast model in Section 6.2 that by using the semi-continuous approach we avoid the need for these intermediate values.

Once the initial estimates of the corrections have been calculated, an elliptic equation for the pressure correction is formulated. In the nonlinear model this is done by first linearizing the equation of state (6.10). We define the time tendencies of ρ, θ and Π in one time step by

$$\rho' \equiv \rho^{n+1} - \rho^n, \qquad \theta' \equiv \theta^{n+1} - \theta^n, \qquad \Pi' \equiv \Pi^{n+1} - \Pi^n, \tag{6.11}$$

where n and $n+1$ indicate the time level. Then linearizing the equation of state in terms of these variables we obtain

$$\kappa \Pi \theta \rho' + \kappa \rho \theta \Pi' + \kappa \rho \Pi \theta' = -\kappa \rho \Pi \theta + \frac{r^2 p}{c_p}, \tag{6.12}$$

where the full model variables are defined at time level n. It is this equation which we solve within the numerical model. We substitute appropriate predicted quantities into (6.12) to obtain an elliptic equation for the pressure correction Π'. This step ensures that the elliptic equation obtained is linear, but at the expense of accuracy. An alternative strategy is to write the continuity equation in logarithmic form and retain the weakly nonlinear elliptic equation which results. This is the strategy adopted by the Canadian Meteorological Centre [16]. The presently used method leads to a linear Helmholtz equation, which is solved using a generalized conjugate residual algorithm as described in [78]. Preconditioning of the problem is performed using an alternating direction implicit (ADI) method, as proposed in [77].

6.2 The perturbation forecast model

6.2.1 The continuous equations

We represent the state vector of the continuous nonlinear model by

$$\mathbf{x_c} = (u, v, w, \Pi, \rho, \theta). \tag{6.13}$$

The continuous equations for the perturbation forecast model are obtained by first setting

$$\mathbf{x_c} = \bar{\mathbf{x}}_\mathbf{c} + \boldsymbol{\delta}\mathbf{x_c}, \tag{6.14}$$

where $\bar{\mathbf{x}}_\mathbf{c}$ is a spatially and temporally varying background state satisfying the nonlinear equations and $\boldsymbol{\delta}\mathbf{x_c}$ is the perturbation vector

$$\boldsymbol{\delta}\mathbf{x_c} = (\delta u, \delta v, \delta w, \delta\Pi, \delta\rho, \delta\theta). \tag{6.15}$$

We then substitute into the nonlinear equations and drop products of perturbations in the usual way to obtain the linearized set of equations.

However, before carrying out this procedure we can use our physical insight to simplify the equation set that we wish to linearize. Firstly we omit in (6.5) and (6.6) the metric and Coriolis terms in which w appears and in the vertical velocity equation we omit the metric and Coriolis terms involving u and v. This is based on the commonly used "traditional approximation" [22]. However, whereas this approximation is usually preceded by assuming that $1/r$ may be replaced by $1/a$, where a is the constant radius of the Earth (the shallow atmosphere approximation) [58], we retain a full three-dimensional height field in the equations. On the basis of a simple scale analysis we also make the extra approximation of ignoring the advection of w, treating the time derivative as a partial derivative. After all of these approximations the full set of momentum equations which we linearize is

$$\frac{Du}{Dt} - 2\Omega \sin\phi v - \frac{uvtan\phi}{r} + \frac{c_p\theta}{rcos\phi}\left(\frac{\partial\Pi}{\partial\lambda} - \frac{\partial\Pi}{\partial r}\frac{\partial r}{\partial\lambda}\right) = 0, \tag{6.16}$$

$$\frac{Dv}{Dt} + 2\Omega \sin\phi u + \frac{u^2 tan\phi}{r} + \frac{c_p\theta}{r}\left(\frac{\partial \Pi}{\partial \phi} - \frac{\partial \Pi}{\partial r}\frac{\partial r}{\partial \phi}\right) = 0, \tag{6.17}$$

$$\frac{\partial w}{\partial t} + g + c_p\theta\frac{\partial \Pi}{\partial r} = 0. \tag{6.18}$$

Having made these approximations we perform the linearization procedure. For the linearization of the approximate momentum equations (6.16), (6.17) and (6.18) we obtain the linearized equations

$$\begin{aligned}\frac{D\delta u}{Dt} \quad & + \boldsymbol{\delta u}.\nabla\bar{u} - 2\Omega\sin\phi\delta v - \frac{\delta u\bar{v}\tan\phi}{r} - \frac{\bar{u}\delta v\tan\phi}{r} \\ & + \frac{c_p\delta\theta}{r\cos\phi}\left(\frac{\partial\bar{\Pi}}{\partial\lambda} - \frac{\partial\bar{\Pi}}{\partial r}\frac{\partial r}{\partial\lambda}\right) + \frac{c_p\bar{\theta}}{r\cos\phi}\left(\frac{\partial\delta\Pi}{\partial\lambda} - \frac{\partial\delta\Pi}{\partial r}\frac{\partial r}{\partial\lambda}\right) = 0,\end{aligned} \tag{6.19}$$

$$\begin{aligned}\frac{D\delta v}{Dt} \quad & + \boldsymbol{\delta u}.\nabla\bar{v} + 2\Omega\sin\phi\delta u + \frac{2\bar{u}\delta u\tan\phi}{r} \\ & + \frac{c_p\delta\theta}{r}\left(\frac{\partial\bar{\Pi}}{\partial\phi} - \frac{\partial\bar{\Pi}}{\partial r}\frac{\partial r}{\partial\phi}\right) + \frac{c_p\bar{\theta}}{r}\left(\frac{\partial\delta\Pi}{\partial\phi} - \frac{\partial\delta\Pi}{\partial r}\frac{\partial r}{\partial\phi}\right) = 0,\end{aligned} \tag{6.20}$$

where $\boldsymbol{\delta u} = (\delta u, \delta v, \delta\dot{\eta})$.

$$\frac{\partial\delta w}{\partial t} + c_p\delta\theta\frac{\partial\bar{\Pi}}{\partial r} + c_p\bar{\theta}\frac{\partial\delta\Pi}{\partial r} = 0. \tag{6.21}$$

For the linearization of the continuity equation (6.8) and the thermodynamic equation (6.9) we obtain

$$\begin{aligned}\frac{\partial\delta\rho}{\partial t} \quad & + \frac{1}{\partial r/\partial\eta}\left[\frac{1}{\cos\phi}\frac{\partial}{\partial\lambda}\left(\frac{(\delta\rho\bar{u} + \bar{\rho}\delta u)}{r}\frac{\partial r}{\partial\eta}\right) + \frac{1}{\cos\phi}\frac{\partial}{\partial\phi}\left(\frac{(\delta\rho\bar{v} + \bar{\rho}\delta v)}{r}\frac{\partial r}{\partial\eta}\cos\phi\right)\right. \\ & \left. + \frac{\partial}{\partial\eta}\left((\delta\rho\bar{\dot{\eta}} + \bar{\rho}\delta\dot{\eta})\frac{\partial r}{\partial\eta}\right)\right] = 0\end{aligned} \tag{6.22}$$

and

$$\frac{D\delta\theta}{Dt} \quad + \boldsymbol{\delta u}.\nabla\bar{\theta} = 0. \tag{6.23}$$

In order to obtain the linearization of the equation of state, we linearize the form that is actually used in the nonlinear model, given by (6.12). We assume that the state about which we are linearizing satisfies the full equation of state, so that the

right hand side of (6.12) is zero. Then ignoring products of perturbations with the time increments ρ', Π' and θ', we obtain the linearized equation

$$\kappa\bar{\Pi}\bar{\theta}(\delta\rho^{n+1} - \delta\rho^n) + (\kappa - 1)\bar{\rho}\bar{\theta}(\delta\Pi^{n+1} - \delta\Pi^n) + \kappa\bar{\Pi}\bar{\rho}(\delta\theta^{n+1} - \delta\theta^n) = 0. \quad (6.24)$$

The six equations (6.19)-(6.24) form the basis of the perturbation forecast model. The symbol ∇ is the three-dimensional gradient operator, defined on a sphere as

$$\nabla = \left(\frac{1}{r\cos\phi}\frac{\partial}{\partial\lambda}, \frac{1}{r}\frac{\partial}{\partial\phi}, \frac{\partial}{\partial\eta}\right)^T. \quad (6.25)$$

At this point it is also useful to note extra diagnostic relationships arising from a linearization of the corresponding relationships in the nonlinear model. A linearization of the definition of Exner pressure gives a relationship between δp and $\delta\Pi$:

$$\delta\Pi = \frac{\kappa\bar{\Pi}\delta p}{\bar{p}}. \quad (6.26)$$

We also have the linearization of the definition of $\dot{\eta}$ (6.3),

$$\delta\dot{\eta} = \frac{1}{\partial r/\partial\eta}\left[\delta w - \frac{\delta u}{r\cos\phi}\frac{\partial r}{\partial\lambda} - \frac{\delta v}{r}\frac{\partial r}{\partial\phi}\right]. \quad (6.27)$$

Once we have defined this set of equations, we need to decide on an appropriate numerical scheme with which to solve them. We try to follow as closely as possible the scheme used in the nonlinear model, but some changes must be made to accommodate extra terms which arise from the linearization and we also find some other approximations necessary. In the following sections we look at the implementation of this scheme.

6.2.2 General formulation of the numerical scheme

Before looking at the detailed discretization of the perturbation forecast model, it is helpful to write the scheme in its matrix formulation, to set out the different steps

of the solution procedure more clearly. We first define a general state of the discrete perturbation forecast model

$$\boldsymbol{\delta}\mathbf{x} = (\delta u, \delta v, \delta w, \delta\Pi, \delta\rho, \delta\theta), \tag{6.28}$$

where the perturbation fields are now understood to be vectors of values over the model grid points. We let

$$\boldsymbol{\delta}\mathbf{x}' = \boldsymbol{\delta}\mathbf{x}^{n+1} - \boldsymbol{\delta}\mathbf{x}^{n}. \tag{6.29}$$

Then the scheme can be written in the simple form

$$\boldsymbol{\delta}\mathbf{x}^{n+1} = \boldsymbol{\delta}\mathbf{x}^{n} + \mathbf{M}^{-1}\mathbf{P}\boldsymbol{\delta}\mathbf{x}^{n}, \tag{6.30}$$

where $\mathbf{P}$ and $\mathbf{M}$ are matrices denoting the predictor and corrector parts of the scheme.

We note that the variable $\delta\dot{\eta}$ is not included within the vector $\boldsymbol{\delta}\mathbf{x}$, but is treated as a diagnostic quantity calculated at the start of each time step. The pressure variable is taken to be $\delta\Pi$, from which we can calculate δp using (6.26).

The first step of the solution procedure is to calculate the application of the matrix $\mathbf{P}$, which we denote

$$\boldsymbol{\delta}\tilde{\mathbf{x}} = \mathbf{P}\boldsymbol{\delta}\mathbf{x}^{n}. \tag{6.31}$$

This corresponds to the predictor step in the scheme. We must then invert the matrix $\mathbf{M}$ to complete the solution of (6.30). In practice we have the matrix in the operator form

$$\mathbf{M}\boldsymbol{\delta}\mathbf{x}' = \boldsymbol{\delta}\tilde{\mathbf{x}}. \tag{6.32}$$

This system is reduced analytically to a single equation for $\delta\Pi'$, of the form

$$\mathcal{L}\delta\Pi' = RHS, \tag{6.33}$$

where $\mathcal{L}$ is an elliptic operator, which can then be solved using a generalized conjugate residual (GCR) method. The value of $\delta\Pi'$ is then substituted into (6.32) to

provide the other components of $\boldsymbol{\delta}\mathbf{x}'$ and the updated values $\boldsymbol{\delta}\mathbf{x}^{n+1}$ are calculated using

$$\boldsymbol{\delta}\mathbf{x}^{n+1} = \boldsymbol{\delta}\mathbf{x}^{n} + \boldsymbol{\delta}\mathbf{x}'. \tag{6.34}$$

For the model being developed here it is preferable to approximate the matrix $\mathbf{M}$ when forming the elliptic equation for $\delta\Pi'$, to avoid coupling the horizontal momentum equations with the thermodynamic equation. The details of this are explained in Section 6.2.5. For the moment we just note how the matrix notation is adapted in this case. We write the approximation to $\mathbf{M}$ as $\mathbf{M_1}$. In order to form the elliptic equation we replace (6.32) by

$$\mathbf{M_1}\boldsymbol{\delta}\mathbf{x}' = \boldsymbol{\delta}\tilde{\mathbf{x}}. \tag{6.35}$$

This can be rearranged to provide a linear equation of the form

$$\hat{\mathcal{L}}\delta\hat{\Pi}' = RHS, \tag{6.36}$$

which can be solved for $\delta\hat{\Pi}'$, again using a GCR method. The increment to the perturbation Exner pressure field is then found by setting $\delta\Pi' = \delta\hat{\Pi}'$. The increments to the other fields can be calculated using either the approximate matrix equation (6.35) or the original equation (6.32). Although using the original equation would be more accurate, the present version of the model uses the approximate equation for this step since it makes the adjoint model easier to derive. However initial tests have shown little difference between the solutions. Once the increments have been calculated the final update of the perturbations is performed using (6.34).

6.2.3 Outline of the numerical scheme

The aim of the numerical scheme in the perturbation forecast model is to discretize the equations of Section 6.2.1 while following as closely as possible the nonlinear model. The scheme is implemented on the same horizontal and vertical grids and

follows a very similar semi-implicit semi-Lagrangian solution procedure. In this section we set out the semi-discretized form of the equations to indicate how the time discretization is implemented. A more complete description of the scheme is then given in Section 6.2.5. First it is necessary to introduce some notation for the representation of the finite difference equations.

Notation

We define finite difference operators for the horizontal and vertical grids. For the horizontal operators we let $X(\lambda_i, \phi_j)$ be a general point on the horizontal grid, where i, j are the indices in the λ and ϕ directions respectively and the vertical level is unspecified for the purpose of the definitions. For the vertical operators we consider a variable $Z = Z(r_{i,j,k})$ for operators involving r and $Z = Z(\eta_k)$ for operators involving η, where i, j represent the indices in the λ and ϕ directions and k is the vertical level. We then have

- Horizontal averaging operators

$$\overline{X(\lambda_i, \phi_j)}^{\lambda} = \frac{1}{2}\left[X(\lambda_{i+\frac{1}{2}}, \phi_j) + X(\lambda_{i-\frac{1}{2}}, \phi_j)\right], \tag{6.37}$$

$$\overline{X(\lambda_i, \phi_j)}^{\phi} = \frac{1}{2}\left[X(\lambda_i, \phi_{j+\frac{1}{2}}) + X(\lambda_i, \phi_{j-\frac{1}{2}})\right]; \tag{6.38}$$

- Horizontal differencing operators

$$\partial_\lambda X(\lambda_i, \phi_j) = \frac{X(\lambda_{i+\frac{1}{2}}, \phi_j) - X(\lambda_{i-\frac{1}{2}}, \phi_j)}{\Delta\lambda}, \tag{6.39}$$

$$\partial_\phi X(\lambda_i, \phi_j) = \frac{X(\lambda_i, \phi_{j+\frac{1}{2}}) - X(\lambda_i, \phi_{j-\frac{1}{2}})}{\Delta\phi}, \tag{6.40}$$

$$\partial_{2\lambda} X(\lambda_i, \phi_j) = \frac{X(\lambda_{i+1}, \phi_j) - X(\lambda_{i-1}, \phi_j)}{2\Delta\lambda}, \tag{6.41}$$

$$\partial_{2\phi} X(\lambda_i, \phi_j) = \frac{X(\lambda_i, \phi_{j+1}) - X(\lambda_i, \phi_{j-1})}{2\Delta\phi}; \tag{6.42}$$

- Vertical averaging operators

$$\overline{Z(r_{i,j,k})}^{r} = \frac{(r_{i,j,k+\frac{1}{2}} - r_{i,j,k})Z(r_{i,j,k+\frac{1}{2}}) + (r_{i,j,k} - r_{i,j,k-\frac{1}{2}})Z(r_{i,j,k-\frac{1}{2}})}{r_{i,j,k+\frac{1}{2}} - r_{i,j,k-\frac{1}{2}}}, \quad (6.43)$$

$$\overline{Z(\eta_k)}^{\eta} = \frac{(\eta_{k+\frac{1}{2}} - \eta_k)Z(\eta_{k+\frac{1}{2}}) + (\eta_k - \eta_{k-\frac{1}{2}})Z(\eta_{k-\frac{1}{2}})}{\eta_{k+\frac{1}{2}} - \eta_{k-\frac{1}{2}}}; \quad (6.44)$$

- Vertical differencing operators

$$\partial_r Z(r_{i,j,k}) = \frac{Z(r_{i,j,k+\frac{1}{2}}) - Z(r_{i,j,k-\frac{1}{2}})}{r_{i,j,k+\frac{1}{2}} - r_{i,j,k-\frac{1}{2}}}, \quad (6.45)$$

$$\partial_{2r} Z(r_{i,j,k}) = \frac{Z(r_{i,j,k+1}) - Z(r_{i,j,k-1})}{r_{i,j,k+1} - r_{i,j,k-1}}, \quad (6.46)$$

$$\partial_\eta Z(\eta_k) = \frac{Z(\eta_{k+\frac{1}{2}}) - Z(\eta_{k-\frac{1}{2}})}{\eta_{k+\frac{1}{2}} - \eta_{k-\frac{1}{2}}}, \quad (6.47)$$

$$\partial_{2\eta} Z(\eta_k) = \frac{Z(\eta_{k+1}) - Z(\eta_{k-1})}{\eta_{k+1} - \eta_{k-1}}. \quad (6.48)$$

We note that the vertical averaging operators perform a piecewise constant averaging. This is different from a standard linear averaging and was chosen to ensure that certain adjoint properties of the continuous equations also hold in the discrete formulation. However, it is less accurate than a linear interpolation and so will be replaced by the latter in a future version of the model.

We also introduce the notation for the time-weighting of particular terms. For a given term δc we define

$$\begin{aligned} \overline{\delta c}^{ti} &= (1-\alpha_i)\delta c_d^n + \alpha_i \delta c_a^{n+1} \\ &= (1-\alpha_i)\delta c_d^n + \alpha_i \delta c_a^n + \alpha_i \delta c'_a \end{aligned} \quad (6.49)$$

where

$$\delta c' = \delta c^{n+1} - \delta c^n. \quad (6.50)$$

The subscript d indicates a value at the departure point and the subscript a a value at the arrival point. The α_i are the time-weighting parameters for the different terms, with $\alpha_i \in [0.5, 1]$. The model time step is written Δt. We also introduce

the parameter $\beta = f\Delta t$, where $f = 2\Omega \sin\phi$ is the Coriolis parameter, and define weightings

$$W_1 = \frac{1 - \alpha_5(1-\alpha_5)\beta^2}{1 + \alpha_5^2\beta^2}, \tag{6.51}$$

$$W_2 = \frac{\beta}{1 + \alpha_5^2\beta^2}, \tag{6.52}$$

for a time-weighting parameter α_5. The derivation of the weightings W_1, W_2 is explained in Section 6.2.4.

A feature of the grid staggering that we are using in the horizontal and vertical is that variables are defined at four different sets of points. The variables p, Π and ρ are defined at the same point on the grid, with the horizontal wind components u and v staggered from these in the east-west and north-south directions respectively. We refer to these as p-points, u-points and v-points respectively. The remaining variables θ, w and $\dot{\eta}$ are defined at the same horizontal positions as p, Π and ρ, but on vertical levels staggered from those on which the other variables are held. These points are referred to as θ-points. In the equations which follow we assume that where no spatial position is indicated, then variables are defined on the appropriate points for that equation. Thus the horizontal momentum equations are defined on u- and v- points, the equation of state and continuity equation on p-points and the vertical momentum equation and thermodynamic equation on θ-points. The diagnostic relationship for $\dot{\eta}$ is also defined on θ-points. We also assume that variables are calculated at time level n where not indicated otherwise.

Time discretization

Having defined the notation we wish to use, we now state the time discretization of equations (6.19) to (6.23). Noting that the chosen grid staggering implies that u, v and θ are held at different points on the grid, we introduce the subscripts du, dv and dt to indicate the departure points associated with each of these grid points

respectively. We then have

$$\begin{aligned}\delta u^{n+1} &- W_1\delta u^n_{du} - W_2\delta v^n_{du} + \Delta t\Bigg[(\boldsymbol{\delta}\mathbf{u}.\nabla\bar{u})^n - \left(\frac{\delta u\bar{v}\tan\phi}{r}\right)^n \\ &+ \overline{\frac{c_p\delta\theta}{r\cos\phi}\left(\frac{\partial\bar{\Pi}}{\partial\lambda} - \frac{\partial\bar{\Pi}}{\partial r}\frac{\partial r}{\partial\lambda}\right)}^{t3} \\ &+ \overline{\frac{c_p\bar{\theta}}{r\cos\phi}\left(\frac{\partial\delta\Pi}{\partial\lambda} - \frac{\partial\delta\Pi}{\partial r}\frac{\partial r}{\partial\lambda}\right)}^{t3}\Bigg] = 0, \end{aligned} \tag{6.53}$$

$$\begin{aligned}\delta v^{n+1} &- W_1\delta v^n_{dv} + W_2\delta u^n_{dv} + \Delta t\Bigg[(\boldsymbol{\delta}\mathbf{u}.\nabla\bar{v})^n + \left(\frac{\delta u\bar{u}\tan\phi}{r}\right)^n \\ &+ \overline{\frac{c_p\delta\theta}{r}\left(\frac{\partial\bar{\Pi}}{\partial\phi} - \frac{\partial\bar{\Pi}}{\partial r}\frac{\partial r}{\partial\phi}\right)}^{t3} + \overline{\frac{c_p\bar{\theta}}{r}\left(\frac{\partial\delta\Pi}{\partial\phi} - \frac{\partial\delta\Pi}{\partial r}\frac{\partial r}{\partial\phi}\right)}^{t3}\Bigg] = 0. \end{aligned} \tag{6.54}$$

We note that the second term containing $\tan\phi$ from (6.19) and half of the $\tan\phi$ term from (6.20) are absorbed into the departure point calculation, following Bates et al. [7].

$$\delta w^{n+1} - \delta w^n + \Delta t\left[c_p\overline{\delta\theta}^{t4}\frac{\partial\bar{\Pi}}{\partial r} + c_p\bar{\theta}\overline{\frac{\partial\delta\Pi}{\partial r}}^{t4}\right] = 0, \tag{6.55}$$

$$\begin{aligned}\delta\rho^{n+1} &- \delta\rho^n + \frac{\Delta t}{\partial r/\partial\eta}\Bigg[\frac{1}{\cos\phi}\frac{\partial}{\partial\lambda}\left(\frac{(\delta\rho\bar{u} + \bar{\rho}\overline{\delta u}^{t1})}{r}\frac{\partial r}{\partial\eta}\right) \\ &+ \frac{1}{\cos\phi}\frac{\partial}{\partial\phi}\left(\frac{(\delta\rho\bar{v} + \bar{\rho}\overline{\delta v}^{t1})}{r}\frac{\partial r}{\partial\eta}\cos\phi\right) \\ &+ \frac{\partial}{\partial\eta}\left((\delta\rho\bar{\dot{\eta}} + \bar{\rho}\overline{\delta\dot{\eta}}^{t\rho})\frac{\partial r}{\partial\eta}\right)\Bigg] = 0, \end{aligned} \tag{6.56}$$

$$\delta\theta^{n+1} - \delta\theta^n_{dt} + \Delta t\left[\frac{\delta u}{r\cos\phi}\frac{\partial\bar{\theta}}{\partial\lambda} + \frac{\delta v}{r}\frac{\partial\bar{\theta}}{\partial\phi} + \overline{\delta\dot{\eta}}^{tw}\frac{\partial\bar{\theta}}{\partial\eta}\right] = 0. \tag{6.57}$$

The term $\overline{\delta\dot{\eta}}^{t\rho}$ in (6.56) is given by

$$\overline{\delta\dot{\eta}}^{t\rho} = \frac{1}{\partial r/\partial\eta}\left[\overline{\delta w}^{t2} - \overline{\frac{\overline{\delta u}^{\eta}}{\overline{r}^{\lambda}\cos\phi}\frac{\partial r}{\partial\lambda}}^{\lambda t1} - \overline{\frac{\overline{\delta v}^{\eta}}{\overline{r}^{\phi}}\frac{\partial r}{\partial\phi}}^{\phi t1}\right] \tag{6.58}$$

and $\overline{\delta\dot{\eta}}^{tw}$ in (6.57) is given by

$$\overline{\delta\dot{\eta}}^{tw} = \frac{1}{\partial r/\partial\eta}\left[\overline{\delta w}^{t2} - \overline{\frac{\overline{\delta u^n}^{\eta}}{\overline{r}^{\lambda}\cos\phi}\frac{\partial r}{\partial\lambda}}^{\lambda} - \overline{\frac{\overline{\delta v^n}^{\eta}}{\overline{r}^{\phi}}\frac{\partial r}{\partial\phi}}^{\phi}\right]. \tag{6.59}$$

6.2.4 Comments on the discretization

It is useful at this point to highlight two particular differences from the scheme used in the nonlinear model. The first arises from the linearization of the advection terms which, as we discussed in Chapter 5, which produces an extra term consisting of the perturbation to the wind field multiplying the gradient of the linearization state field. Within the three-dimensional model we use the approach implemented in PFM2 of the shallow water model in Section 5.2.4, and evaluate this term at the arrival point at time level n.

The second difference from the nonlinear model scheme is in the treatment of the terms involving the Earth rotation rate (the Coriolis terms) in the horizontal momentum equations. Within the nonlinear model theses terms are treated semi-implicitly, giving rise to terms within the elliptic equation. However, since these terms couple the equations for u and v, we find such a treatment in the perturbation forecast model causes problems for the subsequent derivation of the adjoint model. For this reason we wish to remove the Coriolis terms from this part of the solution procedure. Referring to the matrix formulation of Section 6.2.2, this corresponds to requiring that these terms appear only within the operator $\mathbf{P}$ and not within $\mathbf{M}$. However, stability considerations require that these terms be treated implicitly in time. In order to do this we use the method which Gadd [29] introduced into a split-explicit model. We adapt this scheme by applying it as an average along the semi-Lagrangian trajectory and introducing an off-centering parameter in the time-weighting to increase the stability.

We derive the scheme by considering the horizontal momentum equations consisting only of advection and the Coriolis terms, linearized about a constant advecting velocity (U_0, V_0)

$$\frac{D\delta u}{Dt} - f\delta v = 0, \tag{6.60}$$

$$\frac{D\delta v}{Dt} + f\delta u = 0, \tag{6.61}$$

where

$$\frac{D}{Dt} \equiv \frac{\partial}{\partial t} + \frac{U_0}{r\cos\phi}\frac{\partial}{\partial \lambda} + \frac{V_0}{r}\frac{\partial}{\partial \phi}. \tag{6.62}$$

The first step is to implement a semi-Lagrangian treatment of the advection and a semi-implicit treatment of the wind perturbation in the Coriolis terms. We write the semi-discrete equations

$$\delta u_a^{n+1} = \delta u_d^n + (1-\alpha_5)\Delta t f \delta v_d^n + \alpha_5 \Delta t f \delta v_a^{n+1}, \tag{6.63}$$

$$\delta v_a^{n+1} = \delta v_d^n - (1-\alpha_5)\Delta t f \delta u_d^n - \alpha_5 \Delta t f \delta u_a^{n+1}, \tag{6.64}$$

where subscript d indicates a value at the departure point, subscript a indicates a value at the arrival point, α_5 is a time-weighting coefficient and Δt is the model time step. We note that we have not yet fixed the position on the grid at which f is calculated. Substituting for δv_a^{n+1} in (6.63) from (6.64) and for δu_a^{n+1} in (6.64) from (6.63) we obtain

$$\delta u_a^{n+1} = W_1 \delta u_d^n + W_2 \delta v_d^n, \tag{6.65}$$

$$\delta v_a^{n+1} = W_1 \delta v_d^n - W_2 \delta u_d^n, \tag{6.66}$$

with W_1 and W_2 given by (6.51) and (6.52). We fix the evaluation of f (and therefore β) to be at the departure point and implement the form of the scheme given by (6.65) and (6.66) directly in the scheme of the perturbation forecast model. This gives rise to the terms containing W_1 and W_2 in the semi-discrete equations (6.53) and (6.54).

To illustrate that this scheme provides the stability we require, we perform a Fourier stability analysis as described in Section 2.2.4 by substituting the modes

$$\delta u = \delta u_0 e^{i(kx+ly+\omega t)}, \delta v = \delta v_0 e^{i(kx+ly+\omega t)} \tag{6.67}$$

into (6.65) and (6.66). This gives

$$\begin{pmatrix} EE' - W_1 & -W_2 \\ W_2 & EE' - W_1 \end{pmatrix} \begin{pmatrix} \delta u_0 \\ \delta v_0 \end{pmatrix} = \begin{pmatrix} 0 \\ 0 \end{pmatrix}, \tag{6.68}$$

where $E = \exp(i\omega\Delta t)$, $E' = \exp(i(U_0 k\Delta x + V_0 l\Delta y))$. Then a necessary condition for stability is that the modulus of E be less than one. Following Section 2.2.4 we set the determinant of the matrix to zero to obtain the discrete dispersion relation

$$EE' = W_1 \pm iW_2. \tag{6.69}$$

Since $\| E' \| = 1$ we find that

$$\begin{aligned} \| E \|^2 &= W_1^2 + W_2^2 \\ &= \frac{(1-\alpha_5(1-\alpha_5)\beta^2)^2 + \beta^2}{(1+\alpha_5^2\beta^2)^2}. \end{aligned} \tag{6.70}$$

This expression is difficult to analyse in the general case. However, we can obtain the following results for specific cases:

- For $\alpha_5 = 0.5$ we have $\| E \| = 1$ and the scheme is unconditionally stable.
- For $\alpha_5 = 1$ we have

$$\| E \| = \frac{1}{1+\beta^2} < 1$$

and again the scheme is stable.

- For other values of α_5 we plot $\| E \|$ for different values of β. This is shown in Figure 6.1. It is seen that the scheme is stable for all values of $\alpha_5 \geq 0.5$. Thus we conclude that the proposed scheme gives the stability we require, while avoiding the Coriolis terms entering into the pressure equation.

6.2.5 Details of the numerical scheme

We now present the details of the solution procedure for the numerical scheme with reference to the matrix formulation outlined in Section 6.2.2. In order that we can clearly indicate the averaging of different terms on the grid we omit the overbar on the linearization state for this section only. Where a term is averaged in two directions then the first index of the averaging is that which is carried out first. So, for example, $\overline{x}^{r\lambda}$ means first average x in the vertical using r and then do a horizontal

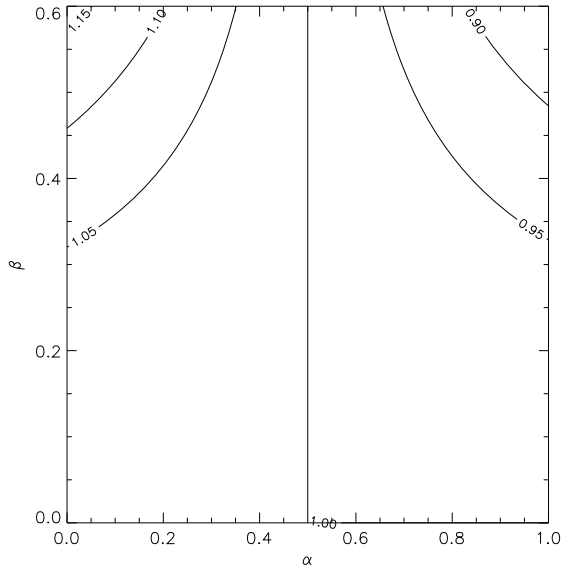

Figure 6.1: $\| E \|$ for different values of α_5 and β.

λ averaging. We assume that all terms are evaluated at the appropriate grid-point for the equation and at time level n unless indicated otherwise. The solution then proceeds as follows.

Computation of $\mathbf{P}\boldsymbol{\delta}\mathbf{x}^n$

The first step is the computation of the predicted values $\boldsymbol{\delta}\tilde{\mathbf{x}} = \mathbf{P}\boldsymbol{\delta}\mathbf{x}^n$. For the horizontal and vertical momentum equations we set

$$\begin{aligned}
\delta\tilde{u} &= W_1\delta u^n_{du} - \delta u^n + W_2\overline{\delta v}^{\lambda\phi^n}_{du} - \Delta t\left[(\boldsymbol{\delta}\mathbf{u}.\nabla u) - \left(\frac{\delta u\overline{v}^{\lambda\phi}\tan\phi}{\overline{r}^{\lambda}}\right)\right] \\
&- \Delta t\Bigg(\Bigg[(1-\alpha_3)\frac{c_p}{\overline{r}^{\lambda}\cos\phi}\left(\overline{\theta}^{r\lambda}\partial_\lambda\delta\Pi - \overline{\theta\partial_r\delta\Pi}^{r\lambda}\partial_\lambda r\right) \\
&+ (1-\alpha_3)\frac{c_p}{\overline{r}^{\lambda}\cos\phi}\left(\overline{\delta\theta}^{r\lambda}\partial_\lambda\Pi - \overline{\delta\theta\partial_r\Pi}^{r\lambda}\partial_\lambda r\right)\Bigg]_{du} \\
&+ \alpha_3\frac{c_p}{\overline{r}^{\lambda}\cos\phi}\left(\overline{\theta}^{r\lambda}\partial_\lambda\delta\Pi - \overline{\theta\partial_r\delta\Pi}^{r\lambda}\partial_\lambda r\right) \\
&+ \alpha_3\frac{c_p}{\overline{r}^{\lambda}\cos\phi}\left(\overline{\delta\theta}^{r\lambda}\partial_\lambda\Pi - \overline{\delta\theta\partial_r\Pi}^{r\lambda}\partial_\lambda r\right)\Bigg); \qquad (6.71)
\end{aligned}$$

$$
\begin{aligned}
\delta\tilde{v} &= W_1\delta v^n_{dv} - \delta v^n - W_2\overline{\delta u}^{\lambda\phi^n}_{dv} - \Delta t\Big[(\boldsymbol{\delta u}.\nabla v) + \Big(\frac{\overline{\delta u}^{\lambda\phi}\overline{u}^{\lambda\phi}\tan\phi}{\overline{r}^{\phi}}\Big)\Big] \\
&- \Delta t\Big(\Big[(1-\alpha_3)\frac{c_p}{\overline{r}^{\phi}}\Big(\overline{\theta}^{r\phi}\partial_\phi\delta\Pi - \overline{\theta\partial_r\delta\Pi}^{r\phi}\partial_\phi r\Big) \\
&+ (1-\alpha_3)\frac{c_p}{\overline{r}^{\phi}}\Big(\overline{\delta\theta}^{r\phi}\partial_\phi\Pi - \overline{\delta\theta\partial_r\Pi}^{r\phi}\partial_\phi r\Big)\Big]_{dv} \\
&+ \alpha_3\frac{c_p}{\overline{r}^{\phi}}\Big(\overline{\theta}^{r\phi}\partial_\phi\delta\Pi - \overline{\theta\partial_r\delta\Pi}^{r\phi}\partial_\phi r\Big) \\
&+ \alpha_3\frac{c_p}{\overline{r}^{\phi}}\Big(\overline{\delta\theta}^{r\phi}\partial_\phi\Pi - \overline{\delta\theta\partial_r\Pi}^{r\phi}\partial_\phi r\Big)\Big); \qquad (6.72)
\end{aligned}
$$

$$
\delta\tilde{w} = -\Delta t\Big[c_p\delta\theta\partial_r\Pi + c_p\theta\partial_r\delta\Pi\Big]. \qquad (6.73)
$$

For the thermodynamic equation we implement a semi-Lagrangian scheme which is non-interpolating in the vertical and which is also used in the thermodynamic equation of the nonlinear model [72]. We calculate the predicted value

$$
\begin{aligned}
\delta\tilde{\theta} &= \delta\theta^n_{dl} - \delta\theta^n - \Delta t[(1-\alpha_2)(w-w^*)\partial_{2r}\delta\theta]_{dl} \\
&- \Delta t\alpha_2(w-w^*)\partial_{2r}\delta\tilde{\theta}_1 - \Delta t\Big(\frac{\overline{\delta u}^{r\lambda}}{r\cos\phi}\partial_{2\lambda}\theta + \frac{\overline{\delta v}^{r\phi}}{r}\partial_{2\phi}\theta + \delta\dot{\eta}\partial_{2\eta}\theta\Big), \qquad (6.74)
\end{aligned}
$$

where the subscript dl indicates the value on the nearest vertical level to the departure point d and

$$
w^* = \frac{r_a - r_{dl}}{\Delta t}. \qquad (6.75)
$$

The quantity $\delta\tilde{\theta}_1$ is an intermediate predictor for the advective part of the equation calculated from the time level n values,

$$
\begin{aligned}
\delta\tilde{\theta}_1 &= \delta\theta^n_{dl} - \delta\theta^n - \Delta t[(1-\alpha_2)(w-w^*)\partial_{2r}\delta\theta]_{dl} \\
&- \Delta t\alpha_2(w-w^*)\partial_{2r}\delta\tilde{\theta}^n. \qquad (6.76)
\end{aligned}
$$

The predictor for the density is

$$
\begin{aligned}
\delta\tilde{\rho} &= -\frac{\Delta t}{\partial_\eta r}\Big(\frac{1}{\cos\phi}\partial_\lambda\Big(\frac{\overline{\delta\rho\partial_\eta r}^{\lambda}u + \overline{\rho\partial_\eta r}^{\lambda}\delta u}{\overline{r}^{\lambda}}\Big) \\
&+ \frac{1}{\cos\phi}\partial_\phi\Big(\frac{(\overline{\delta\rho\partial_\eta r}^{\phi}v + \overline{\rho\partial_\eta r}^{\phi}\delta v)\cos\phi}{\overline{r}^{\phi}}\Big) \\
&+ \partial_\eta\Big((\overline{\delta\rho}^{r}\dot{\eta} + \overline{\rho}^{r}\delta\dot{\eta})\partial_\eta r\Big)\Big). \qquad (6.77)
\end{aligned}
$$

We also have the remaining component of $\boldsymbol{\delta\tilde{\mathbf{x}}}$,

$$\delta\tilde{\Pi} = 0, \tag{6.78}$$

since there is no predictor step for the pressure perturbation.

Computation of $\mathbf{M}^{-1}\boldsymbol{\delta\tilde{\mathbf{x}}}$

The prediction step leaves us with the matrix equation $\mathbf{M}\boldsymbol{\delta}\mathbf{x}' = \boldsymbol{\delta\tilde{\mathbf{x}}}$, given by the equations

$$\begin{aligned}\delta u' &+ \frac{\alpha_3 c_p \Delta t}{\overline{r}^{\lambda}\cos\phi}\left(\overline{\delta\theta'}^{r\lambda}\partial_\lambda\Pi - \overline{\delta\theta'\partial_r\Pi}^{r\lambda}\partial_\lambda r\right)\\ &+ \frac{\alpha_3 c_p \Delta t}{\overline{r}^{\lambda}\cos\phi}\left(\overline{\theta}^{r\lambda}\partial_\lambda\delta\Pi' - \overline{\theta\partial_r\delta\Pi'}^{r\lambda}\partial_\lambda r\right) = \delta\tilde{u};\end{aligned} \tag{6.79}$$

$$\begin{aligned}\delta v' &+ \frac{\alpha_3 c_p \Delta t}{\overline{r}^{\phi}}\left(\overline{\delta\theta'}^{r\phi}\partial_\phi\Pi - \overline{\delta\theta'\partial_r\Pi}^{r\phi}\partial_\phi r\right)\\ &+ \frac{\alpha_3 c_p \Delta t}{\overline{r}^{\phi}}\left(\overline{\theta}^{r\phi}\partial_\phi\delta\Pi' - \overline{\theta\partial_r\delta\Pi'}^{r\phi}\partial_\phi r\right) = \delta\tilde{v};\end{aligned} \tag{6.80}$$

$$\delta w' + \Delta t\left[\alpha_4 c_p\delta\theta'\partial_r\Pi + \alpha_4 c_p\theta\partial_r\delta\Pi'\right] = \delta\tilde{w}; \tag{6.81}$$

$$\delta\theta' + \alpha_2\Delta t\partial_{2r}\theta\delta w' = \delta\tilde{\theta}; \tag{6.82}$$

$$\begin{aligned}\delta\rho' &+ \frac{\Delta t}{\partial_\eta r}\left(\frac{1}{\cos\phi}\partial_\lambda\left(\frac{\overline{\rho\partial_\eta r}^{\lambda}}{\overline{r}^{\lambda}}\delta u_1{}'\right) + \frac{1}{\cos\phi}\partial_\phi\left(\frac{\overline{\rho\partial_\eta r}^{\phi}\cos\phi}{\overline{r}^{\phi}}\delta v_1{}'\right)\right.\\ &+ \left.\partial_\eta\left(\overline{\rho}^{r}\partial_\eta r\delta\dot{\eta}_1{}'\right)\right) = \delta\tilde{\rho};\end{aligned} \tag{6.83}$$

$$\frac{(\kappa-1)\rho\overline{\theta}^{r}p}{\kappa\Pi}\delta\Pi' + p\rho\overline{\delta\theta'}^{r} + p\overline{\theta}^{r}\delta\rho' = 0, \tag{6.84}$$

with

$$\delta u_1{}' = \alpha_1\delta u', \tag{6.85}$$

$$\delta v_1{}' = \alpha_1\delta v', \tag{6.86}$$

$$\delta w_1{}' = \alpha_2\delta w' \tag{6.87}$$

and

$$\delta\dot{\eta}_1{}' - \frac{1}{\partial_\eta r}\left[\delta w_1{}'' - \overline{\frac{\overline{\delta u_1{}'}^{\eta}}{\overline{r}^{\lambda}\cos\phi}\partial_\lambda r}^{\lambda} - \overline{\frac{\overline{\delta v_1{}'}^{\eta}}{\overline{r}^{\phi}}\partial_\phi r}^{\phi}\right] = 0. \tag{6.88}$$

It is at this point that we introduce an approximation into the matrix $\mathbf{M}$ as referred to in Section 6.2.2. In order to avoid coupling updates to the horizontal momentum equations (6.79) and (6.80) with the thermodynamic equation (6.82), we approximate $\delta\theta'$ in these equations with the predicted value $\delta\tilde{\theta}$. Thus this term is moved to the right hand side of the equations. We define

$$\delta\tilde{u}^* = \delta\tilde{u} - \frac{\alpha_3 c_p \Delta t}{\overline{r}^{\lambda}\cos\phi}\left(\overline{\delta\tilde{\theta}}^{r\lambda}\partial_\lambda\Pi - \overline{\delta\tilde{\theta}\partial_r\Pi}^{r\lambda}\partial_\lambda r\right), \tag{6.89}$$

$$\delta\tilde{v}^* = \delta\tilde{v} - \frac{\alpha_3 c_p \Delta t}{\overline{r}^{\phi}}\left(\overline{\delta\tilde{\theta}}^{r\phi}\partial_\phi\Pi - \overline{\delta\tilde{\theta}\partial_r\Pi}^{r\phi}\partial_\phi r\right). \tag{6.90}$$

Then (6.79) and (6.80) become

$$\delta u' + \frac{\alpha_3 c_p \Delta t}{\overline{r}^{\lambda}\cos\phi}\left(\overline{\theta}^{r\lambda}\partial_\lambda\delta\Pi' - \overline{\theta\partial_r\delta\Pi'}^{r\lambda}\partial_\lambda r\right) = \delta\tilde{u}^*; \tag{6.91}$$

$$\delta v' + \frac{\alpha_3 c_p \Delta t}{\overline{r}^{\phi}}\left(\overline{\theta}^{r\phi}\partial_\phi\delta\Pi' - \overline{\theta\partial_r\delta\Pi'}^{r\phi}\partial_\phi r\right) = \delta\tilde{v}^*. \tag{6.92}$$

We also immediately substitute the expression for $\delta\dot{\eta}_1{}'$ (6.88) into (6.83) to eliminate $\delta\dot{\eta}'$, since this is considered only a diagnostic variable. Thus, using also (6.85)-(6.87) we obtain

$$\begin{aligned}\delta\rho' \;+\; & \frac{\Delta t}{\partial_\eta r}\left(\frac{\alpha_1}{\cos\phi}\partial_\lambda\left(\overline{\frac{\rho\partial_\eta r}{\overline{r}^{\lambda}}\delta u'}^{\lambda}\right) + \frac{\alpha_1}{\cos\phi}\partial_\phi\left(\overline{\frac{\rho\partial_\eta r}{\overline{r}^{\phi}}\cos\phi\,\delta v'}^{\phi}\right)\right.\\ & \left. +\; \partial_\eta\left(\overline{\rho}^{r}\left[\alpha_2\delta w' - \overline{\frac{\alpha_1\overline{\delta u'}^{\eta}}{\overline{r}^{\lambda}\cos\phi}\partial_\lambda r}^{\lambda} - \overline{\frac{\alpha_1\overline{\delta v'}^{\eta}}{\overline{r}^{\phi}}\partial_\phi r}^{\phi}\right]\right)\right) = \delta\tilde{\rho}.\end{aligned} \tag{6.93}$$

At this stage we also substitute (6.82) into (6.81) to give

$$\delta w' = \frac{1}{G}\left(\delta w^* - \alpha_4 c_p \Delta t\theta\partial_r\delta\Pi'\right), \tag{6.94}$$

with

$$\delta w^* = \delta\tilde{w} - \alpha_4 c_p \Delta t\delta\tilde{\theta}\partial_r\Pi \tag{6.95}$$

and

$$G = 1 - \alpha_2 \alpha_4 c_p \Delta t^2 \partial_{2r} \theta \partial_r \Pi. \tag{6.96}$$

In order to understand better the matrix structure of the equations, we rewrite this

$$G\delta w' + \alpha_4 c_p \Delta t \theta \partial_r \delta\Pi' = \delta w^*. \tag{6.97}$$

The matrix $\mathbf{M}$ referred to in Section 6.2.2 is given by the left hand sides of (6.79), (6.80), (6.82), (6.84), (6.93) and (6.97). We note that for the w' equation it is the finite difference form of (6.97) that we actually use and not (6.81). This distinction is important, since the above substitution has been made with the analytical equations.

By replacing the horizontal momentum equations with the equations (6.91), (6.92) in the Helmholtz derivation, we are replacing the matrix $\mathbf{M}$ with an approximate matrix $\mathbf{M_1}$. Thus $\mathbf{M_1}$ is given by the left hand sides of (6.91), (6.92), (6.82), (6.84), (6.93), and (6.97), but with $\delta\Pi'$ replaced by $\delta\hat{\Pi}'$.

Solution of implicit step

Using the equations of $\mathbf{M_1}$ and substituting into (6.84), we obtain the elliptic equation

$$\begin{aligned}
&\frac{(\kappa-1)\rho\theta p}{\kappa\Pi}\delta\hat{\Pi}' + p\rho\overline{\left(\delta\tilde{\theta} - \frac{\alpha_2\Delta t\partial_{2r}\theta}{G}\left(\delta w^* - \alpha_4 c_p \Delta t\theta\partial_r\delta\hat{\Pi}'\right)\right)}^{\eta} \\
+ \;& p\theta\Bigg(\delta\tilde{\rho} - \frac{\Delta t}{\partial_\eta r}\Bigg(\frac{\alpha_1}{\cos\phi}\partial_\lambda\Big(\frac{\overline{\rho\partial_\eta r}^{\lambda}}{\overline{r}^{\lambda}}\delta u'\Big) + \frac{\alpha_1}{\cos\phi}\partial_\phi\Big(\frac{\overline{\rho\partial_\eta r}^{\phi}\cos\phi}{\overline{r}^{\phi}}\delta v'\Big) \\
+ \;& \partial_\eta\Big(\overline{\rho}^r\Big[\alpha_2\delta w' - \frac{\alpha_1\overline{\delta u'}^{\eta}}{\overline{r}^{\lambda}\cos\phi}\partial_\lambda r\Big)^{\lambda} - \overline{\frac{\alpha_1\overline{\delta v'}^{\eta}}{\overline{r}^{\phi}}\partial_\phi r}^{\phi}\Big]\Big)\Bigg)\Bigg) = 0,
\end{aligned} \tag{6.98}$$

where $\delta u', \delta v', \delta w'$ are as defined by equations (6.91), (6.92), (6.94), but with $\delta\Pi'$ replaced by $\delta\hat{\Pi}'$. This is a Helmholtz equation which we need to solve iteratively for $\delta\hat{\Pi}'$. The exact form of the equation is given for reference in Appendix B. To solve this equation we use the same generalized conjugate residual method as used in the nonlinear model. In fact, we find that form of the elliptic equation is the

same as that in the nonlinear model, thus allowing the same Fortran code to be used. Having solved (6.98) for $\delta\hat{\Pi}'$ we set $\delta\Pi' = \delta\hat{\Pi}'$.

Final update step

The perturbation Exner pressure is updated with

$$\delta\Pi^{n+1} = \delta\Pi^n + \delta\Pi'. \tag{6.99}$$

The perturbation pressure δp can then be updated using (6.26). To find the other components of $\boldsymbol{\delta}\mathbf{x}^{n+1}$ we back substitute into the equations (6.91), (6.92), (6.82), (6.93) and (6.97). We note that by using the approximate equations (6.91) and (6.92) rather than the original equations (6.79) and (6.80) we are updating using the approximate matrix $\mathbf{M_1}$. Finally the values of the perturbation fields at time level $n+1$ are found by adding the increments on to the time level n values.

6.3 Numerical experiments

Having derived the perturbation forecast model it is necessary to validate the model we have coded. This consists of two steps. The first is to check that the code correctly solves the scheme we have set out above. The second step is to check that the model we have developed represents the evolution of a perturbation to sufficient accuracy, that is the validity of the model as defined by Definition 3.3. As we saw for the shallow water model in Section 5.4.2, testing a perturbation forecast model is much more difficult than testing a tangent linear model, since the model is not correct in the sense of Definition 3.2, that is it is not equal to the first order part of the discrete nonlinear model. Hence error measures such as the relative error do not tend to zero with smaller perturbations. In order to make some effort at checking the code, individual subroutines representing the calculation of the various equations are tested by feeding in data for which it is possible to obtain an analytical solution

and checking that this solution is found. This does not give a complete test, but does help to identify many bugs in the code. The nature of these tests is dependent on the function of the subroutine and results are not presented here.

The validity of the model is tested by comparing the evolution of a perturbation in the perturbation forecast model with the evolution in the nonlinear model, as described in Section 3.1. In order to do this we need to define a set of initial conditions for the nonlinear model and generate an appropriate perturbation. Other studies involving full three-dimensional weather forecasting models have used the model state resulting from the application of a data assimilation system as the initial conditions. Such a state is known as an *analysis* and is used to provide the initial conditions for routine numerical weather prediction forecasts. Studies by Errico et al. [28] and Li et al. [50] used interpolated analyses from the European Centre for Medium-Range Weather Forecasting in tests of a linear model. For our studies it was not possible to use an interpolated analysis directly for reasons explained in Section 6.3.1. Thus a different method for setting up the experiments was required. In the next section we explain the method used. Subsequent sections will then discuss results from particular experiments.

6.3.1 Method

In order to compare the evolution of a perturbation in the perturbation forecast model with the evolution in the nonlinear model it is necessary to define two sets of initial conditions for the nonlinear model, one for the nonlinear base state run and one for the perturbed nonlinear model run. However we would prefer that the difference between them, which will be the initial perturbation for our linear model, be of a similar structure to a typical analysis error. Errico et al. [28] found that the growth of random perturbations, which had no spatial correlations and no prescribed relationships between fields, was described mainly by linear processes. Hence such

perturbations do not provide a realistic test of a linear model. We seek a method of producing initial perturbation fields which have realistic spatial correlations and also realistic inter-correlations between different variables.

The method we use to obtain our initial conditions is described with reference to Figure 6.2. We first take two analyses 24 hours apart, each valid at midnight. We refer to these as analyses valid on Day 0 and Day 1. During the period in which these tests have been carried out the nonlinear model was not connected to a data assimilation system and so no analyses were available for the model we were using. The analyses were therefore taken from the Met Office's current operational Unified Model system. This model is quite different from the nonlinear model we are using, with a different grid staggering of variables in both the horizontal and vertical and also differences in some of the variables being used. A reconfiguration program written at the Met Office is used to convert these analyses to a set of initial conditions for each variable of the new nonlinear model on its own grid. However, these initial conditions cannot be used directly for the perturbation forecast experiments for two reasons. The first is that the reconfiguration can cause imbalances which then affect the evolution of the system. This is particularly noticeable when we consider the evolution of small perturbations. The second reason is that we wish to run with an adiabatic version of the model and these fields have been produced from a diabatic version. Suddenly turning off all physical parametrizations has also been found to cause imbalances.

In order to generate the initial conditions we first run from each of the analyses on the new grid using only the adiabatic version of the nonlinear model, and run until midnight on Day 2. Thus the Day 0 analysis is run for 48 hours and the Day 1 analysis for 24 hours. We follow the usual nomenclature of meteorology and refer to a forecast N hours after the analysis time as a T+N forecast. Then these two model runs result in T+24 and T+48 forecasts, both valid at midnight on Day 2. These two forecasts provide the two sets of initial conditions for the perturbation

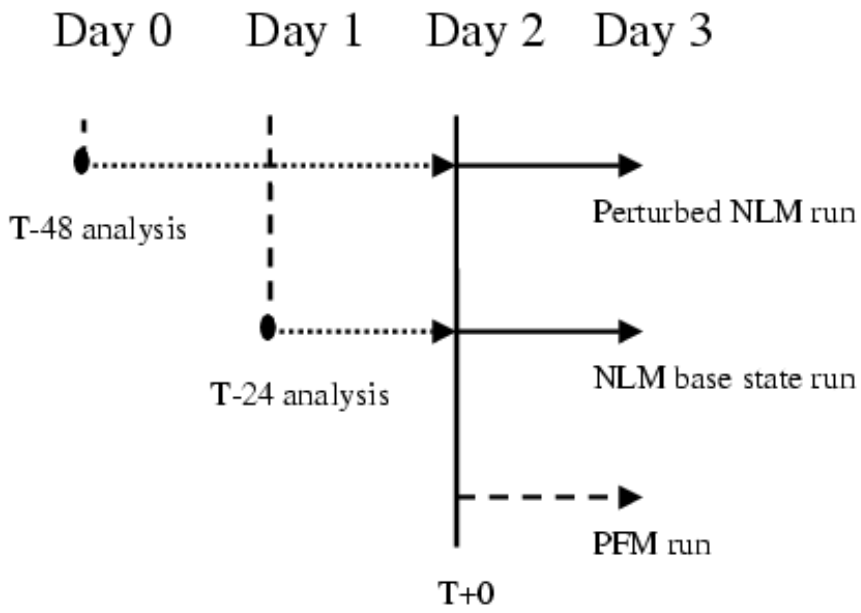

Figure 6.2: Illustration of experimental method. The dotted arrows indicate the 24 and 48 hour forecasts of the nonlinear model run to generate initial fields, the solid arrows indicate the nonlinear model runs from the T+24 and T+48 fields and the dashed line is the run of the perturbation forecast model. Day 2 is taken to be T+0 for the experiments.

experiments. The forecasts are indicated by the dotted arrows in Figure 6.2.

In order to compare the evolution of a perturbation in the nonlinear and linear models we first run the nonlinear model from these two forecasts. The run from the T+24 forecast is taken to be the nonlinear base state run and the run from the T+48 forecast is taken to be the perturbed nonlinear model run. These forecasts are indicated by the solid arrows of Figure 6.2. The initial perturbation, from which we start the perturbation forecast model, is given by the difference between the T+48 and T+24 forecasts. The differencing of two such forecasts is often taken to be an estimate of forecast error [39] and so this should be a reasonable physical perturbation to use.

For the experiments in the following sections the model is run on a regular latitude-longitude grid, with a horizontal resolution of 3.75° in the east-west di-

rection and 2.5° in the north-south direction. There are 38 levels in the vertical, following the orography at the lower levels and gradually flattening out with height. In the results shown the plots of perturbations are chosen around levels of physical interest, for example $250hPa$ where there are the strongest jets. However, the data are plotted on model levels rather than pressure levels and so the pressure given is only an approximate pressure. This avoids any errors due to interpolation and so allows us to compare fields directly as they come out of the model. However, we note that for the Charney-Phillips grid being used the θ and w fields are on levels staggered from the other fields. Each variable is output on the level on which it is stored within the model.

For each of the experiments described we use a model time step of $1800s$ in both the nonlinear and linear models unless stated otherwise. The time-weighting parameters are set to $\alpha_1 = \alpha_3 = 0.6$ and $\alpha_2 = \alpha_4 = 1.0$ for both models, with the extra weighting $\alpha_5 = 0.6$ in the perturbation forecast model. This extra weighting arises from the treatment of the Coriolis terms as described in Section 6.2.3. The linearization state for the perturbation forecast model is taken to be at the start of the time step, except in the experiment of Section 6.4 which is designed to test this approximation.

The data we use are taken from December 1998. The T+0 data time is taken to be midnight on 3rd December, with the fields for the nonlinear runs spun up from analyses at midnight on 1st December and 2nd December. For this case the perturbation generated using the method described has maximum values of approximately $50 - 70ms^{-1}$ in the zonal and meridional wind fields, $25hPa$ in the pressure field and $35K$ in the potential temperature fields. The largest perturbations are in the lowest levels of the model. We note that since we are not using any surface friction or vertical diffusion scheme in either the linear or nonlinear model, it is likely that non-meteorological structures will develop close to the surface [11]. This may lead to a distortion of the results if we consider only global measures of error and so

in the following sections we verify the model distinguishing between the different model levels. For this case we concentrate attention particularly on the following levels:

Level 1: The lowest model level;

Level 12: The top of the boundary layer;

Level 15: Approximately $500hPa$;

Level 21: Approximately $250hPa$;

Level 31: The first constant height level on the vertical grid.

Level 31 is chosen not for its meteorological interest, but because it is a place which numerically could cause problems.

6.3.2 Correctness

Although we have shown that in general a perturbation forecast model will not be correct in the sense of Definition 3.2, since it does not represent the first order part of the discrete nonlinear model, it is useful to examine the behaviour of the model as the perturbation size is reduced. In Chapter 5 we found that the relative error of the perturbation forecast model tended to a non-zero constant as the perturbation size was reduced, which agreed with the theory developed in Section 3.1.2 (we recall Figure 5.4 of page 117). We now investigate the behaviour of the three-dimensional model for a similar experiment. The initial perturbation is taken to be that produced as described in Section 6.3.1 and the linearization test is run with this perturbation multiplied by a factor $\alpha = 10^{-p}$, where $p = 0, 1, 2, 3$. The integration period is taken to be 12 hours. At the end of the period we calculate the relative error (3.17) for each level using the root mean squared norm (3.21) weighted by the area of a grid box. Since for this model we find that most of the decrease in relative error

occurs between values of $\alpha = 1.0$ and $\alpha = 0.1$, we also include experiments with the intermediate values 0.5 and 0.2.

The change of relative error with α is shown in Figure 6.3 for each of the primary model variables $\delta u, \delta v, \delta w, \delta p, \delta \rho, \delta \theta$. We note that here we are using pressure rather than Exner pressure as the output variable, since its physical meaning is more readily interpreted when we look at the perturbation fields themselves. Each plot of Figure 6.3 shows the five model levels chosen in Section 6.3.1, with level 1 in black, level 12 in orange, level 15 in blue, level 21 in red and level 31 in green. The first thing we note is that for all the levels plotted except level 1 we have an initial decrease in error as α decreases followed by a levelling off of the error to a constant value. This is the same pattern that we saw for the shallow water model in Figure 5.4. We also note that for most of the fields the error on level 1 increases in value for the smallest perturbation. A closer examination of the perturbations themselves (not shown) shows that this can be explained by an error at one grid point over the Himalayas when the perturbations are very small.

It is clear from Figure 6.3 that the present version of the perturbation forecast model has a large variation of accuracy with height. Such a variation was not found in studies of the tangent linear model of the MM4 mesoscale model by Errico et al. [28]. However, our experiments do not yet include any friction scheme or vertical diffusion. This is likely to lead to highly nonlinear effects near the lower boundary leading to larger differences between the linear and nonlinear models. We expect that once such schemes have been implemented, the variation of error with height will be less.

In experiments with data from another date, July 1999, the graphs of relative errors show similar patterns as α is reduced (not shown). However, the asymptotic values are found to be quite different. This would be expected since the difference between the perturbation forecast model and a tangent linear model will depend on the linearization state fields and so on the particular meteorological situation.

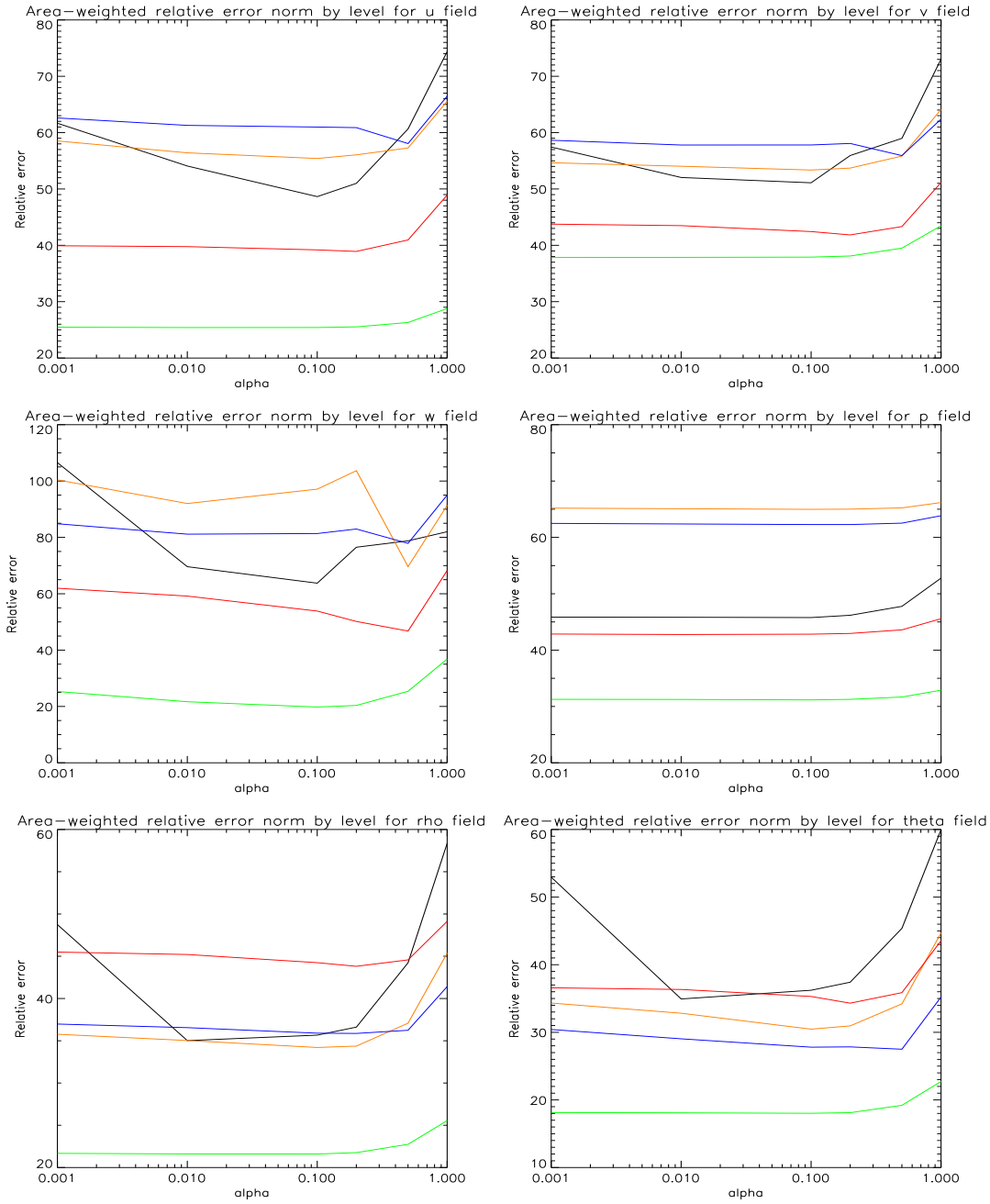

Figure 6.3: Relative error norms at T+12 as a function of α. The different lines are level 1 (black), level 12 (orange), level 15 (blue), level 21 (red) and level 31 (green)

Thus it appears that the asymptotic values of the graphs plotted cannot give any general information about the performance of the model. In order to assess that the perturbation forecast model is performing satisfactorily we therefore require some other criterion with which to measure its validity. In the following sections we make use of the formulae which we proposed in Section 3.3 in order to provide such a criterion.

6.3.3 Error measures

In order to assess the validity of the perturbation forecast model it is useful to know how much of the linearization error we see is due to nonlinear effects and how much is due to the fact that we have not linearized the discrete nonlinear model. For our three-dimensional model we can make use of the method we derived in Section 3.3 and tested for the shallow water model in Section 5.6. We estimate the linearization error we would expect from a tangent linear model by running the nonlinear model from three different initial conditions and using the formula (3.32) to calculate the estimated tangent linear model (TLM) linearization error $\boldsymbol{\mathcal{E}}$. This can then be compared with the actual linearization error $\mathbf{E}$ from the perturbation forecast model (PFM), found from the difference between the perturbation as evolved in the nonlinear model and the PFM solution.

First we must find a suitable value of the parameter γ to use in the linearization error estimate (3.32). To do this we apply the method suggested in Section 5.6 and plot the evolution of the estimated tangent linear model solution error $\hat{E}_S$ given by

$$\hat{E}_S = 100 \frac{rms(\boldsymbol{\mathcal{E}}^n)}{rms(\boldsymbol{N}^n[\boldsymbol{\delta}\mathbf{U}^0])}, \tag{6.100}$$

for different values of γ. In Figure 6.4 the evolution of $\hat{E}_S$ is plotted using values at T+6, T+12, T+18 and T+24, with values of $\gamma = 0.5, 0.2, 0.1, 0.01$ shown by the dotted, dashed, dot-dashed and solid lines respectively. The different coloured lines indicate the different levels in the same way as in Section 6.3.2 and as detailed in

the caption of the figure. We note that for most of the fields away from level 1 all values of γ give approximately the same estimate at T+6. For level 1 there is some variation even at T+6 and this is likely to be due to the fact that we have large perturbations at this level. Thus the terms we are neglecting in the Taylor expansions we use to derive the linearization error estimate may not be negligible. However the order of magnitude of the estimate is similar for most values of γ. For the δw field the estimates diverge on most levels after T+12 indicating that these terms cannot be neglected for this field and the estimate is unlikely to be accurate. We also note that for the $\delta\theta$ field on level 15 and for the δw field on level 1, there is a large deviation in the estimates of the T+18 solution error when a value of $\gamma = 0.01$ is used. A closer examination of the actual fields shows that this is caused by rounding error with such a small value of γ, leading to very large values of the estimate at a few single grid points. For fields other than δw we see that the dashed curve is very close to the converged solution for most levels away from level 1. This curve corresponds to $\gamma = 0.2$ and so we use this value of the parameter for our estimates from this point on.

In Figure 6.5 we compare the evolution of the actual PFM solution error E_S with the estimated TLM solution error calculated using (6.100) and a value of the parameter $\gamma = 0.2$. The PFM error E_S is calculated from (3.22)

$$E_S = 100\frac{rms(\mathbf{E}^n)}{rms(\boldsymbol{N}^n[\boldsymbol{\delta}\mathbf{U}^0])}, \tag{6.101}$$

with the linearization error $\mathbf{E}$ defined by the difference between the nonlinear perturbation and the PFM solution. We plot the same five levels as previously, with the actual PFM solution error shown by the solid line and the estimated TLM error shown by the dashed line. For perturbations to u, v and θ the actual solution error follows a very similar evolution to the estimate for levels 12, 15 and 21 (the orange, blue and red lines). On level 1 we find that the perturbation forecast model performs better than expected, while on level 31 the actual error is much worse for

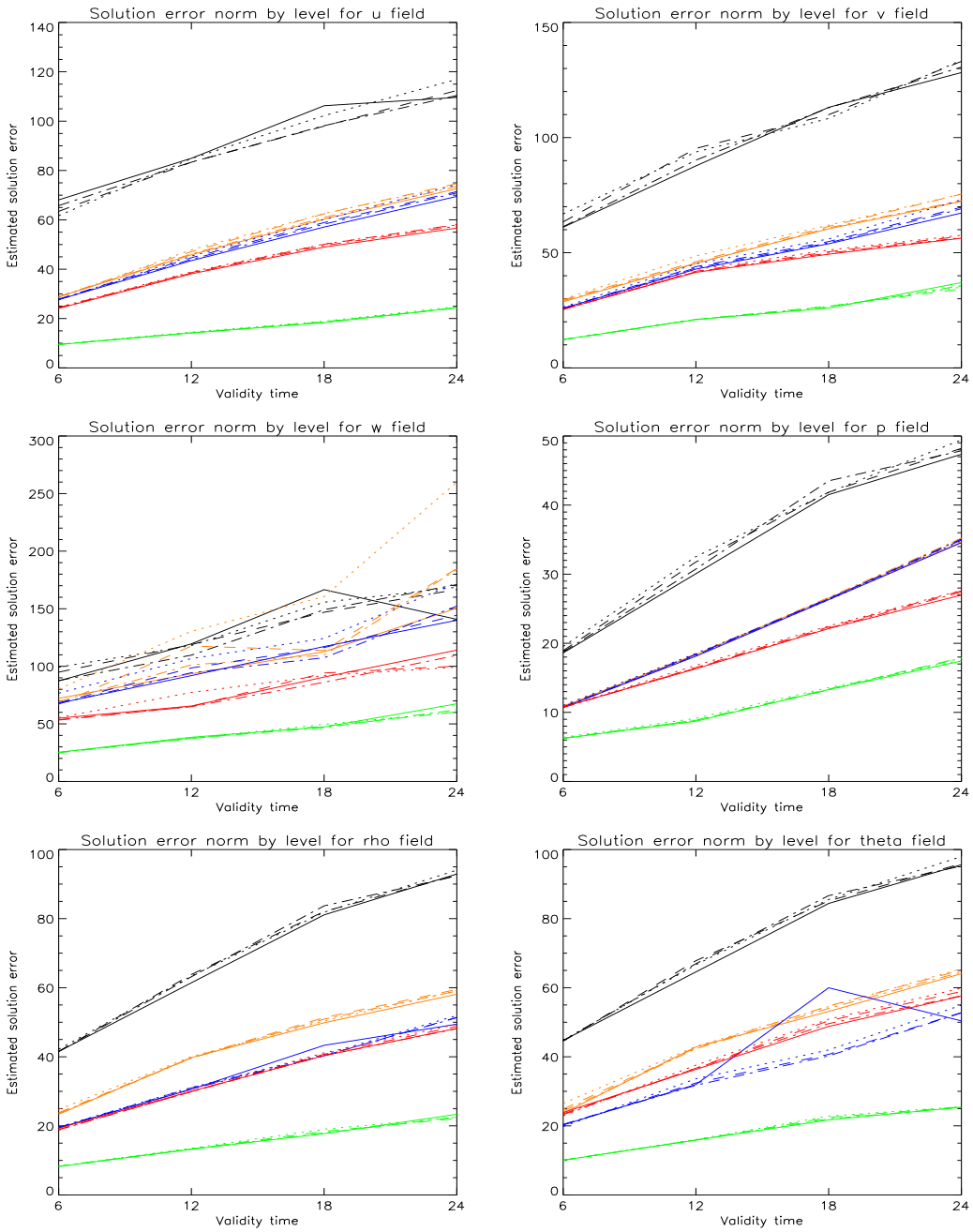

Figure 6.4: Evolution of estimated solution error from T+6 to T+24 on individual levels. The levels shown are level 1 (black), level 12 (orange), level 15 (blue), level 21 (red) and level 31 (green). For each level estimates using values of $\gamma = 0.5, 0.2, 0.1, 0.01$ are plotted using the lines dotted, dashed, dot-dashed and solid respectively.

these fields.

Of particular interest in Figure 6.5 is the solution error for the pressure field. We see that for all the levels plotted the actual error is much higher than the estimated error. The other fields in this figure, $\delta\rho$ and δw, show a reasonable agreement at T+6, but much variation thereafter, with some levels having good agreement and others showing a large error. However, the strong nonlinearity of the δw fields, which is reflected in Figure 6.4 by the large variation of the estimate with changes in γ, means that we are less confident in the error estimate for this field.

To investigate further the errors seen at all levels for the δp field and at higher levels in the other fields, we plot in Figure 6.6 the correlation coefficient (3.23) between the linear and nonlinear perturbations for each level at validity time T+12. We recall from Chapter 3 that the correlation coefficient for two fields $\mathbf{x} = \{x_j\}$ and $\mathbf{y} = \{y_j\}$ of length N is defined by

$$C[\mathbf{x}, \mathbf{y}] = \frac{\sum_{i=1}^{N}(x_i - \bar{x})(y_i - \bar{y})}{\left(\sum_{i=1}^{N}(x_i - \bar{x})^2 \sum_{i=1}^{N}(y_i - \bar{y})^2\right)^{\frac{1}{2}}}, \tag{6.102}$$

where $\bar{x}, \bar{y}$ are the mean values of the components of $\mathbf{x}$ and $\mathbf{y}$ respectively. The validity time of T+12 is chosen since it allows comparison with previously published results. It is also likely that we would want to use the linear model for an incremental 4D-Var data assimilation system with a twelve hour time window and so it is important that the model is valid over this period. We see from Figure 6.6 that all fields except δw have a correlation coefficient of greater than 0.9 above model level 20 and that the pressure perturbation shows a correlation coefficient of greater than 0.93 everywhere. These values compare with correlations published by Li et al. [50] of 0.94 for δu, 0.91 for δv and 0.96 for the perturbation to their pressure variable. We see from Figure 6.6 that our results match the published values at higher vertical levels in the model. The lack of agreement at lower levels may be due to the absence of friction and vertical diffusion in both the perturbation forecast model and the nonlinear model generating the linearization states.

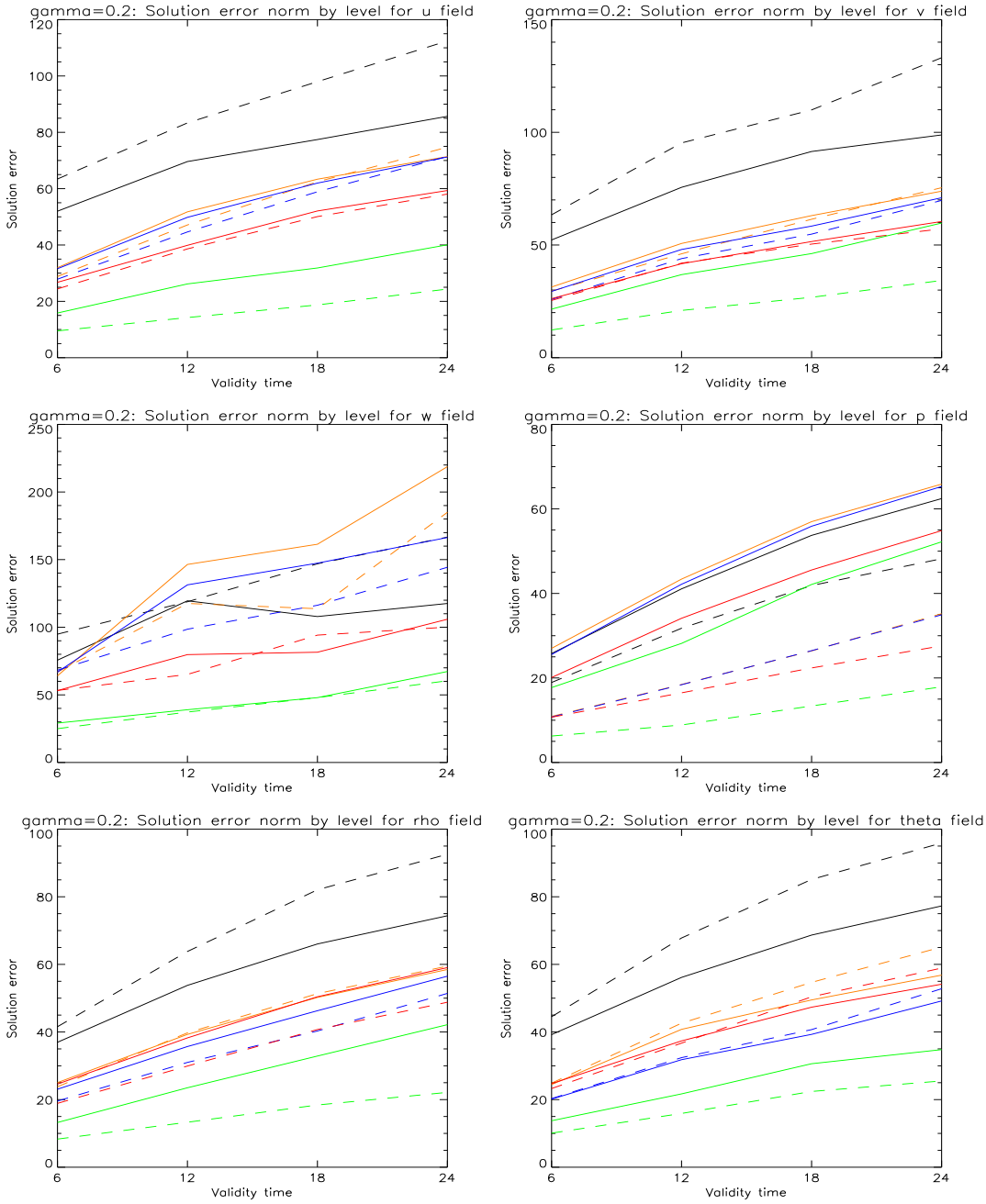

Figure 6.5: Comparison of evolution of actual PFM and estimated TLM solution errors from T+6 to T+24 on individual levels. The levels shown are level 1 (black), level 12 (orange), level 15 (blue), level 21 (red) and level 31 (green). For each level the solid line indicates the actual error from the perturbation forecast model and the dashed line indicates the estimated TLM error.

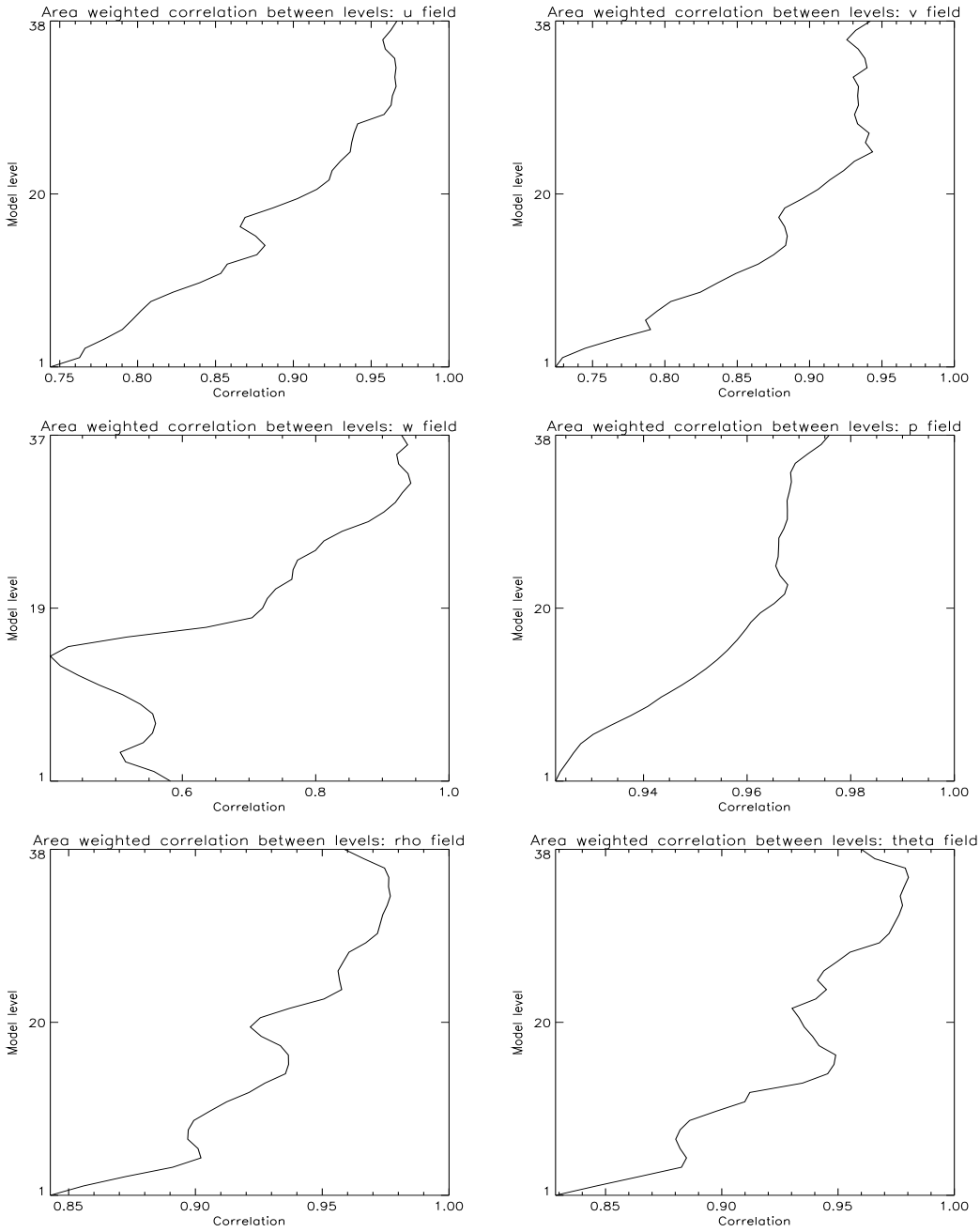

Figure 6.6: Correlation coefficient between nonlinear and linear perturbations plotted against model level for each model field.

From our investigations of different error measures in Section 3.1.2, a good correlation coefficient but high solution error would imply that the linear model is predicting the same pattern of perturbations as the nonlinear model, but that the amplitudes are incorrect. To determine if this is the case we define a damping coefficient C_D by

$$C_D = \frac{rms(\mathbf{L}(t_n, t_0)\boldsymbol{\delta}\mathbf{U^0})}{rms(\boldsymbol{N}^n[\boldsymbol{\delta}\mathbf{U^0}])}. \tag{6.103}$$

Thus for values of $C_D < 1$ the perturbation forecast model field is damped with respect to the nonlinear perturbation. We plot this coefficient for each field in Figure 6.7. It is evident that for all fields except δw the perturbation forecast model is damping with respect to the nonlinear model. The damping is particularly strong for δp between level 12 and 15, but is also present for δu and δv around level 15 and for the other fields slightly higher. For the δw field we have an amplification in the perturbation forecast model with respect to the nonlinear evolution. However, we expect this field to be particularly sensitive to the lack of a friction scheme in the linear model in areas of steep orography. Hence we leave investigation of this field until such a scheme has been implemented. We concentrate our attention on the other fields and now look at the perturbation fields themselves.

6.3.4 Perturbation fields

In this section we continue to look at the fields at validity time T+12 and concentrate our attention on model level 15. This level is chosen for two reasons. Firstly, we have seen from Figure 6.7 that this is the level at which the heaviest damping occurs for the pressure and horizontal wind fields. Secondly, this level is at approximately $500hPa$, which is a level used in other studies we shall compare with. We begin by considering a field which the solution error showed to be in good agreement with the estimated tangent linear model solution error. This will enable us to judge whether our choice of the parameter $\gamma = 0.2$ was suitable. We consider the potential

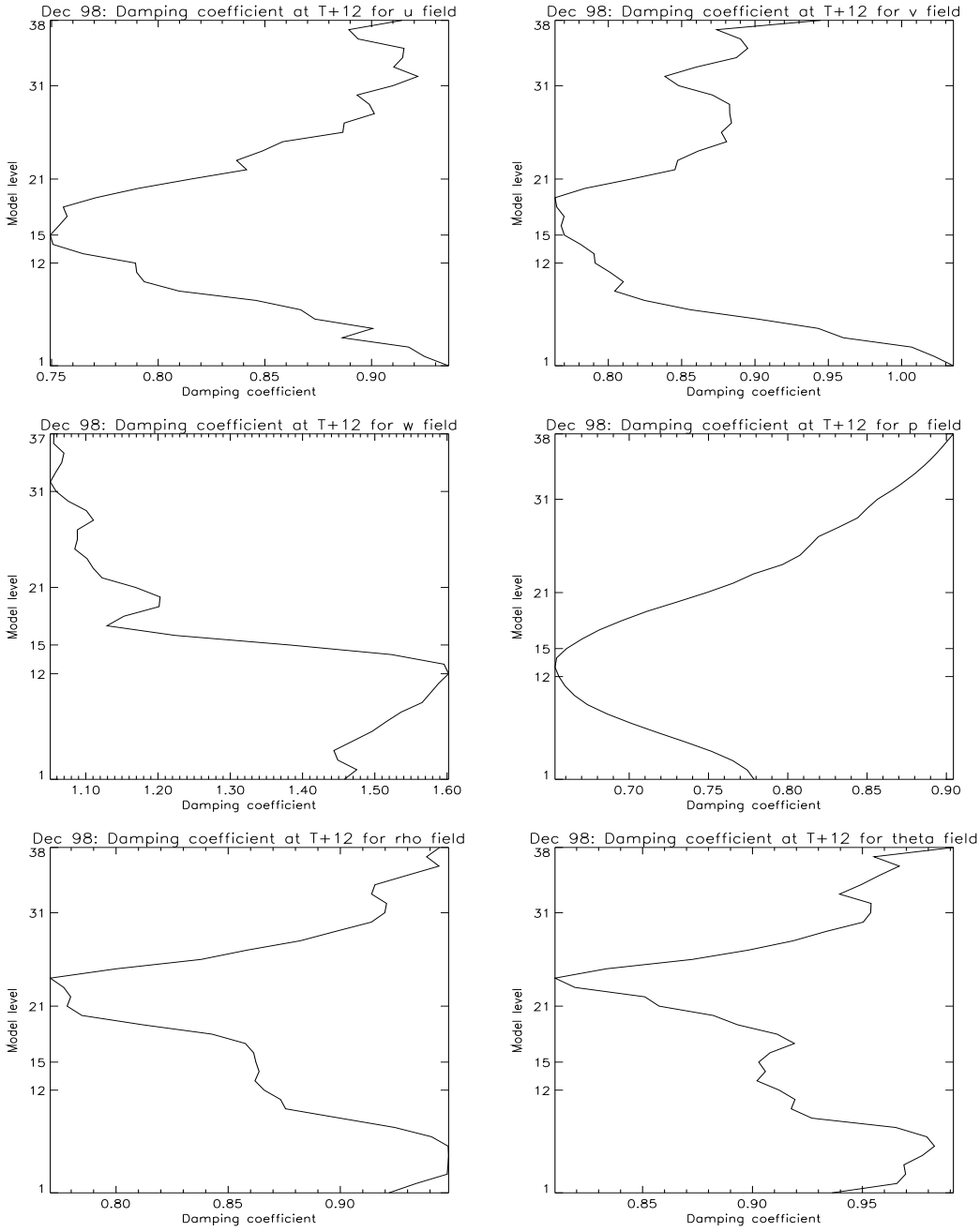

Figure 6.7: Damping coefficient (6.103) plotted against model level for each model field.

temperature field on level 15 at T+12. From Figure 6.5 we see that the actual PFM and estimated TLM solution errors agree very well for this field and Figure 6.6 shows that the correlation coefficient exceeds 0.94. We show a comparison of the nonlinear and linear perturbations in Figure 6.8. In this figure Plot A shows the perturbation predicted by the nonlinear model, Plot B the perturbation predicted by the perturbation forecast model, Plot C the difference between these and Plot D the estimated TLM linearization error calculated from our formula (3.32). It is clear first of all that the general pattern of the perturbations is the same in the linear and nonlinear models. A comparison of plots C and D shows that in general where there are linearization errors in the perturbation forecast model these also appear in our estimate of the TLM linearization error. The RMS value of the PFM linearization error is 0.53 compared with 0.54 for the estimated TLM error. Thus we see that the error arising from the use of a perturbation forecast model is no greater than that which would be expected with a tangent linear model. We conclude that for this field the main differences between the linear and nonlinear perturbations are due to nonlinear effects rather than approximations in the linear model. The similarity between plots C and D in both pattern and magnitude also reinforces the confidence we have in our error estimate with the chosen parameter.

We now consider the perturbations to pressure at T+12. We note however that because of the choice of grid, level 15 for p is staggered from level 15 for θ. We found in Section 6.3.3 that at this level there was a good correlation between the linear and nonlinear perturbations but a high level of damping in the linear model. Figure 6.9 shows the perturbation fields for this level. Again we plot the nonlinear perturbation, the linear model perturbation, the true PFM linearization error and the estimated TLM linearization error. It is immediately noticeable that the linear model perturbation contains many of the same features as the nonlinear perturbation, but is damped in magnitude almost everywhere. A comparison of actual PFM and estimated TLM linearization errors, plots C and D, indicates that

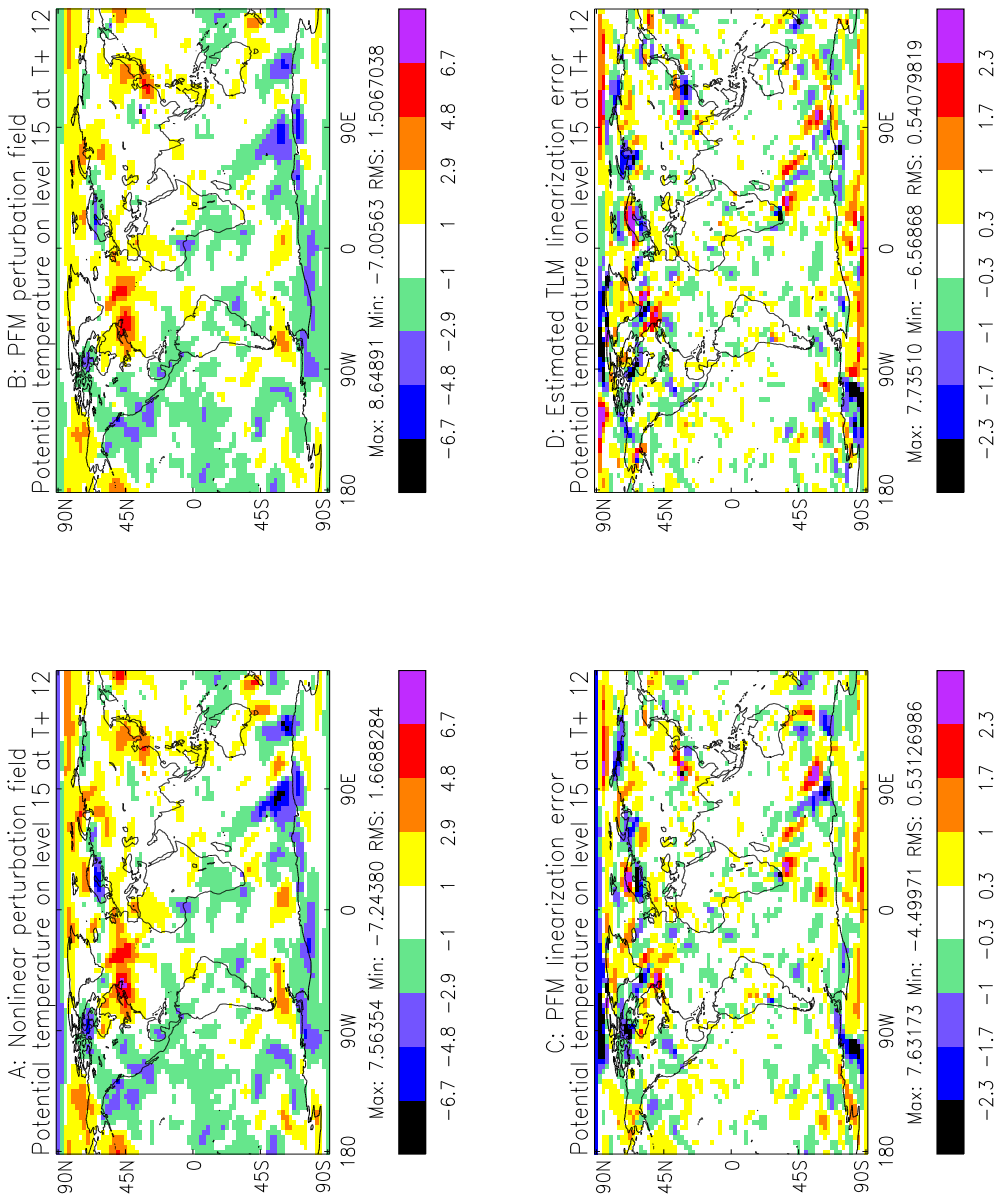

Figure 6.8: θ perturbation on level 15 at T+12. Plot A shows the nonlinear perturbation, Plot B shows the perturbation forecast model perturbation, Plot C shows the actual PFM linearization error, and Plot D shows the estimated TLM linearization error. Units are K.

this is not due to nonlinear effects and would not be expected if we had an exact tangent linear model. Thus it appears that for the pressure field the perturbation forecast model causes a damping which cannot be explained solely by nonlinear effects.

We find a similar damping of the perturbation to the v component of the wind on this level. Figure 6.10 shows the δv on level 15 at T+12, with the four plots as in the previous two figures. For this field we particularly notice a damping of the linear perturbation near the North Pole with respect to the nonlinear perturbation. A comparison of the actual PFM and estimated TLM linearization errors indicates that this damping is not due to nonlinear effects. Although the damping is not as evident in this field as in the pressure, it is useful to note since this field provides a comparison with published results. In studies of the tangent linear of a mesoscale model [27], [28], the authors showed perturbations of the v component of the wind at $500hPa$ to agree well with the nonlinear perturbation after 12 hours. This provides further evidence that the damping we see is due to approximations in the perturbation forecast model rather than nonlinear effects. However this comparison must be made with care, since the nonlinear perturbations themselves were decaying in the experiments of [28] while they are not in our model. This decay in the nonlinear perturbations can probably be explained by the fact that [28] used a limited area model. Other studies have shown that perturbation growth is restricted in limited area models compared to global models by the assumption of zero perturbations on the lateral boundaries [25].

We have seen so far that in general the patterns of the linear and nonlinear perturbation fields match well, with most of the error being in the amplitude. However it is possible that the correct pattern is being predicted simply because the perturbations are not changing very much in time. In order to account for this we would like to measure how well the linear model predicts the change in perturbation from one time step to the next. One way of doing this is to compare tendencies

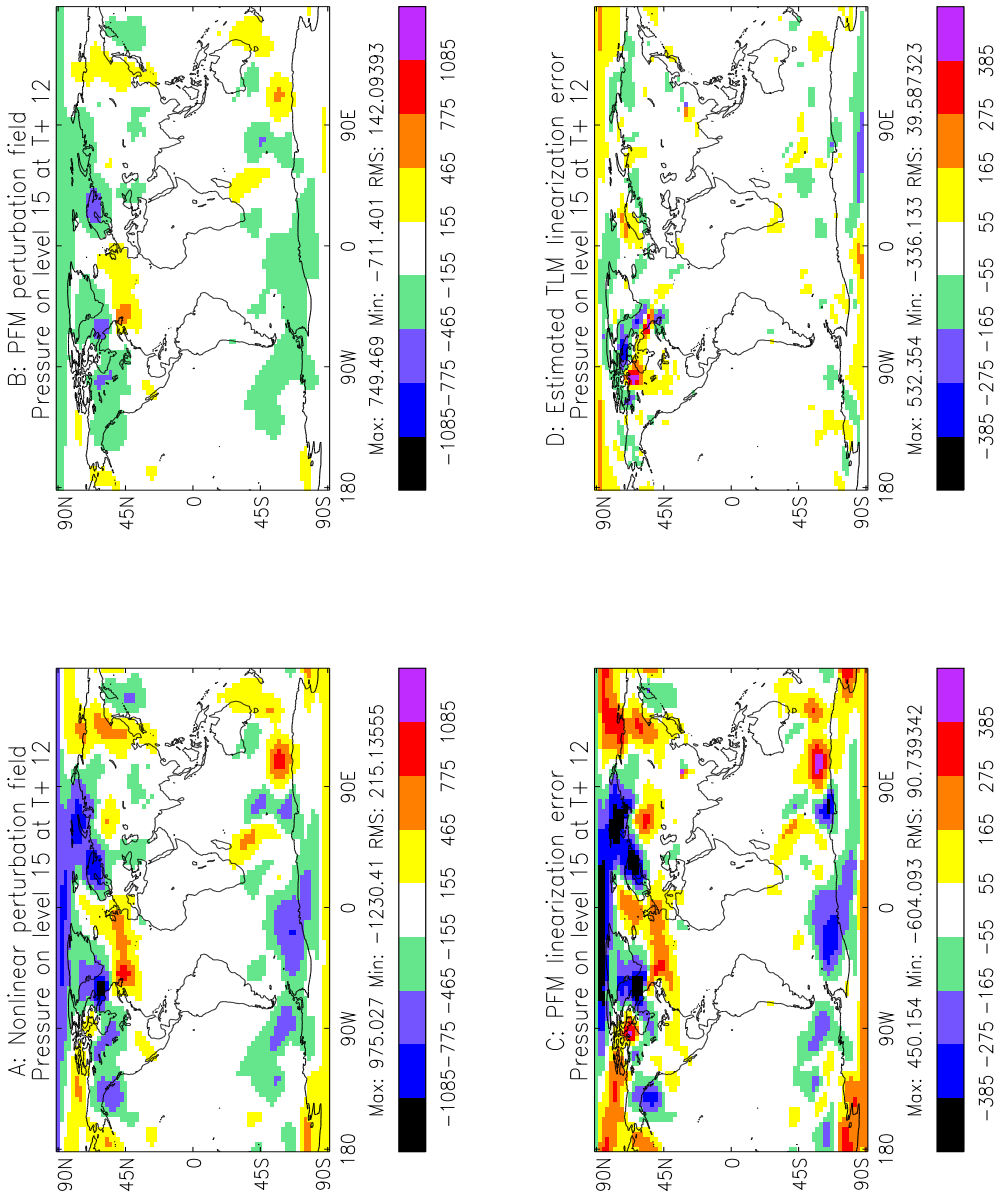

Figure 6.9: Pressure perturbation on level 21 at T+12. Plot A shows the nonlinear perturbation, Plot B shows the perturbation forecast model perturbation, Plot C shows the actual PFM linearization error, and Plot D shows the estimated TLM linearization error. Units are Pa.

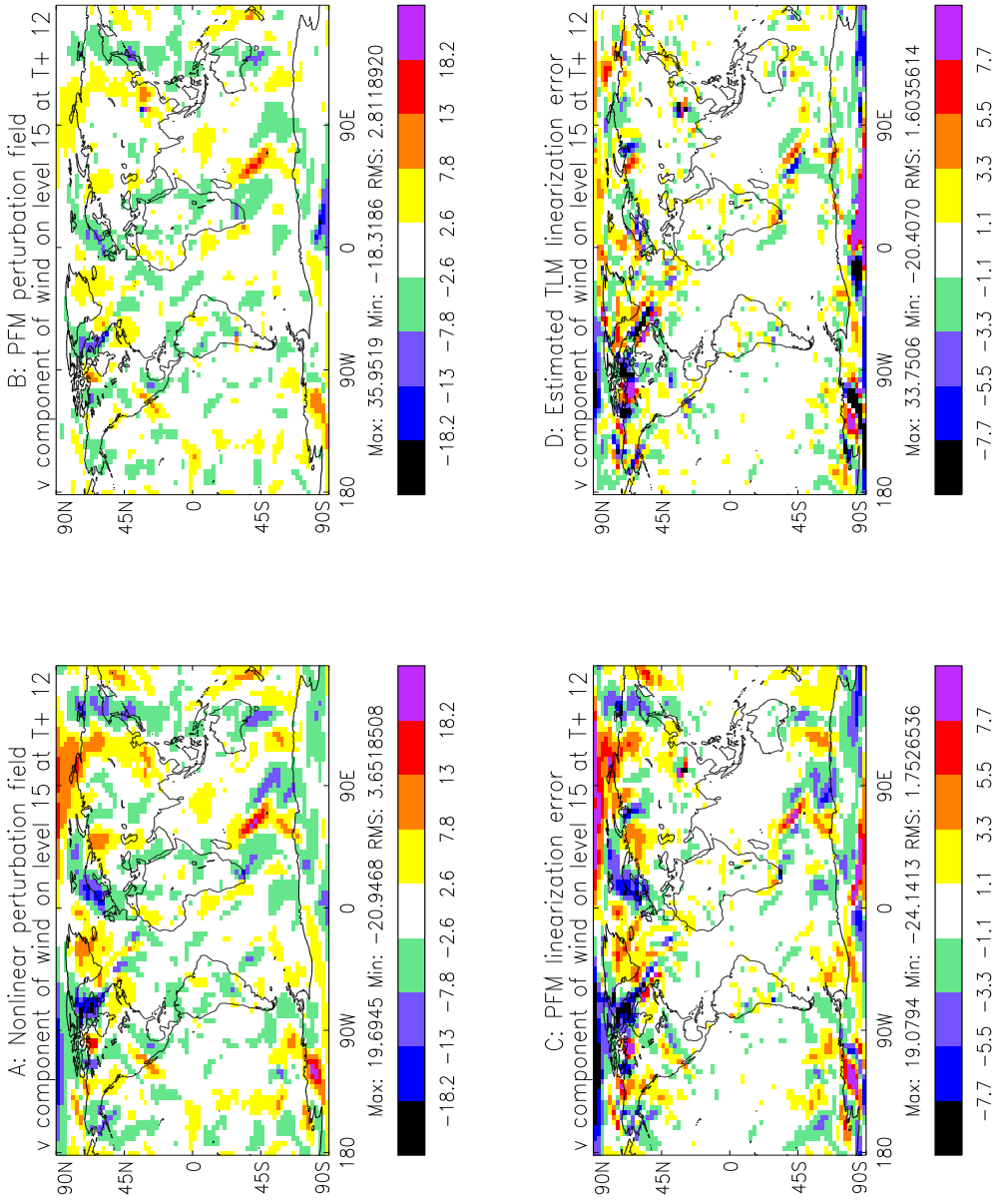

Figure 6.10: v perturbation on level 21 at T+12. Plot A shows the nonlinear perturbation, Plot B shows the perturbation forecast model perturbation, Plot C shows the actual PFM linearization error, and Plot D shows the estimated TLM linearization error. Units are ms^{-1}.

in the perturbations. For the purpose of this study we define the tendency field to be the perturbation field after one time step minus the initial perturbation and do not normalize by the time step. A comparison of this change in the nonlinear and perturbation forecast models allows a judgement to be made as to whether the linear model is changing the initial fields in the correct way.

Before looking at the tendencies it would be useful if we had some estimate of the error we would expect in the tendencies if we had an exact tangent linear model, in a similar way to the error estimate we produced for the fields themselves. We outline a method of achieving this. We suppose that we have an initial perturbation $\boldsymbol{\delta}\mathbf{U^0}$ at time t_0. Now let the nonlinear perturbation after one time step be written $\boldsymbol{N}^{\Delta t}[\boldsymbol{\delta}\mathbf{U^0}]$ and the linear model perturbation be written $\mathbf{L}(t_{\Delta t}, t_0)\boldsymbol{\delta}\mathbf{U^0}$. Then we can write the nonlinear tendency $\Delta_N\boldsymbol{\delta}\mathbf{U^0}$ as

$$\Delta_N\boldsymbol{\delta}\mathbf{U^0} = \boldsymbol{N}^{\Delta t}[\boldsymbol{\delta}\mathbf{U^0}] - \boldsymbol{\delta}\mathbf{U^0} \tag{6.104}$$

and the perturbation forecast model tendency $\Delta_P\boldsymbol{\delta}\mathbf{U^0}$ as

$$\Delta_P\boldsymbol{\delta}\mathbf{U^0} = \mathbf{L}(t_{\Delta t}, t_0)\boldsymbol{\delta}\mathbf{U^0} - \boldsymbol{\delta}\mathbf{U^0}. \tag{6.105}$$

Then the error in the tendency $\mathbf{E}_\tau$ is given by

$$\begin{aligned} \mathbf{E}_\tau &= \Delta_N\boldsymbol{\delta}\mathbf{U^0} - \Delta_P\boldsymbol{\delta}\mathbf{U^0} \\ &= \boldsymbol{N}^{\Delta t}[\boldsymbol{\delta}\mathbf{U^0}] - \mathbf{L}(t_{\Delta t}, t_0)\boldsymbol{\delta}\mathbf{U^0}. \end{aligned} \tag{6.106}$$

Thus we see that the error in the tendency is equal to the difference between the perturbation fields themselves after one time step, or in other words the tendency error is equal to the one-time-step linearization error. Since we have a method of estimating how much of the linearization error is due to the TLM linear approximation, we can apply this method to the one-time-step fields and estimate how much of the tendency error is due to the TLM linear approximation.

We look first at a field that we have already judged to be well forecast at T+12, the potential temperature on level 15. Figure 6.11 shows the tendency field for θ on

level 15. In this figure Plot A shows the tendency field from the nonlinear model, Plot B shows the perturbation forecast model tendency, Plot C is the difference between them and Plot D is the estimated tendency error of a tangent linear model. It is clear that the tendency pattern of the perturbation forecast model is very similar to that of the nonlinear model perturbation and in general is of the same sign, indicating that perturbation forecast model forces the initial perturbation in the correct sense. However, as for the fields themselves, we find a difference in magnitude between the nonlinear and linear tendencies. From Plot D it is clear that most of the errors we do see are associated with areas where nonlinear effects are important. For this field the actual and estimated errors (Plots C and D) agree well both qualitatively and quantitatively.

We now consider the pressure perturbation tendency on this level. Figure 6.12 compares the nonlinear and linear tendencies, with the plots in the same format as Figure 6.11. Again we find that in general the tendencies are in the correct place and are of the correct sign. However we note that the perturbation forecast model has an excessive tendency at the North Pole. This may be due to an error in the formulation or simply a coding bug and will require further investigation in the future. We find for this field the error in the tendencies (Plot C) does not correspond very well with the estimated TLM error (Plot D). Experiments to investigate the sensitivity of this estimate to the value of the parameter γ in the estimate formula have shown that while the extreme values at a few grid points may be sensitive to this, the general pattern is not. The pressure tendency error we see in the perturbation forecast model is quite different from that which we would expect from a tangent linear model. Nevertheless the linearization error of the perturbation forecast model is smaller than the expected error. Thus it would seem that at least the initial tendencies are not responsible for the damping we see in the pressure field.

In order to understand how dependent the damping we see is on the particular

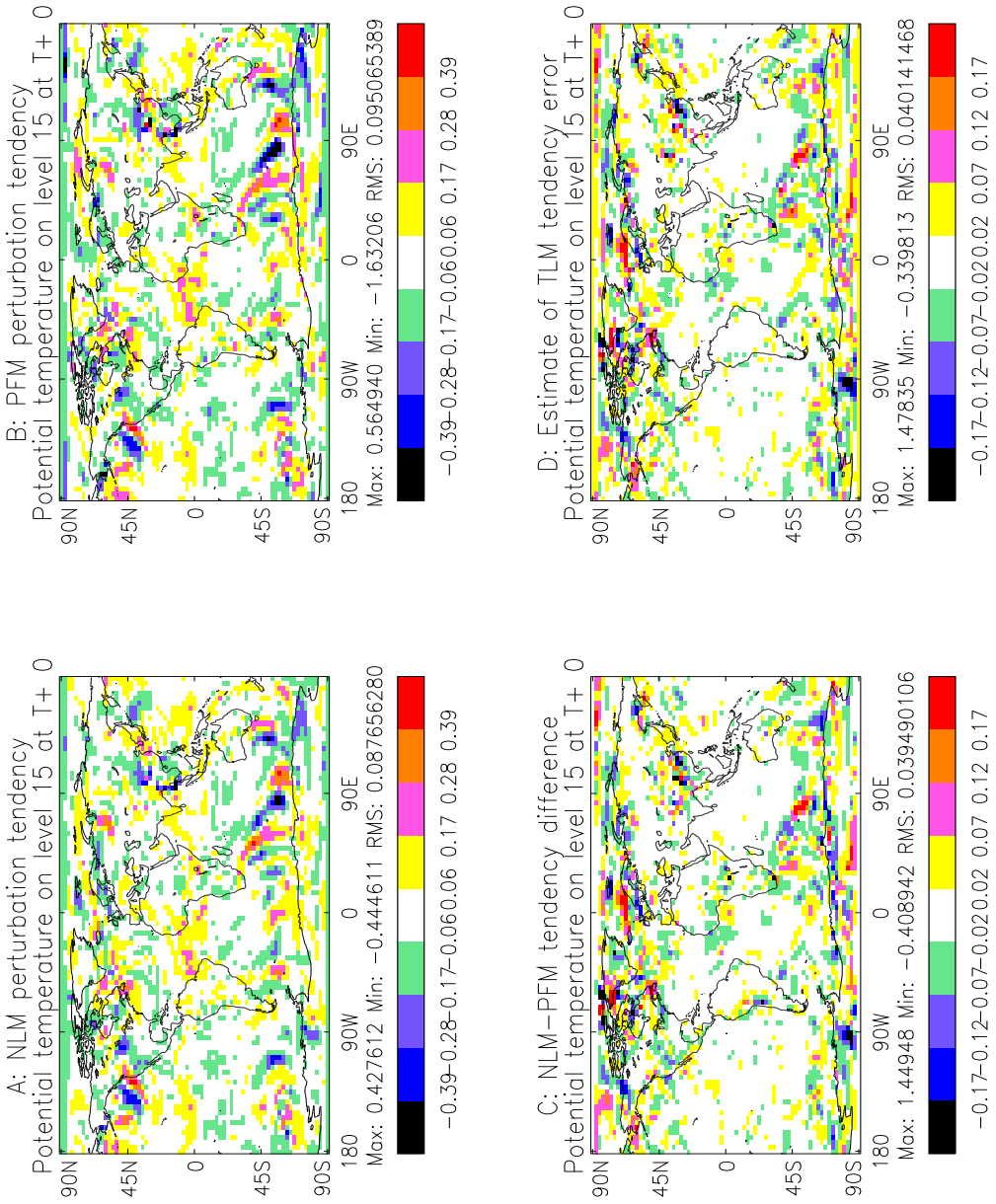

Figure 6.11: Initial tendency of perturbation to θ on level 15. Plot A shows the NLM tendency, Plot B shows the PFM tendency, Plot C shows the difference between them and Plot D shows the estimated TLM tendency error. Units are K.

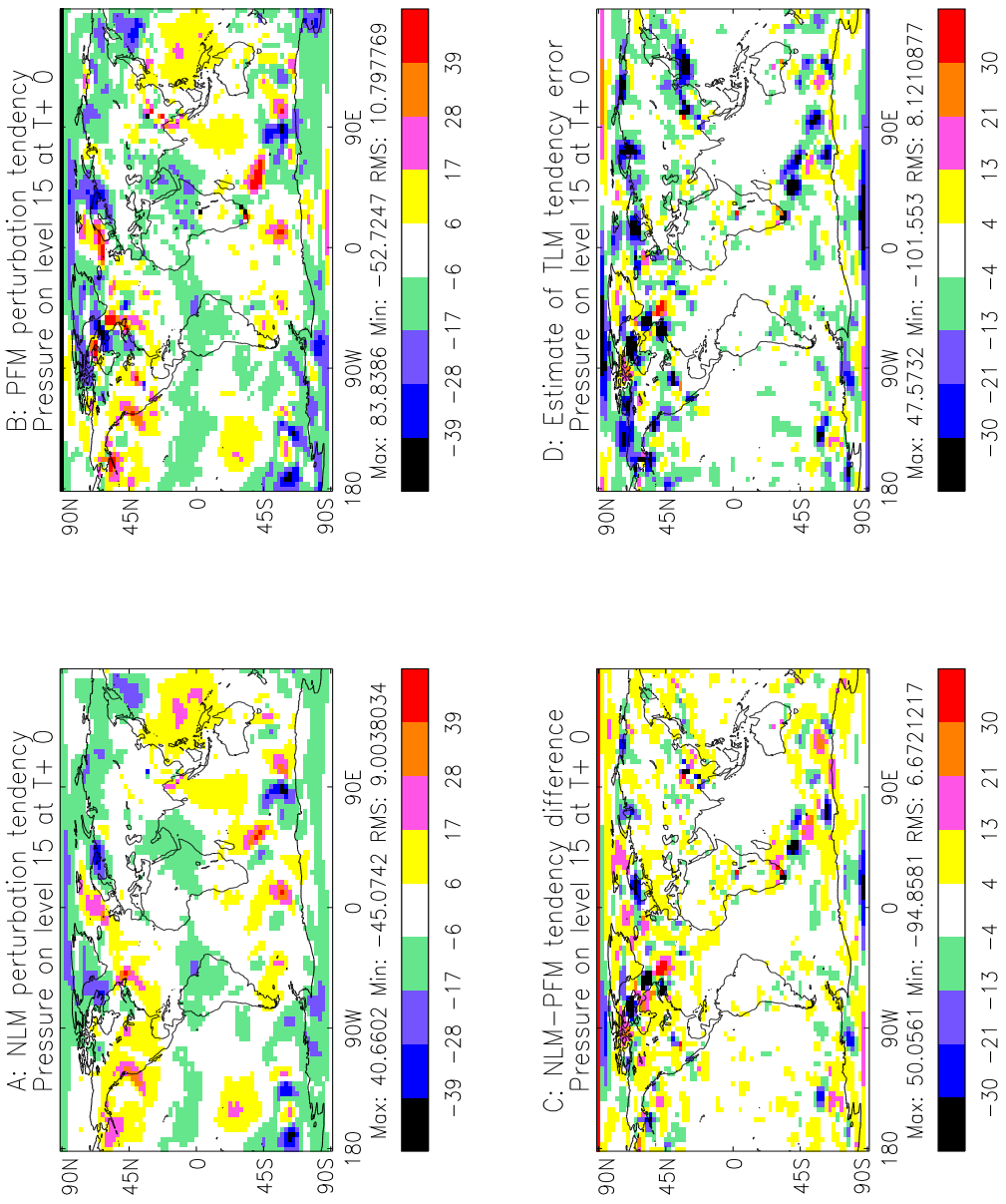

Figure 6.12: Initial tendency of pressure perturbation on level 15. Plot A shows the NLM tendency, Plot B shows the PFM tendency, Plot C shows the difference between them and Plot D shows the estimated TLM tendency error. Units are *Pa*

case chosen, we have also run from another set of data, changing from a Northern Hemisphere winter to a Northern Hemisphere summer period, July 1999. The initial data were produced in the same way as described in Section 6.3.1. For this case the levels were set up differently and so we have that level 14 is the top of the boundary layer, level 19 is at $500hPa$, level 27 is at $250hPa$ and the first constant height level is level 35. We plot the damping coefficient (6.103) for this case in Figure 6.13. A comparison with Figure 6.7 on page 187 shows that for this case the perturbations from the linear model are damped in a similar way to the December 1998 case. Again we see a large damping of pressure, which is worst between the boundary layer top and $500hPa$, and a damping of the u and v perturbations, peaking slightly higher than $500hPa$. A look at the fields themselves also reveals a similar behaviour to those of the December 1998 case (not shown). Thus we find that the damping for both cases follows the same pattern and even though the model levels are set up differently for the two experiments, the damping peaks at approximately the same pressure level.

Since the damping does not seem to be dependent on the data we must assume that it is caused by a difference between the schemes of the linear and nonlinear models. One likely candidate for the problem is the fact that we have a first order time error in the treatment of the perturbation wind term arising from the linearization of the advection step. This comes from the fact that we treat this term at the arrival point at time level n, as in the second perturbation forecast model of Chapter 5. Although this did not show up as a problem in the shallow water model experiments of Chapter 5, this may be just because of the restricted set of tests we were able to run. It has been shown by Durran that for a linear finite difference scheme of order r applied to the oscillation equation, the amplitude error is of order Δt^n, where $n = r + 1$ if r is odd and $n \geq r + 2$ if r is even [20]. This means that for a first order scheme the amplitude error is $O(\Delta t^2)$, whereas for a second order scheme it is at most $O(\Delta t^4)$. We would therefore expect that the first order error in

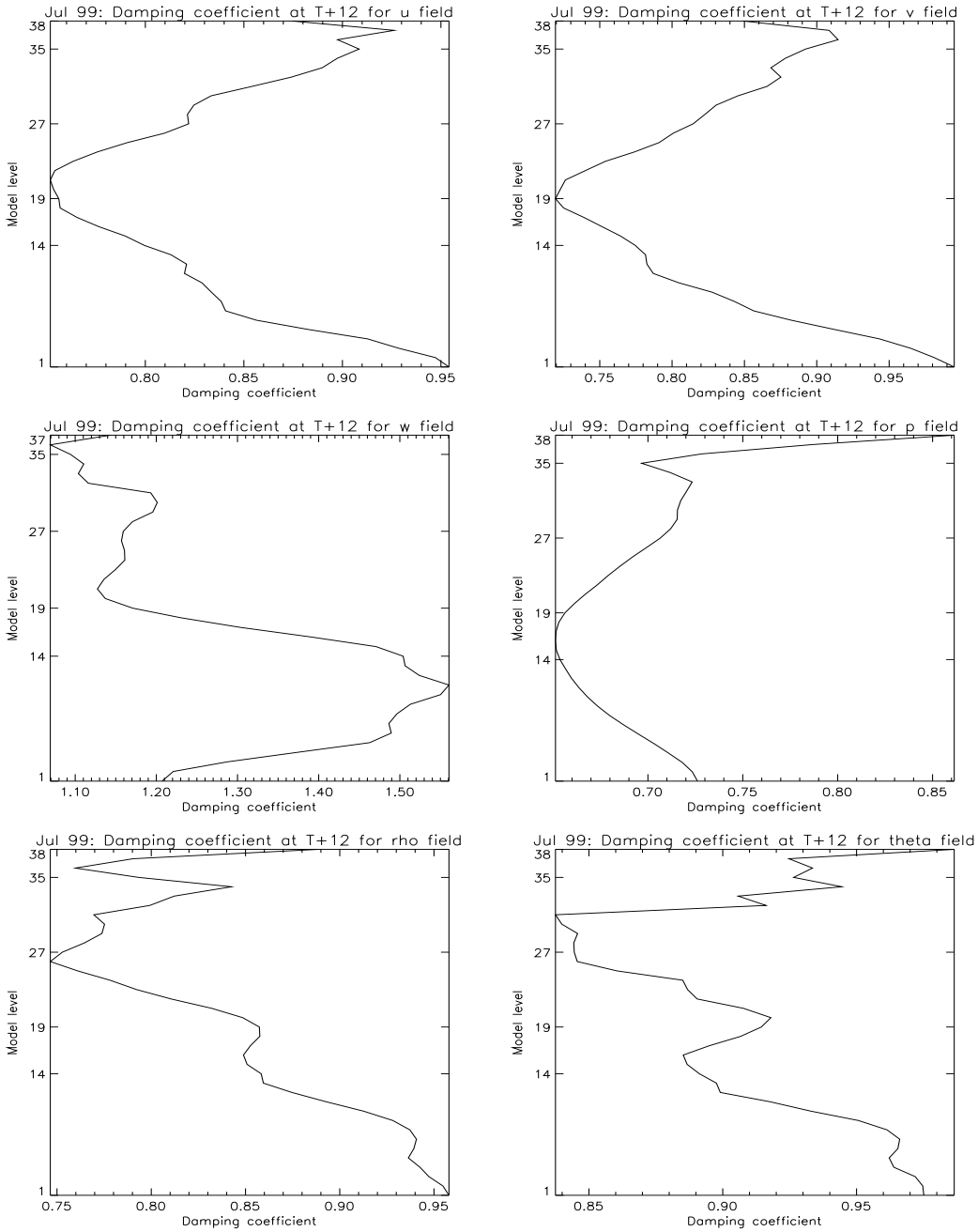

Figure 6.13: Damping coefficient (6.103) plotted against model level for each model field for the July 1999 case.

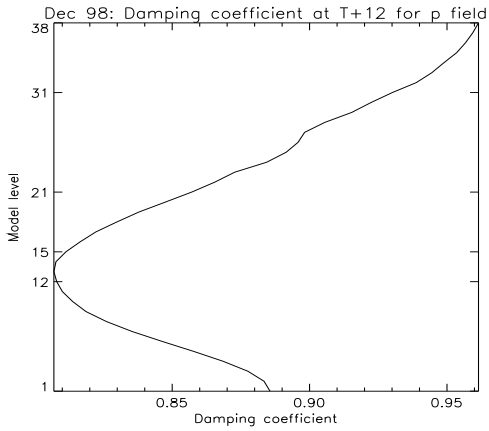

Figure 6.14: Damping coefficient (6.103) for δp plotted against model level for each model field for the December 1998 case with a $900s$ time step.

the linear model could contribute to the difference in amplitude between the linear and nonlinear perturbations.

Ideally we would like to test the effect of truncation error on our results by running the experiment with a different time step and a different spatial resolution such that the ratio of the spatial and temporal steps remains constant. For the three-dimensional model this is not yet possible, since we do not have facilities to change spatial resolution easily. To give some kind of insight as to whether the truncation error may be the source of the damping problem we run the linear model using half the original time step ($900s$), but keeping the spatial resolution as before. The nonlinear model is run with the original $1800s$ time step and so the linearization state in the linear model is only updated every $1800s$ or two time steps. This avoids the extra complication as to the effect of a change in linearization state. In Figure 6.14 we plot the damping coefficient (6.103) for the pressure perturbation for this run, using the data from December 1998. A comparison with the corresponding plot for the run with an $1800s$ time step in Figure 6.7 shows that the variation of damping with height is unchanged. However the minimum value of the damping coefficient has been changed from 0.65 in the $1800s$ time step run to over 0.8 in the

900s time step run, with the damping reduced at all other levels. Plots for other variables show a similar reduction of the damping. Thus we see that running with a smaller time step results in a much more accurate prediction of the amplitude of the perturbations. Although this does not provide a strict test of truncation error, since the spatial resolution remains constant, it does provide some evidence that the amplitude errors are caused by our first order treatment of these extra terms. We outline in Section 7.2 how we propose to investigate this hypothesis further.

6.4 Linearization state

In each of the above experiments we have taken the nonlinear base state to be at the start of the time step, time level n. We have shown in Section 5.5 that in general this will be only first order in time, whereas averaging the linearization state to the centre of the time step for the forcing terms will be second order in time. However, in the three-dimensional perturbation forecast model we are treating the extra term arising from the linearization of advection $(\boldsymbol{\delta}\mathbf{u}.\nabla)$ as in the shallow water model PFM2 of Section 5.2.4, which we found in Section 5.3.3 to be always first order in time. Thus for our three-dimensional model we do not expect any extra accuracy from averaging the linearization state to the centre of the time step.

In order to test this we ran again the experiment described in Section 6.3, but with the linearization state taken to be the average of the time level n and time level $n+1$ values. The control run with which we compare is the run described above with the nonlinear base state taken at time level n. We summarize the results in Table 6.2. In this table we show for each variable the maximum absolute difference between the new perturbation forecast model run and the control (Column A), the model level on which this difference occurs (Column B) and the maximum absolute PFM linearization error on this level (Column C). For each of the variables we find that the maximum change from averaging the nonlinear base state is less than 10%

of the maximum linearization error. We conclude that for this particular model the more accurate linearization state does not have a significant impact, as expected from the theory. However, a greater sensitivity to the linearization state may be found if we were to replace the present first order scheme with one which is second order.

	A	B	C
Field	Maximum absolute difference	Level	Maximum absolute linearization error
δu	4.5 ms^{-1}	3	78.6 ms^{-1}
δv	3.8 ms^{-1}	2	62.7 ms^{-1}
δw	0.05 ms^{-1}	15	1.75 ms^{-1}
δp	49.8 Pa	1	1530 Pa
$\delta \rho$	0.01 kgm^{-3}	1	0.32 kgm^{-3}
$\delta \theta$	3.5 K	1	48.0 K

Table 6.2: Comparison of difference between run of the perturbation forecast model with the nonlinear base state at the start and the centre of the time step. Column A shows the maximum absolute difference between the fields, Column B shows on what level this difference occurs and Column C shows the maximum PFM linearization error from the control run on this level.

6.5 Summary

In this chapter we have applied the semi-continuous method to derive the linearization of a full three-dimensional numerical weather prediction model. In doing so we have made use of the study of the shallow water model in Chapter 5 to help validate our results. Firstly, we have seen clearly that deriving a perturbation forecast model for a partial differential equation system implies some degree of freedom in the choice of the scheme made. One example of this is the perturbation wind term

arising from the linearization of advection. In the three-dimensional model of this chapter we treated this term at the arrival point at time level n, in a similar way to the shallow water model PFM2 of Section 5.2.4. However, in Section 5.3.3 we showed that the scheme is only first order accurate in time. Although this did not seem to be a problem in the simple shallow water model, it may have a greater effect in the three-dimensional model.

Another example of a particular choice we made for this model is in the treatment of the Coriolis terms. Considerations for developing the adjoint model required that these terms be treated in a different way from corresponding terms in the nonlinear model. In order to treat them in a stable manner but outside our elliptic equation we developed an alternative scheme particular to the perturbation forecast model.

We have also seen that as for the shallow water perturbation forecast model of Chapter 5 testing was made more difficult by the fact that the linearization error does not tend to zero as the perturbation size is reduced. In order to provide a method for validating our perturbation forecast model, we have made use of the formula derived in Section 3.3 to estimate the error that a tangent linear model would give. This has proved invaluable in tests of the three-dimensional model, since it has allowed us to evaluate how much of the errors we see are likely to be due to approximations we have made rather than nonlinear effects. For example, at middle levels we have seen a damping in the perturbations, especially in the pressure field. For this case we have seen that this damping would not be expected if we had an exact tangent linear model and so this indicates that the present formulation of our perturbation forecast model is not sufficiently accurate for the purposes we require. The evidence we have suggests that this damping may be due to the first order treatment of terms arising from the linearization of advection. We return to this question in Section 7.2 where we consider how we may increase the accuracy of these terms.

However despite such problems, experiments with this first version of the model

are encouraging. As for the simple models developed in Chapters 4 and 5, we have found for the three-dimensional model that the linear model developed using the semi-continuous method is able to predict the approximate evolution of a perturbation. For some of the fields we have validated this prediction was as accurate as that which we would expect from a tangent linear model, even for a 24 hour forecast. This was particularly true for perturbations to the horizontal wind components and the potential temperature away from the model boundaries. We expect that with considered modifications of the numerical scheme this accuracy could also be achieved for the other fields. We discuss some further ideas for achieving this in Section 7.2.

Chapter 7

Conclusions and future work

In Chapter 3 we posed the question "Can the semi-continuous method provide us with a linear model which is as accurate as the tangent linear model formed by the discrete method while avoiding some of the problems associated with linearizing discrete numerical models?" We now summarize the results we have found which begin to answer this question and discuss some ideas for further work.

7.1 Summary of results

In examining the linear model formed by the semi-continuous method we have considered its accuracy from three different perspectives which we defined in Chapters 2 and 3. These are truncation error, correctness and validity. For the ordinary differential problem of Chapter 4 it was also possible to examine the linear stability of the models.

We have seen that the linear model is 'correct', as defined by Definition 3.2, if it is formed by the discrete method, whereas the perturbation forecast model formed by the semi-continuous method is not usually correct in this sense. This became more apparent when we looked at a PDE problem in Chapter 5, since it is clear that some degree of freedom is available when discretizing the continuous linear equations.

In terms of truncation error, for the examples of the schemes we studied the tangent linear model was found to be as accurate as the discrete nonlinear model from which it is derived. For the perturbation forecast model this is not necessarily the case. The example of the ODE problem of Chapter 4 and the shallow water problem of Chapter 5 have shown that the accuracy of the perturbation forecast model may be compromised by two factors, the way in which the numerical scheme is applied and the choice of linearization state. The first of these arises only in the PDE problem, again from the freedom with which the linearized equations may be discretized. This was illustrated by the two versions of the perturbation forecast model for the shallow water problem of Chapter 5. We found that two slightly different discretizations gave schemes with different orders of accuracy. In Chapter 6 we proposed this as a possible reason for the damping we see in the three-dimensional perturbation forecast model and we discuss how we intend to investigate this further in Section 7.2.

The choice of linearization state on the other hand was found to influence the truncation error of both the ODE and PDE problems. We have shown that changing the point at which the linearization state is taken within the time step window can change the order of the scheme. It may be possible that this formal loss of accuracy may not be important in practice. Other studies using tangent linear models have shown that provided the linearization state is not too rapidly changing, acceptable results can be obtained without updating every time step, even though this formally introduces an error in the linearization (for example [28]). However, in the case of the shallow water problem of Chapter 5 we found that by averaging the linearization state within the semi-Lagrangian advection step it was possible that the scheme produced was no longer consistent. This may pose more of a problem for the general use of perturbation forecast models, since it implies that for similar schemes the linearization state must be updated on every time step. This is probably the most serious restriction on the use of the semi-continuous method that we have

discovered in this work. Although it is not relevant to the present three-dimensional model of the Met Office, any future changes to the numerical scheme introducing the semi-Lagrangian advection of nonlinear quantities may cause problems for the present design of the linear model.

The validity of a linear model is a more subjective test than correctness and truncation error and yet is probably the one of most interest. In tests of simple models of an ODE problem in Chapter 4 and a PDE problem in Chapter 5 the perturbation forecast model was demonstrated to have a similar validity to the tangent linear model. However we recognize that the range of possible tests on these models was limited. Ways of extending these are discussed in Section 7.2. The study of the shallow water model also allowed the verification of a formula designed to estimate the linearization error of the tangent linear model. This formula has formed the basis of our validation of the three-dimensional perturbation forecast model. By means of this formula we have shown that much of the linearization error that we see in tests of the three-dimensional model is due to nonlinear effects rather than the fact of deriving the model by the semi-continuous method. Nevertheless, other significant errors are apparent, particularly in the damping of the pressure perturbation.

Overall we have shown that a linear model formed by the continuous method may be as accurate as a tangent linear model. This will depend particularly on how the numerical scheme is applied to the continuous linear equations and on how the linearization state is chosen. The viability of using this method has been shown in simple models. In the three-dimensional model the results were encouraging, but it is clear that the present version of the model is not yet satisfactory. Further modifications to the scheme will be tested in order to improve this.

There still remains to summarize the answer to the second part of our question, that is does the semi-continuous method allow the avoidance of problems associated with discretizing the discrete numerical models? In the shallow water model of

Chapter 5 it was not clear that either method held any advantage from this point of view. The linearization of interpolation associated with semi-Lagrangian schemes, while not necessarily resulting in a 'correct' tangent linear, does not appear to cause problems for the validity of the model in time. This confirms the results found by Tanguay et al. [81]. For the iterative solution of the elliptic equation, it was straightforward in the shallow water model to derive the linearized equation to solve in the tangent linear model. Hence neither the semi-Lagrangian advection nor the iterative solver caused any problem for deriving the tangent linear.

For the three-dimensional model the use of the semi-continuous method did provide an extra advantage, since the nonlinear model has several predictor-corrector steps in the solution procedure. A derivation of the tangent linear model would have required either the storage or recalculation of the intermediate values from these steps, which was not necessary for the perturbation forecast model. It was also possible to make some extra approximations in the equations and in the discretization, for example by simplifying the way in which the Coriolis terms were treated. However it is clear that some of these approximations have led to a poor prediction of the pressure perturbation and so further investigation is required to understand the effects of each of them on the final solution.

A major practical advantage of using a perturbation forecast model will come when parametrizations of physical processes are introduced into the linear model. As we discussed in Section 3.2 these parametrizations often contain discontinuous processes which cause problems for tangent linear models. It is also the case that as the schemes for the nonlinear models become more complex, their linearizations will themselves be complex and expensive without adding any extra useful information to the linear system. The perturbation forecast model allows simpler parametrizations to be added with more thought as to what the scheme is trying to do in the linear model. Thus advantages of the semi-continuous method do remain and it is clear that perturbation forecast models can be designed to be as accurate as tangent

linear models. Nevertheless great care must be taken in the design of a perturbation forecast model to ensure that the accuracy is as good as is required.

7.2 Further work

Having begun to answer the question which we posed, we now consider how this work may be extended in order to provide further insight into the two methods for deriving a linear model. The first extension concerns the shallow water model of Chapter 5. Although the studies of that chapter showed very little difference between the tangent linear model and perturbation forecast model, the experiments we were able to carry out were limited in scope. This was partly due to the fact that it was only possible to find simple problems for the system which were not too highly nonlinear. A useful exercise would be to extend this model to include rotation. Such an extension would allow a greater range of experiments to be run. It would also result in the system having a Rossby mode solution as well as the two gravity modes. This would enable a study of how well the linear models treat a Rossby mode, which could be compared with the results found for the gravity waves.

A second extension of the problem would be to derive the adjoints of the different linear models. We expect the accuracy of the adjoint to be linked to that of the linear model. However it may be that using the adjoints in simple sensitivity or assimilation tests would give a better quantative measure of the difference between the linear models. This would also be a more stringent test of the adjoint model formed via the semi-continuous method, since although the application of incremental four-dimensional variational data assimilation allows an approximate linear model and adjoint, other applications of adjoints require the gradient to be as accurate as possible.

At the same time, it is clear that further work is required on the three-dimensional

model. One problem remaining from this study is the damping effect of our perturbation forecast model which we reported in Chapter 6. We conjectured that this may be due to the treatment of the term arising from the linearization of advection, which we showed in the study of the shallow water model to be first order in time. Although this did not seem to be detrimental to the performance of the simple model it is certainly not desirable to have such an error. The alternative considered in the shallow water model was to average the term along the trajectory, but this holds extra complications for the three-dimensional model since it adds extra coupling between the equations. We therefore require another second order discretization of this term. The scheme we have identified and intend to test is an extrapolation in time at the mid-point of the trajectory, in much the same way as the departure point calculation is performed. Thus, for example in the linearized thermodynamic equation, we would have

$$\boldsymbol{\delta u}.\nabla\theta = \frac{3}{2}(\boldsymbol{\delta u}.\nabla\theta)^{n}_{m} - \frac{1}{2}(\boldsymbol{\delta u}.\nabla\theta)^{n-1}_{m}, \tag{7.1}$$

where m indicates a calculation at the mid-point. We can show that this scheme is second order in time, but it does contain a small instability ([21], p.55). Its usefulness will have to be determined experimentally. However, the analysis of the shallow water model showed that for the linear model to remain second order in time we also require a second order estimate of the linearization state at the centre of the time step. Thus it is probable that to see the benefit of this new scheme we will also need to revise the strategy of using the start of time step linearization state.

Recently other investigations elsewhere in the Met Office have shown that the damping in the perturbation forecast model is also sensitive to the treatment of the Coriolis terms. We introduced in Section 6.2.4 a discretization of these terms designed to avoid problems when deriving the adjoint of the linear model. Alternative discretizations tested more recently have been shown to lessen the damping

effect seen in the linear model. However, more work is needed to investigate the comparative stability and accuracy properties of these different schemes.

Appendix A

Convergence of iterative procedure

We prove here the conditions for which the iterative procedure of the nonlinear shallow water model of Section 5.2.1 converges to the solution of the discrete elliptic equation we are trying to solve. The equation we wish to solve is equation (5.51) on page 93,

$$-C\phi'_{i+1} + \Big(2C + \frac{1}{\Phi_{ref}}\Big)\phi'_i - C\phi'_{i-1} = R_i - \ln(\Phi_{ref} + \phi'_i) + \frac{\phi'_i}{\Phi_{ref}}, \tag{A.1}$$

with $C > 0, \Phi_{ref} > 0$ and $\Phi_{ref} + \phi'_i > 0$ for $i = 1, \ldots, N$. This equation can be represented symbolically by the vector notation

$$\mathbf{L}\boldsymbol{\phi}' = R - N(\boldsymbol{\phi}'), \tag{A.2}$$

where $\boldsymbol{\phi}' = \{\phi'_i\}$. The matrix $\mathbf{L}$ and vector function N are defined by their components

$$(\mathbf{L}\boldsymbol{\phi}')_i = -C\phi'_{i+1} + \Big(2C + \frac{1}{\Phi_{ref}}\Big)\phi'_i - C\phi'_{i-1}, \tag{A.3}$$

$$N_i(\boldsymbol{\phi}') = \ln(\Phi_{ref} + \phi'_i) - \frac{\phi'_i}{\Phi_{ref}}, \tag{A.4}$$

and R is the vector of components R_i. The iterative procedure proposed to solve this equation is given by equation (5.52) on page 93,

$$\begin{aligned} -C{\phi'_{i+1}}^{(m+1)} &+ \left(2C + \frac{1}{\Phi_{ref}}\right){\phi'_i}^{(m+1)} - C{\phi'_{i-1}}^{(m+1)} \\ &= R_i - \ln(\Phi_{ref} + {\phi'_i}^{(m)}) + \frac{{\phi'_i}^{(m)}}{\Phi_{ref}}. \end{aligned} \tag{A.5}$$

This is a fixed point iteration which can be written in the form

$$\boldsymbol{\phi}'^{(m+1)} = \mathbf{L}^{-1}(R - N(\boldsymbol{\phi}'^{(m)})). \tag{A.6}$$

In order to show the conditions under which this iteration will converge, we make use of the fixed-point theorem, taken from [62]. We first define a general iteration of the form

$$\mathbf{g}(\mathbf{x}^{(m+1)}, \mathbf{x}^{(m)}) = 0, \qquad m = 0, 1, 2, \ldots \tag{A.7}$$

We denote by $\mathbf{g_x}$ and $\mathbf{g_y}$ the $n \times n$ matrices

$$\mathbf{g_x}(x, y) = \left(\frac{\partial \mathbf{g}_i}{\partial x_j}(x, y)\right), \qquad \mathbf{g_y}(x, y) = \left(\frac{\partial \mathbf{g}_i}{\partial y_j}(x, y)\right). \tag{A.8}$$

We also require the definition of the spectral radius of a matrix:

Definition A.1 *Let* $\mathbf{C}$ *be a matrix with eigenvalues* $\lambda_1, \lambda_2, \ldots, \lambda_n$. *Then the* spectral radius *of* $\mathbf{C}$, *written* $\rho(\mathbf{C})$, *is defined by*

$$\rho(\mathbf{C}) = \max_i |\lambda_i|. \tag{A.9}$$

We then have the following theorem:

Theorem A.1 (Fixed-point theorem) *Let* S' *be an open neighbourhood of a point* $\mathbf{x}^* \in R^n$. *Assume that* $\mathbf{g} \in C^1(S' \times S')$, $\mathbf{g_x}^{-1}$ *is defined and continuous on* $S' \times S'$ *and* $\mathbf{g}(\mathbf{x}^*, \mathbf{x}^*) = 0$. *Define*

$$\mathbf{C} \equiv -[\mathbf{g_x}(\mathbf{x}^*, \mathbf{x}^*)]^{-1}\mathbf{g_y}(\mathbf{x}^*, \mathbf{x}^*) \tag{A.10}$$

and suppose that $\rho(\mathbf{C}) \equiv \lambda < 1$. *Then there exists a neighbourhood* S *of* $\mathbf{x}^*$ *such that for any initial vector* $\mathbf{x_0} \in S$ *the sequence generated by (A.7) converges to* $\mathbf{x}^*$.

In order to apply this theorem to our iteration (A.6) we first note that it can be written in the form (A.7) by defining

$$\mathbf{g}(\boldsymbol{\phi}'^{(m+1)}, \boldsymbol{\phi}'^{(m)}) = \mathbf{L}\boldsymbol{\phi}'^{(m+1)} + N(\boldsymbol{\phi}'^{(m)}) - R. \tag{A.11}$$

We define matrices

$$\mathbf{D} = \frac{\partial}{\partial \phi_j}(N_i - R), \tag{A.12}$$

$$\mathbf{C} = -\mathbf{L^{-1}D}. \tag{A.13}$$

From (A.4) we see that $\mathbf{D}$ is a diagonal matrix with entries along the diagonal given by

$$-\frac{1}{\Phi_{ref}} + \frac{1}{\Phi_{ref} + \phi_i'} = -\frac{1}{\Phi_{ref}}\left(1 - \frac{\Phi_{ref}}{\Phi_{ref} + \phi_i'}\right). \tag{A.14}$$

Then using Theorem A.1 the fixed point iteration (A.6) will converge to a correct solution of the nonlinear system (A.2) if

$$\rho(\mathbf{C}) < 1. \tag{A.15}$$

It remains to find the conditions under which (A.15) holds.

We first set out two lemmas.

Lemma A.1 (Similarity transform) *Let* $\mathbf{P}$ *be a nonsingular matrix. Then for matrices* $\mathbf{C}, \tilde{\mathbf{C}}$ *with* $\tilde{\mathbf{C}} = \mathbf{P^{-1}CP}$*, the eigenvalues of* $\tilde{\mathbf{C}}$*, denoted* $\lambda(\tilde{\mathbf{C}})$*, are equal to the eigenvalues of* $\mathbf{C}$*,* $\lambda(\mathbf{C})$*. Hence we also have* $\rho(\tilde{\mathbf{C}}) = \rho(\mathbf{C})$*.*

Lemma A.2 (Symmetric transform) *Let* $\mathbf{P}$ *be a nonsingular matrix and let* $\mathbf{C}, \tilde{\mathbf{C}}$ *be matrices with* $\tilde{\mathbf{C}} = \mathbf{P^T CP}$*. Then* $\mathbf{C}$ *is a symmetric positive definite matrix if and only if* $\tilde{\mathbf{C}}$ *is a symmetric positive definite matrix.*

We now note that the matrix $\mathbf{L}$ is symmetric and strictly diagonally dominant with positive diagonal entries and hence $\mathbf{L}$ is symmetric positive definite. This

implies that $\mathbf{L}$ and $\mathbf{L^{-1}}$ have unique symmetric positive definite square roots which we write $\mathbf{L}^{\frac{1}{2}}$, $\mathbf{L}^{-\frac{1}{2}}$ respectively (see, for example, [36]). We define a matrix

$$\mathbf{A} = \mathbf{L}^{\frac{1}{2}}\mathbf{C}\mathbf{L}^{-\frac{1}{2}} \tag{A.16}$$

$$= -\mathbf{L}^{-\frac{1}{2}}\mathbf{D}\mathbf{L}^{-\frac{1}{2}}. \tag{A.17}$$

Then from Lemma A.1 the eigenvalues of $\mathbf{A}$ are equal to the eigenvalues of $\mathbf{C}$ and we also have that $\mathbf{A}$ is symmetric, since $\mathbf{D}$ is diagonal. The eigenvalues of $\mathbf{A}$, denoted λ_i, are therefore real. We consider matrices $\mathbf{B_1} = \mathbf{I} + \mathbf{A}$, $\mathbf{B_2} = \mathbf{I} - \mathbf{A}$ and establish the following lemma:

Lemma A.3 *If $\mathbf{B_1}, \mathbf{B_2}$ are symmetric positive definite matrices then the convergence criterion (A.15) is satisfied.*

Proof of Lemma A.3

Let μ_i, ν_i be the eigenvalues of $\mathbf{B_1}, \mathbf{B_2}$ respectively. Then $\mu_i = 1 + \lambda_i$ and $\nu_i = 1 - \lambda_i$. If $\mathbf{B_1}, \mathbf{B_2}$ are symmetric positive definite then we have $\mu_i > 0$ and $\nu_i > 0$ for all i. Hence

$$\begin{aligned} 1 + \lambda_i &> 0 \\ \text{and} \quad 1 - \lambda_i &> 0, \end{aligned}$$

which implies that $|\lambda| < 1$. Hence $\rho(\mathbf{A}) < 1$ and so by Lemma A.1 $\rho(\mathbf{C}) < 1$ and the convergence criterion (A.15) holds.□

It remains to find the conditions for which $\mathbf{B_1}, \mathbf{B_2}$ are symmetric positive definite. We now consider the matrices

$$\mathbf{L}^{\frac{1}{2}}(\mathbf{I} \pm \mathbf{A})\mathbf{L}^{\frac{1}{2}} = \mathbf{L} \pm \mathbf{D}. \tag{A.18}$$

Since $\mathbf{L}^{\frac{1}{2}}$ is symmetric, by Lemma A.2 we have that $\mathbf{I} \pm \mathbf{A}$ will be symmetric positive definite if $\mathbf{L} \pm \mathbf{D}$ is symmetric positive definite. Since $\mathbf{L}$ is a tridiagonal matrix and

$\mathbf{D}$ is a diagonal matrix with entries given by (A.14), we find that $\mathbf{L} \pm \mathbf{D}$ is the tridiagonal matrix with entries

$$\left(-C, 2C + \frac{1}{\Phi_{ref}} \pm \frac{1}{\Phi_{ref}}\left(1 - \frac{\Phi_{ref}}{\Phi_{ref} + \phi_i'}\right), -C\right). \tag{A.19}$$

A sufficient condition for this matrix to be symmetric positive definite is that it be strictly diagonally dominant. This will certainly occur if

$$\frac{1}{\Phi_{ref}} \geq \left|\frac{1}{\Phi_{ref}}\left(1 - \frac{\Phi_{ref}}{\Phi_{ref} + \phi_i'}\right)\right|. \tag{A.20}$$

For $\phi_i' > 0$ this condition always holds. For $\phi_i' < 0$ (A.20) holds for

$$|\phi_i'| < \frac{\Phi_{ref}}{2}. \tag{A.21}$$

Hence (A.21) provides a sufficient condition for the convergence of the iteration (A.5).

We note also that from (5.48) we have $\Phi_{ref} + \phi_i{}' = \phi_i^{n+1}$, the value of ϕ_i at the new time level, and so we can write the convergence condition (A.20) as

$$\frac{1}{\Phi_{ref}} \geq \left|\frac{1}{\Phi_{ref}}\left(1 - \frac{\Phi_{ref}}{\phi_i^{n+1}}\right)\right|. \tag{A.22}$$

Hence a sufficient condition for convergence is that $\Phi_{ref} < \phi_i^{n+1}$. We can therefore guarantee convergence by choosing a value of Φ_{ref} less than any expected value of ϕ_i at the new time level.

Appendix B

Helmholtz equation for 3-dimensional model

The Helmholtz equation for the perturbation forecast model resulting from substitution into (6.98) takes the following form:

$$\begin{aligned} &\frac{1}{\cos\phi}\partial_\lambda\left(C_{xx1}X\right)+\frac{1}{\cos\phi}\partial_\phi\left(C_{yy1}Y\right) \\ &+\partial_\eta\left[C_{zz}\delta_\eta\delta\hat{\Pi}'-C_5\left(\overline{C_{xz}\overline{X}^{\eta}}^{\lambda}+\overline{C_{yz}\overline{Y}^{\eta}}^{\phi}\right)\right] \\ &+C_3\left[\overline{C_z\partial_\eta\delta\hat{\Pi}'}^{r}\right] \\ &-C_4\delta\hat{\Pi}' \;=\; RHS, \end{aligned} \tag{B.1}$$

with X and Y are defined by

$$X=C_{xx2}\left(\partial_\lambda\delta\hat{\Pi}'-C_{xp}\overline{C_2\partial_r\delta\hat{\Pi}'}^{r\lambda}\right), \tag{B.2}$$

$$Y=C_{yy2}\left(\partial_\phi\delta\hat{\Pi}'-C_{yp}\overline{C_2\partial_r\delta\hat{\Pi}'}^{r\phi}\right), \tag{B.3}$$

and the notation following that introduced on Page 160. The coefficients are given by

$$C_{xx1}=\frac{\overline{\rho\partial_\eta r}^{\lambda}}{\overline{r}^{\lambda}}, \tag{B.4}$$

$$C_{xx2} = \frac{\alpha_1\alpha_3\Delta t c_p \overline{\theta}^{r\lambda}}{\overline{r}^{\lambda}\cos\phi}, \tag{B.5}$$

$$C_{yy1} = \frac{\overline{\rho\partial_\eta r}^{\phi}\cos\phi}{\overline{r}^{\phi}}, \tag{B.6}$$

$$C_{yy2} = \frac{\alpha_1\alpha_3\Delta t c_p \overline{\theta}^{r\phi}}{\overline{r}^{\phi}}, \tag{B.7}$$

$$C_{zz} = \frac{\alpha_2\alpha_4 c_p \Delta t \overline{\rho}^{r}\theta}{\partial_\eta r G}, \tag{B.8}$$

$$C_{z} = \frac{\alpha_2\alpha_4 c_p \Delta t \theta\partial_{2r}\theta}{\partial_\eta r G}, \tag{B.9}$$

$$C_{xz} = \frac{\partial_\lambda r}{\overline{r}^{\lambda}\cos\phi}, \tag{B.10}$$

$$C_{yz} = \frac{\partial_\phi r}{\overline{r}^{\phi}}, \tag{B.11}$$

$$C_{xp} = \frac{\partial_\lambda r}{\overline{\theta}^{r\lambda}}, \tag{B.12}$$

$$C_{yp} = \frac{\partial_\phi r}{\overline{\theta}^{r\phi}}, \tag{B.13}$$

$$C_{2} = \theta, \tag{B.14}$$

$$C_{3} = \frac{\rho\partial_\eta r}{\overline{\theta}^{r}}, \tag{B.15}$$

$$C_{4} = \frac{(1-\kappa)\rho\partial_\eta r}{\kappa\Pi\Delta t}, \tag{B.16}$$

$$C_{5} = \overline{\rho}^{r}, \tag{B.17}$$

$$\begin{aligned} RHS &= \frac{\partial_\eta r}{p\theta\Delta t}\Bigg(- p\rho\overline{\Big(\delta\tilde{\theta} - \frac{\alpha_2\Delta t\partial_{2r}\theta}{G}\delta w^*\Big)}^{r} - p\theta\delta\tilde{\rho}\Bigg) \\ &+ \frac{1}{\cos\phi}\partial_\lambda\Bigg(\alpha_1\frac{\overline{\rho\partial_\eta r}^{\lambda}}{\overline{r}^{\lambda}}\delta u^*\Bigg) + \frac{1}{\cos\phi}\partial_\phi\Bigg(\alpha_1\frac{\overline{\rho\partial_\eta r}^{\phi}}{\overline{r}^{\phi}}\cos\phi\delta v^*\Bigg) \\ &+ \partial_\eta\Bigg(\overline{\rho}^{r}\Big(\frac{\alpha_2\delta w^*}{G} - \frac{\overline{\alpha_1\overline{\delta u^*}^{\eta}}^{\lambda}}{\overline{r}^{\lambda}\cos\phi}\partial_\lambda r - \frac{\overline{\alpha_1\overline{\delta v^*}^{\eta}}^{\phi}}{\overline{r}^{\phi}}\partial_\phi r\Big)\Bigg). \end{aligned} \tag{B.18}$$

Bibliography

[1] W.K. Anderson and V. Venkatakrishan. Aerodynamic design optimization on unstructured grids with a continuous adjoint formulation. *Computers and Fluids*, 28:443–480, 1999.

[2] J-W. Bao and Y-H. Kuo. On/off switches in the adjoint method: Step functions. *Mon. Wea. Rev.*, 123:1589–1594, 1995.

[3] J-W. Bao and T.T. Warner. Treatment of on/off switches in the adjoint method: FDDA experiments with a simple model. *Tellus*, 45A:525–538, 1993.

[4] M.C. Bartholomew-Biggs. Using forward accumulation for automatic differentiation of implicitly-defined functions. *Computational Optimization and Applications*, 9:65–84, 1998.

[5] M.C. Bartholomew-Biggs, S. Brown, B. Christianson, and L. Dixon. Automatic differentiation of algorithms. *Journal of Computational and Applied Mathematics*, 124:171–190, 2000.

[6] G.K. Batchelor. *An introduction to fluid dynamics.* Cambridge University Press, 1967.

[7] F.H.M. Bates, J.R. Semazzi and R.W. Higgins. Integration of the shallow water equations on the sphere using a vector semi-Lagrangian scheme with a multigrid solver. *Mon. Wea. Rev.*, 118:1615–1627, 1990.

[8] J.R. Bates, S. Moorthi, and R.W. Higgins. A global multilevel atmospheric model using a vector semi-Lagrangian finite-difference scheme. Part I: Adiabatic formulation. *Mon. Wea. Rev.*, 121:244–263, 1993.

[9] C. Bischof, A. Carle, G. Corliss, A. Griewank, and P. Hovland. ADIFOR: Generating derivative codes from Fortran programs. *Scientific Programming*, 1:11–29, 1992.

[10] C.H. Bischof. Automatic differentiation, tangent linear models and pseudo-adjoints. In Le Dimet [47], pages 59–80.

[11] R. Buizza. Sensitivity of optimal unstable structures. *Quart. J. Roy. Meteor. Soc.*, 120:429–451, 1994.

[12] R. Buizza and T.N Palmer. The singular-vector structure of the atmospheric global circulation. *J.A.S.*, 52:1434–145, 1995.

[13] R. Buizza, J. Tribbia, F. Molteni, and T.N Palmer. Computation of optimal unstable structures for a numerical weather prediction model. *Tellus*, 45A:388–407, 1993.

[14] W.C. Chao and L-P. Chang. Development of a four-dimensional variational analysis system using the adjoint method at GLA. Part I: Dynamics. *Mon. Wea. Rev.*, 120:1661–1673, 1992.

[15] G. Chavent, M. Dupuy, and P. Lemonnier. History matching by use of control theory. *Society of Petroleum Engineers Journal*, pages 74–86, 1975.

[16] J. Côté, S. Gravel, A. Méthot, A. Patoine, M. Roch, and A. Staniforth. The operational CMC-MRB global environmental multiscale (GEM) model. Part I: Design considerations and formulation. *Mon. Wea. Rev.*, 126:1373–1395, 1998.

[17] P. Courtier, J-N. Thepaut, and A. Hollingsworth. A strategy for operational implementation of 4D-Var, using an incremental approach. *Quart. J. Roy. Meteor. Soc.*, 120:1367–1387, 1994.

[18] M.J.P. Cullen, T. Davies, M.H. Mawson, J.A. James, S.C. Coulter, and A. Malcolm. An overview of numerical methods for the next generation U.K. NWP and climate model. In C.A. Lin, R. Laprise, and H. Ritchie, editors, *Numerical methods in atmospheric and oceanic modelling*, pages 425–444. Canadian Meteorological and Oceanographic Society, 1997.

[19] T. Davies, M.J.P. Cullen, M.H. Mawson, and A.J. Malcolm. A new dynamical formulation for the UK Meteorological Office Unified Model. In *Recent developments in numerical methods for atmospheric modelling* [23], pages 202–225.

[20] D.R. Durran. The third-order Adams-Bashforth method: An attractive alternative to leapfrog time differencing. *Mon. Wea. Rev.*, 119:702–720, 1991.

[21] D.R. Durran. *Numerical methods for wave equations in geophysical fluid dynamics*. Springer-Verlag, 1999.

[22] C. Eckart. *Hydrodynamics of oceans and atmospheres*. Pergamon Press, 1960.

[23] ECMWF. *Recent developments in numerical methods for atmospheric modelling*, Seminar proceedings, 7-11 September 1998.

[24] G. Erbes. A semi-Lagrangian method of characteristics for the shallow-water equations. *Mon. Wea. Rev.*, 121:3443–3452, 1993.

[25] R.M. Errico and D. Baumhefner. Predictability experiments using a high-resolution limited-area model. *Mon. Wea. Rev.*, 115:488–504, 1987.

[26] R.M. Errico and K.D. Raeder. An examination of the accuracy of the linearization of a mesoscale model with moist physics. *Quart. J. Roy. Meteor. Soc.*, 125:169–195, 1999.

[27] R.M. Errico and T. Vukićević. Sensitivity analysis using an adjoint of the PSU-NCAR mesoscale model. *Mon. Wea. Rev.*, 120:1644–1660, 1992.

[28] R.M. Errico, T. Vukićević, and K. Raeder. Examination of the accuracy of a tangent linear model. *Tellus*, 45A:462–477, 1993.

[29] A.J. Gadd. Two refinements of the split explicit integration scheme. *Quart. J. Roy. Meteor. Soc.*, 106:215–220, 1980.

[30] C.W. Gear. *Numerical initial value problems in ordinary differential equations.* Prentice-Hall, 1971.

[31] M. Ghil and P. Malanotte-Rizzooli. Data assimilation in meteorology and oceanography. *Advances in Geophysics*, 33:141–266, 1991.

[32] R. Giering and T. Kaminski. Recipes for adjoint code construction. *ACM Trans. On Math. Software*, 24:437–474, 1998.

[33] M.B. Giles and N.A. Pierce. An introduction to the adjoint approach to design. *European Journal of Flow, Turbulence and Combustion*, 2000. To appear.

[34] A. Griewank. On automatic differentiation. In Iri and Tanabe [47], pages 83–108.

[35] A. Griewank, C. Bischof, G. Corliss, A. Carle, and K. Williamson. Derivative convergence for iterative equation solvers. *Optimization Methods and Software*, 2:321–355, 1993.

[36] N.J. Higham. Stable iterations for the matrix square root. *Numerical Algorithms*, 15:227–242, 1997.

[37] M. Hortal. The development and testing of a new two-time-level semi-Lagrangian scheme (SETTLS) in the ECMWF forecast model. *Quart. J. Roy. Meteor. Soc.*, 1999. Submitted.

[38] D.D. Houghton and A. Kasahara. Nonlinear shallow fluid flow over an isolated ridge. *Comm. Pure Appl. Math.*, 21:1–23, 1968.

[39] N.B. Ingleby. The statistical structure of forecast errors and its representation in the Met Office global 3-dimensional variational data assimilation scheme. *Quart. J. Roy. Meteor. Soc.*, 2001. To appear.

[40] A. Jameson, N. Pierce, and L. Martinelli. Optimum aerodynamic design using the Navier-Stokes equations. *J. Theor. Comp. Fluid Mech.*, 10:213–237, 1998.

[41] M. Janiskova, J-N. Thepaut, and J-F. Geleyn. Simplified and regular physical parametrizations for incremental four-dimensional variational assimilation. *Mon. Wea. Rev.*, 127:26–45, 1999.

[42] H. Kreiss and J. Oliger. *Methods for the approximate solution of time dependent problems.* Number 10 in GARP publications series. World Meterological Organization, 1973.

[43] K. Krishna. Commutativity of differentiation and discretization with special reference to finite element and finite difference discretizations. *Numer. Funct. Anal. and Optimiz.*, 7:235–265, 1984.

[44] J.D. Lambert. *Computational methods in Ordinary Differential Equations.* John Wiley and Sons, 1973.

[45] J.D. Lambert. *Numerical methods for Ordinary Differential Systems.* John Wiley and Sons, 1991.

[46] A.S. Lawless and N.K. Nichols. A comparison of two methods of deriving the tangent linear model. Forecasting Research Technical Report 257, The Met Office, 1998.

[47] F.-X. Le Dimet, editor. *High-performance computing in the geosciences.* Kluwer Academic Publishers, Boston, Mass., 1995.

[48] F-X. Le Dimet and O. Talagrand. Variational algorithms for analysis and assimilation of meteorological observations: theoretical aspects. *Tellus*, 38A:97–110, 1986.

[49] Y. Li et al. Variational data assimilation with a semi-Lagrangian semi-implicit global shallow-water equation model and its adjoint. *Mon. Wea. Rev.*, 121:1759–1769, 1993.

[50] Y. Li et al. Four-dimensional variational data assimilation experiments with a multilevel semi-Lagrangian semi-implicit general circulation model. *Mon. Wea. Rev.*, 122:966–983, 1994.

[51] A. Lorenc. Analysis methods for numerical weather prediction. *Quart. J. Roy. Meteor. Soc.*, 112:1177–1194, 1986.

[52] P. Lynch. Richardson's marvellous forecast. pages 61–73. Amer. Met. Soc., Boston, 1999.

[53] A. McDonald. Accuracy of multiply-upstream, semi-Lagrangian advective schemes. *Mon. Wea. Rev.*, 112:1267–1275, 1984.

[54] A. McDonald. Accuracy of multiply-upstream, semi-Lagrangian advective schemes II. *Mon. Wea. Rev.*, 115:1446–1450, 1987.

[55] A. McDonald and J.R. Bates. Improving the estimate of the deparure point position in a two-time level semi-Lagrangian semi-implicit scheme. *Mon. Wea. Rev.*, 115:737–739, 1987.

[56] F. Molteni, R. Buizza, T.N. Palmer, and T. Petroliagis. The ECMWF ensemble prediction system: Methodology and validation. *Quart. J. Roy. Meteor. Soc.*, 122:73–119, 1996.

[57] K.W. Morton and D.F. Mayers. *Numerical solution of partial differential equations.* Cambridge University Press, 1994.

[58] R. Muller. A note on the relation between the "traditional approximation" and the metric of the primitive equations. *Tellus*, 41A:175–178, 1989.

[59] S.K. Nadarajah and A. Jameson. A comparison of the continuous and discrete adjoint approach to automatic aerodynamic optimization. Technical Report AIAA-2000-0667, American Institute of Aeronautics and Astronautics.

[60] E.J. Nielsen and W.K. Anderson. Aerodynamic design optimization on unstructured meshes using the Navier-Stokes equations. *AIAA Journal*, 37:1411–1419, 1999.

[61] J.M. Ortega and W.C. Rheinboldt. On discretization and differentiation of operators with application to Newton's method. *J. SIAM Numer. Anal.*, 3:143–156, 1966.

[62] J.M. Ortega and M.L. Rockoff. Nonlinear difference equations and Gauss-Seidel type iterative methods. *J. SIAM Numer. Anal.*, 3:497–513, 1966.

[63] T.N. Palmer, R. Gelaro, J. Barkmeijer, and R. Buizza. Singular vectors, metrics and adaptive observations. *J.A.S.*, 55:633–653, 1998.

[64] S. Polavarapu and M. Tanguay. Linearizing iterative processes for four-dimensional data assimilation schemes. *Quart. J. Roy. Meteor. Soc.*, 124:1715–1742, 1998.

[65] S. Polavarapu, M. Tanguay, R. Menard, and A. Staniforth. The tangent linear model for semi-Lagrangian schemes: linearizing the process of interpolation. *Tellus*, 48A:74–95, 1996.

[66] J. Pudykiewicz, R. Benoit, and A. Staniforth. Preliminary results from a partial LRTAP model based on an existing meteorological forecast model. *Atmos. Ocean*, 23:267–303, 1985.

[67] F. Rabier and P. Courtier. Four-dimensional assimilation in the presence of baroclinic instability. *Quart. J. Roy. Meteor. Soc.*, 118:649–672, 1992.

[68] F. Rabier, P. Courtier, and O. Talagrand. An application of adjoint models to sensitivity analysis. *Beitr. Phys. Atmosph.*, 65:177–192, 1992.

[69] F. Rabier, E. Klinker, P. Courtier, and A. Hollingsworth. Sensitivity of forecast errors to initial conditions. *Quart. J. Roy. Meteor. Soc.*, 122:121–150, 1996.

[70] L.F. Richardson. *Weather Prediction by Numerical Processes.* Cambridge University Press, 1922.

[71] R.D. Richtmyer and K.W. Morton. *Difference methods for initial-value problems.* Wiley-Interscience, 1967.

[72] H. Ritchie. Application of the semi-Lagrangian method to a multilevel spectral primitive-equations model. *Quart. J. Roy. Meteor. Soc.*, 117:91–106, 1991.

[73] H. Ritchie and C. Beaudoin. Approximations and sensitivity experiments with a baroclinic semi-Lagrangian spectral model. *Mon. Wea. Rev.*, 122:2391–2399, 1994.

[74] C. Rivest, A. Staniforth, and A. Robert. Spurious resonant response of semi-Lagrangian discretizations to orographic forcing: diagnosis and solution. *Mon. Wea. Rev.*, 122:366–376, 1994.

[75] N. Rostaing, S. Dalmas, and A. Galligo. Automatic differentiation in Odyssée. *Tellus*, 45A:558–568, 1993.

[76] Z. Sirkes and E. Tziperman. Finite difference of adjoint or adjoint of finite difference? *Mon. Wea. Rev.*, 125:3373–3378, 1997.

[77] W.C Skamarock and J.B. Klemp. Preconditioned conjugate-residual solvers for Helmholtz equations in nonhydrostatic models. *Mon. Wea. Rev.*, 125:587–599, 1997.

[78] P.K. Smolarkiewicz and L.G. Margolin. Variational elliptic solver for atmospheric applications. Report LA-12712-MS, Los Alamos, 1994.

[79] A. Staniforth and J. Côté. Semi-Lagrangian integration schemes for atmospheric models - a review. *Mon. Wea. Rev.*, 119:2206–2223, 1991.

[80] O. Talagrand and P. Courtier. Variational assimilation of meteorological observations with the adjoint vorticity equation. I: Theory. *Quart. J. Roy. Meteor. Soc.*, 113:1311–1328, 1987.

[81] M. Tanguay, S. Polavarapu, and P. Gauthier. Temporal accumulation of first-order linearization error for semi-Lagrangian passive advection. *Mon. Wea. Rev.*, 125:1296–1311, 1997.

[82] C. Temperton. Tangent linear and adjoint models. In *Recent developments in numerical methods for atmospheric modelling* [23], pages 12–20.

[83] C Temperton and Staniforth A. An efficient two-time-level semi-Lagrangian semi-implicit integration scheme. *Quart. J. Roy. Meteor. Soc.*, 113:1025–1039, 1987.

[84] C Temperton, M. Hortal, and A. Simmons. A two-time-level semi-Lagrangian global spectral model. *Quart. J. Roy. Meteor. Soc.*, 1999. Submitted.

[85] J-N. Thepaut and P. Courtier. Four-dimensional variational data assimilation using the adjoint of a multilevel primitive-equation model. *Quart. J. Roy. Meteor. Soc.*, 117:1225–1254, 1991.

[86] J-N. Thepaut, R.N. Hoffman, and P. Courtier. Interactions of dynamics in a four-dimensional variational assimilation. *Mon. Wea. Rev.*, 121:3393–3414, 1993.

[87] J. Thuburn and T.W.N. Haine. Adjoints of nonoscillatory advection schemes. *J. Comput. Phys.*, 2000. Submitted.

[88] T. Vukićević and J-W. Bao. The effect of linearization errors on 4DVAR data assimilation. *Mon. Wea. Rev.*, 126:1695–1706, 1998.

[89] A. Wiin-Nielsen. The birth of numerical weather prediction. *Tellus*, 43AB:36–52, 1991.

[90] Q. Xu. Generalized adjoint for physical processes with parameterized discontinuities. Part I: Basic issues and heuristic examples. *J.A.S.*, 53:1123–1155, 1996.

[91] J. Zhu and M. Kamachi. The role of time step size in numerical stability of tangent linear models. *Mon. Wea. Rev.*, 128:1562–1572, 2000.

[92] X. Zou. Tangent linear and adjoint of 'on-off' proceses and their feasibility for use in 4-dimensional variational data assimilation. *Tellus*, 49A:3–31, 1997.

[93] X. Zou, Y-H. Kuo, and Y-R. Guo. Assimilation of atmospheric radio refractivity using a nonydrostatic adjoint model. *Mon. Wea. Rev.*, 123:2229–2249, 1995.

[94] D. Zupanski and D Mesinger. Four-dimensional variational data assimilation of precipitation data. *Mon. Wea. Rev.*, 123:1112–1125, 1995.

[95] M. Zupanski. Regional four-dimensional variational data assimilation in a quasi-operational forecasting environment. *Mon. Wea. Rev.*, 121:2396–2408, 1993.